CONTRACT REPORT S-75-5

THE MECHANICS OF PILE-SOIL INTERACTION IN COHESIONLESS SOILS

by

D. Michael Holloway, G. Wayne Clough, Aleksandar S. Vesic
School of Engineering, Department of Civil Engineering
Duke University, Durham, N. C. 27706

December 1975

Final Report

Approved For Public Release; Distribution Unlimited

Prepared for Office, Chief of Engineers, U. S. Army
Washington, D. C. 20314

Under Contract No. DACW39-73-C-0137

Monitored by Soils and Pavements Laboratory
U. S. Army Engineer Waterways Experiment Station
P. O. Box 631, Vicksburg, Miss. 39180

REPORT DOCUMENTATION PAGE

READ INSTRUCTIONS BEFORE COMPLETING FORM

1. REPORT NUMBER: Contract Report S-75-5
2. GOVT ACCESSION NO.:
3. RECIPIENT'S CATALOG NUMBER:

4. TITLE (and Subtitle): THE MECHANICS OF PILE-SOIL INTERACTION IN COHESIONLESS SOILS

5. TYPE OF REPORT & PERIOD COVERED: Final Report

6. PERFORMING ORG. REPORT NUMBER:

7. AUTHOR(s)
D. Michael Holloway
G. Wayne Clough
Aleksandar S. Vesic

8. CONTRACT OR GRANT NUMBER(s): DACW39-73-C-0137

9. PERFORMING ORGANIZATION NAME AND ADDRESS
School of Engineering
Duke University
Durham, N. C. 27706

10. PROGRAM ELEMENT, PROJECT, TASK AREA & WORK UNIT NUMBERS:

11. CONTROLLING OFFICE NAME AND ADDRESS
Office, Chief of Engineers, U. S. Army
Washington, D. C. 20314

12. REPORT DATE: December 1975

13. NUMBER OF PAGES: 297

14. MONITORING AGENCY NAME & ADDRESS (if different from Controlling Office)
U. S. Army Engineer Waterways Experiment Station
Soils and Pavements Laboratory
P. O. Box 631, Vicksburg, Miss. 39180

15. SECURITY CLASS. (of this report): Unclassified

15a. DECLASSIFICATION/DOWNGRADING SCHEDULE:

16. DISTRIBUTION STATEMENT (of this Report)

Approved for public release; distribution unlimited.

17. DISTRIBUTION STATEMENT (of the abstract entered in Block 20, if different from Report)

18. SUPPLEMENTARY NOTES

19. KEY WORDS (Continue on reverse side if necessary and identify by block number)

Cohesionless soils
Computer applications
DUKFOR (computer program)
Pile driving
Pile load tests
Pile-soil interaction
Soil-structure interaction

20. ABSTRACT (Continue on reverse side if necessary and identify by block number)

A one-dimensional, discrete element formulation was developed to simulate single pile performance during impact driving and subsequent load testing. The computer program, DUKFOR, combines a multiple-blow wave equation solution with an incremental static equilibrium formulation. Static equilibrium at the end of the simulated blow provides the initial conditions for a subsequent hammer blow or for load test simulation. In this way residual driving stresses are included in the simulation. Nonlinear or bilinear static load transfer properties may be assigned along the shaft and at the pile point. The incremental static equili-

20. ABSTRACT (continued).

brium solution permits arbitrary load test path simulation. Pile tests from two sites were analyzed using DUKFOR: Jonesville Lock and Dam (JLD) near Jonesville, La., where prestressed concrete piles were driven or jetted and driven into dense to very dense, fine silty sands; and Lock and Dam No. 4 (LD4), Arkansas River Project, near Pine Bluff, Ark., where closed-end pipe piles were impact-driven, vibratory-driven, or jetted and driven into medium dense, fine silty sands. Each pile was load tested both in compression and tension. DUKFOR predictions of pile driving (when applicable) and load testing performance were made using fundamental geotechnical assumptions for the resistance distributions. Measured pile capacities were used to backcalculate the appropriate failure parameters for use in the analyses. The shaft load transfer mechanism was described by hyperbolic interface shear test parameters. Hyperbolic point load transfer parameters were developed from LD4 pile test measurements. The DUKFOR predictions of pile performance were generally quite good. Predicted residual point loads for the LD4 test piles were in fair agreement with field measurements. Predicted compression load-displacement behavior was excellent. Tension load-displacement predictions showed the significant effects of residual compression load distribution on tension test performance; however, the displacement predictions at loads near failure were not very good. DUKFOR predicted LD4 load distribution data fairly well, though a "strain-hardening" effect was noted in the load transfer measurements. An axisymmetric finite element code, AXISYM, was developed to provide a direct comparison of analytical results with those of DUKFOR. It was shown that the "strain-hardening" effect could be the result of increasing shear strength due to compression load transfer to the surrounding soil. The opposite effect is predicted by AXISYM for tension loading; the tension load transferred to the surrounding soil reduces confining stress levels and "softens" the pile-soil system response. It was concluded that these tendencies are of minor importance in predicting load-displacement behavior, at least for the pile tests studied. Residual driving load distributions were shown to directly affect pile performance due to the manner in which soil resistance is mobilized. They play a major role in the correct interpretation of pile test results for use in design. DUKFOR is the only method available to predict the residual pile load effects on single pile behavior. Having investigated the analytical capabilities and limitations of the two computer codes, the authors performed parametric studies to establish appropriate stability and convergence criteria. In addition, a parametric study was included to determine the effects of different hammer-assembly-pile-soil system properties on the predicted blow counts and residual load distributions using DUKFOR. Finally, a direct comparison of DUKFOR and AXISYM solution costs was made. In order to obtain load test predictions of comparable accuracy, it was found that the AXISYM analysis was at least 10 to 30 times more expensive in computational effort alone. On the basis of solution capabilities and practical considerations, it is believed that DUKFOR provides the better method.

THE CONTENTS OF THIS REPORT ARE NOT TO BE USED FOR ADVERTISING, PUBLICATION, OR PROMOTIONAL PURPOSES. CITATION OF TRADE NAMES DOES NOT CONSTITUTE AN OFFICIAL ENDORSEMENT OR APPROVAL OF THE USE OF SUCH COMMERCIAL PRODUCTS.

PREFACE

The work described in this report was performed under Contract No. DACW39-73-C-0137, "Analyses of Pile-Soil Interaction," between the U. S. Army Engineer Waterways Experiment Station (WES) and Duke University. The study was sponsored by the Office, Chief of Engineers, U. S. Army (OCE), through the Civil Works R&D Program under CWIS 31203, "Analyses of Structure and Foundation Interaction."

This study, which was begun in July 1973, was performed under the supervision of Professor A. S. Vesić, Dean, School of Engineering, Duke University, and Professor G. Wayne Clough of Stanford University (Duke University during the conduct of this study).

The investigation described in this report was conducted by Mr. D. Michael Holloway, who was a graduate research fellow in the Department of Civil Engineering during the course of the project. This report is essentially the dissertation of Mr. Holloway submitted to Duke University in partial fulfillment of the requirements for the Doctor of Philosophy degree. Documentation, utilization guidelines, and listings of the computer programs developed in this effort will be published separately by WES.

Messrs. Walter C. Sherman, Jr., Research Civil Engineer, Soil Mechanics Division (SMD), and Stanley J. Johnson, Special Assistant, Soils and Pavements Laboratory (S&PL), provided technical review and advice. Mr. Hugh M. Taylor, Jr., Engineer, SMD, provided technical assistance at WES. Mr. Lucien Guthrie was technical monitor for OCE.

The work was carried out under the general direction of Messrs. Clifford L. McAnear, Chief, SMD, and James P. Sale and Richard G. Ahlvin, Chief and Assistant Chief, respectively, S&PL.

Director of WES during the study was COL G. H. Hilt, CE. Technical Director was Mr. F. R. Brown.

CONTENTS

LIST OF FIGURES

LIST OF TABLES

List of Tables (con't) Page

LIST OF SYMBOLS

English Letters

$\bar{a}$	acceleration vector
A	cross sectional area
A_p	pile point area
A_s	pile shaft surface area
B	base width
c	soil cohesion; or superscript denoting at compression failure; or normal stress wave velocity
c'	modified soil cohesion
c_a	pile-soil adhesion
C	compression
CC	cyclic compression
CIGRAV	gravity force coefficient
crit	subscript denoting critical value
CT	cyclic tension
CPU	computer processing units
D	depth of embedment
D/B	relative depth of embedment
DIAG	vector of values on stiffness matrix diagonal
D/	driving simulated
e	coefficient of restitution or subscript denoting explosive force
E	Young's Modulus or energy term

Symbols (con'd)

f	subscript denoting failure condition
f_o	unit shaft capacity
$\bar{f}_o$	average unit shaft capacity
F	force
$\bar{F}$	force vector
FE	finite element
FACTOR	ratio of integration time interval to the critical value in the pile driving model
g	acceleration of gravity
h	stroke
h_e	equivalent stroke
i	subscript denoting initial value or elemental value
IBLOWS	number of simulated blows
IS	interface shear
I/O	computer input/output
J_p, J_s	point and shaft nonlinear viscous dampint constants
$\bar{J}_p, \bar{J}_s$	point and shaft linear viscous damping constants.
JLD	Jonesville Lock and Dam
k	spring stiffness value
$\bar{k}$	soil stiffness value
K_s	ratio of normal stress on the pile shaft to in situ effective overburden stress
L	length
LD4	Lock and Dam No. 4
max	subscript denoting maximum or failure value
MO	number of the first pile segment

Symbols (con'd)

n	exponent parameter
N_c, N_q, N_γ	bearing capacity factors
N_q	bearing capacity factor for deep circular foundations
o	superscript or subscript denoting initial value
p	pressure or subscript denoting pile point
q	effective vertical stress
q_o	unit point bearing capacity
q_f	effective overburden pressure at failure at foundation base level
Q	force in pile
Q_p	point bearing capacity
Q_s	shaft bearing capacity
R	soil resistance force
r, θ, z	spatial coordinates, maybe used as subscripts
$\bar{r}$	radius to the centroid of an element
$RESID_i$	sum of dynamic forces on an element
$RESID_{p+1}$	sum of dynamic forces on all pile elements
RMAX,RMIN	maximum, minimum static resistance force
RDYNAM	dynamic resistance force
s	subscript denoting pile shaft
S	subscript denoting soil
SF	stress free
SAREA	element surface area
t	time; as a subscript it denotes a tangent value; as a superscript it denotes a tension failure value
u	displacement at a point

Symbols (con'd)

ult	subscript denoting hyperbolic assymptote value
UR	unload/reload
v,V	velocity term or subscript denoting vertical
W	weight
x,y,z	spatial coordinates, may be used as subscripts
z_{str}	zone of stretching
z_w	depth of water table

Greek Letters

γ	unit weight, may be used as subscript
γ_w	unit weight of water
δ	interface friction angle
Δ	relative displacement
$\Delta x, \Delta t$	incremental change in x,t
ε	strain
η	driving system mechanical efficiency
Θ	angle characteristic of bearing failure zone geometry
$\overline{\Theta}$	interval of revolution in element stiffness derivation
ν	Poisson's ratio
π	pi = 3.14159 . . .
ρ	mass density
σ	total
$\overline{\sigma}$	effective stress
σ_1, σ_3	principal stresses

Symbols (con'd)

$(\sigma_1 - \sigma_3)$	deviator stress
$\overline{\sigma}_n$	interface normal stress
$\overline{\sigma}_o$	mean normal stress
Σ	summation
τ	shear stress
ϕ	angle of internal friction
ϕ'	modified angle of internal friction
χ	correction coefficient
ζ	coordinate location along pile
$\zeta_c, \zeta_q, \zeta_\gamma$	bearing capacity shape factors
$\frac{\partial}{\partial x}, \frac{\partial}{\partial t}$	first partial derivative with respect to x, t
$\frac{\partial^2}{\partial x^2}, \frac{\partial^2}{\partial t^2}$	second partial derivative with respect to x, t

CONVERSION FACTORS, BRITISH TO METRIC UNITS OF MEASUREMENT

British units of measurement used in this report can be converted to metric units as follows:

Multiply	By	To Obtain
inches	2.54	centimeters
feet	0.3048	meters
miles (U.S. statute)	1.609344	kilometers
pounds (force) per square inch	0.6894757	newtons per square centimeter
kips (force) per square foot	47.8803	newtons per square meter
pounds (mass) per cubic foot	16.0185	kilograms per cubic meter
inches per second	2.54	centimeters per second
feet per second	0.3048	meters per second

THE MECHANICS OF PILE-SOIL INTERACTION IN COHESIONLESS SOILS

Chapter I

INTRODUCTION

Purpose of Study

Foundation conditions and structural constraints often require the use of pile foundations to support the structure and to minimize objectionable settlements. The accurate prediction of foundation performance and the effective interpretation of field load tests are urgent economic and technical needs of geotechnical engineering practice.

This study represents the final phase of an investigation into the analysis of pile load tests. Overall study objectives have been: (a) to compile and make available to the Corps of Engineers (CE) offices the results of pile load tests performed by CE offices and other investigators; (b) to review analytical solutions for determining pile load capacity; (c) to compare pile load test results with theoretical solutions; (d) to develop improved methods for conducting and interpreting pile load tests; and (e) to develop design guidelines.

In a previous report by Sherman, Holloway and Trahan[1], objectives (a) through (c) were accomplished. Very few of the many pile test results compiled supplied sufficient data to permit detailed analyses of pile-soil system performance. In most cases the data were incomplete. In others

the pile was not loaded far enough to cause failure, but rather only far enough to satisfy design criteria. Only a few carefully instrumented pile load tests with adequate soils data could be examined effectively. Some of the observations of that report deserve further comment.

It was found that for pile tests in soft to medium clays, conventional bearing capacity theory (assuming undrained shear strengths) provided generally satisfactory load test predictions. Moreover, such assumptions probably provide conservative estimates of long-term behavior. Sparse data from pile tests in stiffer cohesive soils suggest that many uncertainties cause difficulties in assessing both short- and long-term pile performance. Transient phenomena involving remolding, excess pore pressure dissipation and reconsolidation, make the analytical determination of the resistance to penetration a most difficult task. It was decided, therefore, that efforts could best be applied to analyses of pile-soil interaction in cohesionless soils, for which such transient phenomena should not dominate the behavior.

Analyses of pile tests in cohesionless soils suggest that conventional static formulae do not adequately predict pile performance. Additional investigations into the mechanism of pile-soil interaction in cohesionless soils were thereafter begun. A rational analytical procedure was developed to better predict or interpret the pile-soil system response of single, axially-loaded piles. A one-dimensional discrete element formulation, FDFOR, was generated to incorporate one-dimensional interface and tip deformation models to simulate nonlinear and/or bilinear elemental resistance behavior. The results of FDFOR analyses partially satisfied objective (d) of the overall study.[2] Predictions agreed reasonably well

with compression load-displacement behavior; however, load distribution predictions and tension test results compared poorly with field measurements. The discrepancies were attributed to residual driving stresses and residual stresses after compression testing, though only qualitative simulations could be performed using a static formulation.

In a related study analytical (wave equation) solutions to pile driving problems were examined. Numerical solutions of one-dimensional wave equation representations of pile driving behavior were the primary interest. The computer code developed at Texas A&M University (TAMU), patterned after A.E.L. Smith's algorithm, was adapted for use on the Waterways Experiment Station (WES) computer facilities. The pile driving results of test piles used in FDFOR analyses were analyzed using TAMFOR, the WES time sharing version of the TAMU program. The investigation of wave equation applications is published in a separate report.[3]

In view of the observations made and the expertise developed during the execution of these projects, it was determined that the influence of residual load distributions on pile performance should be examined analytically. To accomplish this objective a computer code was proposed which could simulate the pile installation-load test behavior in a unified procedure.

Scope

As a final product of this research effort, a combined dynamic/static, one-dimensional discrete element formulation, DUKFOR, has been developed. The dynamic solution scheme permits multiple blow analyses to model impact pile driving behavior more accurately. The incremental

static equilibrium algorithm (after FDFOR) is used to satisfy static equilibrium at the end of each hammer blow, as well as to solve arbitrary static loading conditions. DUKFOR incorporates all the features of FDFOR in a complete procedure that analyzes the whole pile installation/load test sequence continuously. The "static only" solution option in DUKFOR is an improved version of the FDFOR formulation.

An axisymmetric finite element (FE) code, AXISYM, was developed to directly compare the one-dimensional and axisymmetric idealizations of the problem. The plane strain, multi-purpose FE code SOIL-STRUCT, developed by G.W. Clough and Y. Tsui was modified to include an axisymmetric idealization that can model pile test behavior.

Chapter II discusses pile installation behavior. Particular attention is given to mathematical models of impact pile driving. Chapter III reviews the analyses used to estimate the behavior of axially-loaded single piles. Comparisons with experimental observations, and a description of the effects of residual loads in pile test performance/interpretation complete the chapter. The development of computer codes DUKFOR and AXISYM is presented in Chapter IV.

Chapter V documents the results of DUKFOR and AXISYM analyses performed to evaluate analytical capabilities. Pile tests were analyzed using DUKFOR, and one test pile was carefully studied using AXISYM and DUKFOR. Solution stability and convergence criteria are evaluated for both codes in Chapter VI. Parametric investigations of system variables were made to determine their effects on (DUKFOR) predicted pile driving behavior. A discussion of AXISYM and DUKFOR code capabilities completes the chapter.

Chapter VI contains the conclusions that may be drawn from the overall study, and general recommendations to engineers for applying the techniques in practice and in future research. The Appendix provides some essential details needed to prescribe pile-soil system parameters in applying these methods.

Chapter II

ANALYSES OF PILE INSTALLATION

In order to analyze a pile-soil interaction problem a multitude of factors affecting the behavior must be quantified into a grossly simplified mathematical model. Laboratory model tests under carefully monitored conditions indicate that many variables profoundly influence subsequent pile performance. Predetermination of these conditions for field pile load test behavior is an even more difficult task. To accurately extrapolate single pile load test behavior to the performance of foundation piles supporting the structure requires far more judgement than available analytical methods can justify.

The efforts described in this study focus on axial load-deformation behavior of single pile foundations in cohesionless soils. This chapter discusses analyses of pile performance during installation.

Methods of pile installation are briefly discussed and impact pile driving is emphasized. Analytical methods used to examine pile driving behavior involve either energy formulae or solutions to a one-dimensional wave equation representation of the problem. Basic assumptions and limitations of these methods are described. The final section of this chapter reviews several fundamental concepts that are essential to

develop a basic understanding of impact pile driving phenomena. A review of wave equation applications to pile driving problems fulfills this purpose.

Methods of Pile Installation

The purpose of foundation piles is to transfer structural loads to bearing strata that will prevent structural failure. With this purpose in mind, the installation of a suitable pile requires judicious consideration of the structural requirements, the alternatives most appropriate for the site conditions, and certainly the cost and reliability of the installed foundation.

One diverse category is described as cast-in-place construction. The foundation element (pile, pier, drilled shaft or caisson) is built in situ with all necessary care to insure the structural integrity of the finished product. A vast number of procedures have been used successfully under quite varied circumstances. Quite often, a method must be adapted to accommodate the specific site conditions encountered. The discussion will be limited to the broad category of cast-in-place piles.

The method of construction for cast-in-place piles can have a significant influence upon the performance of the foundation. Disturbance caused during installation can alter the in situ stress conditions and deformation properties in the vicinity of the pile. As an example, the drilling of a shaft into a cohesionless deposit may require the use of drilling mud to prevent the soil from sloughing into the cavity. Not only do radial stresses decrease considerably near the cavity (increasing shear stresses and strains), but the mud may also intrude into the adjacent soil

affecting the frictional characteristics along the pile shaft. The concrete placement will restore the radial stresses to some degree, depending upon the method of placement used.

A related means of installation to cast-in-place methods employs predrilling or jetting to develop the hole into which a prefabricated pile is placed. Either method is generally applied when impact driving encounters very high resistance to pile penetration. Predrilling or jetting may be used to assist penetration of an impact driven pile through very stiff cohesive or very dense cohesionless soil strata to achieve the necessary penetration.

Drilling methods may be used in both cohesive and cohesionless soils with proper care to maintain the hole as needed. Jetting employs a high pressure stream of air and/or water to cause high excess pore fluid pressures that reduce effective stresses in the vicinity of the advancing pile point. The liquified soil is usually flushed up along the pile shaft. Jetting is suitable only in cohesionless soils. Cohesive soils typically have too high resistance to erosion by water jets.

It is important to note the influence of each method of installation on the engineering solution. Cast-in-place methods and predrilling/jetting methods typically involve substantial changes in the stress-strain state of the soil near the pile from the in situ conditions. Indeed, these methods may cause a reduction in effective stresses around the pile resulting in a low shaft resistance. The accurate estimation of construction effects and quality control of the final product are frequently formidable tasks. For piles designed to sustain substantial shaft resis-

tance, such procedures as predrilling and jetting are generally restricted. For end bearing piles these same techniques would be well suited.

The final method of installation to be mentioned in this section is pile driving. There are two basic types of pile drivers: vibratory hammers and impact hammers. Each type may be subdivided according to specific hammer characteristics.

Vibratory pile drivers apply an oscillatory axial force pulse at the pile butt. Low frequency (5 to 35 cycles per second) vibrators lift and push downward the entire pile with each cycle. These hammers are most commonly used to drive and extract sheet piling, soldier beams, and light cross-section non-displacement piles. High frequency (40 to 140 cycles per second) vibrators generate sufficient energy at a controlled frequency to cause resonance of the pile-soil system. The vibrations reduce shaft friction resistance and transmit significant energy to the pile tip. The vibratory energy at the tip causes the soil to flow from beneath the pile tip as penetration proceeds. Resonant vibrators have been used successfully on a number of projects to drive displacement piles over 100 feet in length.[4]

Vibratory pile drivers offer some attractive advantages including[4]: increased installation speed; reduction of objectionable installation noise; ability to drive lighter cross-section piles more effectively to the necessary penetration than impact hammers can accomplish; and finally, the reduction of the amplitude of vibrations transmitted to adjacent structures near the site. The costs of equipment and maintenance are two recognized drawbacks at this time. Documented performance of vibratory hammer-driven foundation piles is lacking in the geotechnical literature.

Impact pile driving is the most common method of foundation pile installation. The energy causing pile penetration is delivered in impact stress transmission from a propelled ram to the pile. Impact pile drivers have been used to install piling since early in recorded history. Nonetheless, a fundamental understanding of the phenomena pertaining to pile driving performance has not been generated until very recently. Rational methods for analyzing pile driving behavior are just beginning to find acceptance in foundation engineering practice. The next section discusses the mechanics of impact pile driving and includes a summary of the available analytical methods that are applied to this class of problems.

Impact Pile Driving Behavior

The performance of the hammer-pile-soil system during impact pile driving involves a combination of extremely complex phenomena. The nature of impact energy transmission from the ram to the pile may require analytical formulation of ram-capblock-drivehead-cushion-pile interaction behavior in a general problem. The pile penetration behavior due to ram impact adds the pile-soil interaction to the system variables. Incorporation of accurate representations of all the variables affecting pile driving behavior is truly beyond the "state-of-the-art" in geotechnical engineering. Nevertheless, the engineer frequently needs to determine a solution to pile driving problems in practice. A fundamental understanding of the nature of the problem and of the available analytical methods is essential.

Energy Formulae

The most basic mathematical model of impact pile driving employs the assumption of simple Newtonian (point mass) impact between the ram and the pile. The simplest formulae equate an "adjusted" ram output energy at impact to the work performed to cause pile penetration.

"Adjustments" to the ram energy output involve considerations of energy losses during impact. These losses may include cushion inelasticity, mechanical losses, component inertial forces and related empirical adjustments based upon field experience. Some pile driving formulae incorporate a variety of considerations in obtaining the energy transmitted to the pile.

"Adjustments" to pile and pile-soil behavior assumptions can include total pile inertia (point mass), pile impedance, a rheological (spring) model of the total soil resistance, and even the distribution of resistance along the pile in particular formulae. Empirical correlation factors have been recommended for any or all of these possible parameters to match each author's pile test results and generate a "new" formula to add to an ever-growing list of formulae published in the literature.

The important point to note in this discussion is that the most "accurate" formulae are often derived from a correlation study of a set of pile test results, and then compared with similar pile test results to verify their utility. No matter how sophisticated the formulation, a host of important problem variables are lumped in gross parameters and adjusted to match a limited set of field data. Moreover, a number of significant causative variables are not even accounted for quantitatively in these energy formulae. This fact is vividly described in Table II-1 from Parola.[5]

Table II-1

The Wave Equation Versus Energy Formulae, From Parola[5].

	Varieties						
	Pile Impedance or Area	Hammer Cushion	Pile Cushioning Effect	Soil Resistance Distribution	Hammer Energy	Ram Velocity	Drivehead Weight
1. Engineering News					X		
2. Modified Engineering News	U				X		
3. Gow	U				X		
4. Vulcan Iron Works	U				X		
5. Bureau of Yards and Docks					X		
6. Rankine	X			X	X		
7. Dutch	U				X		
8. Ritter	U				X		
9. Eytelwein	U				X		
10. Navy-McKay	U				X		
11. Sanders					X		
12. Gates					X		
13. Danish	X				X		
14. Janbu	X				X		
15. Hiley	X			X	X		
16. Redtenbacker	X			X	X		
17. Pacific Coast Uniform Building Code	X				X		
18. Canadian National Building Code	X			X	X		
19. Olson and Flaate					X		
Wave Equation Analysis	X	X	X	X	X	X	X

Legend: Blank Space - variable not accounted for
U - variable unsatisfactorily accounted for
X - variable accounted for

Nineteen common energy formulae (of some several hundred published and, no doubt, many hundreds more unpublished) are listed versus significant variables affecting pile driving behavior. The lack of representation given to so many variables by every energy formula is glaringly obvious. In contrast to these formulae, the one-dimensional wave equation formulation is also included. It accommodates all the variables in a quantitative manner such that it represents the best available solution to the general problem.

In fairness, however, it must be recognized that energy formulae have been used quite successfully in many cases. The reliability of a given formula is usually as good as the degree to which the engineering problem matches the cases for which the formula has been accurate. In a case where the hammer-pile-soil system closely resembles the successful field experience with a specific formula, it is probably the most reliable analytical method. When hammer and/or pile and/or site conditions deviate from those proven by experience, beware!

One-Dimensional Wave Equation Solutions

A thorough review of analytical solutions to the one-dimensional wave equation and their applications to impact pile driving problems is given elsewhere.[3] In this section a summary of the essential information described in that report is provided.

Stress wave propagation behavior is described by Newton's Second Law: The vector sum of the forces acting on a body is equal to the product of the mass times the resulting acceleration. Continuum mechanics generalizes the statement in the (dynamic equilibrium) equations of motion at a point, employing the appropriate constitutive representation of the

physical materials. This system of equations may be greatly simplified when the physical problem can be described in one dimension, as the dynamic equilibrium at a point on a one-dimensional rod in response to propagation of a longitudinal stress wave.

The free body diagram of an infinitesimal rod element is given in Fig. II-1. The equation of equilibrium for the rod element is written directly as,

$$\Sigma \bar{F} = \left(\frac{W}{g}\right) \bar{a} \quad . \tag{II-1}$$

In other words, regardless of deformation properties of the rod, the resultant force applied to the element equates with the elemental mass times the resultant element acceleration at any instant in time.

Rewriting equation II-1 in terms of stresses and element properties and cancelling or factoring corresponding terms the elemental equilibrium equation may be written as

$$A\frac{\partial \sigma_x}{\partial x} - R = \rho A \frac{\partial^2 u}{\partial t^2} \tag{II-2}$$

where, in general,

$u(x,t)$; displacement at a point x on the rod,	L
$\sigma_x(x,t)$; stress at a point x on the rod,	F/L^2
$R(x,t)$; external resistance force at x,	F/L
$A(x)$; cross-section area at x,	L^2
$\rho(x)$; mass density at x,	F/L^3

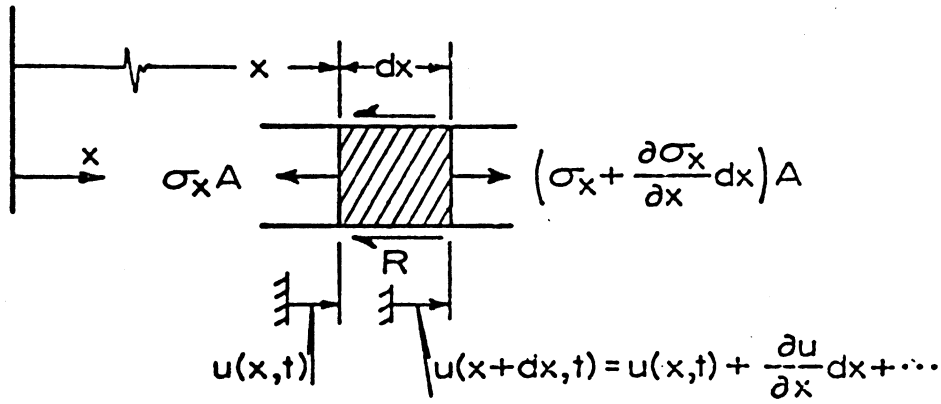

$u(x,t)$ = Displacement, L

$\sigma_x(x,t)$ = Stress, F/L^2

$R(x,t)$ = Resistance, F/L

$A(x)$ = Cross Section Area, L^2

$\rho(x)$ = Mass Density, M/L^3

Figure II-1. Rod Element Free Diagram.

Most pile materials may be assumed to deform as a Hookean (linear elastic) solid subjected to infinitesimal strains, such that the stress-strain relation may be assumed as,

$$\sigma_x = E\varepsilon_x = E \frac{\partial u}{\partial x} \tag{II-3}$$

where

$E(x)$ = Young's Modulus at x, F/L^2.

Applying this assumption the general differential wave equation is written in terms of unknown displacements, $u(x,t)$, as

$$A \frac{\partial}{\partial x}\left(E \frac{\partial u}{\partial x}\right) - R = \rho A \frac{\partial^2 u}{\partial t^2} \tag{II-4}$$

Determination of material properties and the resistance behavior fully described the differential equation. In order to solve a problem, initial conditions and appropriate boundary conditions must also be specified. The complete formulation of a problem may, therefore, be written in the form,

<u>The differential equation (wave equation)</u>:

$$A \frac{\partial}{\partial x}\left(E \frac{\partial u}{\partial x}\right) - R = \rho A \frac{\partial^2 u}{\partial t^2} \tag{II-5}$$

<u>Initial conditions at $t = t_o$</u>:

$$u(x,t) = u_o(x)$$

$$\frac{\partial u}{\partial t}(x,t) = v_o(x)$$

$$R(x,t) = R_o(x)$$

Boundary conditions:

$$u(x,t) \text{ or } \frac{\partial u}{\partial x}(x,t) \text{ at } x = 0$$

$$u(x,t) \text{ or } \frac{\partial u}{\partial x}(x,t) \text{ at } x = L$$

The exact solution of such a system of equations is available only for a few special cases. To solve the general class of problems described by equations II-5 approximate methods must be applied. A numerical solution scheme was formulated by A.E.L. Smith[7] in 1955. However, the solution of the system of resulting different equations is too cumbersome for manual computations. Its more general use became possible only after the development of high-speed digital computers.

The development of high-speed, digital computers made solutions of large systems of linear algebraic equations easily accomplished. Smith presented the algorithm and problem formulation logic necessary to solve impact pile driving problems for a discrete element (finite-difference) model in a comprehensive paper published in 1960.[8] Most of the literature published thereafter has extended or clarified points necessary to refine Smith's procedure.

The terms written in equations II-5 may be quite complicated functions of several variables. A, E and/or ρ may vary for a particular problem with respect to location in the system. Cushion modulus values are usually different from that for pile materials, for example. The pile may vary in cross-section or material properties, as well. Resistance to penetration, R(x,t), is usually considered to be a function of pile dis-

placement and instantaneous velocity for the general case. Therefore, the direct application of difference equation approximations to the differential equation is a cumbersome chore.

Smith developed the solution using the equations of motion for discrete (lumped-parameter) elements. Elemental representation of all the component parts of the hammer-pile-soil system requires the use of equivalent weights, springs, and resistance forces. A schematic diagram of the discrete element model is provided in Fig. II-2. In his 1960 paper Smith also proposed a rheological model for the penetration resistance of the soil. Figure II-3 describes its static and dynamic behavior and the parameters necessary to define the response.

Smith's algorithm uses a nest of five elemental equilibrium equations to integrate the elemental equation of motion with respect to a finite time increment, subject to interelement and penetration resistance to motion. The solution marches out in finite time increments from the initial conditions to determine pile element displacements and driving stresses during one hammer blow. The "standard" procedure has applied a single hammer blow at t_0 integrating the difference equations of motion with time until the pile tip begins to rebound. The pile set is then computed as the difference between the maximum tip displacement and the assumed full tip rebound.

The details of Smith's formulation have been thoroughly reviewed in the author's previous report.[3] Discussion will be limited to the most significant information needed to apply this method.

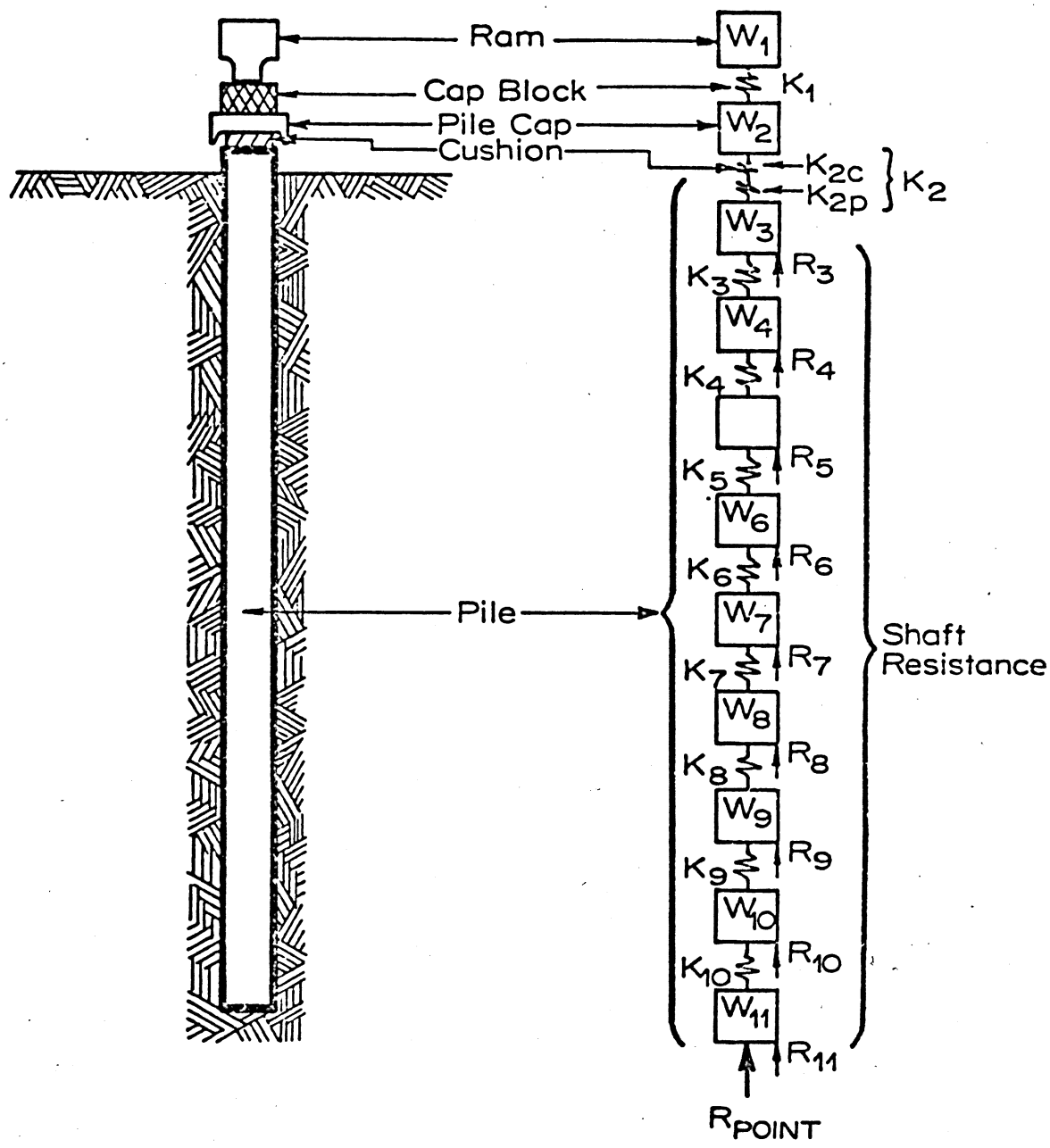

Figure II-2. Discrete Element Model of Hammer-Pile-Soil System.

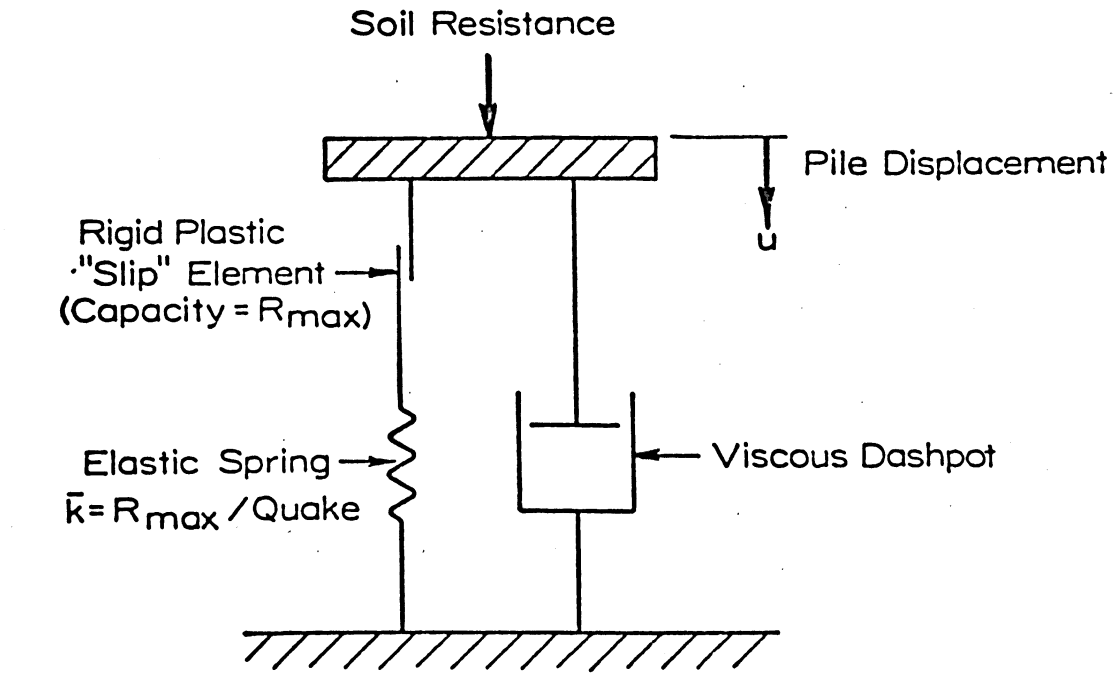

a) Rheological Model

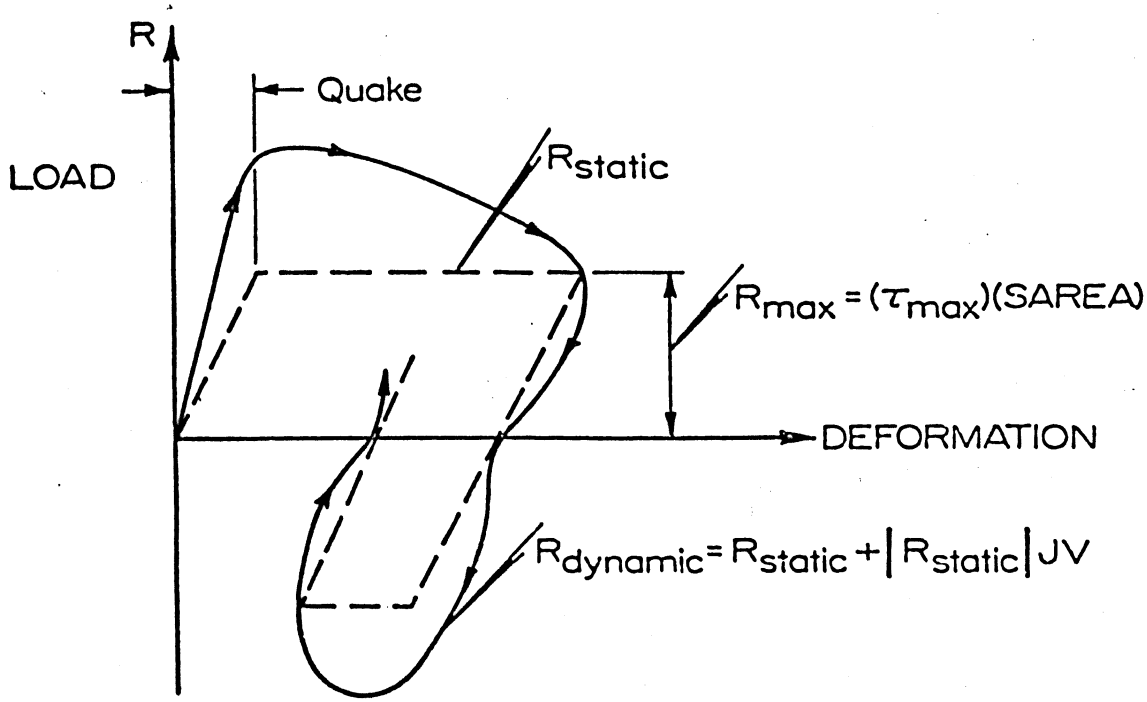

b) Load-Deformation Behavior

Figure II-3. Smith's Rheological Model of Soil Resistance.[8]

A primary consideration is the discretization of the system variables; pile element lengths and time increment magnitude. For typical pile properties Smith suggested that pile segment lengths should not exceed 10 feet, to ensure a smooth representation of the transmitted stress wave. In addition be recommended that no fewer than ten elements be used to describe the system components.[8] The selection of the necessary time increment magnitude is determined as a function of the stress wave velocity in the pile.

Stresses transmitted in a freely suspended elastic rod travel at a wave speed given by the quantity $c = \sqrt{E/\rho}$, a physically measurable quantity. The time required for the stress wave front to travel Δx distance along the rod is simply $\Delta t = \Delta x/c$. For a system of interconnected elements a "critical" value of Δt would represent the shortest time interval necessary for the stress wave front to pass any element spring in either direction. If Δt were chosen larger than the critical value the stress wave would tend to bypass an element whose Δt was smaller, causing solution instability. For a freely suspended rod with uniform segments the use of the critical time increment would generate the "exact" solution.[8]

For pile driving behavior the component element properties, soil resistance and boundary conditions, affect the stress wave transmission behavior. In order to insure convergence a smaller time interval is usually selected (commonly one-half the critical time interval). For further treatment of stress wave propagation analyses refer to appropriate engineering texts.[9, 10, 11]

Smith's rheological model assumes that the static resistance to penetration can be described as a linear elastic-plastic spring and slip element combination, see Fig. II-3. The dynamic resistance is added to the static resistance as a function of the instantaneous element velocity and static resistance force in the form,

$$R_{dynamic} = R_{static} + |R_{static}| \ (JV) \qquad \text{(II-6)}$$

where R_{static} is defined uniquely by the displacement, the elastic quake, Q, and the ultimate resistance force, RU. The velocity term, V, is the instantaneous element value, and the damping parameter, J, has inverse units of velocity (e.g., seconds per foot). It should be noted that the behavior in Fig. II-3 is modeled as shown using Equation II-6. The equations described by Smith[8] and TAMU[12] do not model the behavior of Fig. II-3 in the "negative" loading range. This probably has minor influence on their results since calculations are halted at the onset of tip rebound. Within this investigation, however, the behavior described in Equation II-6 and Fig. II-3 is called "Smith's formulation."

In general, each element may be assigned quake and damping parameters, though most commonly, the behavior is separated only as shaft or point values for quake and damping parameters. Smith prescribed values for the different parameters based upon his own experience. Subsequent investigators have determined related values based upon correlation studies from additional field observations. The description of these parameters is given in the Appendix, and in the next section.

Smith recommended that the inelastic response of cushion materials could be defined as an equivalent bilinear relationship. The loading

stiffness for the cushion is determined from the relationship

$$K = \frac{AE}{\Delta L} \tag{II-7}$$

where ΔL is the cushion thickness. The unload/reload behavior can be written conveniently in the form

$$K_{UR} = K/e^2 \tag{II-8}$$

where e is the coefficient of restitution for the cushion material, see Fig. II-4. Subsequent investigators have verified the accuracy of this assumed behavior.[12] Figure II-5 describes the stress-strain behavior of hard (micarta) and soft (pine plywood) cushion materials after Lowery et al.[12]

No tension conditions are readily accommodated between elements to simulate physical behavior. The ram rebounds from impact with no tension stresses to restrain it. Pile helmet, capblock, cap and cushion elements are usually loosely fitted to reduce tension stresses/strains at the pile butt. Smith described the algorithm logic necessary to proved these conditions.[3]

Smith generated a basic algorithm, applicable to impact pile driving, to solve the one-dimensional wave equation in finite difference form using numerical integration techniques. The procedure is sufficiently versatile to adapt to any impact pile driving problems. Subsequent investigations have refined his method to facilitate code usage and incorporate field observations. Most of these efforts have involved accurate determination of input parameters through laboratory testing and field measure-

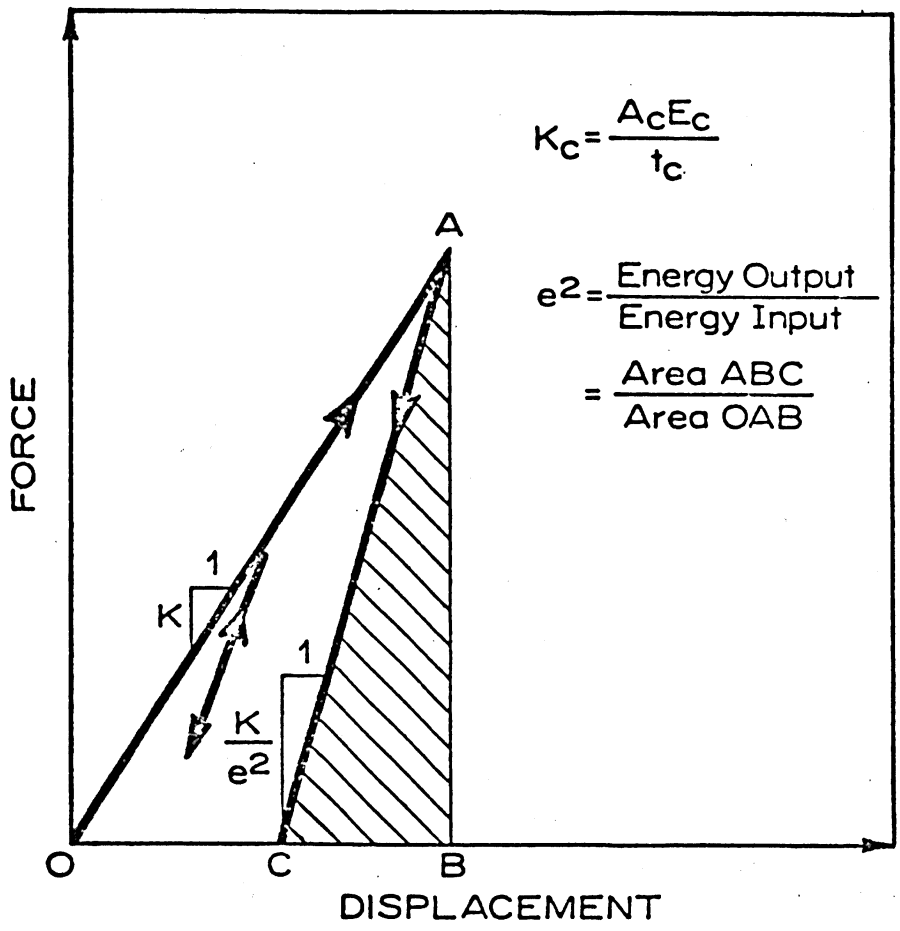

Figure II-4. Bilinear Cushion Spring Model.[8]

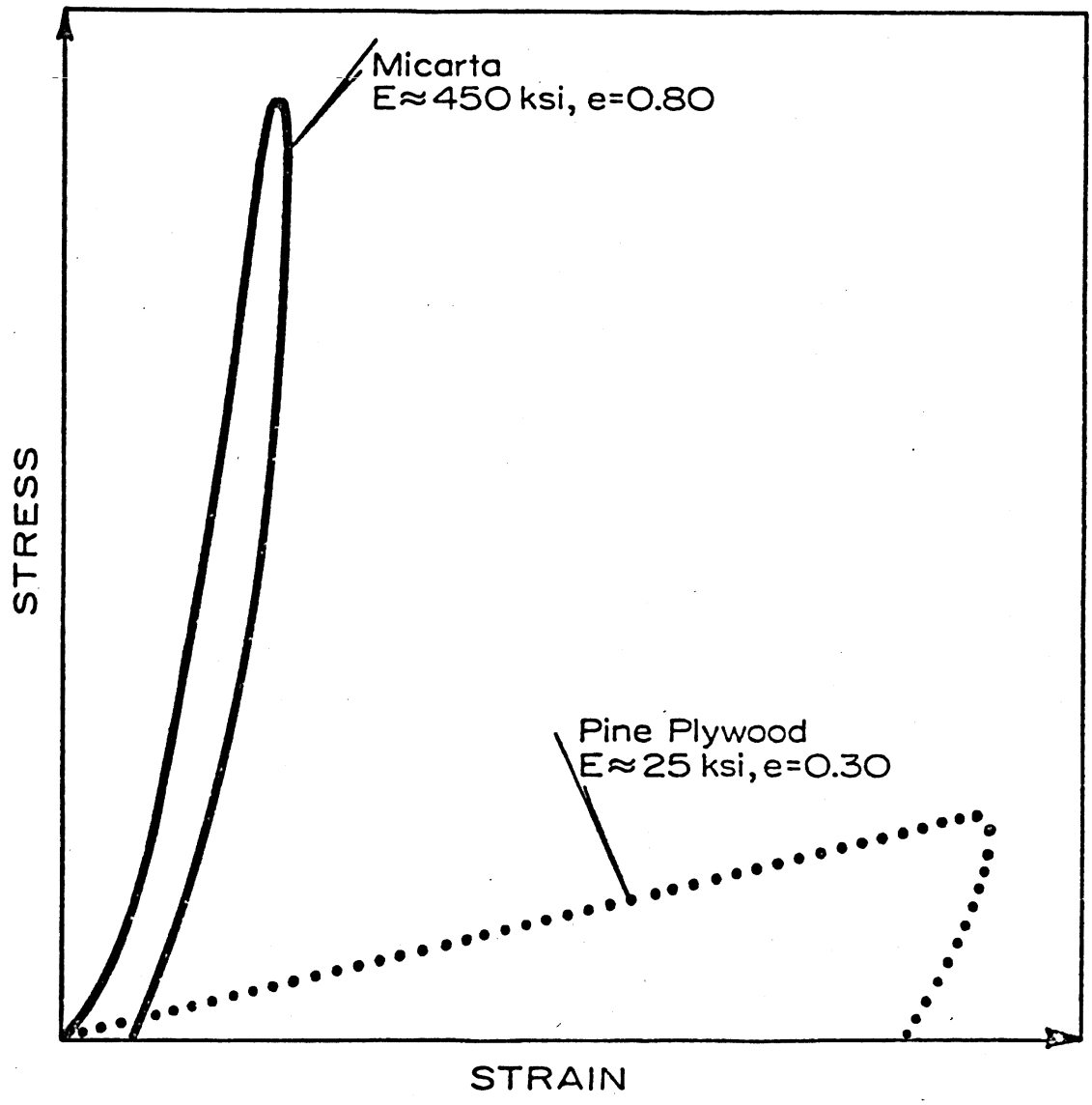

Figure II-5. Stress-Strain Behavior of Cushion Materials: Micarta and Pine Plywood.[20]

ment correlations. Results pertaining to driving system variables are summarized in the Appendix.

An alternative method for determining solutions to some types of differential equations employs the electronic analog of the mathematical problem. Parola[5] developed an analog computer program to simulate ram-drive head impact and energy transmission to an infinite elastic rod. He employed a simple two degree of freedom system for the ram and drivehead, respectively, and simplified the equations by neglecting the drivehead weight (but not mass). By assuming an infinitely long elastic rod without external resistance to motion, no reflected stress waves are transmitted, allowing considerable equation simplification.

Using the concept of impedance to motion,[9,10] Parola parametrically examined energy transmission from the ram to the pile as a function of system impedance. Based upon a series of analyses using a range of hammer-cushion-pile properties commonly used in practice, Parola found that under these assumptions a range of pile/hammer impedance values would assure at least 90 percent efficient energy transfer to the pile. This range is described by the relationship:[5]

$$\rho cA = [0.6 \text{ to } 1.10]\sqrt{\frac{W_{ram}}{g} K} \qquad \text{(II-9)}$$

The quantity ρcA is defined as the pile impedance, while the term $\sqrt{\frac{W_{ram}}{g} K}$ represents the driving impedance, with K describing the capblock spring constant.

This fundamental concept is intuitively obvious in considering elastic impact. Too stiff a pile will cause the ram to rebound, reflect-

ing input energy. Piles having too low impedance obtain only a portion of the ram energy, as the ram will follow the pile and retain energy. Either condition causes inefficient driving and may cause pile damage.[5] Adhering to this formula alone will not insure the most efficient driving conditions, however. Not only should the energy transfer be maximized by impedance match of the driving system, but also the shape of the transmitted stress wave must be considered. Parametric studies by Parola (using a finite difference solution scheme) indicate that the driving efficiency (penetration per blow) is also a function of stress wave shape.[5] The results of his analyses are discussed in the next section.

One adaptation of the wave equation formulation that employs a different system of variable unknowns has been developed at Case Western Reserve University (CWRU). The CWRU methods employ sophisticated instrumentation to measure continuous impact force and acceleration data at the pile butt during pile driving. Details of the instrumentation and formulations devised by CWRU investigators are provided in an earlier CWRU progress report.[13] Articles published in various technical journals and presented at professional conferences describe the ongoing research by CWRU investigatiors.[14, 15, 16, 17] A recent Ph.D. dissertation by Rausche[18] is also available.

The basic CWRU wave equation procedure employs a predictor-corrector algorithm to adjust soil resistance behavior such that the solution for butt element force, from input (measured) butt acceleration, converges on the field-measured force record. They use a generalized Kelvin rheological model with a linear viscous dash pot, instead of Smith's model.

A particular advantage avilable by measuring force and/or acceleration at the pile butt is, of course, that inaccuracies in simulating the impact interaction of the drive system are no longer a problem. The actual transmitted pulse to the pile is recorded directly. Adapting the finite difference algorithm to accommodate the force-time record is a straight-forward procedure. Nevertheless, routine measurement of these data is not yet available in practice.

In addition to the wave equation method, CWRU has also devised a simplified, one-degree of freedom procedure which incorporates these field measurements in an on-site specialized computer solution. Integration circuitry computes the pile top velocity from acceleration input. The pile is assumed to respond as a rigid mass, and the resistance to penetration is computed as the average (measured) force at the time of zero velocity, t_o, and at one full wave pass later, $t = t_o + 2L/c$, less the average computed inertia force over the time interval $(t_o, t_o + 2L/c)$. The field computer instantaneously performs this function calculation and displays the computed resistance for every hammer blow or every nth blow as specified.[13,17]

The field computer and field instrumentation have been presented and demonstrated at seminars given at CWRU, and also recently at the Specialty Conference held at Purdue University in June 1972.[19] Instrumentation developed for these purposes has included pipe section-sized force transducers, clip-on type force transducers, and piezoelectric accelerometers. These devices are arranged in order that bending effects may be cancelled out. The most notable advances are in the four channel magnetic tape recording capability and in the analog-to-digital conversion process

that allow analyses of continuous driving records, immeasurably streamlining the operation.

Wave Equation Applications

Much of the pile driving research efforts of the past decade have been aimed at determining input parameters to the wave equation analyses. The discussion of driving system parameters is given in detail in a previous report,[3] and a summary of the information is provided in the Appendix.

The algorithm devised by Smith has been developed by Texas A&M University (TAMU) research engineers for the Texas Transportation Institute (TTI). The modifications to Smith's original computer code have improved usage flexibility, provided additional computation information and modified computation logic somewhat to better model the field behavior.

A highly versatile, research oriented code has been developed by Lowery, et al.,[20] to examine the effect of virtually any problem variable on the wave equation analysis. The TTI research report includes a listing of the program and usage guidelines, along with some results of code applications.

For most practical problems a simpler version of the wave equation solution scheme will usually suffice. The design-analysis oriented finite difference code, developed from Smith's original program, is documented in TTI Research Report 33-11, "Pile Analysis Wave Equation Utilization Manual."[21] Example problems, code listing, and usage guidelines are included in this TAMU publication. A batch computer deck prepared

from this information was adapted to the Waterways Experiment Station (WES) computer facilities during a previous study.[3]

A streamlined version of the design-oriented TAMU code was revised for use on the WES time-sharing computer facilities. The only modifications involved the revision of input and output modes to accomodate the advantages and limitations of the time-sharing mode. Details and the description of the time-sharing version, TAMFOR (TAMU FORmulation), including usage guidelines adapted from the TTI publication,[21] and developed example problems are provided in an earlier report.[3]

Wave equation methods have clarified several fundamental concepts of impact pile driving that even vast field experience could not effectively explain. A brief summary of these concepts should facilitate a basic understanding of the related pile driving phenomena.

Pile driving stresses are a critical concern to the contractor and the designer. Driving conditions, hammer and accessory selection, and pile driveability all interrelate with the driving stresses transmitted to the pile.

For a specified driving system the peak impact stresses are proportional to the ram impact velocity. This is easily recognized in considering the influence of increasing the ram stroke of a single-acting hammer since the input energy is proportionally increased with the stroke. For two different driving systems delivering the same impact energy, the lighter ram must strike at a higher velocity to impart the same energy, causing higher peak stresses and shorter impact duration (therefore,

shorter stress wave length) than the hammer with the heavier ram. Deisel hammers typically employ lighter rams than comparable single- and double-acting steam/air hammers.

Pile impedance has a significant influence on peak driving stresses. Higher impedance piling (heavier and/or stiffer sections) induce higher peak stresses and shorter impact durations under otherwise similar conditions.[5,22]

Pile driving accessories also affect the shape of the stress wave transmitted to the pile. The primary purpose for using cap block and pile cushions in the hammer assembly is to maintain ram impact stresses and resulting pile stresses at tolerable levels. A stiffer cushion transmits higher peak stresses of shorter duration than a softer cushion. Cushion stiffness is a function of both the material deformation properties and its dimensions, (see equation II-7). The transmitted force pulse is also affected by the coefficient of restitution of the material.[5,12]

The influence of transmitted force pulse shape on pile driveability under various driving conditons has been examined by Parola.[5] His results indicate that pile driveability is directly influenced by stress wave shape. For easy driving conditions (low resistance to penetration) it was found that longer impact duration (longer stress wave length) was more effective in increasing penetration per blow than was the magnitude of the impact stress. For hard driving conditions the opposite tendency was observed: pile penetration was increased more effectively by increased stress amplitude than by increased impact duration.[5]

Recognizing the influence the driving system variables on the stress wave transmitted to the pile butt, two different "extremes" can be represented graphically as in Fig. II-6 after Parola.[5] Each curve represents a driving system transmitting roughly the same impact energy to the pile-soil system. Under otherwise identical conditions the selection of each of the variables listed with the appropiate curve will have a direct influence on stress wave shape.

Use of a lighter ram at higher impact velocity, a stiffer cushion, a higher impedance pile and the existence of harder driving conditions all tend to produce a higher stress wave of shorter duration. As previously mentioned, this stress wave shape will drive piling more efficiently under hard driving conditions. Under easy driving conditions the selection of the opposite trend in any of these variables will produce more penetration per blow. In other words, the judicious selection of a compatible hammer assembly-pile-soil system could "optimize" driveability and minimize installation cost. Wave equation methods offer the only engineering solution capable of incorporating all the pertinent system variables in a rational analytical model.

Problems of pile damage may prove quite expensive. Several potential causes of damage may be cited. Ram impact eccentricity or system misalignment can transmit bending and torsion stresses that may cause pile damage. The one-dimensional wave equation cannot analyze these effects, of course. For damage caused by excessively hard driving (high resistances, obstructions, etc.) potential pile damage can be predicted as excessive peak stresses along the pile. Peak compression stresses are readily

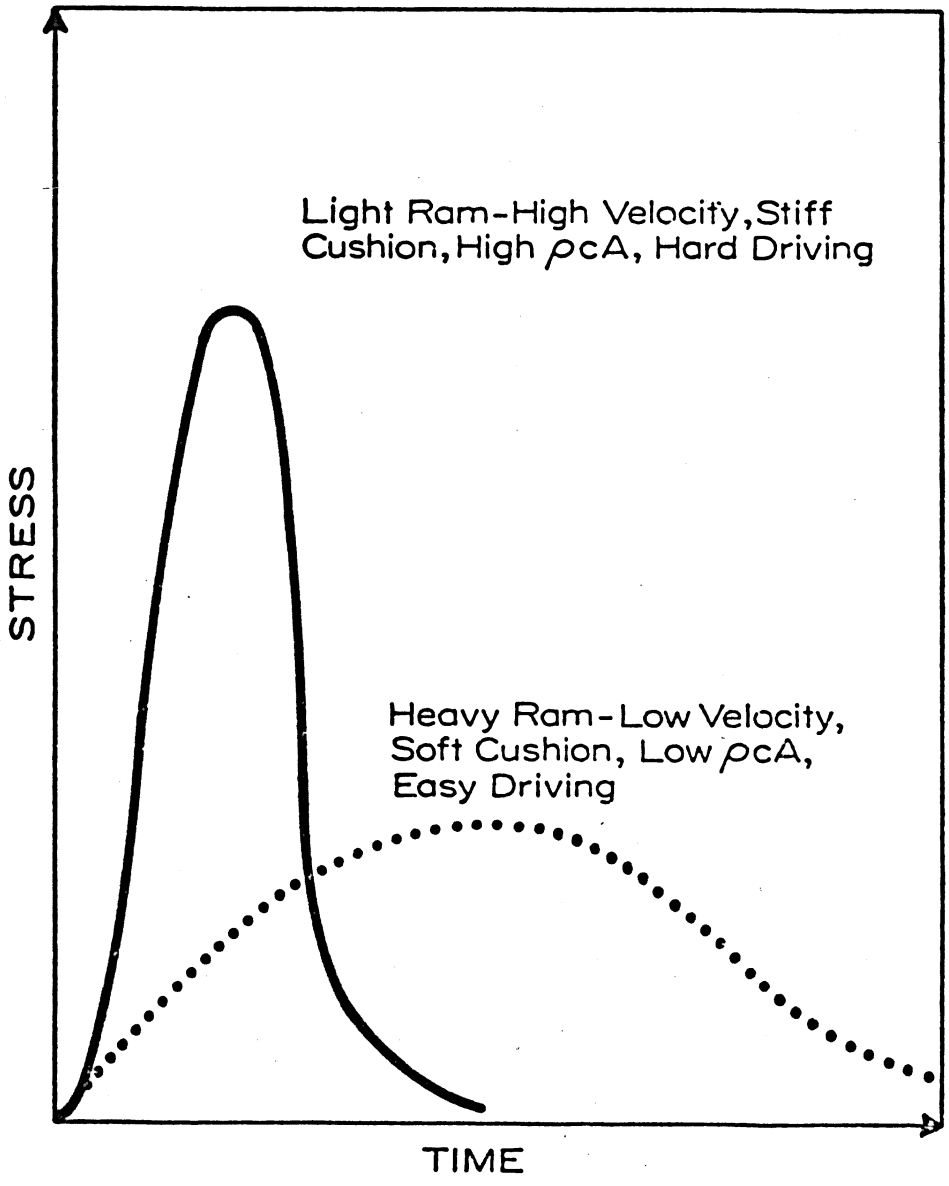

Figure II-6. Factors Affecting Impact Stress Transmission and Penetration.[5]

estimated and field measurements have verified the accuracy of the wave equation solutions.[12,13]

Precast, reinforced concrete piles may be damaged due to excess tensile stresses/strains. An incident compression stress wave reflects at a "free end" as an equal magnitude tension stress wave. Depending upon pile length and driving resistance behavior, breakage may develop at particular locations along driven piles. A TAMU research report[23] provides specific recommendations for driving prestressed, reinforced concrete piling based on wave equation analyses and field observations.

The influence of pile length upon pile driveability was examined parametrically by Parola.[5] Relatively stiff piles were little affected by pile length as the stress wave transmitted was of short duration. Piles having lower impedance tend to develop longer stress waves (longer impact duration) such that the reflected stress wave stacking at the pile tip interacts for a longer duration. Parola's results indicate that piles of low impedance drive more efficiently for shorter pile lengths; the influence of pile length on driveability for high impedance piling is negligible.[5]

The greatest success in wave equation applications may be gained in the selection of the most effective driving system. Hammer assembly and pile properties are readily available in the literature, see the Appendix. The major uncertainties that have been found are in usage of the method to determine pile bearing capacities and the related question of whether or not penetration is possible under very hard driving.

The inaccuracies found in applying the wave equation solutions are generally attributed to the inadequacy of the assumed rheolgical model of soil resistance. The nature of pile-soil interaction behavior is extremely complex. As a pile penetrates, discontinuous shear deformations develop at the pile tip and along the shaft. Simultaneously the material beneath the tip is compressed and displaced as the region adjacent to the tip is sheared and deformed in extension. As the pile penetrates further the soil along the shaft is severely sheared.

Soils exhibit an extremely complex deformation and failure behavior in the laboratory under well-controlled stress-deformation conditions. Soil behavior may be a function of stress/deformation history, stress level, stress path, and (particularly important for impact driving behavior) deformation rate. The development and dissipation of excess pore fluid pressures affects the effective stresses, deformation and failure response of the soil. It is essential, therefore, to recognize that the determination of representative soil parameters as input to a pile driving analysis is truly a crude exercise of engineering judgement, at best!

Smith proposed that the bilinear elastic-plastic model for static behavior and the nonlinear (interdependent) viscous dashpot be applied for the soil resistance behavior in lieu of "more accurate" representation of the behavior, see Fig. II-3. He suggested that the elastic soil quake be prescribed as 0.10 in. for both point and shaft resistance springs, while the point damping parameter, J_p, be given a value of 0.15 sec/ft. He assumed that the shaft damping value, J_s, would be approximately $J_p/3 = 0.05$ sec/ft. These were average values established from his own experience.[8]

Static and dynamic triaxial tests have been performed to evaluate these soil parameters. Reeves et al.[24] examined these parameters for saturated sands, and Gibson and Coyle[25] included tests on clay soils as well. Impact loading conditions for these triaxial soil samples suggested that the damping parameter J should be velocity dependent. They introduced an exponential correlation factor, N, to obtain constant J values modifying equation II-6 in the form,

$$R_{dynamic} = (1 + JV^N),\ 0 \leq N \leq 1 \qquad \text{(II-10)}$$

the dimensions of J depending upon the exponent, N.

It was assumed that J corresponds to the tip damping parameter, J_p, over the range of impact velocities applied in the field. The side damping parameter, J_s, was studied for model piles in clays.[26,27] The results of these TTI research reports indicated that the tip quake and damping parameters more closely matched those suggested by Smith, (i.e. N = 1 in equation II-10 above). The shaft resistance parameters for the model piles were evaluated parametrically to determine values for equation II-10 as follows:[28]

Point:

$$QUAKE_p = 0.10 \text{ in.},\ J_p = 0.15 \text{ sec/ft},\ N = 1.0$$

Shaft:

$$QUAKE_s = 0.03 \text{ in.},\ J_s = 1.25 \ (\text{sec/ft})^N,\ N = 0.35$$

Soil disturbance due to pile installation may drastically affect the resistance to penetration during driving and the static behavior, as

well. For sensitive clays the remolded strength may be substantially less than "undisturbed" strengths such that a driven pile may show very little resistance during driving or immediately after driving. A strength regain and, therefore, an increase pile capacity may develop as reconsolidation (excess pore pressure dissipation) of the disturbed soil proceeds with time. Strength regain may continue in some sensitive cohesive soils over several years as a result of consolidation and thixotropic effects. This strength regain is commonly described as pile "set-up," or "freeze."

Dense deposits of fine cohesionless soils may develop negative pore pressures during pile driving, giving high transient strengths. A pile load test or subsequent redriving after these excess pore pressures dissipate often reveals a much lower resistance to penetration than the initial driving resistance would indicate. The development of high resistances during high rate of deformation loading that do not prevail under static loading conditions is commonly termed "relaxation."

In many cases the actual soil resistance to penetration during driving bears little resemblance to the resistance observed during a load test performed after transient phenomena have passed. In order to correlate wave equation predictions with pile load test data an estimate of the set-up or relaxation must be provided for in the analysis. The resistance predicted in the pile driving simulation clearly represents an approximation of the behavior during pile driving. An alternate method of accommodating these phenomena to some degree would be to redrive the piles after sufficient time has elapsed to dissipate transient effects, and accurately measure the response of the first few hammer blows. Neverthe-

less, the loading conditions may still be misleading due to deformation rate dependency, for instance.

The most recent efforts of the TAMU researchers[29,30] have returned to Smith's original rheological model, equation II-6, in lieu of equation II-10. Values of soil damping parameters have been correlated by Foye et al.,[30] after giving due consideration to adjust resistance during driving for estimates of pile set-up or relaxation. In their analyses the quake parameters were prescribed as 0.10 in., as Smith had recommended. These values are given in Table II-2.

The blow count correlations used to determine the damping parameters in any of the investigations represent the passage of the resistance versus predicted blow count curve through a single point corresponding to the estimated resistance during driving and the final blow count at full penetration. It will be shown in Chapter V that such a correlation is in no way unique. Within reasonable bounds one may assume a point damping value and determine a side damping value that will match the blow count accurately. Such a correlation may also be somewhat sensitive to problem discretization as well. The variables are all interrelated in the approximation and, in a mathematical sense, the damping "constants" are correlation variables at best. As these properties are not yet physically measurable, such parameters are the best alternative.

It is useful at this point to compare Smith's bilinear static model with laboratory interface shear test results. Figure II-7 describes interface shear test results for medium-dense Chattahooche River sand-on-mortar. Superimposed on these data is Smith's bilinear model with 0.10 in.

Table II-2

TAMU Soil Damping Parameter[30]

Soil Type	J_s (SEC/FT)	J_p (SEC/FT)
Clay (CL, CH, Hardpan)	0.20	0
Partially saturated sands and silts	0.05	0
Saturated sands and silts	0.50	0
Soft peat	0.00	0

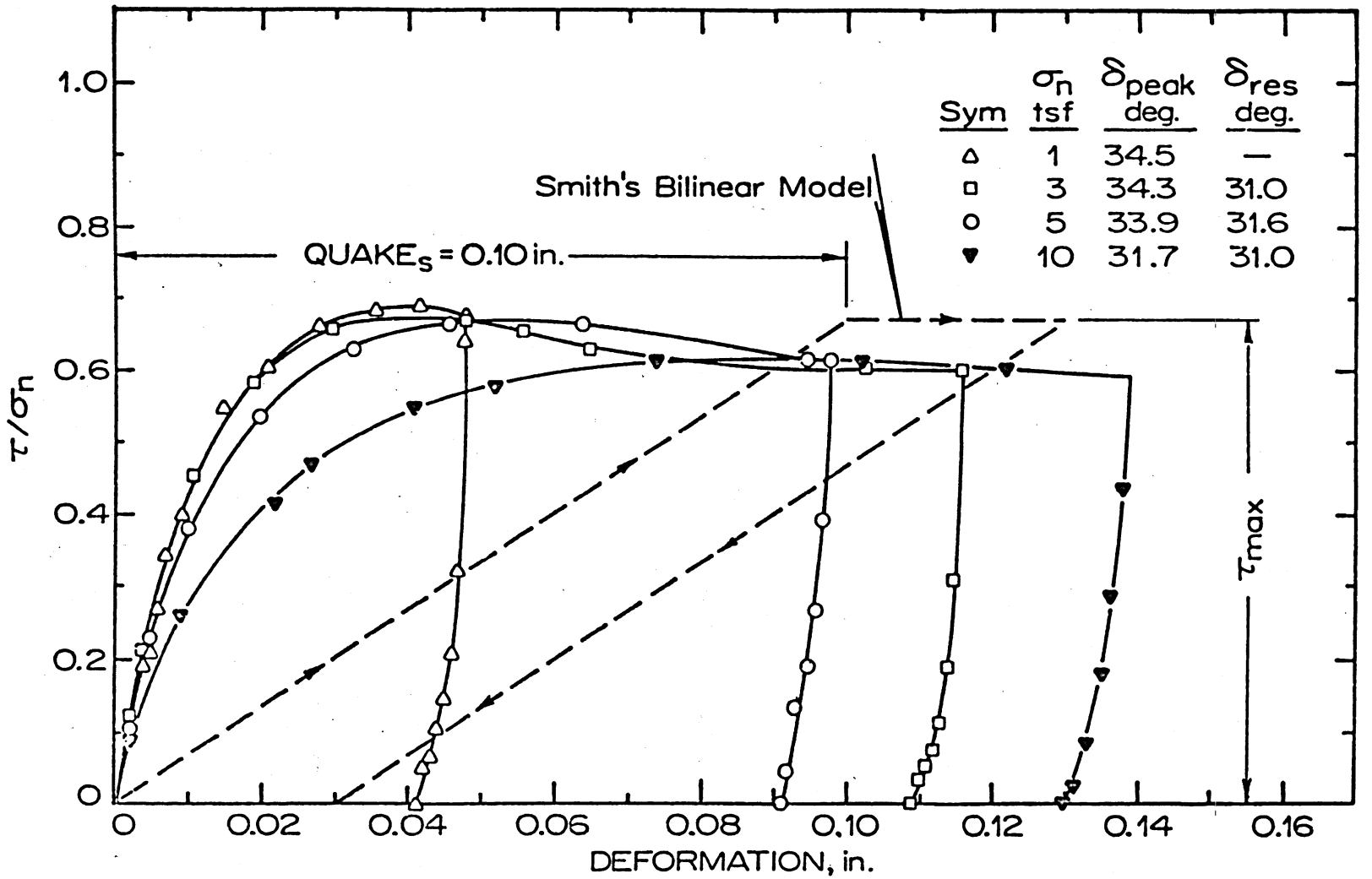

Figure II-7. Typical Interface Shear Test Results: Chattahooche River Sand-on-Mortar.

elastic quake. The measurements show nonlinear, stress level-dependent behavior quite different from the bilinear model. Deformation in the surrounding soil should probably cause the load transfer displacements to be somewhat greater than the pure relative displacement at the interface. Load test analyses during this investigation suggest that using laboratory interface shear data directly in the analyses may provide a good approximation to field load-displacement behavior. These analytical results are presented in Chapter V.

Pile-soil interaction is generally subdivided into two separate problems: pile installation; and pile performance thereafter. The influence of installation on the resulting pile performance has long been recognized as significant. Nevertheless, in lieu of a rational model, gross assumptions have typically been made to account for installation effects on subsequent pile behavior. Indeed, the influence of subsequent hammer blows on pile driving behavior has not been examined analytically.

In keeping with the approach taken in the literature, analytical models of static pile behavior will be treated separately in the next chapter. It cannot be overemphasized that the effects of pile installation play an integral part in the subsequent foundation behavior. The separation is an artificial step at best, and the potential danger of misinterpreting the behavior of carefully conducted pile tests is ever-present.

Chapter III

ANALYSES OF PILE TEST BEHAVIOR

The performance of single, axially loaded piles under carefully controlled field load test conditions has been examined frequently in foundation engineering practice. Numerous field investigations and model pile test studies have been published in a wide variety of technical publications. In spite of the vast stores of data and, in large measure, because of the discrepancies these studies suggest, expensive pile load tests are still routinely performed to evaluate the foundation designs. In many ways the prediction of pile test performance continues to contain a strong element of art.

As previously discussed, many factors may affect profoundly the behavior of single piles. Some factors influencing pile test behavior include: pile geometry and material properties; installation and loading conditions; the heterogeneous nature of most soil deposits; and the stress-deformation history of the pile-soil system. It should come as no surprise that no analytical procedure exists which incorporates all variables in a rational manner.

Two broad categories separate analytical solutions to pile-soil interaction problems: limit equilibrium (bearing capacity) methods; and

load-deformation procedures, which simulate the entire load test history. These two approaches are discussed hereafter. The final section of this chapter presents some pertinent laboratory and field observations described in the literature.

Limit Equilibrium Methods

Limit equilibrium theories were reviewed in detail in a previous project report.[1] A summary of that review is included in this section.

Conventional bearing capacity theories for deep foundations (static formulae) usually compute pile capacity as the sum of two independent components; shaft (skin) friction, Q_s, and point resistance, Q_p. Unit point bearing capacity is given as $q_o = Q_p/A_p$, where A_p is the effective point bearing area. Unit shaft capacity, f_o, usually varies along the pile and an average value is described as $\overline{f}_o = Q_s/A_s$, where A_s is the total shaft area. Values for q_o and f_o are generally assumed mutually independent terms and, thus, they are evaluated separately.

Point Bearing Capacity

The value of q_o is often obtained from limit equilibrium solutions of plasticity theory. The most common assumptions for soil behavior include:[31]

a. Mohr-Coulomb failure criterion.

b. Shear strength independent of strain.

c. Elastic deformations negligible with respect to plastic deformations.

d. Volume changes due to shear and normal stresses are negligible.

The use of all these conditions describe a rigid-plastic, Mohr-Coulomb solid.

Limit equilibrium methods analytically approximate the physical system behavior using a representative kinematic failure mechanism, with associated boundary and discontinuity conditions. It must be stressed that such methods provide approximate solutions to idealized continuum mechanics problems which only approximate pile-soil interaction behavior. Three basic kinematic failure mechanisms that have been assumed for point bearing capacity problems are described in figure III-1 after Vesić.[31] The remainder of this section discusses some applications of these failure patterns to pile bearing capacity problems.

The Prandtl-Reissner-Terzaghi failure pattern is shown in figure III-1a. The original solutions to the bearing capacity problems are attributed to Prandtl[32,33] and Reissner.[34] Most of the subsequent theories describe extensions and modifications of their findings.[31] Caquot[35] and Buisman[36] were the first to apply this failure pattern to deep foundations.[31]

Prandtl and Reissner solved the problem of plastic flow in a rigid-plastic, Mohr-Coulomb half space having strength components c and ϕ. Three plastic equilibrium shear zones are combined: an active Rankine zone beneath the smooth foundation base; two passive Rankine zones which intersect the plane of the foundation base; and two Prandtl zones of radial shear in transition between active and passive failure zones. A uniform surcharge, q, is assumed to act on the foundation base plane.

Figure III-1. Kinematic Failure Mechanisms for Deep Foundations After Vesić.[31]

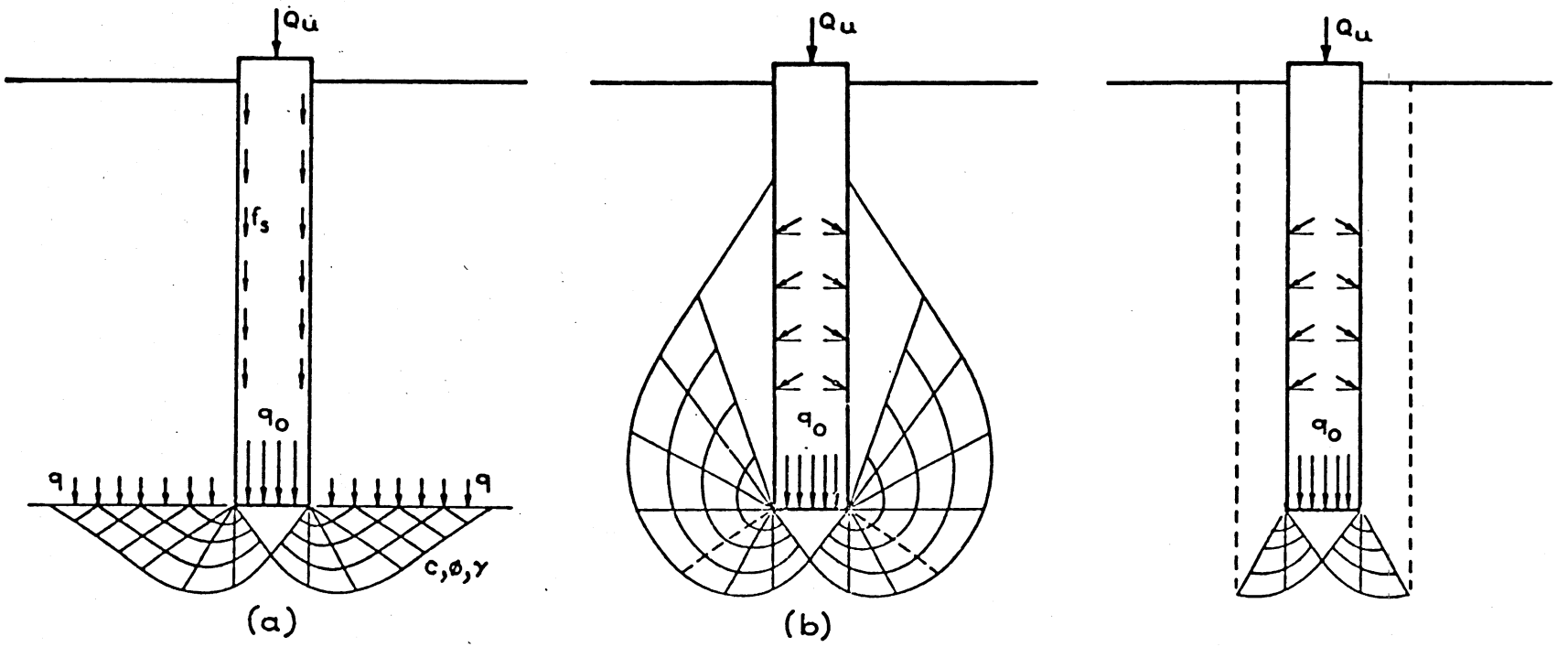

Terzaghi described this failure mechanism as general shear failure. The bearing capacity of an infinite strip is computed as the sum of three related solutions as[37]

$$q_o = cN_c + qN_q + \frac{\gamma B}{2} N_\gamma \qquad \text{(III-1)}$$

where the terms N_c, N_q and N_γ are dimensionless bearing capacity factors which depend only on ϕ. The first term, cN_c, represents the unit bearing capacity supported by a weightless, Mohr-Coulomb solid without a surcharge ($\gamma = 0$, $q = 0$, $c \geq 0$, $\phi \geq 0$). The second term, qN_q, is the unit load supported by a weightless, cohesionless solid under a surcharge, $q(\gamma = 0, q \neq 0, c = 0, \phi \geq 0)$. The third term, $\frac{\gamma B}{2} N_\gamma$, describes the load supported by a cohesionless solid with non-zero body forces but without surcharge ($\gamma \neq 0$, $q = 0$, $c = 0$, $\phi \geq 0$). In the case of deep foundations, the third term is quite small compared with the other two, and may be neglected.

Terzaghi presented the equations of Prandtl and Reissner for N_c and N_q for an assumed smooth foundation base. He also described a solution for a rough base, in which he assumed the friction fully mobilized along the base (a slip line). This latter assumption, and therefore, the rough base solution is statically incorrect.[58]

Terzaghi characterized local shear failure as sinkage of the base without fully mobilizing the general shear failure pattern. In such cases he recommends that modified strength parameters $c' = 2/3\ c$ and $\phi' = \tan^{-1}(2/3 \tan \phi)$ be used in determining N_c and N_q, and in equation III-1. He suggests that the failure mode can be predicted from laboratory test results. When the soil behaves in a ductile manner (increasing

resistance with strain, having no pronounced peak) local shear failure is expected.

To account for shallow foundations of finite length and different shapes, Terzaghi applied shape factors. These quantities were multiplied times each term in equation III-1. For deep cylindrical foundations Terzaghi derived a complicated expression for an assumed general shear failure at the base. The overburden pressure is determined as a function of the interaction of the cylinder of soil extending above the failure zone. He noted that soil compressibility and installation effects greatly influence the foundation behavior. He also noted that these bearing capacity factors assume plane strain behavior which hardly resembles pile-soil interaction conditions.[37] Nevertheless, many investigators thereafter neglected his advice.

Brinch Hansen[38] modified the N_c and N_q values of Prandtl using a semi-empirical approach. He prescribed shape and depth factors to deep foundation problems (neglecting the N_γ-term) as functions of ϕ and relative depth.

Note that the dimensionless bearing capacity factors for strip foundations and the associated shape factors are related by equations of the form[31]

$$N_c = (N_q - 1) \cot \phi \qquad (\phi \neq o) \tag{III-2}$$

$$\zeta_c = \frac{\zeta_q N_q - 1}{N_q - 1} \tag{III-3}$$

where ζ_c and ζ_q are dimensionless shape factors. The general form of equation III-1 for deep foundations may be written approximately as

$$q_o = cN_c\zeta_c + q_f N_q \zeta_q \qquad \text{(III-4)}$$

where the quantity q_f represents the effective overburden pressure at failure at the foundation base level.[31]

In order to simplify comparisons between different analytical expressions, Vesić described the combined term $N_q^* = N_q\zeta_q$ as the bearing capacity factor for deep circular foundations. Figure III-2 describes several N_q^* curves of different investigators, given as functions of ϕ.[31]

The DeBeer-Jáky-Meyerhof failure pattern extends the slip line field above the foundation base to include the shear resistance of the overburden soil. DeBeer[39] used this pattern to evaluate the upper limit of penetration resistance for an incompressible soil, see figure III-2b. Jáky employed a similar failure pattern to solve the problem of bearing capacity of a pile.[40] The most extensive use of this failure mechanism has been developed by Meyerhof.[41]

The fundamental difference between values of N_c and N_q, given by Meyerhof and Prandtl, involves development of the kinematic mechanism above the foundation base. The N_q-term in equation III-1 is the only one altered as[41]

$$q_o = cN_c + p_o N_q + \frac{\gamma B}{2} N_\gamma \qquad \text{(III-5)}$$

where p_o is described as the unit normal stress on the "free surface,"

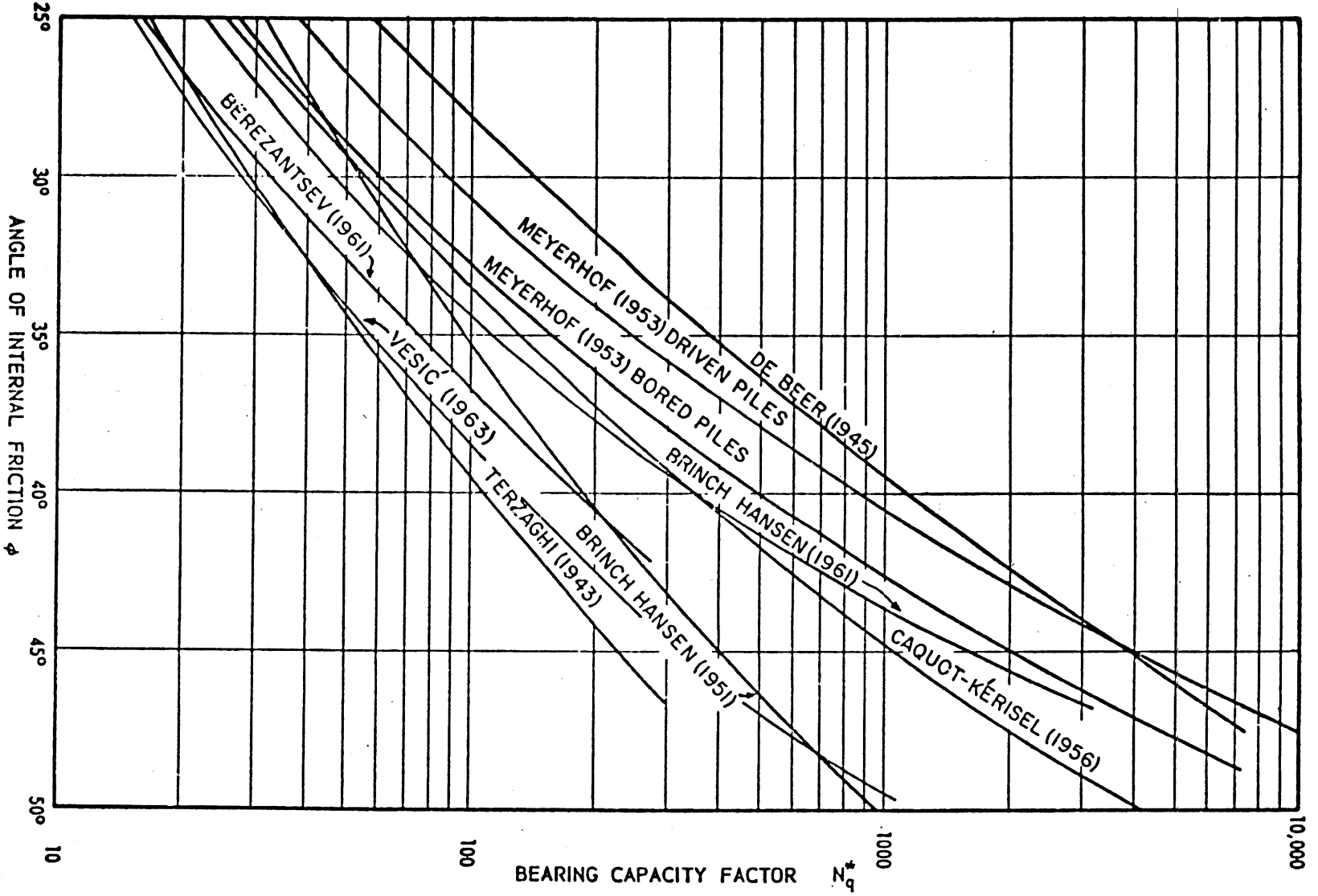

Figure III-2. Bearing Capacity Factors N_q^* for Deep Circular Foundations from Vesić.[31]

which is the line connecting the foundation base with the soil surface. The bearing capacity factors have different values, of course.

For shallow strip foundations p_o depends on the unit skin friction along the foundation shaft, the weight of the wedge of soil above the equivalent free surface (above a straight line extending from the base) which intersects the soil surface at an angle, and the shear resistance mobilized tangential to the free surface. The values of the general bearing capacity factors depend upon depth, geometry and roughness of the foundation base, as well as the friction angle. Interrelated depth parameters uniquely define these values.[41] Further discussions of Meyerhof's method are provided by Scott,[42] including some useful simplifying assumptions.

Curves representing Meyerhof's N_c, N_q and N_γ values suggest that the mobilized shear stress on the equivalent free surface has little effect on the point bearing capacity. For deep foundations the failure pattern reverts to the pile shaft, and the N_γ term is quite small. The unit normal stress, p_o, is therefore given as the average normal stress acting on the pile shaft within the failure zone. Computed as an earth pressure equivalent it is given as[41]

$$p_o = \frac{K_s^c \gamma D}{2} \qquad \text{(III-6)}$$

where K_s^c is the lateral earth pressure coefficient at failure. For buried foundations in cohesionless soils Meyerhof recommends K_s^c values between (0.5 - 1.0) for loose to dense deposits, respectively. For driven foundations K_s^c is evaluated using in situ testing techniques.[41]

Meyerhof introduced a semi-empirical shape factor for point bearing capacity. Its value depends upon base shape, relative depth, friction angle and installation method.[41] For deep foundations in compressible sands his solution predicts much higher capacities than field measurements indicate. Meyerhof attributed the difference to soil compressibility and related local shear phenomena. He prescribed a modified strength parameter

$$\phi' = \tan^{-1}(\chi \tan \phi) \qquad \text{(III-11)}$$

where $\chi = 0.85$ for buried foundations, and $\chi = 0.95$ for driven foundations due to soil compaction during driving.[41]

N_q^* curves derived after Meyerhof[43] for bored and driven deep foundations are shown in figure III-2. In a subsequent paper Meyerhof extended the solution for point bearing capacity to consider compaction effects.[44] He assumed driving caused prestressing and an increased friction angle near the base to adjust N_q values. In later articles Meyerhof treats other aspects of bearing capacity theory.[45,46,47,48]

The Berezantzev-Yaroshenko-Vesić failure pattern described in figure III-1c, represents a modified pattern to model local shear failure beneath foundations. Berezantzev and Yaroshenko[49] were the first to employ the modified pattern to such problems. Vesić derived values for N_q based upon experimental observations of local shear failure.[50,51]

Vesić examined the load-deformation behavior of foundations in sand using laboratory and field tests under carefully controlled conditions,[50] similar to the procedure employed in a separate investigation

reported by Kérisel.[52,53] Model tests in the laboratory by Vesić evaluated effects of relative depth and base shape, relative density of the sand, and method of foundation installation. Care was taken to control homogeneity of the air-dried cohesionless material, Chattahoochee River Sand. Field tests were conducted on large-scale piles installed at a site consisting of a fairly homogeneous, moist sand.[50]

In order to establish failure criteria in the model tests, Vesić described three characteristic modes of failure for surface foundations; general shear failure, local shear failure and punching shear failure. "Failure" in the latter two cases is defined as the load at which the settlement rate becomes a maximum. Vesić determined that in the case of deep circular foundations (depth to diameter ratio greater than 5) the failure mode was always punching failure, regardless of relative density.[50]

Vesić developed an expression for the point bearing capacity of deep foundations making the usual rigid-plastic, Mohr-Coulomb solid assumptions for the soil. He assumes that the weight of soil within the failure pattern could be neglected as compared with the overburden pressure. He next assumes that the effective overburden pressure at failure, q_f, represents the minor principal stress, and derives an expression patterned after Reissner's equations[34] to evaluate the unit tip capacity, q_0, in sands as[50,51]

$$q_0 = q_f \tan^2\left(\frac{\pi}{4} + \frac{\theta}{2}\right) e^{2\theta \tan \phi} \qquad \text{(III-8)}$$

where θ is an angle defined by the geometry of the failure zone. Based upon experimental results Vesić assumed $\theta = 1.9\phi$ in equation III-8.

Combining shape and bearing capacity factors he determined the value N_q^{*50} which is plotted versus ϕ in figure III-2.

Experimental observations from field and model tests by Vesić and others lead to several interesting conclusions. As mentioned previously static formulae for point bearing capacity of deep foundations in cohesionless soils typically assume that in the relationship

$$q_o = q_f N_q^* \qquad \text{(III-9)}$$

the quantity q_f describes the effective overburden pressure. Such an assumption predicts that if N_q^* is relatively constant, q_o should increase proportionally with depth. Vesić found that such increases only occurred at relatively shallow depths ($D/B \leq 4$, where D is embedment depth). He noted that for greater depths ($D/B \geq 15$ to 20) the measured value of q_o remained essentially constant, independent of depth. Kérisel obtained similar results which led him to conclude that N_q should be a complex function of ϕ, D/B and B, decreasing with depth.[52,53] Vesić, however, suggests that at greater depths q_f is no longer proportional to in situ overburden stress, becoming constant below a critical depth.[50]

The rational explanation for asymptotic values of q_o is based upon an arching phenomenon in the soil surrounding the pile, similar to the yielding pattern assumed in silo analysis.[37] The mass of soil beneath the base moves downward causing stretching (extension strains) in the soil mass and, consequently, vertical stress relief.[50] Laboratory observations indicate the loosening of dense sand adjacent to model pile tips.[50,51] X-ray studies clearly demonstrate the arching phenomenon in model pile tests.[54] Axisymmetric finite element analyses of pile-soil interaction

predict the development of extension and vertical stress relief in the vicinity of the pile point.[55,56]

In the most recent studies at Duke, Al-Awkati[57] has performed cone penetrometer, pressurementer, and related tests in the laboratory under carefully controlled placement and confinement conditions. The results of his investigations indicate the q_0 is a function of effective mean normal pressure, $\bar{\sigma}_0$. He also demonstrated the sensitivity of q_0 to soil compressibility using different amounts of mica in Chattahoocie River sand. Under otherwise "identical" conditions the more compressible soil exhibited significantly less bearing capacities for dense sand. In all the theories based on classical plasticity developed in the literature soil compressibility is at best treated empirically, and most often ignored. For deep foundations the "punching" mode of failure is usually developed, and the soil compressibility plays a major role in such behavior.

To better account for soil compressibility, Vesić has developed a new theory which incorporates soil compressibility in the formulation.[58] He assumes an elastic-plastic Mohr-Coulomb material and applies the limit pressure surrounding a cylindrical cavity to confine the cylinder of soil (in elastic-plastic equilibrium) beneath the pile point. For the range of soil compressibility typical of most medium to dense sands the highly complicated expression is reasonably closely approximated as[58]

$$q_0 = \bar{\phi}_0 \, (1 + \tan\phi) \, e^{\pi \tan\phi} \, \tan^2\left(\frac{\pi}{4} + \frac{\phi}{2}\right) \qquad \text{(III-10)}$$

Note that $\bar{\sigma}_0$ replaces the term q_f in equation III-9, and describes the in situ effective mean normal stress. The quantity $(1 + \tan\phi)$ represents the "shape factor" for deep foundations. The remaining portion of equation

III-10 is the value of N_q given by Prandtl.[32]

The tip displacement required to mobilize full bearing capacity, q_o, depends upon the base diameter, the method of installation and the initial relative density of the sand. For a driven pile in sand the tip displacement at q_o is roughly 8 to 10 percent of the base diameter. For a bored or buried pile tip displacement of at least 25 percent of the base diameter may be required to fully develop q_o. These values increase with decreasing density.[50,52]

Shaft Resistance

Resistance to relative pile-soil movement at the shaft is generally assumed to obey the Mohr-Coulomb failure criterion. The maximum unit shaft resistance, f_o, is prescribed in the relationship

$$f_o(z) = c_a + p_s(z)\tan\delta \qquad \text{(III-11)}$$

where c_a is pile-soil adhesion, $p_s(z)$ is the normal stress on the pile surface at depth z at failure, and δ is the interface friction angle. Equation III-11 implicitly assumes that failure occurs at the pile-soil interface.

For piles in cohesionless soils the adhesion term is zero, and the shaft resistance is entirely frictional. The magnitude of δ depends on pile roughness and may depend upon relative density. Values of the various parameters needed to describe the behavior may be determined from laboratory tests, in situ tests, or estimated from published results.

The value of $p_s(z)$ may depend upon in situ stress conditions, installation and loading history. These effects are often roughly estimated by applying the relationship

$$p_s(z) = K_s \bar{\sigma}_v \qquad \text{(III-12)}$$

where $\bar{\sigma}_v$ is the in situ effective overburden stress, and K_s is the coefficient of lateral earth pressure on the pile shaft at failure. The shaft capacity is often determined by assuming K_s is constant along the pile shaft, producing a "triangular" distribution of f_o along the pile.

Experimental measurements of pile load distributions for piles installed in reasonably homogeneous sands indicate that the unit skin friction, f_o, is proportional with depth only at shallow depths ($D/B \leq 4$). Thereafter, f_o increases at a decreasing rate approaching a limiting value at some critical relative depth.[50,51,52,59,60] The critical relative depth varies between 10 and 20 diameters, depending upon relative density. Vesić attributes this behavior to the arching phenomenon discussed previously. Extension behavior in the vicinity of the pile point causes confining stress relief and thereby reduces the maximum shear stress near the pile point. Finite element analyses predict the reduction of p_s only within a few diameters of the pile point.[55,56] Results of analyses performed during this investigation suggest that if the effects of residual driving loads are neglected it may lead to gross errors in load distribution measurements and interpretation. A discussion of the influence of residual loads on interpretation of load test results is included in the final section of this chapter. Analytical treatment of residual loads will be presented in Chapter V.

Load-Deformation Solutions

Bearing capacity is a vague term in applications to pile foundation problems. The assumptions imposed in limit equilibrium calculations are extremely restrictive and, more specifically, these methods model the physical system behavior rather poorly. What further compounds the difficulties is the "inexactness" of the definitions of failure in the best field load tests. Piles in cohesionless soils rarely exhibit "failure" in a brittle sense, the assumption applied in limit equilibrium theory. The pile-soil system will generally sustain greater loads at increasing displacement levels on beyond what is defined as failure. Most often pile load tests in sand prescribe failure using settlement or settlement rate criteria at load levels somewhat below a "maximum sustainable" value. It is therefore of greater importance to predict the load-displacement behavior of the pile than to determine the bearing capacity alone. In the following paragraphs some analytical methods which determine load-deformation behavior are examined.

Three different methods have been applied to analyze single pile behavior: one-dimensional, load transfer idealizations of the pile-soil system; elasticity theory formulations; and axisymmetric finite element techniques. Each approach employs fundamental assumptions which reduce the physical problem to an approximate mathematical model for which a solution is obtained. Some details of these methods are presented in the following sections.

Load Transfer Analyses

Load transfer analyses are defined herein as one-dimensional, formulations of pile-soil interaction behavior. Vesić described such methods as the transfer function approach.[59] Load transfer functions are prescribed along the pile shaft and at the point. A discrete element model of this type is shown in figure II-2. Pile driving solution methods employing these techniques were discussed in Chapter II. In describing pile load test behavior a static (elemental) equilibrium equation is solved.

Reese and his colleagues[61,62,63,64] developed a numerical procedure employing a transfer function approach. They analyzed various model and full scale pile tests in cohesive soils. Their procedure employs an iteration technique which incorporates nonlinear, strain-softening load transfer behavior in a compact solution scheme. The load-displacement curve and load distribution curves are determined by imposing element equilibrium from the tip element upward, element by element, for a sequence of applied tip displacements. Coyle and Reese[63] generalized the algorithm to apply separate load transfer data curves for each pile element, permitting variations with depth and/or material type. A substantial amount of load transfer data for piles in cohesive soils is published in the paper.[63] Interface deformation relationships were developed for load transfer versus displacement in terms of undrained shear strengths using laboratory and in situ tests and analyses of instrumented pile test data.

Coyle and Sulaiman[65] used the same numerical procedure to analyze pile tests in sand. Laboratory tests were conducted in a modified triaxial cell ("miniature" piles) to determine load transfer functions. The computer

code was used to analyze a series of instrumented field pile tests from which load transfer functions were calculated using load distribution measurements. Their results indicate that the magnitude of maximum load transferred decreased with depth. Note that these data neglect residual driving loads in the pile which had a marked effect. The discussion of the importance of residual loads on load test interpretation is provided in the final section of this chapter.

During the course of this project a load transfer method was developed to analyze pile test behavior.[2] The load transfer function is modeled either as bilinear (elastic-plastic) or nonlinear (hyperbolic) for both interface and tip element load-deformation response. The hyperbolic interface shear representation incorporates stress-level dependent behavior. An incremental (piecewise-linear) equilibrium formulation was developed to permit an arbitrary load application sequence.

Pile tests were analyzed from two sites consisting of cohesionless alluvial deposits. Laboratory interface (direct) shear tests results were used to obtain average hyperbolic parameters, which were used directly as the load transfer functions. Results of the analyses performed using the static algorithm, FDFOR, suggested that residual pile loads play an important role in load test performance.[2] It was decided that a formulation capable of including residual driving loads in the static analyses was essential. The algorithm DUKFOR was developed to analyze the installation/load test behavior in sequence. Details of the formulation are given in Chapter IV. Results of field test analyses performed to verify and document code capabilities are presented in Chapter V.

The one-dimensional idealization of pile-soil interaction lumps the highly complex phenomena at the "mathematical" interface. In order to predict pile performance the load transfer function for each discrete element must be prescribed. Estimates of pile bearing capacity and skin friction distribution are required and assumptions must be made concerning deformation characteristics of the resistance behavior. The load transfer analysis then permits the evaluation of pile test performance.

The major advantages of load transfer procedures over more sophisticated methods include mathematical simplicity and solution economy. Parametric variations on design studies are economical and the results provide load-deformation predictions which evaluate the analytical assumptions directly. The primary arguments against such methods suggest that the assumption of "unique" transfer functions is inconsistent with reality.[59] Load transfer and deformations in the surrounding soil mass and point/shaft behavior interdependancy cause the major concerns. Alternate methods which include these phenomena in the problem formulation are discussed below.

Elasticity Analyses

In order to describe the pile-soil system in a more rigorous formulation some description of load-deformation behavior of the adjacent soil mass is needed. The first approximation to such behavior assumes that the soil may be modeled as a linear elastic (Hookean) solid. Several applications of this approach have been presented in the literature.

D'Appolonia and Romualdi[66] developed an elastic solid solution for end-bearing steel H-piles in uniform soil. Their procedure applied the equations given by Mindlin[67] (for a point load applied in the interior of an elastic half-space) to analyze load transfer behavior. Thurman and D'Appolonia[68] generalized the approach to include pile-soil interaction in layered elastic systems using a numerical procedure. Their method models pile-soil interface behavior as a rigid-plastic, Mohr-Coulomb slip response. The tip resistance is assumed to be bilinear elastic-plastic with an elastic (limit) quake of 5 to 10 percent of the pile diameter.[68] Each soil layer is assigned two elastic constants; Young's modulus and Poisson's ratio. A few pile tests were analyzed and satisfactory solution accuracy was obtained.

Poulos and his colleagues [69,70] applied a similar approach to solve single pile-soil interaction problems. In a recent paper Poulos[71] summarizes much of the theoretical work done by his group in the form of design/analysis charts. He also presents tables and curves decribing soil moduli as functions of soil properties. These data were obtained by parametric fitting of field load test results. Poulos offers a simplified method for constructing load-settlement curves using two bilinear models (one for point resistance and one for total shaft resistance) which are functions of an average soil modulus. Slip at the pile-soil interface was neglected.

Though elastic solid solutions incorporate deformations in the soil skeleton, the assumptions imposed are inconsistent with the observed behavior of soils. Nonlinear, stress level-dependent behavior of soils

and pile-soil interfaces make the assignment of equivalent linear elastic constants an extremely arbitrary task. Effects of residual loads and/or loading history cannot be estimated by these techniques.

Finite Element Analyses

The finite element method has provided the means for solving many geotechnical engineering problems heretofore considered unsolvable. Finite element solutions applied recently to pile-soil interaction problems have contributed much to the understanding of the complex phenomena governing load test performance.

Finite element techniques describe the continuous physical system as an assemblage of (finite) elements connected at discrete points (nodes). The behavior of the overall system is formulated in terms of the response at these nodes. A description of finite element techniques may be found in texts on the subject.[42,43] The discussion hereafter treats pile-soil interaction solutions specifically.

One of the advantages of the finite element method is that arbitrary geometry and material properties may be modeled more effectively. Layered systems, geometric and material discontinuities, and nonlinear deformation characteristics may be prescribed element-by-element throughout the finite element mesh. A sample finite element mesh for a pile-soil mesh is shown in figure III-3, from reference 56.

Ellison[55] modeled the pile-soil system using an axisymmetric idealization. A subsequent paper presented a portion of his work.[74]

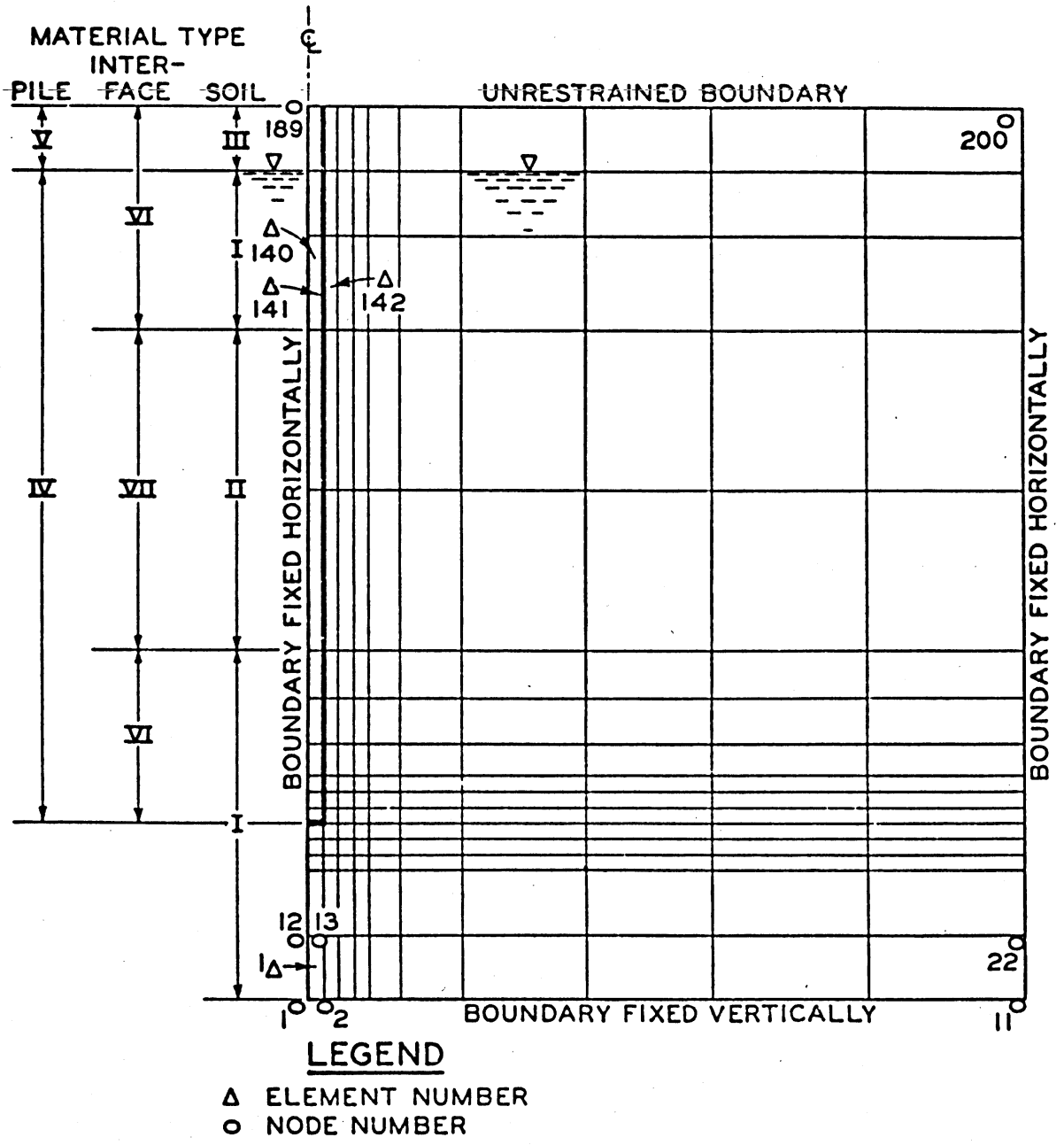

Figure III-3. Typical Finite Element Idealization of the Pile-Soil System.[56]

Ellison employed a trilinear pseudoelastic constitutive model for the soil, a linear model for the pile, and rigid-plastic point spring elements at the pile-soil interface in an incremental formulation. Deformations at point spring-connected pile and soil element nodes are the same until the shear force in the spring exceeds the Mohr-Coulomb strength at the interface, whereupon slip occurs. Ellison analyzed bored piles in cohesive soils and buried piles in cohesionless soils with reasonable success in predicting pile behavior. He noted that accurate simulation of the installation procedure was needed to model pile-soil interaction in cohesionless soils.[55]

Desai and Holloway[56] analyzed a jetted and driven pile placed in medium to dense cohesionless soil, see figure III-3. Stress level-dependent, nonlinear (hyperbolic) pseudoelastic formulations were applied for the soil and the pile-soil interface elements. "One-dimensional" axisymmetric joint elements were used to describe the interface deformation behavior. Constitutive parameters for the interface shear elements were determined from laboratory test results. Desai presented the same results, analyses of other pile tests, and some parametric studies in a recent paper.[76]

In all these finite element investigations reasonable agreement was obtained between "predicted" and measured load-displacement behavior. Each study indicates the development of an extension zone in the soil adjacent to the pile tip, providing analytical verification of the arching phenomena observed in the vicinity of the pile point in model tests.

The finite element method offers the most rigorous formulation available for pile-soil interaction problems. However, much information must be supplied as input to the analysis to accurately describe the properties of the soil and interface elements throughout the pile-soil system. The stress-deformation behavior near the pile is quite complicated. Soils are known to exhibit significant stress path dependency and one primary deficiency in applying these techniques to pile-soil interaction problems rests with the accuracy of the constitutive formulations employed.

A more serious limitation of the finite element solutions used to date concerns neglecting the affects of pile installation on subsequent behavior. Existing analyses assume a "stress-free" pile with at rest pressures in the pile-soil system. This is especially important in analyses of piles driven in cohesionless soils. Simulation of increased lateral stresses, soil densification and residual pile stresses caused by pile driving have not been modeled using the axisymmetric idealization. The prediction of load distributions, cyclic loading and tension loading response are formidable tasks. The importance of residual loads in predictions and interpretations of load test behavior is discussed in the following section.. The axisymmetric finite element code applied in the current study, AXISYM, is described in Chapter IV. Analytical results obtained using AXISYM are included in Chapter V.

Experimental Observations

As previously discussed, measurements of load distribution with depth for field and model piles in cohesionless soils indicate that unit shaft capacity, f_o, tends to reach a limiting value at some critical relative depth.[50,51,52,59,60] The measurements show this tendancy occurs at 10 to 20 pile diameters depth, depending upon relative density. This behavior has been explained as an arching phenomenon along the pile shaft. Finite element analyses predict such behavior only within a few diameters of the pile point.[55,56] Laboratory investigations corroborate this observation.[53,54,59] Hanna and Tan performed model tests using relatively long piles; the critical depth was found to reach 40 pile diameters.[77]

The causes of the critical depth phenomena and constant f_o well above the pile point remain somewhat of a mystery. A critical concern which accompanies these observations is the measurement of limiting point bearing capacity values with depth. The assumption of uniform shaft friction and constant point bearing capacity values below a critical relative depth gives considerably different results than assuming "triangular" distributions and tip capacities increasing with depth.

The most obvious discrepancy noted in some cases is that the pile was not loaded to failure, though some bearing capacity criterion was satisfied. If such were the case the load transferred to the soil with depth might drop off as the lower portion of the pile may not have moved enough to mobilize the full resistance. This would indicate an apparent uniform distribution of f_o and reduction near the point. Likewise, in such instances a "maximum sustainable" point load, q_o, would not have

been reached. This is a common error in the interpretation and performance of pile tests. Nevertheless, in some cases definite "plunging" characteristics are described by the load-displacement curve, while the instrumentation measurements describe the same tendancies in skin friction distribution and point bearing values. Many prediction inconsistencies have been attributed to "residual driving stresses" in lieu of any other explanation. In this case the existence of residual driving stresses plays a major role.

Residual Stress Effects

Pile test performed at Lock and Dam No. 4, Arkansas River Project, CE, were studied in detail by Hunter and Davisson.[76] Their paper represents the most prominent description in the literature of residual driving loads for piles in cohesionless soils. Instrumented steel pipe, H-piles and precast concrete piles were load tested in compression and thereafter, in tension. Measured tension loads as high as 100 kips at the pile point represent residual compression loads after driving. since the instrumentation was zeroed at the start of the compression load test, the unload of the residual point load (compression) would be measured in tension. They used a graphical procedure to estimate "corrected" load distribution curves based on the assumption that no residual loads remained at the end of the tension test. Their procedure was used to analyze the load tests described in a previous project report.[1]

It is important to note that unless gages are zeroed prior to installation or after extraction of the load test pile, actual residual

load distributions cannot be determined. The correct values of point capacity and total shaft capacity can be obtained from subsequent tension load test data, provided load/strain measurements are made near the pile point. The shapes of unit skin friction distribution and load distribution curves at failure in both compression and tension remain indeterminate, however.

A hypothetical example of load transfer behavior in compression and tension is presented in figure III-4. A triangular distribution of skin friction at failure is assumed for convenience, though any other shape could be used. Curves (0) and (0') describe the residual load/shear stress distribution state at the start of the compression and tension load tests, respectively. The shapes of these residual curves resemble compression unload curves from FDFOR analyses.[2] Note, of course, that the value of the unit skin friction at any depth describes the slope of the respective load distribution curve. In other words, the slopes of the load versus depth curves (left figure of each pair) are plotted as unit skin friction, τ, in the companion figures (on the right.)

Compression load test behavior near failure is described in figure III-4a. Load distribution curve (1) is parabolic for a linear increase of skin friction with depth. The differences between curves (1) and (0) are plotted as curves (1M). Strictly speaking curves (1M) describe forces and shear stresses "mobilized" in the pile-soil system at the current load level. In most instrumented pile tests reported in the literature, the measurements assume, implicitly, that residual loads due to driving are negligible; i.e., that curves (0) coincide with the origins

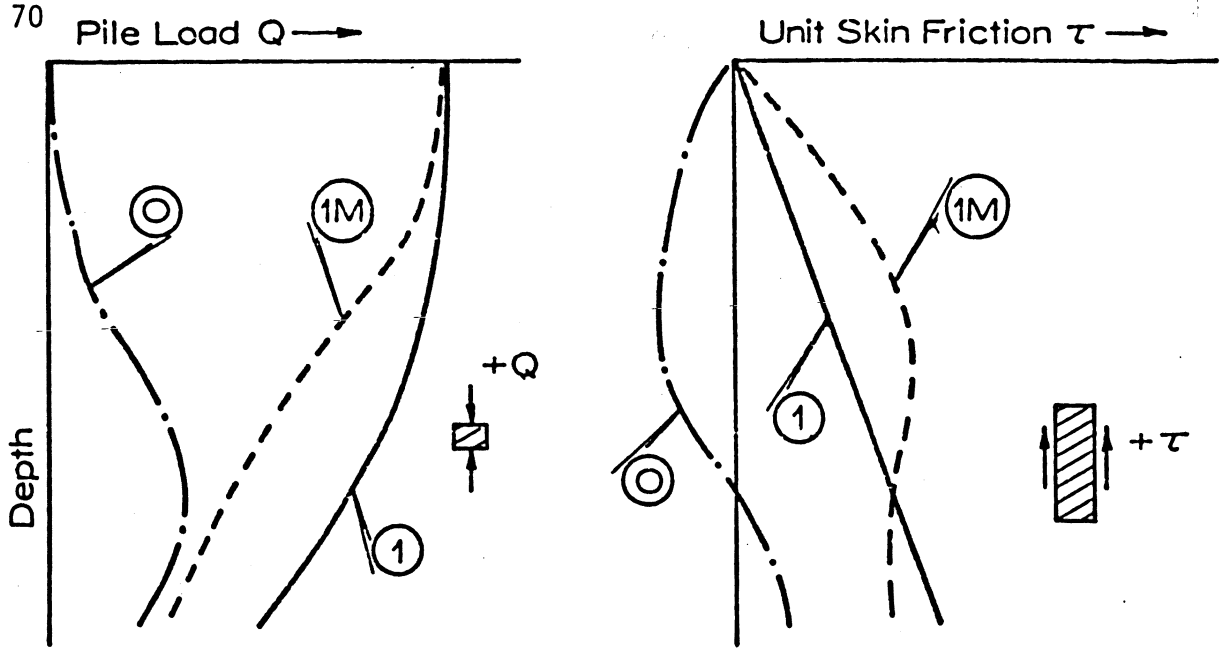

a-COMPRESSION TEST RESULTS

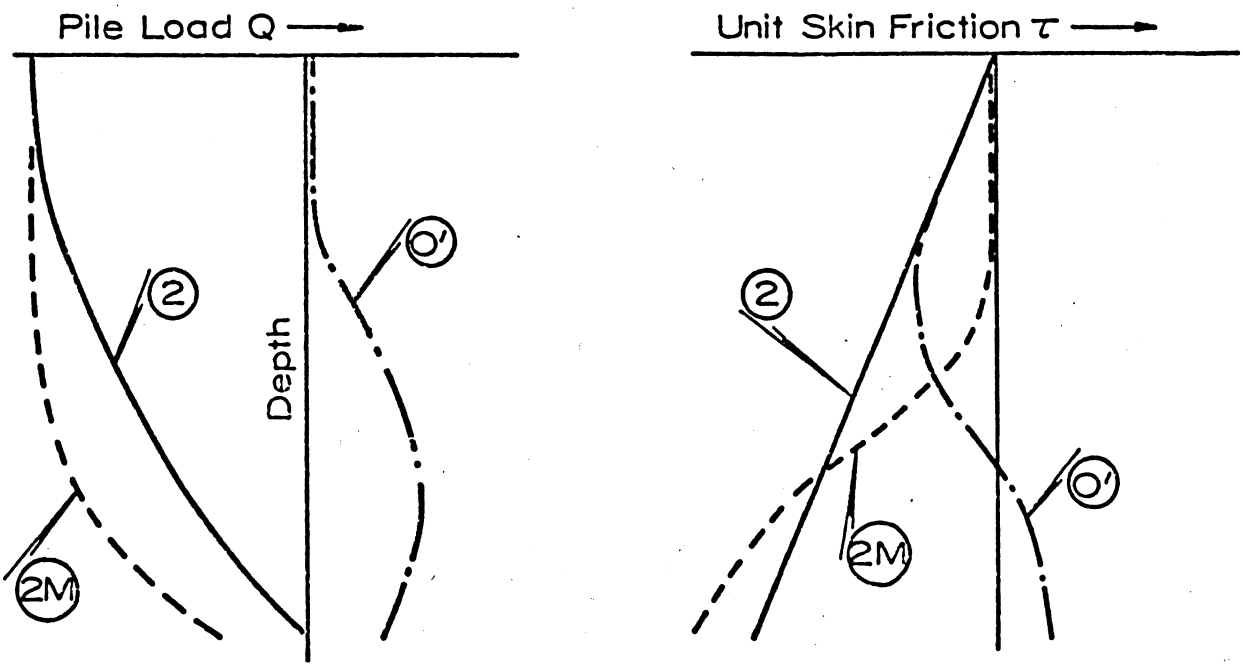

b-TENSION TEST RESULTS

Note: (0)/(0') residual Q,τ curves in compression/tension
(1)/(2) "actual" Q,τ curves at failure in compression/tension
(1M)/(2M) "mobilized" or measured Q,τ curves in compression/tension

Figure III-4. Pile Test Interpretation; Residual Load Distribution Affects.

of the load distribution and skin friction distribution curves. Therefore, curves (1M) describe the shapes of the (hypothetical) measured load and computed shear stress curves, uncorrected for the residual load distribution. Note in particular the unit shaft resistance curve (1M) shows a linear increase of shear stress only at shallow depth, after which it drops to a near constant value. Likewise, the measured (uncorrected) value of point bearing capacity underestimates the true value by the magnitude of the residual point load.

For tension tests curves (2) in figure III-4b represent the actual forces and shear stresses acting on the system. Curve (0') represents the residual load distribution for which the instruments were zeroed (for the tension test.) Once again curves (2M) describe "mobilized" or measured data. Note the measured tension force at the pile tip corresponds to the residual compression load at the tip at the time the gage was zeroed. In some cases that occurs at the start of the tension test. If the strain gages were zeroed at the start of the tension test, subsequent to a compression test, the shapes of curves (0) and (0') would probably be different.

These examples demonstrate that ignoring significant residual loads in analyses of pile test performance could lead to serious difficulties in applying the results in design. Skin friction curve (1M), figure III-4a, describes a greater area beneath the curve and, thus, a higher shaft capacity than is actually present. Were the shape of the curve unavailable (e.g., only measured load at the point and the butt) one might incorrectly estimate the design requirements. This could prove unconservative and/or costly if a significant design change from

the load test pile is warranted by pile test results.

In light of these observations an analytical procedure which can include residual load effects in the formulation is urgently needed. Load test results for which significant residual loads are neglected are the rule rather than the exception in the geotechnical practice. A procedure has been developed which will approximate pile-soil interaction behavior throughout installation and loading testing. Formulations of the methods used in this study are described in Chapter IV. Analyses of pile tests using these techniques are presented in Chapter V.

Chapter IV

CODE DEVELOPMENT

Two finite element computer programs have been developed during the current phase of the investigation. The one-dimensional formulation of pile-soil interaction is called DUKFOR (DUKe FORmulation). It incorporates two solution schemes which mathematically model impact pile driving behavior and static (axial) load test behavior either sequentially or separately as needed. In conjunction with DUKFOR an axisymmetric finite element code, AXISYM, was developed to compare the predictive capabilities and practical applications of each solution method. AXISYM provides for static load test simulation only.

Specific details of each computer code, including program listing, documentation, usage guidelines and sample problems are provided in separate user manuals.[78,79] Essential descriptions of the features developed for each computer code are given in subsequent sections of this chapter.

One-Dimensional Code: DUKFOR

During the previous phase of this study a one-dimensional formulation, FDFOR, was generated to mathematically model static load test behavior using a discrete element representation. This code considered linear elastic interelement behavior for the pile with provision for

bilinear (elastic-plastic) or nonlinear (hyperbolic) deformation behavior at the pile-soil interface and at the pile tip.[2]

The present study has adapted this representation into a combined solution method that predicts pile driving and load testing behavior in a unified procedure. DUKFOR represents the final product of this research effort.

Basic Considerations

The representation of pile-soil interaction behavior in one dimension assumes that all component system behavior can be approximated along the pile axis. In one dimension the finite element and discrete element approaches are virtually the same. The pile is represented as discrete segments (point masses) inter-connected with equivalent elastic springs. The pile driving system is described in a similar fashion, as discussed in Chapter II.

As noted in Chapters II and III, the element displacements are absolute quantities, whereas, the physical system behaves in a more complex manner. The load transferred to the soil is dependent upon both relative deformations at the pile-soil interface and the stress-deformation behavior of the soil mass surrounding the pile. The one-dimensional model combines this affect as an "equivalent" load-deformation at a mathematical "interface."

DUKFOR applies body forces in the pile as initial conditions using an equivalent element load vector in a static equilibrium calculation;

these forces may be excluded, if necessary. Pile driving simulation may be included or not for each specific problem. The pile driving behavior is modeled similarly to the procedure presented originally by Smith.[8]

One significant variation from Smith's method involves the capability of applying a sequence of blows during the pile driving analysis. Instead of terminating computations when the tip rebounds, DUKFOR allows for continuous computation of the response over an arbitrary time interval. At the end of this interval the numerical integration (with time) is halted, and the transient dynamic forces remaining are "statically" equilibrated. Residual pile driving stresses are determined after each blow. A subsequent blow, or the beginning of the load test sequence, or the start of a new problem may then be specified.

One important detail should be emphasized at this stage. Wave equation computations require the evaluation of interelement forces as a function of displacement differences. Accurate and smooth simulation of the stress wave requires discretization in both space and time dimensions. Greater refinement directly reduces the magnitude of the displacement differences determined in the solution. Therefore, it was found that the use of double precision variables is absolutely essential to determine a convergent and stable numerical solution.

The remaining sections pertaining to DUKFOR describe program usage flexibility and solution capabilities. The next section describes the elemental representations necessary as input for a general problem.

Element Representations

A schematic diagram of the hammer-pile-soil system of the one-dimensional model is described in figure II-1. The finite difference formulation of the elemental equations of motion requires lumped-parameter values for the various system components.

The pile driving system coded in DUKFOR presently models either single- or double-acting impact hammers. Diesel hammer behavior includes energy transmitted during bounce chamber compression and combustion, in addition to the impact phenomena.[18,80] The TAMU codes approximate the bounce chamber pressure effects in their formulations. Davisson[80] described the available methods of modeling diesel hammer behavior as particularly inaccurate. He recommends a new formulation which incorporates all the necessary improvements to effectively represent diesel hammers. No details of the procedure were provided, however.

An alternative to simulating impact behavior is, of course, to record the impact stress wave transmitted to the pile, and use the record as a force-time input at the pile butt. DUKFOR does not have such capability at this writing, though the necessary algorithm logic may be readily accommodated. One word of caution should be stressed however. As discussed in Chapter II, numberous factors affect the shape of the transmitted force pulse. The use of a "standard" force pulse could misrepresent the actual interaction behavior. If the force-time record is not that measured from the analyzed pile, ram impact simulation is recommended.

DUKFOR determines the necessary ram input variables using three

quantities: the rated hammer energy, E_{ram}, ft-lb;* the hammer mechanical efficiency, η; and the total weight of striking parts, W_{ram}, lb. An "equivalent" free-fall stroke, h_e, is given by

$$h_e = \eta\, E_{ram}/W_{ram} \quad , \text{ ft.} \qquad \text{(IV-1)}$$

The initial ram velocity at impact is then computed from the equation

$$V_{ram} = \sqrt{2gh_e} \quad , \text{ ft/sec.} \qquad \text{(IV-2)}$$

For most problems single- and double-acting hammer rams may be assumed as rigid point masses. An option for discretizing the ram (recommended for long, slender rams)[12] is provided in the formulation. The algorithm logic required to adapt the solution for mandrel driven pile behavior has not been included in DUKFOR. Code revision would be necessary to model such behavior.

Capblock deformation properties are needed in terms of the loading spring constant (lb/in.) and the coefficient of restitution (a decimal) of the cushion material. Its load and unload/reload spring constants are computed after Smith's bilinear representation, see figure II-4. The weight of the helmet or drive head is specified and it is assumed rigid. The pile cushion material properties are specified in the same manner as those of those of the capblock. In the event no capblock is present, an

---

*Note: programmed constants require compatible British units. For appropriate conversions to the metric system refer to page xvii.

equivalent spring constant for the ram impact head should be used. Should no pile cushion be provided, the value for the cushion spring constant is specified as zero. An equivalent spring constant and related coefficient of restitution are computed by the code as a series combination of the pile cushion and first pile element spring, as recommended by the TAMU findings.[12]

Program usage flexibility dictates the manner in which problem variables are defined. A three-layered soil system is described as an example in figure IV-1. The material properties for each soil layer are defined or determined separately from the pile parameters. Zones for each stratum are specified with respect to the ground surface. The deformation and failure criterion parameters are defined for each soil layer. All of these quantities are directly related to depth z. Provision is made to accommodate either bilinear elastic-plastic or nonlinear (hyperbolic) interface shear resistance to "static" penetration for each soil stratum. Similarly, a bilinear or nonlinear tip resistance must be defined.

Pile geometry and related quantities are prescribed separately with respect to the ζ-coordinate. Three options provide for simplified program input. Pile material(s) must be defined with respect to ζ; one option accounts for composite pile segments. Similarly, truncated pile sections (connected lengths of different, but constant, cross-sections) may be defined with respect to ζ. Finally, a pile of constant cross-section may be described. Having the material properties of the pile defined in this manner, these options subdivide the pile into an arbitrary number of equal length segments. The program computes all the lumped-parameter constants needed for the analysis.

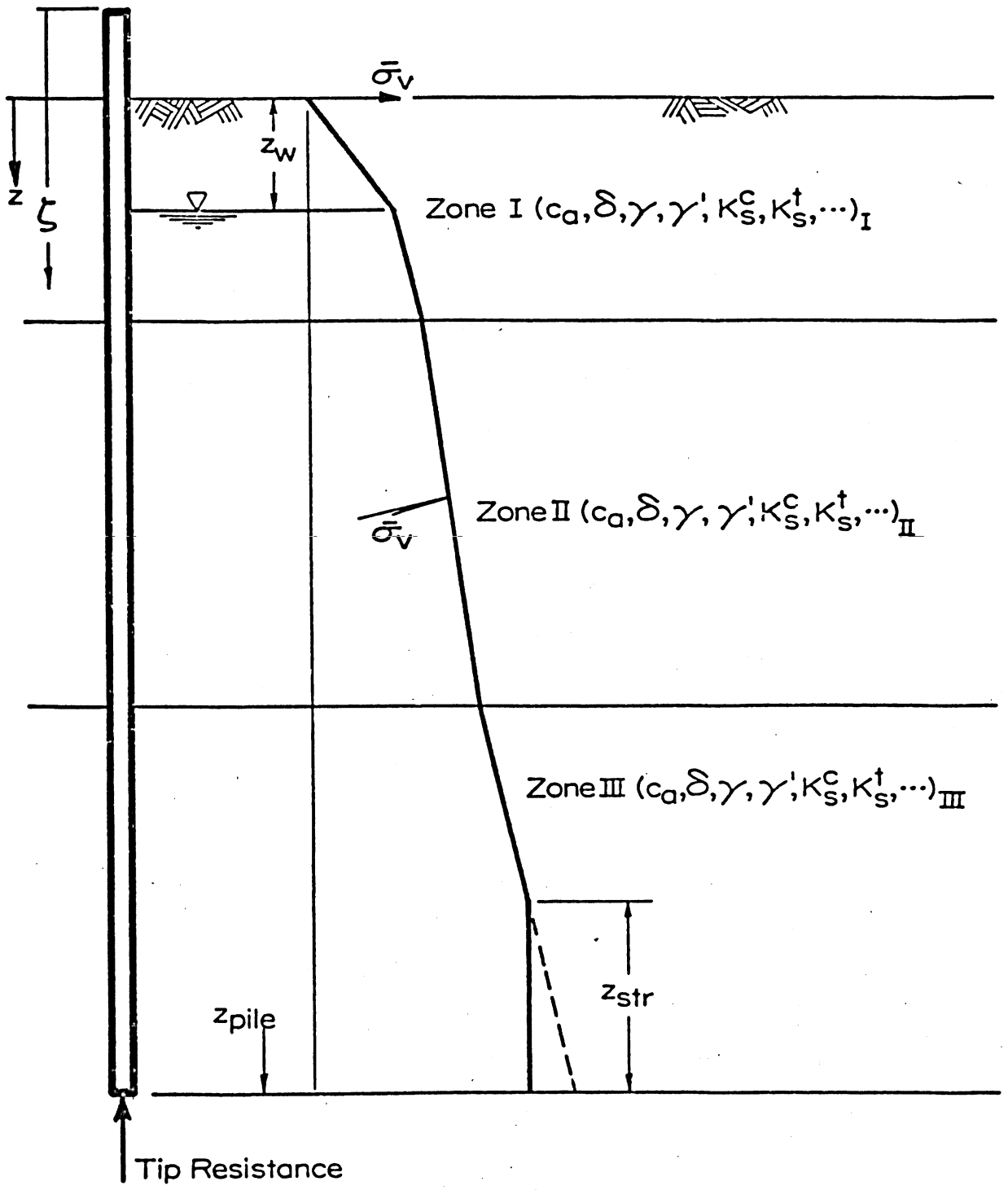

Figure IV-1. Pile-Soil System Parameters: DUKFOR.

The user may alternatively choose to input all of the pile element properties individually with another option. This would be necessary in the case of tapered pile representation for instance, since the cross section and surface area of each element would depend on ζ. For non-tapered piling, however, the first three options are preferable.

The overall geometry problem variables are thereafter specified. The depth of penetration, z_{pile}, water table depth, z_w, and a potential "zone of stretching" z_{str}, (having constant overburden pressure above the pile point) are input values. Finally, lateral earth pressure coefficients at failure are defined for each soil layer, and tip behavior quantities of maximum resistance and initial "quake" are given to completely describe the problem variables.

The computer code determines all of the pile-soil interface resistance parameters in terms of the overall problem geometry and the necessary material properties. The effective overburden stress "at rest" for each element centroid is computed as a function of depth. The value of the normal stress on the pile element-soil interface is determined as this overburden pressure times the coefficient of lateral earth pressure on the shaft at failure, using a superscript to denote values for compression failure, K_s^c, or tension failure, K_s^t. These K_s values are assumed constant within each layer. The overburden stress, $\bar{\sigma}_v$, near the pile is affected by the load-deformation conditions throughout the installation and load test sequence. Nevertheless, the assumptions prescribed in the one-dimensional formulation provide the simplest approximation.

The Mohr-Coulomb failure criterion is applied in the computation of maximum shear resistance values for the i-th element in the form

$$\tau^{c}_{max}\ (z_i) = c_a + K^{c}_{s}\ \bar{\sigma}_v\ (z_i)\ \tan\ \delta$$

$$\tau^{t}_{max}\ (z_i) = c_a + K^{t}_{s}\ \bar{\sigma}_v\ (z_i)\ \tan\ \delta \qquad \text{(IV-3)}$$

where the pile-soil adhesion, c_a, the coefficients of lateral earth pressure at failure, and the interface friction angle, δ, are properties of the penetrated soil layer at z_i, the element centroid depth. The maximum resistance forces on the element are computed as the product τ^{c}_{max} or τ^{t}_{max} times the element surface area. This attributes a difference between compression and tension loading shaft resistance to a change in normal stress on the shaft.

The code provides for either bilinear or hyperbolic (static) deformation behavior at the pile-soil interface and at the pile point. The parametric representation of hyperbolic interface behavior was formulated by Clough and Duncan.[81,82] This procedure used correlation factors to fit a hyperbola to the loading curve of an interface (direct) shear test. From a series of tests performed at different normal stress levels the results may be reduced to a set of average constants. These can effectively incorporate nonlinearity and stress level dependency directly. A description of the procedure and discussion of soil model representation is included in the Appendix.

Note that the simple equation forms for the hyperbola and its slope make it a powerful approximation to use in numerical applications.

The hyperbolic representation of a curve requires the assumption of two parameters to uniquely define a hyperbola: the initial tangent slope to the curve, and the horizontal assymptote. For nonlinear tip behavior the maximum tip load is assumed as the assymptote. The initial tangent slope is computed as the ratio of maximum tip load divided by the assumed (initial tangent) elastic quake.

The bilinear representation of resistance to penetration is easily defined by the same two parameters: the initial slope and the maximum value. Both shaft and tip resistance can be defined uniquely by the linear elastic slope (maximum resistance divided by quake) and the maximum resistance after which perfectly plastic deformation occurs.

The program represents unload/reload behavior as linear elastic. It assumes that the ratio of the unload/reload modulus to the initial tangent modulus, RULRL, is a constant for each material. The unload/reload modulus is selected whenever the current resistance is less than the maximum computed value during the element's load cycle. Whenever the load reverses sign the maximum value is reset to zero. No tension conditions are applied at the pile point.

Figure IV-2a describes a typical nonlinear interface behavior under static conditions. The initial slope A is generated from hyperbolic fit and stress-dependent parameters. The slope B is the unload/reload modulus given as A times RULRL. The figure indicates less tension resistance than compression resistance in this example. The slope A' will be less since the initial tangent modulus generally decreases with decreasing normal stress. Note that the hyperbolic formulation describes purely

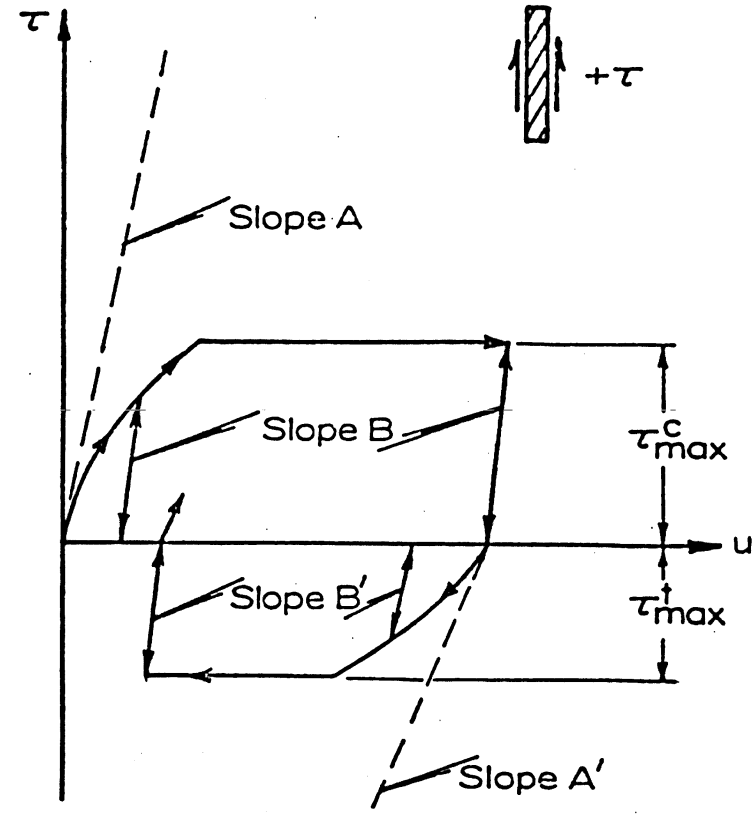

a) Hyperbolic Deformation Model

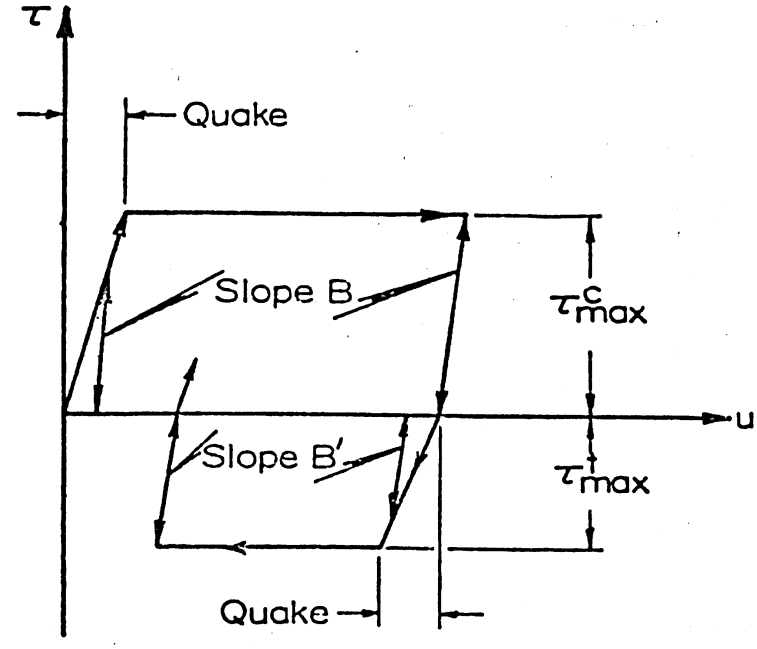

b) Bilinear Deformation Model

Figure IV-2. Interface Shear Load Transfer Models: DUKFOR.

plastic deformation after the maximum shear resistance is reached. Note also that a "loading" condition exists in either deformation direction, depending on the change in displacement with respect to the shear stress level.

Figure IV-2b gives the program representation of a bilinear resistance model. The elastic loading modulus in each shear direction is simply the ratio of maximum element shear stress divided by the quake. The unload/reload moduli are computed as before.

In each of these figures the slopes B and B' were drawn assuming RULRL > 1. Note that the assumptions $\tau^{c}_{max} = \tau^{t}_{max}$ and RULRL = 1 in figure IV-2b reproduce the rheological model in figure II-3 after Smith.[8] Three different dynamic penetration resistance models have been included in DUKFOR. The simplest approach, of course, is to assume that the dynamic and static resistance behavior are identical. The second option, consistent with Smith's formulation, provides for a nonlinear viscous dashpot in parallel with the static resistance "spring," see figure II-3 and equation II-6. Finally, the dynamic resistance may be computed using a linear viscous dashpot model. The equation describing this behavior is written as

$$R_{dynamic} = R_{static} + \bar{J}V \qquad \text{(IV-3)}$$

where $\bar{J}$ has units of force-sec/length.

These last two models assume that the dynamic component of resistance is added to the static behavior during driving. This implies that the static behavior is unaffected by installation. There are numerous

references in the literature citing transient phenomena of soil set-up or relaxation with time, which may significantly limit the use of these models. Under conditions of set-up or relaxation after driving, these models (equation II-6 or equation IV-3) are crude approximations, at best, of the "static" resistance during pile driving. They may correlate adequately with pile tests performed immediately after driving. Correlation parameters matching pile driving data with pile test data in soils expected to set-up or relax the resistance with time, may require the adjustment of driving resistance to compensate for these phenomena.[5,30]

To restate the argument, load tests performed after transient phenomena have passed may describe pile-soil system behavior that hardly resembles the conditions during pile driving. To analyze such cases using DUKFOR the dynamic and static behavior must be treated separately.

To simplify program logic DUKFOR employs specific subroutines to perform repeated operations, especially when these tasks are called upon at different stages in the solution scheme. In order to accommodate nonlinear behavior models both incremental and total (accumulated) values of pertinent variables are retained. The sign convention applies vector-related quantities as positive downward and assumes compression stresses positive. Interface shear stresses are positive when resisting downward pile movement. The next section describes the pile driving simulation algorithm. Significant program steps are outlined and briefly discussed.

Pile Driving Solution Algorithm

The dynamic formulation has been developed based upon lumped parameter elemental equilibrium equations analagous to Smith's procedure.[8] This representation permits a direct assembly of any combination of driving system components in simple terms. Total force dynamic equilibrium is solved at the end of each arbitrary time interval, marching out with time using an Euler-type numerical integration scheme. A piecewise linear approximation is applied to represent the interacting spring forces during each time increment calculation.

In order to simplify the presentation the pile driving algorithm has been listed, step-by-step, in Table IV-1. A discussion of important details is provided below.

Step 1 calls subroutine DTCALC to compute the critical time increments (see Chapter II) for each element in the total system, Δt_i. The sum of these values, $\sum \Delta t_i$, represents the time needed to transmit the impact stress wave front down to the pile point and back to the ram. The minimum Δt_i value is labeled Δt_{crit}, and the integration time step, Δt, is computed as a fraction of Δt_{crit},

$$\Delta t = \Delta t_{crit}/\text{FACTOR} \qquad \text{(IV-4)}$$

where FACTOR is a user-assumed constant.

Step 2 establishes the first blow initial conditions and boundary conditions for all the elements in the system. All element velocities, displacements, and spring forces are set to zero. If gravity forces are specified, the pile element weights are applied as a static load vector.

Table IV-1
PILE DRIVING ALGORITHM: DUKFOR

Step	Comment	Subroutine Called
1	Compute Δt_i, $\sum \Delta t_i$, Δt_{crit} $\Delta t = \Delta t_{crit}/FACTOR$	DTCALC
2	Specify first blow initial and boundary conditions	
3	Specify new blow initial and boundary conditions BEGIN SINGLE BLOW ITERATION LOOP	
4	Compute static soil resistance spring constants, $\overline{k}_i$, $\overline{k}_{tip}$	RSOIL
5	Compute incremental displacements and total displacements $\Delta u_i = V_i(12\ \Delta t)$ $u_i = u_i + \Delta u_i$	
6	Compute static resistance stresses/forces $\Delta\tau_i$, τ_i, R_i, $RMAX_i$, $RMIN_i$	SSOIL
7	Compute interelement spring forces, F_i $FMAX_i$, $FMIN_i$	FORCE
8	Compute dynamic resistance forces using model a, b, or c. a) $RDYNAM_i = R_i$ b) $RDYNAM_i = R_i + \lvert R_i \rvert\ JV_i$ c) $RDYNAM_i = R_i + \overline{J}V_i$	
9	Compute resultant (unbalanced) element forces $RESID_i = F_{i-1} - F_i - RDYNAM_i + W_i(CIGRAV)$	
10	Compute element velocities $V_i = V_i + RESID_i(\Delta t)\ (g/W_i)$ and check for termination of blow computation. END SINGLE BLOW ITERATION LOOP	
11	Statically equilibrate inertia forces $\Delta\overline{F}_i = RESID_i$	

The resulting quantities are supplied as the first blow initial and boundary conditions. The initial velocity of the striking parts, V_{ram}, is computed from equation IV-3.

Step 3 prescribes initial and boundary conditions for a new hammer blow. The initial velocities are reset according to Step 2, but the total displacements and forces (equilibrated statically after the previous blow) are used at the start of the new blow. Control parameters are reset and current blow variables (e.g. displacements, and maximum value terms) are set to zero. Hereafter the calculation enters the single blow iteration loop where the numerical integration of the equations of motion is performed.

Step 4 evaluates the static resistance stiffness values, $\overline{k}_i$, and $\overline{k}_{tip}$, for the shaft and tip resistance models, respectively. These quantities are determined in subroutine RSOIL using the algorithm logic described in the previous section. Recall that the static resistance behavior is treated independently within the solution assumptions. The quantities $\overline{k}_i$ and $\overline{k}_{tip}$ are functions of the instantaneous static shear stress and tip load levels, as well as the assumed material representations.

Step 5 calculates the incremental element displacements, Δu_i, (assuming V_i constant during Δt) and accumulates the total displacements, u_i, in an integration step given as

$$\Delta u_i = V_i (12\ \Delta t)$$
$$u_i = u_i + \Delta u_i \qquad \text{(IV-5)}$$

where V_i is the instantaneous element velocity in ft/sec.

Step 6 calls SSOIL to determine static soil resistance stresses, $\Delta\tau_i$ and τ_i, and resistance forces R_i, as well as saving maximum/minimum quantities for use in modulus selection during the next time increment. These quantities are computed using the equations

$$\Delta\tau_i = \bar{k}_i \, \Delta u_i$$

$$\tau_i = \tau_i + \Delta\tau_i \qquad \text{(IV-6)}$$

$$R_i = \tau_i \, (SAREA_i)$$

where $SAREA_i$ is the pile element surface area, ft^2.

Step 7 calls subroutine FORCE to calculate interelement spring forces based upon total displacement differences times the spring constant. Maximum/minimum values are stored for each spring during the hammer blow. Smith's bilinear cushion spring behavior, figure II-4, is included in the FORCE algorithm. All "no tension" spring conditions are also satisfied within FORCE.

Step 8 evaluates the instantaneous dynamic element resistance forces using one of three dynamic models: no damping; Smith's damping, equation II-6; or linear viscous damping, equation IV-3.

Step 9 solves the elemental (total) equilibrium equations for the resultant unbalanced forces, $RESID_i$, applying the computed internal and external forces in the form

$$RESID_i = F_{i-1} - F_i - RDYNAM_i + W_i \, (CIGRAV) \qquad \text{(IV-7)}$$

where the parameter CIGRAV is given as zero or one wnen body forces are to be excluded or included, respectively. For the case when i = 1 in equation IV-7, the term F_{i-1} drops out. When i = p the dynamic tip resistance force is specified as F_p. The sum of these quantities for the pile elements, is stored as $RESID_{p+1}$.

Step 9 computes the changes in velocity during the integration step and the element velocities at the end of this step as

$$\Delta V_i = RESID_i \ (\Delta t) \ (g/W_i)$$
$$V_i = V_i + \Delta V_i \qquad \text{(IV-8)}$$

Note that this assumes $RESID_i$ as constant over the time interval Δt. A check for calculation termination is made at this stage, completing the single blow iteration loop.

To continue the integration with time, steps 4 thru 9 are repeated sequentially over an arbitrary time interval. Intermediate print out of dynamic equilibrium data may be specified by the user. For each blow the computation proceeds in time over NPASS passes of the stress wave front, where NPASS is a user-assumed parameter. After this point is reached the program checks the value of $RESID_{p+1}$ ($= \sum RESID_i$) to select a moment in time to halt the computations.

The value of $RESID_{p+1}$ represents the driving force causing pile motion. Its amplitude is a rough measure of the total energy remaining in the pile. As the pile vibrates longitudinally under the force system applied, the value of $RESID_{p+1}$ oscillates with the total pile acceleration.

The quantities $RESID_i$ indicate instantaneous force values equilibrated by inertia forces.

With these concepts in mind, it is important to select a value of NPASS after which no more pile penetration will occur. There may still be appreciable $RESID_i$ values the system, but their total influence is minimal.

In order to complete one blow and establish the initial conditions for the next blow (or for the static analysis phase) it is necessary to satisfy static equilibrium. As the static formulation uses incremental behavior, a reasonable criterion to terminate the single blow calculation at a moment when $RESID_{p+1}$ is relatively small. The criterion used in DUKFOR is of the form

$$\left|RESID_{p+1}\right| \leq RESCK \qquad \text{(IV-9)}$$

where RESCK is a "tolerable" error. In the event equation IV-9 is not satisfied, calculations are automatically halted one full wave pass thereafter.

In conjunction with the necessary conditions for continuing the analyses it is necessary to eliminate the transient inertia forces and satisfy static equilibrium. When one writes Newton's Second Law, equation II-1, the sum of the applied forces ($RESID_i$) is equated with the element mass times the resulting acceleration. The inertia force is equal to $RESID_i$ but opposite in sign. In order to satisfy static equilibrium this inertia force must be "unloaded."

Step 11 unloads the inertia forces in the pile by simply applying the unbalanced element forces in a static equivalent (incremental) load vector,

$$\Delta \bar{F}_i = \text{RESID}_i \qquad \text{(IV-10)}$$

This may be equated in a simple spring-mass, one degree of freedom system, as the restoring force necessary to return the oscillating mass to its static equilibrium position. The implicit assumption in the pile driving solution application of equation IV-10 is that the RESID_i are causing only linear elastic response of the pile-soil system when the integration is stopped. This restriction is realized approximately when the solution has proceeded far enough in time that the element velocities are small (minimal damping forces) and each element is oscillating about a stable displacement value. More details of the implications will be discussed in Chapter VI.

After applying the static equilibration load vector to the system, the results represent the system conditions at the end of the blow. These may be applied as initial and boundary conditions for a next blow. The program will perform the single blow solution steps 3 through 11 for as many blows as the user requires. Thereafter, the computations enter the static load test phase of the anlysis. Input parameters provide for the dynamic/static, dynamic only or static only sequences according to the needs of the user. The next section describes the static solution method.

Static Solution Algorithm

The basic features of the static equilibrium solution method incorporated in DUKFOR were developed during the previous phase of the investigation, for a load test simulation code, FDFOR.[2] The primary formulation changes introduced the combined treatment of compression and tension load (interface) behavior such that sequential simulation of the entire load test could be performed. Subprogramming duplicated algorithms for both dynamic and static solution usage, and linking the process into a coherent package represent the major tasks accomplished. An outline of the computation steps employed by the static solution algorithm is given in Table IV-2. A brief description of these steps follows.

Step 1 assumes appropriate initial conditions and defines the incremental load vector. Three loading cases use the static solution method. The first two were described in the previous section; gravity force vector and the "static equilibrating" force vector. The gravity forces may be applied to generate initial conditions before driving (or before load testing if no dynamic solution is requested). The static equilibrating force vector "unloads" inertia forces in the pile remaining at the end of each hammer blow computation, approximately satisfying static equilibrium. The respective values of these forces are applied as an equivalent load vector, $\{\Delta\bar{F}\}$, in each case.

The third loading case is generated from a load test simulation procedure. Program input parameters specify the end points of arbitrary loading paths, for which static solution data will be printed. The load is applied incrementally to each successive end point such that any mono-

Table IV-2

STATIC SOLUTION ALGORITHM: DUKFOR

Step	Comment	Subroutine Called
1	Assume appropriate initial conditions and establish incremental load vector: a) Gravity forces: $\Delta\bar{F}_i = W_i$ b) Pile driving equilibration forces; $\Delta\bar{F}_i = RESID_i$ c) Load test loading increment; $\Delta\bar{F}_{MO} = QINCR$	
2	Determine soil resistance spring constants	RSOIL
3	Assemble tridiagonal stiffness matrix [K] in three vectors DIAG, SUB, SUP	TRIDST
4	Solve the static equilibrium equations $[K]\{\Delta u\} = \{\Delta\bar{F}\}$ for $\{\Delta u\}$ using a tridiagonal equation solver and compute total displacements $u_i = u_i + u_i$	TRID
5	Compute resistance stresses and forces	SSOIL
6	Compute interelement forces	FORCE

tonic, cyclic, and/or load reversal (e.g. compression to tension) loading sequence may be applied. Upon simultaneous failure of all element resistance springs the calculations are stopped and the previous load increment data are printed out.

Each load increment is applied as an external force to the pile butt element. All other element forces are zeroed. The force vector is, therefore, prescribed as

$$\Delta\bar{F}_{MO} = \pm QINCR$$

$$\Delta\bar{F}_i = 0 \quad i \neq MO \tag{IV-11}$$

where MO is the number of the first pile segment. The plus or minus sign describes the incremental load direction; a positive change in force is applied downward.

The load increment magnitude, QINCR, is an input parameter given in kips. It represents the maximum loading step size. At the start of each applied load path, however, the program uses a series of one kip increments, QINCR in number, to begin the path. This modification allows a change in modulus to be made while the load step is relatively small. During a loading reversal (e.g. compression to tension increment change) the transition from load to unload modulus (or vice versa) is made with minimal "overshoot" problems. Note that modulus selection is done in subroutine RSOIL based upon the previous loading increment results.

Step 2 calculates the tangential soil resistance spring constants, $\bar{k}_i$, for the load transfer model and the appropriate point spring stiffness, $\bar{k}_{tip}$. Subroutine RSOIL calculates these quantities.

Step 3 assembles the static equilibrium equations in arrays. The general form of these may be written in incremental matrix form as

$$[K] \left\{\Delta u\right\} = \left\{\Delta \bar{F}\right\} \tag{IV-12}$$

using a displacement formulation. The direct solution for unknown changes in displacement due to the applied loading increment, $\Delta \bar{F}$, requires an inversion process. The elements in the stiffness matrix, [K], are generated by the recursion formulas

$$K_{ii} = \begin{cases} k_{MO} + \bar{k}_{MO}, & i = MO \\ k_{i-1} + k_i + \bar{k}_i, & i = MO + 1, p \\ k_{p-1} + k_{tip} + \bar{k}_p, & i = p \end{cases} \tag{IV-13a}$$

$$K_{i,i+1} = K_{i+1,i} = -k_i \qquad i = MO, p-1 \tag{IV-13b}$$

These terms describe coefficients of a tridiagonal system of linear algebraic equations. All other elements of the stiffness matrix are zero. The stiffness matrix can be compactly written into three linear arrays: $DIAG_I = K_{ii}$, the main diagonal; and $SUB_I = SUP_I = K_{i,i+1}$, the subdiagonal and superdiagonal, respectively. The subscript I represents a shift operation in which I = 1 corresponds to i = MO. Subroutine TRIDST assembles the tridiagonal equations in this manner.

Step 4 calls upon subroutine TRID, a tridiagonal equation solver routine,[83] to calculate the unknown incremental displacements. The total displacements are then accumulated.

Step 5 evaluates the changes in element soil resistance forces using subroutine SSOIL. Incremental and total shear stresses, and total resistance forces are determined for use in the next program step. Maximum/minimum values of the resistance forces are retained for use in the modulus selection process of RSOIL.

This step completes the computations needed for the loading increment. When the applied load has not reached the load path end point, the execution returns to Step 1 of the static algorithm. When the end of the current load path has been reached the program proceeds to Step 6. For the gravity load option and the static equilibration option Step 6 is performed.

Step 6 calculates the pile spring forces as a function of total element displacements in subroutine FORCE. Upon return from the subroutine the type of loading conditions determine the next operation. For the gravity loading case, the static results are printed out. The program returns, thereafter, to commence the dynamic or static computations, depending upon the problem requirements. For static equilibration at the end of the hammer blow the execution resumes within the pile driving output loop. When the load path end point has been reached, the static solution data is printed out. Thereafter, the control reverts back to Step 1 to initialize a new load path and resume static computations. Upon completion of the load test sequence the program seeks problem input data.

Additional features of the static formulation deserve some attention. A supplementary system of variable arrays is established at the beginning of the pile load test simulation. Current values of total displacement and pile spring loads are defined as zero (initial values)

to monitor the change in these quantities after installation. Many pile tests with sophisticated instrumentation implicitly assume these conditions, by assuming that residual load distributions after driving are negligible.

Another parameter zeroed after driving is the "mobilized" total shear stress in each element. In this fashion both overall and mobilized (after driving) quantities are printed out with the static results. The use of these quantities and further discussion of them is deferred to Chapter V.

The static pile load distribution is computed two ways. The pile spring forces are based upon interelement displacement differences from subroutine FORCE. The second method employs a numerical integration procedure, instead, evaluating the pile load with depth as the total applied load (plus element weights above that depth, if included) minus the load transferred to the soil in shear above z. The load transferred is computed by integrating the skin friction times the element surface area from ground surface to depth z. Two independent solutions are provided for the load distribution results, in addition to the mobilized values already described.

DUKFOR simulates the pile-soil interaction problem in a one-dimensional idealization which greatly reduces problem formulation mathematics. It also grossly simplifies some system variables considered to affect pile performance. In order to better assess the effects of these assumptions, a more sophisticated mathematical formulation is required. A brief discussion of the axisymmetric finite element formulation developed for this study is described below.

Axisymmetric Code: AXISYM

Basic Considerations

Early in the development of this investigation some questions were raised concerning the assumptions of the one-dimensional formulation. It was decided that comparisons of results from DUKFOR analyses with those using an axisymmetric finite element representation could prove quite useful. To accomplish this goal a highly versatile finite element code, SOIL-STRUCT, developed by G.W. Clough and Y. Tsui, was selected. It was necessary to modify the existing formulation to provide an axisymmetric solution capability.

The first version of the SOIL-STRUCT code was developed for the C E to simulate the construction and subsequent performance of U-frame locks.[81,82] This code permitted any arbitrary sequence of incremental loading conditions involving: excavation, fill and structure placement loads; seepage pressure loads; boundary pressure, concentrated force and nodal displacement loads; and loads generated by temperature changes in the structural elements. A displacement formulation modeled plane strain behavior using four node quadrilateral and one-dimensional interface slip elements. Nonlinear, stress-dependent deformation behavior could be specified using hyperbolic fit and stress level-dependent formulations for both solid and interface element behavior. An updated version of this code, LOCKS, is in use at WES.

The original code has been revised to better model soil-structure interaction behavior. The present version, SOIL-STRUCT, incorporates additional loading conditions needed to model tied-back wall construction

behavior.[84] An iteration sequence has been added to improve solution convergence, and a better quadrilateral finite element has been introduced.

The modified five node quadrilateral element, QM5,[85] was included in SOIL-STRUCT to take advantage of its superior shear distortion characteristics. A five node quadrilateral element allows linear strain variation within the element, while constant strains are prescribed at the element boundaries, satisfying interelement compatibility. The modification applied for the QM5 element assigns the element shear strain a constant value throughout (that computed at the central node). This incompatibility allows more element flexibility in bending shear distortion than any other four or five node quadrilateral element formulation. In addition, it can be used as a constant strain triangular element simply by assigning two adjacent nodes to the same coordinate location.[85]

The assumption of axial symmetry greatly simplifies a three-dimensional problem. For the purpose of this investigation full axial symmetry is assumed with respect to problem geometry, material properties, and loading conditions. Cylindrical coordinates (r, z, θ) describe a "solid of revolution" about the z-axis. Within the axisymmetric idealization, any θ-plane (containing the z-axis) represents a principal plane such that $\sigma_{r\theta} = \sigma_{z\theta} = 0$. The value of σ_θ depends only on the material properties and the remaining stress/strain components at a point (r,z), all of which are independent of θ. The vector of effective stress components, $\{\bar{\sigma}\}$, at any point includes only four terms,

$$\{\bar{\sigma}\}^T = (\bar{\sigma}_r, \bar{\sigma}_z, \bar{\sigma}_\theta, \tau_{rz}) \qquad \text{(IV-14)}$$

An axisymmetric finite element problem is fully described by discretization in two dimensions, r and z. Each element represents its solid of revolution about the z-axis. For axisymmetric interface elements the idealization describes a surface of revolution.

Modifications for AXISYM

AXISYM incorporates all necessary changes in SOIL-STRUCT needed to simulate either plane strain or axisymmetric problems of boundary pressure loading exclusively. Subroutines used to perform other loading case computations were not revised to include the axisymmetric option, and therefore, these subroutines were removed for future revision. All the main program control logic has been left intact to accomodate these revised subroutines when they are available.

The quadrilateral (QM5) element stiffness derivation and the algorithm steps needed to provide the axisymmetric option in SOIL-STRUCT are described by Doherty et al.[85] The modifications to SOIL-STRUCT were essentially translating notation from Doherty's code and linking the axisymmetric option to produce AXISYM. An axisymmetric interface element representation was also included after Desai and Holloway.[56]

One comment should be added at this point. The derivation of axisymmetric element stiffness matrices involves volume integrals of terms that are functions of r. The QM5 element formulation employs a four point integration formula to accomplish this task.[85] The axisymmetric approximation to the interface stiffness is given as the product of the plane strain stiffness quantity[81,82] times the term $\bar{r}\,\bar{\theta}$, where $\bar{r}$ is the radius of the element centroid and $\bar{\theta}$ is the interval of revolution used in the

element stiffness formulation (one radian for the QM5 element). For an interface element parallel to the axis of symmetry this gives the exact stiffness as

$$\left[\overline{k}_i\right]_{\mathcal{C}_L} = \overline{r}\left[\overline{k}_i\right]_{R_L} \qquad \text{(IV-15)}$$

since the integration limits are coincident in r.

For interface elements not parallel with the z-axis, equation VI-15 is approximate. For such elements near the centerline and/or within a zone of expected high strain gradients, shorter element lengths should improve solution accuracy.

Problem Formulation

A rectangular element mesh generation routine was developed to punch the input data required by AXISYM. The program, MESHPN, determines element geometries and material types using nodal rows and columns defined by their z and r coordinates, respectively. The overall mesh is subdivided into rectangular zones of material types according to the "boundary" rows and columns. The punched mesh details include nodal coordinates, element nodes and material types. Horizontal and/or vertical lines of interface elements may be included by specifying coincident rows and/or columns of nodes and appropriate material zones using MESHPN.

A sample mesh designed to analyze test pile 2, Lock & Dam No. 4, Arkansas River Project, C E , is shown in Fig. IV-3. Note the refinement used in the vicinity of the pile tip. The line of vertical pile-soil interface elements extends beneath the pile tip in the soil while the

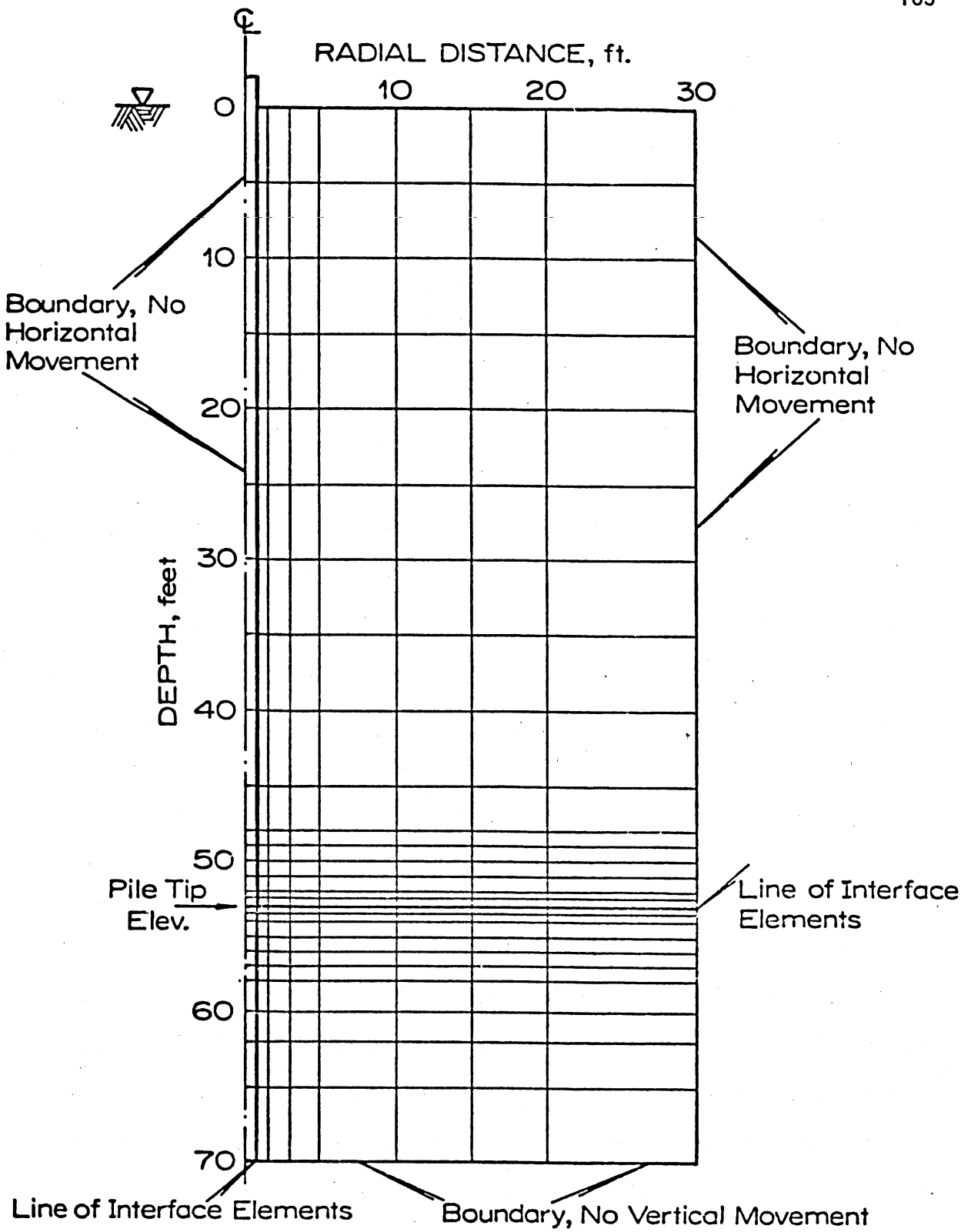

Figure IV-3. Refined Axisymmetric Finite Element Mesh, Test Pile 2, Lock and Dam No. 4, Arkansas River Project.

horizontal plane at the pile tip elevation also extends interface elements across the plane. These elements are assigned "soil-soil" interface properties.

The corner of the pile tip is a geometric and material discontinuity at which infinite stress/strain occurs during penetration. The mesh refinement, and especially the refined interface elements intersecting at this point, keep the analytical singularity localized. The horizontal interface element adjacent to the tip tends to fail in extension, a phenomenon observed analytically and experimentally by others, see Chapter III. Ellison used point springs to connect the element boundary nodes across this plane in a similar application.[55] In this investigation the use of vertical interface elements extending beneath the tip allows interelement slip (punching) to relieve extremely high shear stresses. This combination of interface element zones enhances solution stability and better matches the physical behavior. Further attention to these conditions will be given in Chapter V.

In addition to the finite element mesh data, material properties of the pile, interface, and soil elements must be provided. AXISYM results will include the behavior of the pile, pile-soil interface and soil elements such that the pile-soil system is modeled more "correctly." It is done, however, at the expense of far greater computational effort and more restrictive initial conditions and loading conditions than DUKFOR permits. A brief outline of the AXISYM algorithm is given in Table IV-3. Some comments on the program steps are included below.

Step 1 calculates initial conditions within subroutine INITAL. At the beginning of a new problem a gravity turn on loading step is applied to

TABLE IV-3 AXISYMMETRIC SOLUTION ALGORITHM

STEP	COMMENT	SUBROUTINE CALLED
1	Establish Initial Conditions (a or b)	
	a) Gravity Turn-on Analysis	INITAL
		STRSTF
		BANSOL
		STRESS
	Generate Horizontal Stresses	INITAL
	$\bar{\sigma}_r = \bar{\sigma}_\theta = K_s^0 \bar{\sigma}_z$	
	Determine Element Moduli	MODCAL
	b) Read in Data	INITAL
2	Perform Incremental Loading Case (a thru d)	
	a) Assemble Structural Stiffness Matrix and Load Vector	STRSTF
	$[K]\{\Delta u\} = \{\Delta \bar{F}\}$	
	b) Solve Simultaneous Equations for Unknown Displacements	BANSOL
	c) Compute Element Stresses (at center nodes)	STRESS
	d) Determine Element Moduli	MODCAL
3	Print Output Data	
4	Punch Output Data (as initial conditions)	

determine vertical stresses in the entire system. Nodal displacements and element shear stresses are set equal to zero, and the horizontal effective stresses are calculated for each element as $\bar{\sigma}_r = \bar{\sigma}_\theta = K_s^0 \bar{\sigma}_z$, where K_s^0 is the initial lateral earth pressure coefficient. Based upon these initial stresses, initial element moduli values are generated by subroutine MODCAL. For the continuation of a previous loading history (see Step 4) the initial conditions may be read in directly from data cards, instead.

Step 2 performs the incremental loading step calculations. Subroutine STRSTF assembles the structural stiffness matrix block by block and writes the equations on tape. Subroutine QUAD is called by STRSTF to evaluate quadrilateral element stiffness values, while JTSTF performs this task for joint (interface) elements.

The system of simultaneous equations is solved for nodal (incremental) displacements using subroutine BANSOL, a bandwidth-type Gaussian elimination equation solver. Subroutines STRESS and JSTRES are thereafter called to evaluate element stresses at the center nodes. Subroutine MODCAL is called by STRESS and JSTRES to evaluate new element moduli during this step. An additional program feature particularly useful in some problems allows the user to override algorithm moduli selection and specify either load or unload/reload moduli for all unfailed elements. Further discussion of this option will be included in Chapter V.

Step 3 prints out all computation results. Incremental and total nodal displacements, (center node) element stresses (both principal and r-z-θ), new element moduli and stress levels are listed in the printout.

In the event another iteration is requested, the program returns to Step 2 and repeats the loading increment using adjusted moduli from the previous iteration. SOIL-STRUCT provides the option of additional iterations for each individual loading step. Iteration allows more rapid convergence for larger loading increments, and is especially useful for correcting overshoot difficulties and eliminating tension stresses in soil and interface elements. AXISYM leaves this option intact.

Upon completion of Step 3 the program returns to Step 2, and applies the next loading increment. The sequence is repeated for each loading step specified. When all input loading steps have been applied the program proceeds to Step 4.

Step 4 is a particularly useful feature that is provided in SOIL-STRUCT. All necessary initial conditions for a subsequent loading step are punched on data cards at the end of the computations. The punched output allows step-by-step debugging and verification without the need to repeat previous (proven) loading case history. This capability also provides "computed" initial conditions as a branch point to examine different alternative cases applied thereafter, an especially useful and economical design usage feature. This step has been retained in AXISYM.

Chapter V

PILE TEST ANALYSES

Introduction

Two computer programs were developed during this investigation to represent the mechanics of pile-soil interaction. The code DUKFOR is a one-dimensional load transfer formulation which models the entire sequence of pile driving and load testing. An axisymmetric finite element code, AXISYM, which models only static behavior, was developed to compare with the DUKFOR approach in order to define the advantages and disadvantages of these two analytical models. The development of each code is discussed in the preceeding Chapter. The results of pile test analyses performed with these codes are presented hereafter.

In order to assess capabilities and limitations of the two methods, several instrumented pile tests were analyzed. Only one pile test was studied in detail using both computer codes; additional pile tests were analyzed using the DUKFOR program. Furthermore, parametric studies were made to evaluate stability and convergence criteria for each code. The effects of various hammer-pile-soil system components on pile driving performance and on residual driving loads were examined parametrically using DUKFOR. The results of the parameter studies are presented in Chapter VI.

Pile Test Data: Lock and Dam No. 4

A comprehensive series of pile tests was performed at Lock and Dam No. 4 (LD4), Arkansas River Navigation Project for the U.S. Army Engineer District, Little Rock, by Fruco and Associates.[86] The general subsurface conditions at the test site consist of three major soil strata: an overlying 13 foot thick surface blanket of silts and fine sands; an intermediate stratum of relatively dense, medium to fine sand approximately 93 feet thick; and a Basal stratum of Tertiary clay. The in situ dry density of the deep sand strata ranged between 90 and 109 pcf, showing no consistent trend with depth. Twenty feet of soil was excavated prior to the pile tests. Piezometers indicated that the water table remained 2 to 3 feet below excavation grade during pile driving and load test operations.[86]

Laboratory tests on the soils were performed by the U.S. Army Engineer Division, Southwestern, Laboratory, Dalas, Texas.[87] Direct shear and interface shear tests were performed on the (SP-SM) sand samples prepared in the laboratory at selected densities. The angle of internal friction for the soil, ϕ, ranged between 31° and 35° with an average of 32°. The interface friction angle, δ, for sand-on-steel measured between 23° and 30°, with the higher values associated with the higher relative densities. For the purpose of the analyses performed herein the average value of ϕ was assumed (ϕ = 32°); the value of δ was assumed as 29.8°, a high value chosen because of the likely densification of the sand near the pile shaft.

Soil deformation parameters are needed for the constituitive model used in AXISYM. As no triaxial test data was obtained for LD4 sands,

deformation properties obtained from tests on Jonesville Lock and Dam (JLD) sand were assumed,[56] as has been done in previous finite element studies of these piles.[75,88,89] Hyperbolic pseudoelastic parameters from triaxial tests on remolded 80 percent relative density JLD sand were generated using the standard procedures discussed in the Appendix. Interface shear test data were reduced to average hyperbolic parameters in an analogous procedure. Values of the deformation and failure parameters used in the present study are described in the Appendix.

In order to model shaft load transfer in the DUKFOR model one must approximate the pile-soil system response at the interface. Deformations in the adjacent soil should soften the measured pile load transfer relative to laboratory interface shear test behavior. The effects of pile driving on pile shaft behavior (soil densification and repeated load/unload cycles) should stiffen the measured response. It is assumed for all the DUKFOR analyses presented herein that the laboratory interface shear test behavior represents the field load transfer mechanism directly.

The test piles installed at LD4 included steel H-piles (14 BP 73), steel pipe piles (12-, 16-, and 20 in. O.D.), prestressed concrete piles (16- and 20- in. square), timber piles and steel sheet piles. Details of the properties of test piles which were analyzed are given in Table V-1. Each pile was instrumented with strain rods and/or strain gages. All the analyzed piles are 55 feet long steel pipes which were installed closed-ended with approximately 53 ft embedment. Three of the test piles (TP) were driven to grade using a Vulcan 140 C double-acting steam hammer, LD4TP1, LD4TP2, and LD4TP3. A Bodine vibratory pile driver was used to

Table V-1

Properties and Installation Data, LD4

Test Pile	Type & Details	Net Cross-Section (SQ IN.)	Effective Perimeter (FT)	Gross Tip Area (SQ. FT.)	Hammer Type	Blow Count Final Foot (BLOWS/FT)	Instrumentation
LD4TP 1	12.75 IN. OD PIPE, 0.330 IN. THICK WALL,[a] 2, 4U7.25	17.12	3.90	0.970	VULCAN 140C	16	STRAIN RODS
LD4TP 2	16. IN. OD PIPE, 0.312 IN. THICK WALL,[a] 4, 4U7.25	23.86	5.32	1.568	VULCAN 140C	38	STRAIN RODS & STRAIN GAGES
LD4TP 3	20. IN. OD PIPE, 0.375 IN. THICK WALL,[a] 2, 4U7.25	27.36	5.80	2.270	VULCAN 140C	44	STRAIN RODS
LD4TP 10	SAME AS LD4TP2	23.86	5.32	1.568	BODINE	—	STRAIN RODS & STRAIN GAGES
LD4TP 16	16. IN. OD PIPE, 0.312 IN. THICK WALL,[a] 2, 4U7.25	19.62	4.75	1.482	VULCAN 140C	24[b]	STRAIN GAGES

NOTES: a. ASTM A-252, grade 2 steel pipes b. Jetted 40 ft., driven final 13 ft.

place LD4TP10; LD4TP16 was jetted to 40 ft depth and thereafter impact-driven to grade with a Vulcan 140 C.

Ram impact simulation is employed in the DUKFOR pile driving algorithm, see Chapter IV. The parameters used to describe the Vulcan 140C hammer assembly are listed in Table V-2. Pile driving analyses were carried out on all piles except LD4TP10, since no vibratory driver simulation was possible with the present version of DUKFOR.

All five test piles were loaded to failure in compression and thereafter to failure in tension. Near plunging-type failure developed in each test such that the maximum applied load was assumed as the failure load for each case. Compression test results are described in Table V-3; tension test results are summarized in Table V-4.

Each pile was instrumented along its length in order to measure pile load distribution. Significant residual driving loads were observed in the piles[86] and subsequent analyses were performed by Hunter and Davisson[76] to evaluate the residual loads more precisely. As previously mentioned in Chapter III, these investigators determined the residual driving load distribution as the difference between the magnitude of the measured residual tension loads at the end of the tension test unload, and the magnitude of the measured residual loads at the end of the compression test after unloading. This technique assumed implicitly that there are no residual axial loads anywhere along the pile after unloading at the end of the tension test. This assumption is correct at the pile tip and at the pile butt; however, it is only a rough approximation elsewhere along the pile. Without knowledge of the actual stress-free gage data, the actual shape of the residual load curve is indeterminate.

Table V-2

IMPACT HAMMER ASSEMBLY DATA, LD4

Hammer	
Vulcan 140C double-acting steam hammer	
Ram Weight W_1	14000 lb.
Rated Energy	36000 ft-lb.
Efficiency (assumed)	0.78
Cap Block	
Micarta	
10 x 1.0-in. - thick disks, 17.5 in. O.D. with 4.5 in. bored center hole	
Cross-section	224.6 $in.^2$
Thickness	10. in.
Secant Modulus (stress level dependent)	4.5×10^5 $lb/in.^2$
Coefficient of Restitution (assumed)	0.80
Pile Cap (no cushion block)	
Weight, W_2	1710 lb.

Table V-3

Compression Load Test Behavior, LD4

Test Pile	Maximum Compression Load, Q^c_{max} (KIPS)	Mobilized Compression Capacity TIP (KIPS)	Mobilized Compression Capacity SHAFT (KIPS)	Adjusted[a] Compression Capacity TIP (KIPS)	Adjusted[a] Compression Capacity SHAFT (KIPS)	Lateral Earth Pressure Coefficient[b] K^c_s MOBILIZED	Lateral Earth Pressure Coefficient[b] K^c_s ADJUSTED
1	344	96	244	170	174	1.15	0.821
2	502	150	352	240	262	1.22	0.906
3	516	224	292	320	196	0.926	0.622
10	456	166	290	166	290	1.00	1.00
16[c]	330	100	230	180	150	0.891	0.581

NOTES:

a. Adjusted for measured residual tip load after Hunter and Davisson[86].

b. Effective overburden stress assumed; Interface friction angle $\delta = 29.8^o$; WT at 2 Ft depth, $\gamma = 125$ pcf, $\gamma' = 63$ pcf.

c. Jetted and driven 40 ft. and driven final 13 ft.

Table V-4

TENSION LOAD TEST BEHAVIOR, LD4

Test Pile	Maximum Tension Capacity, Q^t_{max} (KIPS)	Lateral Earth Pressure Coefficient K^t_s
1	184	0.868
2	232	0.802
3	240	0.761
10	220	0.761
16	146	0.565

For LD4 piles analyzed in this report measured residual point loads are directly available. Hunter and Davisson[86] present results giving residual point loads for all the piles studied herein. Compression test results for measured (mobilized) point capacity, Q_p, and shaft capacity, Q_s, are listed in Table V-3. Lateral earth pressure coefficients at failure, K_s^c, were back calculated from respective Q_s values assuming that the skin friction distribution is proportional to the in situ effective overburden stress. Note that the K_s^c values are significantly reduced when residual point loads are correctly considered, see Table V-3. These values are only approximate, however, since the shape of the actual skin friction curve at failure is no doubt more complex than that assumed. Discussion of the effects of this assumption is covered in a subsequent section of this chapter.

Similar procedures were used to analyze tension test results. Because there is no residual tip load at failure in tension ($Q_p = 0$) there is no need to adjust the value of Q_s. Backcalculated values of K_s^t are listed in Table V-4. Based upon results reported by other investigators the K_s^t values should be less than K_s^c; however, this is not the case for LD4TP1 and LD4TP3 which show K_s^c values less than K_s^t. The reason for this is not readily apparent. Based upon these data, however, and in lieu of load transfer measurements at another site, the assumption of $K_s^c = K_s^t$ appears reasonable. This conclusion was stated previously by Vesić.[90]

An additional comment is warranted at this point concerning the magnitudes of the K_s values. Backcalculations of these parameters are sensitive to the value of δ assumed as well as to the shape of the skin friction distribution curve. Using $\delta = 25°$, corresponding to the minimum value measured in the laboratory, K_s^c and K_s^t would be 25 percent larger.

DUKFOR Analysis: LD4TP2

The 16-in. O.D. pipe pile, LD4TP2, was instrumented with both strain gages and strain rods. The pile was impact-driven to full embedment. A cyclic compression test followed by a cyclic tension test were performed on the pile; load-displacement and load distribution data were collected throughout the test phase.

Pile Driving Analysis

Pile driving performance was studied using the dynamic analysis option of DUKFOR. This pile was one of several piles previously studied by the writer using the Texas A&M University (TAMU) computer code (TAMFOR) which was adapted for use on WES computer facilities.[3] The basic difference between the computer codes rests in the approach to the problem. TAMFOR simulates the behavior of the hammer assembly-pile-soil system for a single blow up until the pile point rebounds, whereupon full rebound is assumed to occur. DUKFOR simulates the entire blow, statically equilibrating the system after the driving forces have dissipated (see Chapter IV). With this new technique a series of hammer blows may be applied, taking proper account of the residual driving stresses from previous blows.

In discretization of the pile and time increments numerous choices are possible. As discussed in Chapter II, one should select a pile segment length that is small with respect to the impact stress wave length. A compatible time interval of integration must be chosen smaller than the time required for the stress wave front to pass in either direction through any "driving system" element. Smith prescribed $\Delta t = \Delta t_{crit}/\text{FACTOR}$ using

FACTOR = 2. To satisfy the first criterion Smith recommended no fewer than ten pile segments, not greater than 10 ft in length.[8] For the LD4 test piles using DUKFOR multiple blow, nonlinear resistance models and relatively long (integration) intervals, it was found that PILSEG = 15, FACTOR = 4 and NPASS = 6 (6 stress wave front passes in time) were the best values. It should be noted that for single blow analyses (e.g. TAMFOR solutions) Smith's recommendations are quite satisfactory.

In developing DUKFOR it was expected that for a prescribed resistance distribution a "steady state" pile driving solution would be obtained after a series of hammer blows was simulated. That is, the blow count, and residual load distribution would become essentially constant thereafter for each successive blow. For the LD4 test piles the steady state condition was usually developed after three hammer blows. In order to insure convergence in all cases for the LD4 pile driving solutions described hereafter the input parameters included IBLOWS = 5 (five hammer blows), NPASS = 6, FACTOR = 4, PILSEG = 15. Some of the details involved in selecting these parameters are discussed in Chapter VI.

Figure V-1 describes the parametric determination of point and shaft damping constants, J_p and J_s. All of the data in this figure represent static equilibrated results for the fifth blow. Data obtained using both bilinear and nonlinear resistance models in DUKFOR analyses are described. It was noted in a previous report[3] that the soil damping parameters are actually correlation constants, not intrinsic soil properties. Figure V-1 highlights the fact that J_p and J_s are interdependent quantities such that for a given value of J_p a new value of J_s may be found which

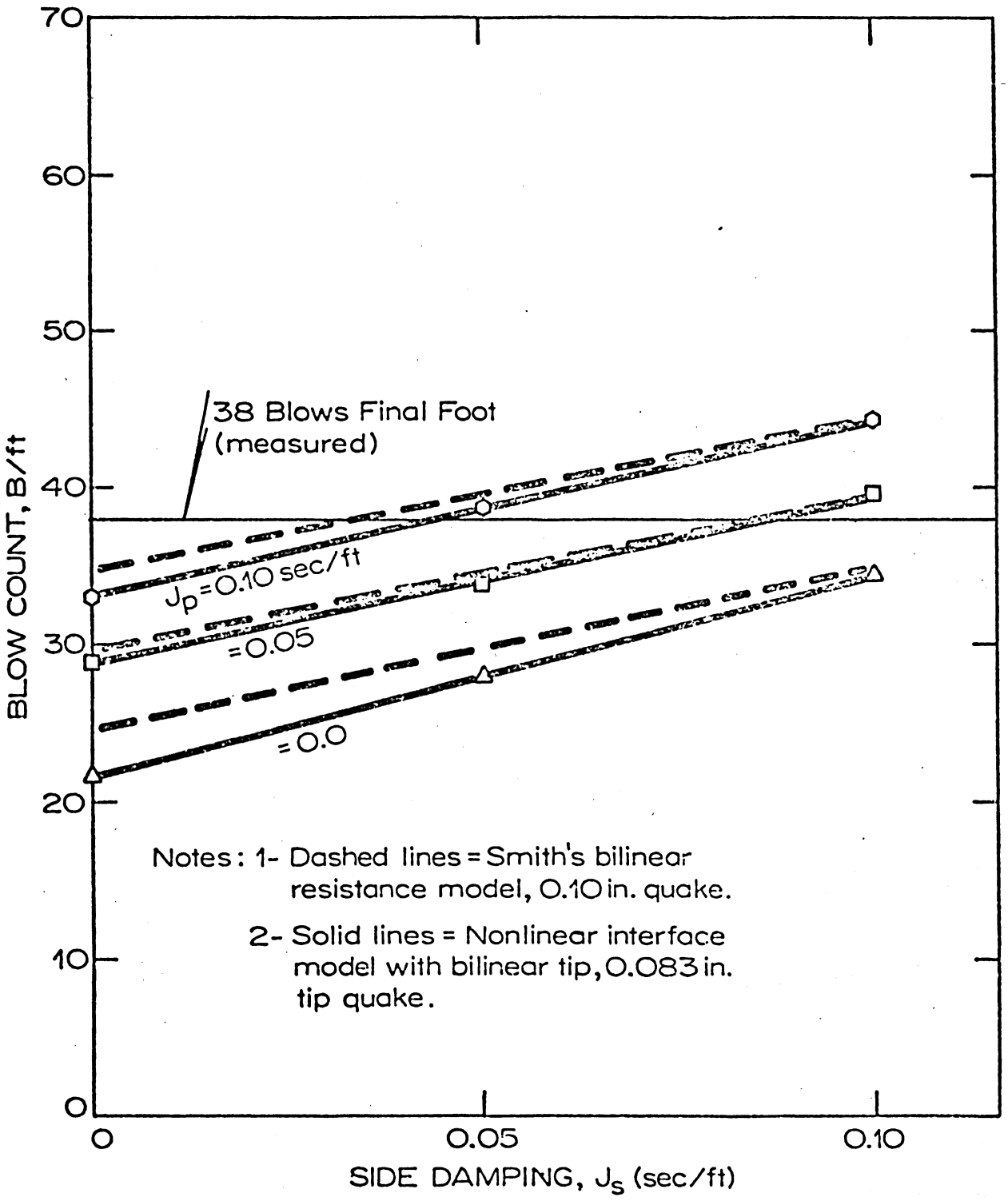

Figure V-1. Pile Driving Results: Evaluation of Damping Affects on Predicted Blow Count, LD4TP2.

correlates with blow count exactly. These values are in no way unique, though a general range may be defined for them. It is interesting to note that the use of bilinear interface deformation properties makes little difference in the predicted blow counts versus those obtained using the nonlinear model.

In addition to blow count, a second measurement for which correlations from the BUKFOR analyses could be made concerns the residual point load. Figure V-2 presents damping correlation data for residual point load using both the bilinear and nonlinear resistance models. These data suggest that the actual field behavior lies somewhere between these two assumptions. From these results and subsequent static analyses the nonlinear deformation model was chosen for the remaining analyses. By correlating damping values directly with blow count and selecting a pair of J_p, J_s values best fitting the residual point load, values of J_p = 0.10 sec/ft and J_s = 0.05 sec/ft, were used for LD4TP2 analyses. Values of J_p and J_s obtained in this manner for all the LD4 piles are listed in Table V-5.

It is interesting to note that the initial tangent quake value listed in Table V-5 satisfy the relationship $QUAKE_p$ = 0.05 in/ft of pile diameter for impact driven piles. These data are reasonably consistent with hyperbolic fits of LD4 tip load transfer measurements. Since the measurements start from a substantial residual point load for all but LD4TP10, the initial portion of the load-displacement curve is unknown. Thus, the hyperbolic fit of the measured data is a rough approximation.

Static load-displacement behavior at the tip was modeled as the hyperbola defined by the initial tangent stiffness ($Q_p/QUAKE_p$) and the

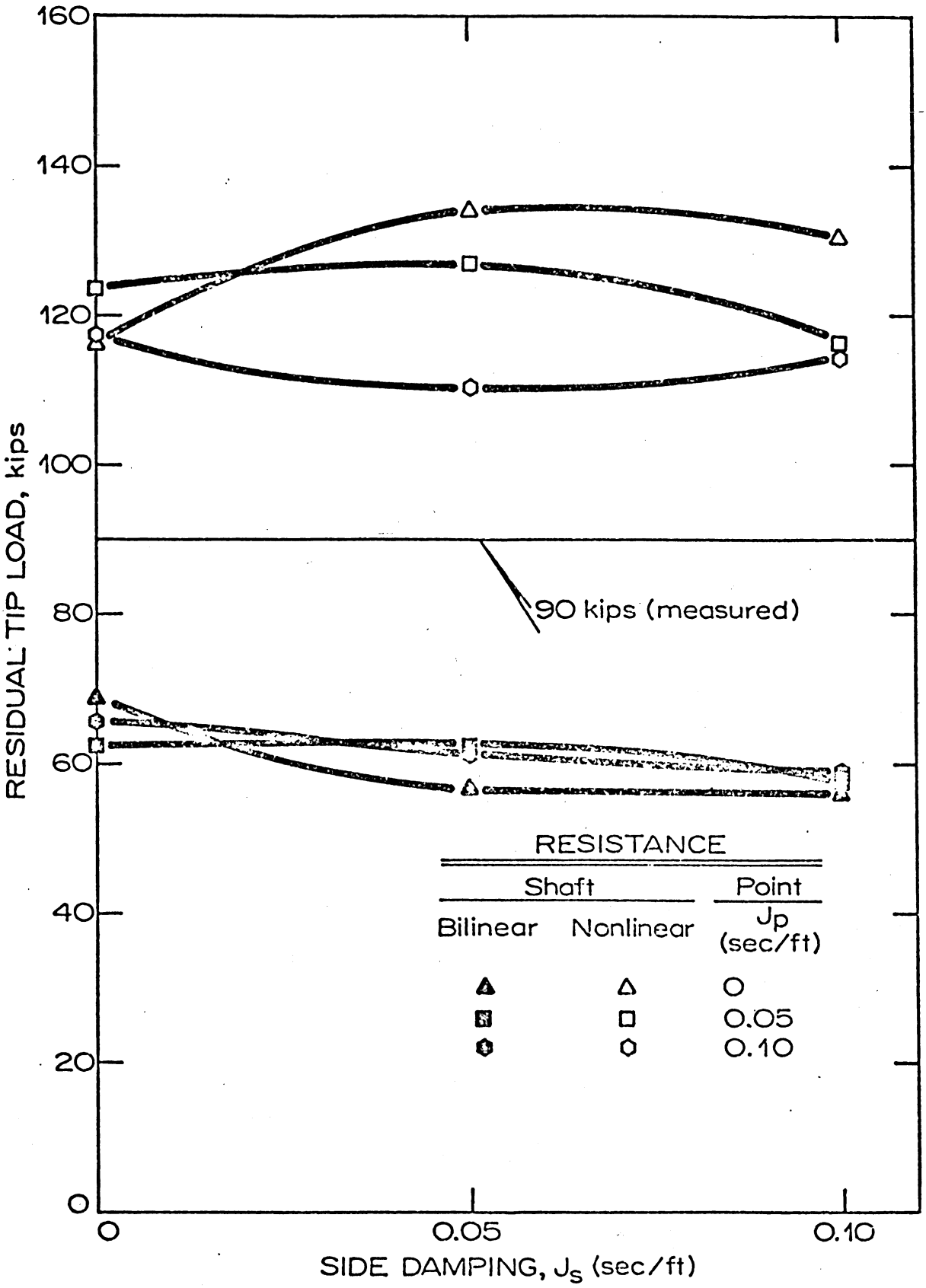

Figure V-2. Pile Driving Results: Evaluation of Damping Affects on Predicted Residual Point Load, LD4TP2.

Table V-5

SOIL PARAMETERS EMPLOYED IN THE PILE TEST ANALYSES, LD4

Test Pile	CORRELATED DAMPING PARAMETERS		ASSUMED INITIAL TANGENT QUAKE
	J_p (sec/ft)	J_s (sec/ft)	QUAKE $(in.)^p$
1	0.0	0.05	0.056
2	0.10	0.05	0.083
3	0.10	0.05	0.100
10	—	—	0.325
16	0.10	0.13	0.083

horizontal assymptote, point capacity Q_p. During driving the static component of tip stiffness is assumed equal to the unload/reload stiffness (bilinear). In lieu of any data it was assumed equal to the initial tangent stiffness. Preliminary analyses indicated that the use of the hyperbolic loading stiffness at the start of driving converged to the same solution as that using the bilinear tip stiffness, but twice as many hammer blows were required.

One more point that cannot be overemphasized is that the shaft resistance and point capacity values used for the pile driving analyses throughout are values adjusted for residual tip loads. For LD4TP2 the lateral earth pressure coefficients $K_s^c = 0.906$, $K_s^t = 0.802$ and tip capacity $Q_p = 240$ kips (see Table V-3) were all input to the pile driving analyses. This is particularly significant in terms of predicting residual load distributions and load test behavior.

Load Test Analysis

Using the correlated damping parameters the dynamic analysis was repeated for LD4TP2. At the end of each hammer blow static equilibrium is established. For the dynamic/static analysis this static equilibrium condition at the end of simulated driving after the fifth blow defines the initial residual stress state for the load test simulation. The maximum applied load to LD4TP2 was 502 kips. The load was applied in cyclic compression to failure. Cyclic load test simulation was performed using unload/reload cycles at 100 kip intervals (as used in the pile test) up to 475 kips. Load-displacement predictions using DUKFOR with hyperbolic and bilinear deformation models are shown in figure V-3, along with the

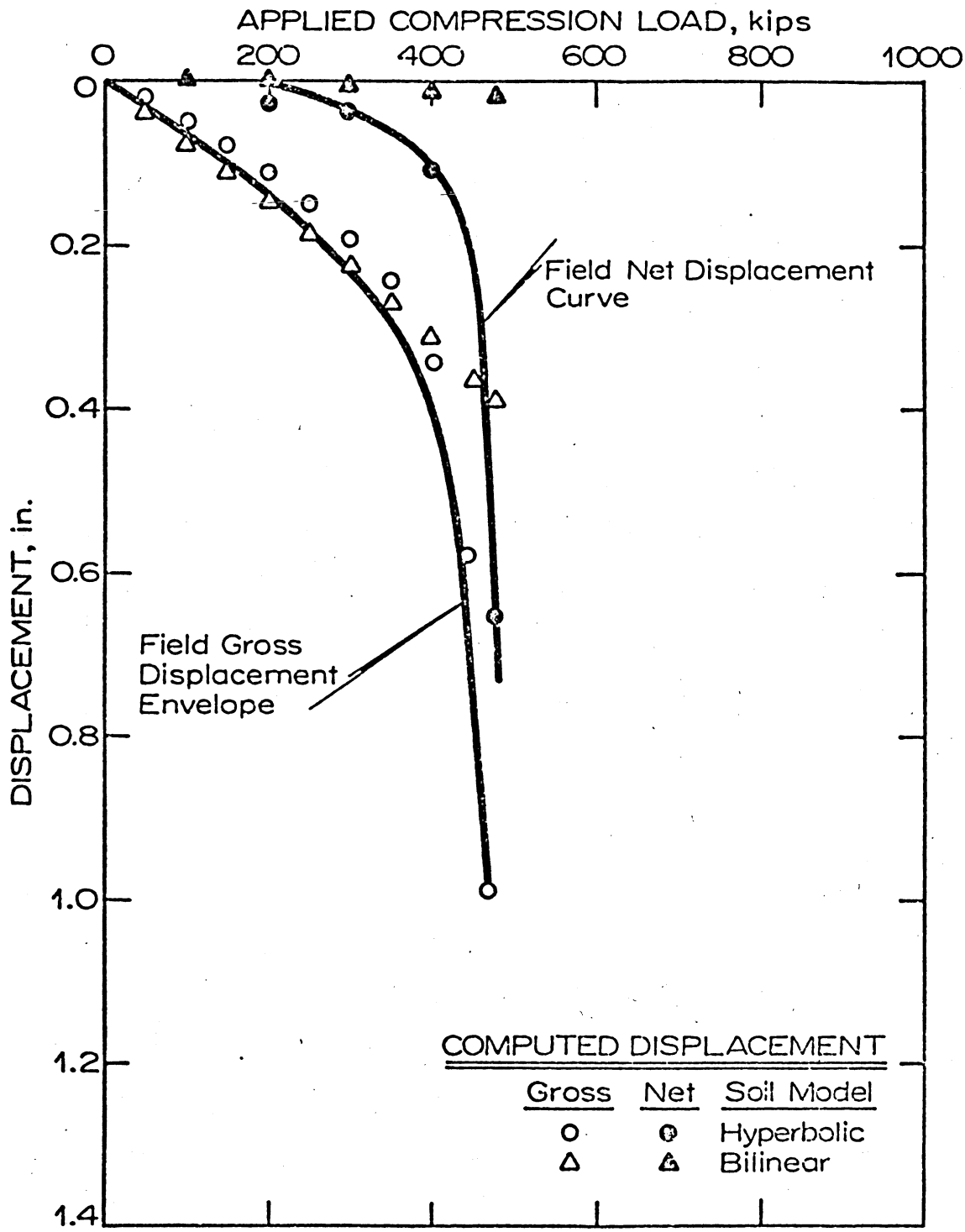

Figure V-3. Cyclic Compression Test Results: Load-Displacement Data; Nonlinear Versus Bilinear Resistance Models, LD4TP2.

field measurements.

The load-displacement predictions using either soil model indicate close agreement with field-measured gross displacements in the initial linear portion of the curve. At higher load levels the bilinear model is less accurate. However, the nonlinear model does remarkably well throughout the load range. In terms of net displacements (permanent settlement upon unload) the nonlinear deformation model yields acceptible agreement with field observations. The bilinear representation gives only a poor estimate of net settlements.

A second comparison with observed data may be made between the mobilized and adjusted bearing capacity parameters. In order to demonstrate these concepts a static only DUKFOR analysis (assumed initially "stress free" pile) was made using mobilized parameters (K_s^c = 1.22, K_s^t = 0.906, Q_p = 150 kips.) One would expect that the stress free initial conditions and mobilized resistance parameters would give essentially the same load-displacement behavior as the driven pile case using parameters adjusted for residual point load, since the mobilized resistance to penetration during loading are essentially the same. This expectation is realized in figure V-4. Both gross and net displacements describe almost identical values for each set of assumptions. These predictions corroborate the statements made in Chapter III regarding the effects residual loads have on load test interpretation (see figure III-4). Without adjustment for residual loads the coefficient of lateral earth pressure at (compression) failure, K_s^c, is overestimated by 35 percent. The tip capacity Q_p is underestimated by 38 percent. Reliable design estimates of K_s^c and Q_p for LD4TP2 are only obtained by correctly accounting for residual driving load at the point.

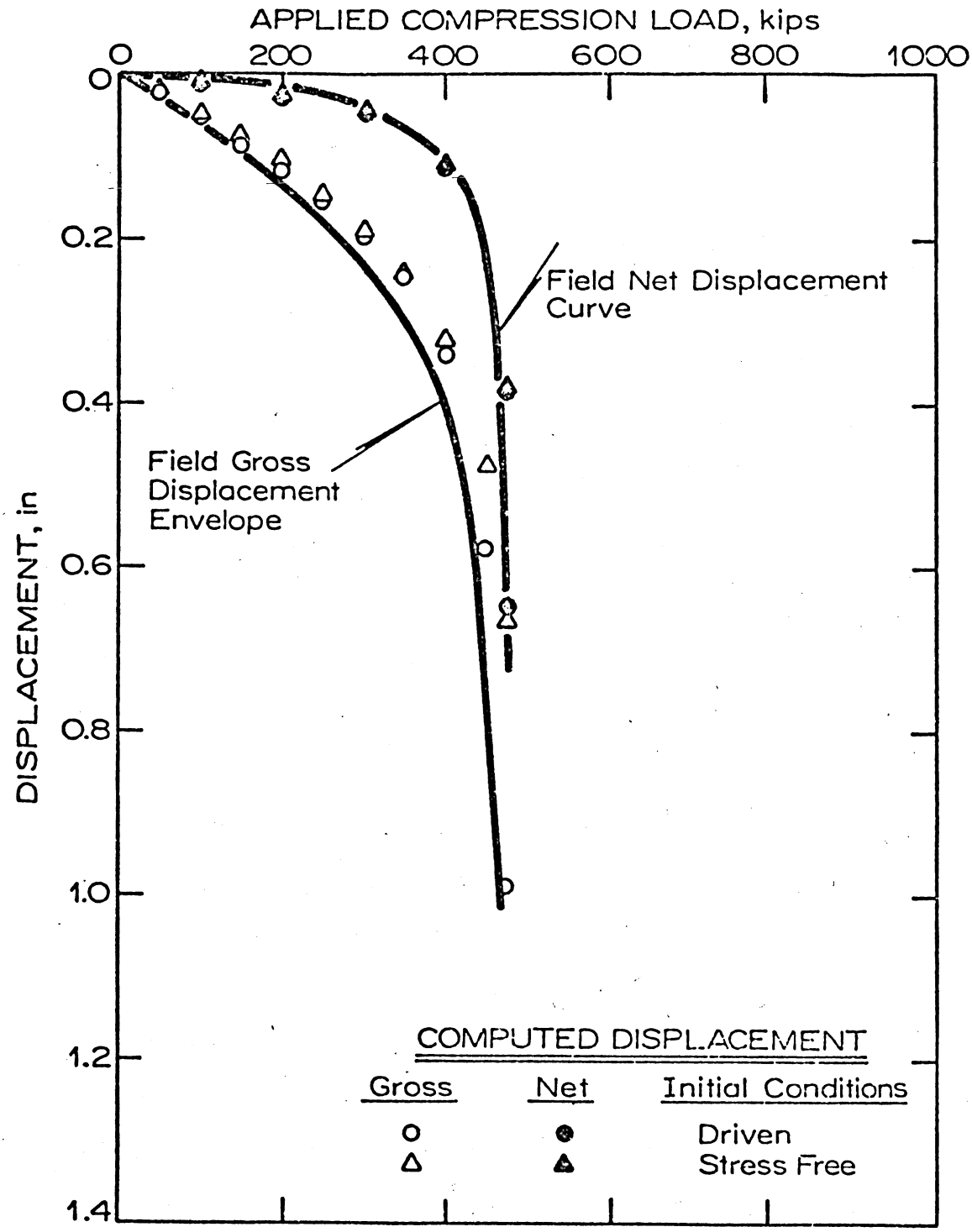

Figure V-4. Cyclic Compression Test Results: Load-Displacement Data; Driven Versus Stress-Free Initial Load Test Conditions, LD4TP2.

The interpretation of load distribution data was discussed in Chapter III using figure III-4. The effects of residual driving loads on compression load distribution measurements were described in detail. Essentially, residual driving loads are subtracted from the actual load distribution to obtain what was called a "mobilized" load distribution. For the LD4 pile tests the instrumentation was zeroed at the start of the compression load test such that measurements should resemble mobilized distributions. As no measurements of residual driving loads were made, the true shape of any load distribution curve remains unknown.

In analyzing the pile driving/cyclic compression/cyclic tension test, DUKFOR predicts load distribution data. Since the dynamic/static analysis option of DUKFOR incorporates residual driving loads as the initial load test conditions, the predicted load distribution data should correspond to the actual pile load distribution, not the measured (mobilized) data. DUKFOR dynamic/static load distribution results for LD4TP2 are shown in figure V-5 as computed data. Curve (0) is the predicted residual driving load at the start of the compression test. Curves (1) and (2) are predictions of the actual pile load distributions at 200 kip and 400 kip applied load, repsectively. In order to obtain an estimate of the measured (mobilized) load distributions one must plot the difference between the curves (1) and (2) and the residual driving load distribution curve (0). The predicted mobilized curves are shown as (1M) and (2M), respectively, in figure V-5. Curves (A) and (B) are drawn through strain rod/strain gage field measurements reported by FRUCO and Associates.[86] The field-measured data are also included in figure V-5.

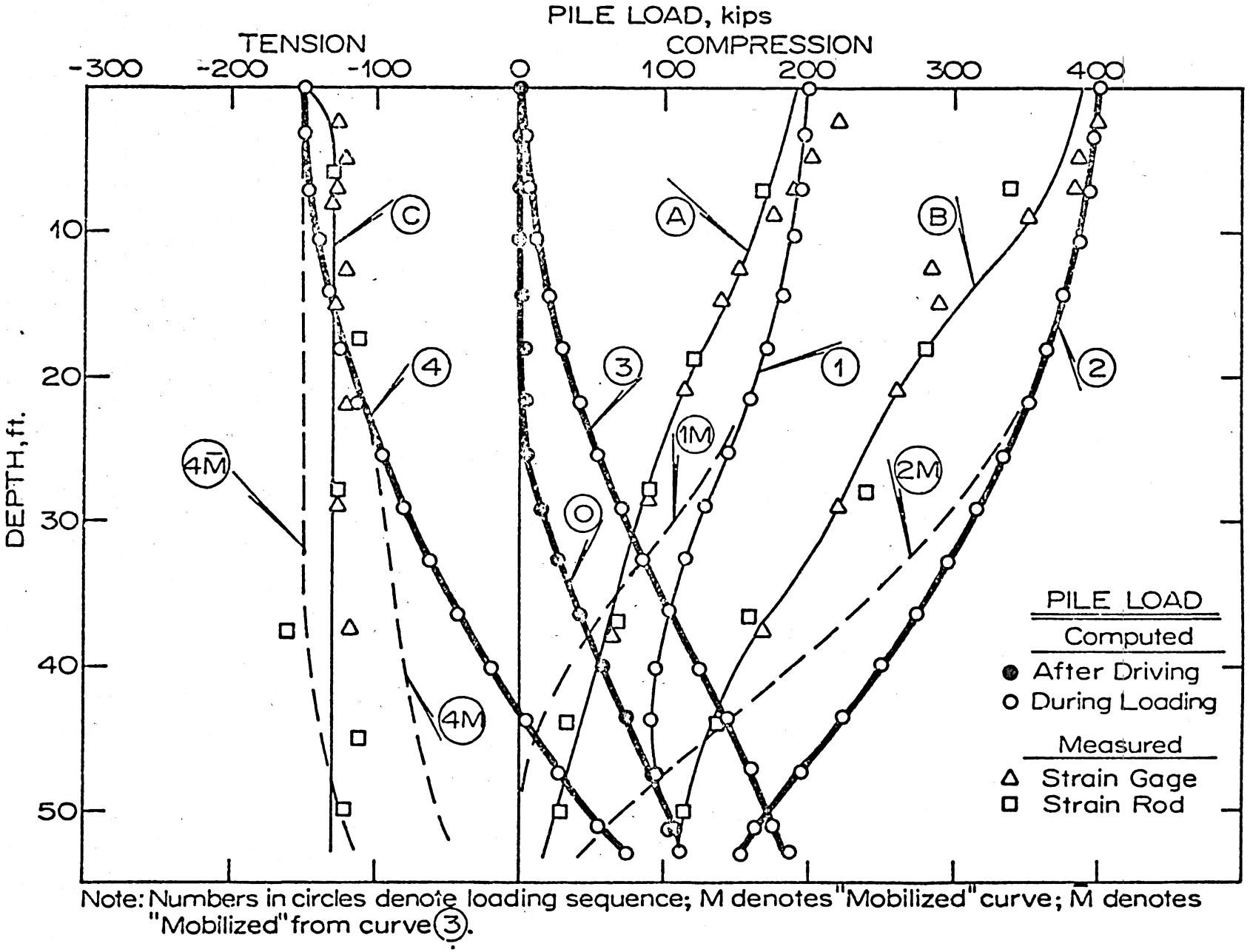

Note: Numbers in circles denote loading sequence; M denotes "Mobilized" curve; $\bar{M}$ denotes "Mobilized" from curve (3).

Figure V-5. Pile Test Results: Load Distribution Data, LD4TP2.

Comparison of the predicted mobilized load distributions and the field measurements indicate fair agreement, in general. Differences between curves (A) and (1M) in the upper half of the pile increase with the higher applied load, as shown between curves (B) and (2M) . This tendency suggests that the load transfer mechanism in the field increased in the upper portion of the pile at higher applied compression loading. This observation was noted by Vesić[59] in a state-of-the-art review which included LD4 pile test results. The trend suggests that unit skin friction increased in magnitude rather than reaching a constant failure level (as assumed by DUKFOR methods.) This point will be clarified in a subsequent discussion of AXISYM results.

Cyclic tension test analyses were performed using three separate sets of assumptions: (1) a sequence of driving/cyclic compression-cyclic tension testing simulation (D/CC-CT), which most closely represents the field behavior; (2) assuming an initially stress free pile with mobilized K_s^c and Q_p values which is loaded first in cyclic compression, then in cyclic tension (SF/CC-CT); and finally, (3) an initially stress free pile which is loaded only in cyclic tension (SF/CT).

The results of the cyclic tension test analyses are plotted in terms of load-displacement behavior in figure V-6. The load-displacement predictions for the first two cases, (D/CC-CT) and (SF/CC-CT) are essentially similar since the initial conditions at the start of the cyclic tension test are quite similar. These predictions agree reasonably well up to about -100 kips, whereafter the field behavior shows increasingly greater displacements than DUKFOR predicts. The tension test response of the DUKFOR model is too stiff. There appears to be a softening tendency of

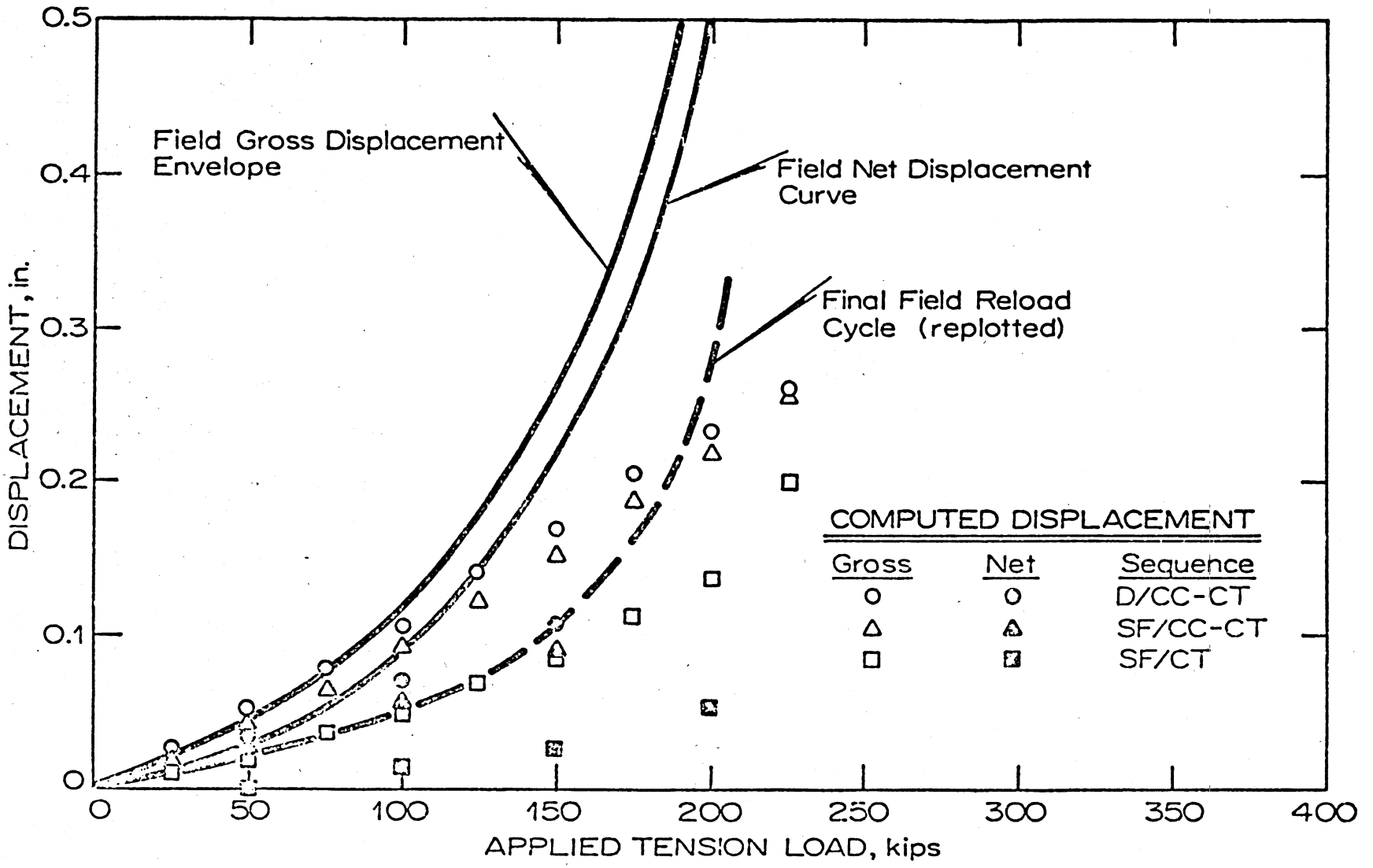

Figure V-6. Cyclic Tension Test Results: Load-Displacement Data, LD4TP2.

the system at higher tension loads/displacements.

The third case (SF/CT) provides a direct estimate of the effect of residual compression stresses on tension test performance. Residual compression forces cause much of the skin friction in the upper section of the pile to be acting downward at the start (negative slope of the compression unload curve, figure V-5). When tension load is applied the upper portion of the pile cannot "mobilize" as much resistance, causing the mobilized shaft resistance to develop deeper, see figure III-4b. As a result, for cases D/DD-CT and SF/CC-CT, the elastic deformations of the pile are greater near the top, causing noticeably greater measured displacements than the SF/CT (having no residual compression stresses) assumptions will predict.

Further evidence to support this argument is offered by comparison of the SF/CT test predictions with the final field reload cycle. Prior to the last load cycle the pile has been loaded almost to failure in tension and then unloaded. As a result the residual compression forces will have been "unloaded" and the initial conditions for the final tension load cycle would probably involve primarily residual tension forces at depth along the pile. The shaft friction sustaining residual tension forces would act upward on the pile near the pile butt. Subsequent application of tension load would yield substantially less displacement than the gross displacement curve. The SF/CT test predictions, therefore, give the best estimate of the reload cycle behavior. This observation was cited previously in static analyses using the code FDFOR.[2]

The comparison of measured versus predicted tension load distribution data is included in figure V-5. Curve (4) describes the -150 kip load results for the loading cycle determined in case D/CC-CT. As before, the field data should agree with the DUKFOR prediction curve minus the residual distribution curve corresponding to the gage zero stage of the test. Two occasions for zeroing the gages are possible: continuous reading from the start of the compression test (residual load curve (0)); and zeroing values at the start of the tension test (residual load curve (3)). Using Curve (0) Curve (4M) is obtained. If Curve (3) is used one finds Curve (4$\bar{M}$), instead. In either case the data describes a "mobilized" load distribution curve. Curve (4$\bar{M}$) approximately predicts the measured data, curve (c). For LD4TP2 it appears that the gages were rezeroed at the start of the tension test since curve (4$\bar{M}$) provides the closer agreement.

Summary

DUKFOR analyses of LD4TP2 indicate that the dynamic/static procedure provides an effective model of the pile-soil interaction problem. The predictions of compression load-displacement behavior are quite good. Discrepancies between predicted and measured load distribution data suggest a more complex response of the physical system than that assumed using DUKFOR. The analyses of cyclic tension test behavior demonstrate the profound influence of residual compression loads on the load-displacement behavior. The differences between predicted and measured displacements indicate that the physical pile-soil system behaves in a "softer" manner as the load level approaches the failure load. Analyses of LD4TP2 using the axisymmetric idealization of AXISYM can help to explain these differences. ASIXYM results are discussed in the following paragraphs.

AXISYM Analysis: LD4TP2

The code AXISYM was described in detail in Chapter IV. The pile-soil interaction problem has been analyzed using axisymmetric finite element (FE) techniques in previous investigations. Ellison[55] used "dimensionless" point spring elements (rigid-plastic slip behavior) to describe response at the pile soil interface and across the horizontal plane at the pile tip. The spring elements adjacent to the pile tip permitted the soil elements to "fail" in tension and propagate a tensile crack. Desai and his colleagues[56,75,88,89] used joint elements to describe the pile-soil interface behavior using interface shear test deformation properties. All of these studies demonstrate effective applications of the FE technique in modeling the physical problem.

The primary difference between the previous FE analyses and these discussed in this presentation is the simulation of punching of the pile point into the soil beneath it. This is accomplished by the FE mesh design shown in figure IV-3. Note that joint elements are used to describe the pile-soil interface behavior. A row of "soil-soil" interface elements are used in the horizontal plane at the pile tip elevation, and a vertical column of soil-soil interface elements extend into the soil beneath the pile point. These soil-soil interface elements are assigned high shear stiffness values prior to failure, providing a near continuous deformation across the element boundaries. The average friction angle of the soil ($\phi = 32°$) is assigned as the soil-soil interface friction angle. Once the shear stresses exceed the Mohr-Coulomb strength for these elements the interface shear stiffness values are reduced to one-thousandth the original values, such that relative slip develops between the adjacent soil elements.

In this manner a punching effect is simulated.

The FE mesh described in figure IV-3 contains 254 nodes, 33 joint elements, 16 pile elements and 167 soil elements (216 elements in all). Parameters obtained from laboratory interface shear tests of LD4 sand-on-steel were used as the pile-soil interface properties (see Appendix). As discussed previously, in lieu of LD4 sand triaxial test data, values obtained from triaxial tests on JLD sand were used herein.

LD4TP2 AXISYM analyses model the pile using solid elements having equivalent axial stiffness, using a circular section having a perimeter equivalent to the actual pile. This is necessary to correctly account for the surface area of the channels protecting the instrumentation, see Table V-1. The tip element is thus larger in bearing area than the physical pile. If one assumes that the point bearing scale effects are negligible, the applied load may be reduced to account for the difference between assumed and actual tip bearing areas. The AXISYM load-displacement predictions employ this assumption.

The in situ dry densities reported from the pile test site ranged between 109 pcf and 90 pcf with a rough estimate of an "average" dry density on the order of 105 pcf, which corresponds to 81 percent relative density. Thus the deformation properties of 80 percent relative density JLD sand were assumed. Assuming a high degree of compaction near the pile shaft, the pile-soil interface shear parameters for 100 percent relative density LD4 sand-on-steel were used for the driven pile.

AXISYM is a static solution method exclusively, such that residual driving stresses could not be obtained using this approach. Thus, an

initially stress-free pile having the mobilized K_s^c value throughout the soil system was assumed in order to account for the manner in which skin friction resistance was developed in the field. To simplify the FE idealization the water table was assumed at the soil surface, though it was recorded at 2 to 3 ft depth throughout the load test. In all the DUKFOR analyses of LD4 pile tests Z_w was assumed at 2 ft.

AXISYM compression load-displacement predictions for LD4TP2 are described in figure V-7 along with the DUKFOR results (D/CC-CT case). The AXISYM results are basically similar to LD4TP2 predictions given by Desai.[75] The AXISYM results describe a slightly softer pile-soil system response than DUKFOR predicts. This is due, in part, to deformations in the adjacent soil mass, which were not included in the DUKFOR analysis assumptions. Alghouth K_s^c was applied in the "gravity turn-on" step, the small (but necessary) pile-soil interface stiffness caused the soil to "hang up" on the stiffer pile. As a result the computed $\bar{\sigma}_v$ stresses in the soil elements near the pile were less than the computed in situ overburden stresses. As a result, assignment of $\bar{\sigma}_n = K_s^c \bar{\sigma}_v$ in the interface elements ($\bar{\sigma}_v$ for the soil element immediately adjacent to the pile shaft) caused the ratio of $\bar{\sigma}_n$ to in situ effective overburden pressure to be less than K_s^c. In figure V-8 this ratio is described as K_s^o. The AXISYM values of $\bar{\sigma}_n$ in the interface elements start out lower in magnitude than assumed in DUKFOR.

An interesting point shown in figure V-8 is a tendency for the magnitude of $\bar{\sigma}_n$ to increase with increasing applied compression load. The load transferred to the soil increases as the confining (and normal) stress levels increase, exhibiting a strain-hardening behavior resembling that noted in figure V-5. Figure V-9, however, indicates that in spite of the

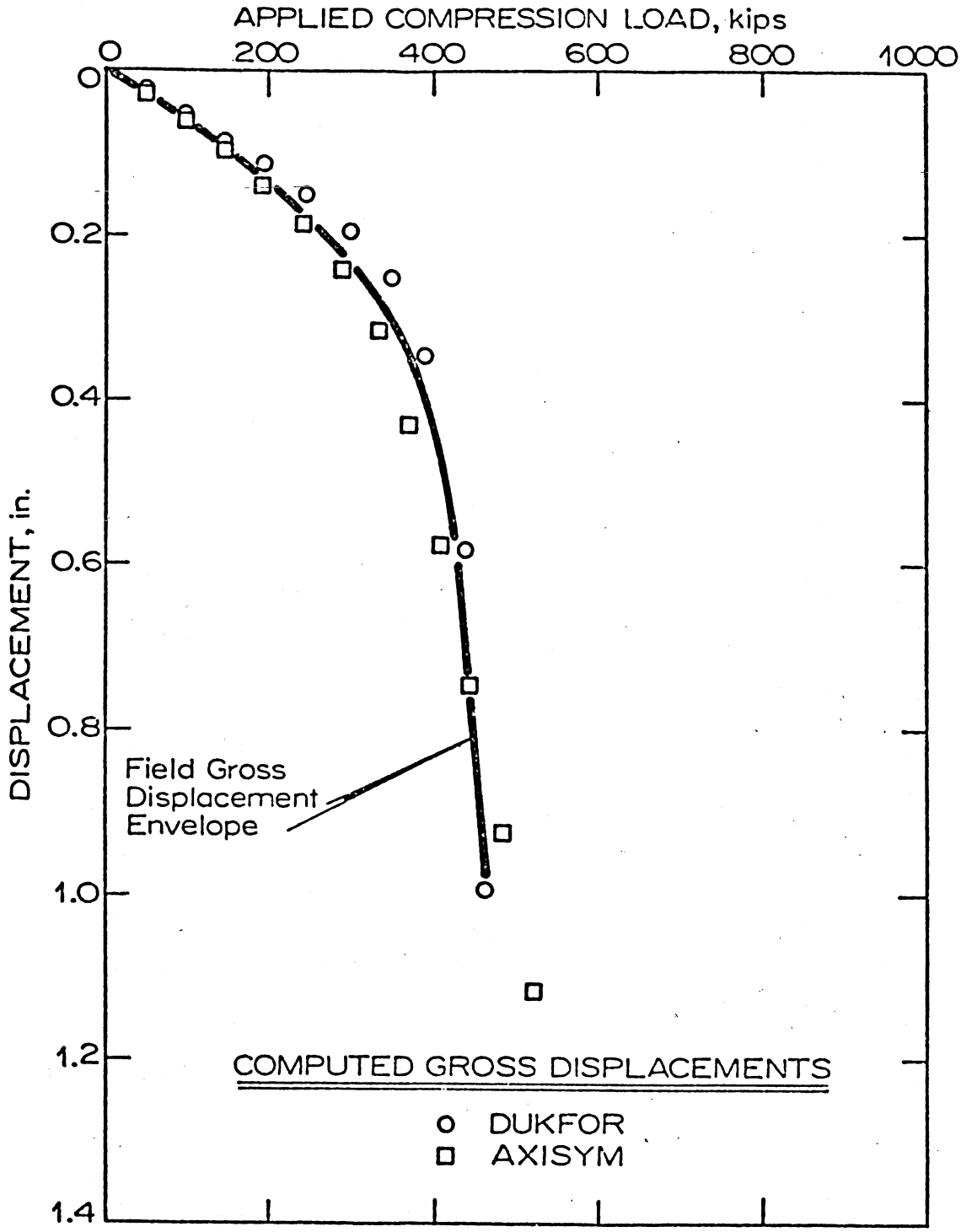

Figure V-7. Cyclic Compression Test Results: Load-Displacement Data; AXISYM versus DUKFOR, LD4TP2.

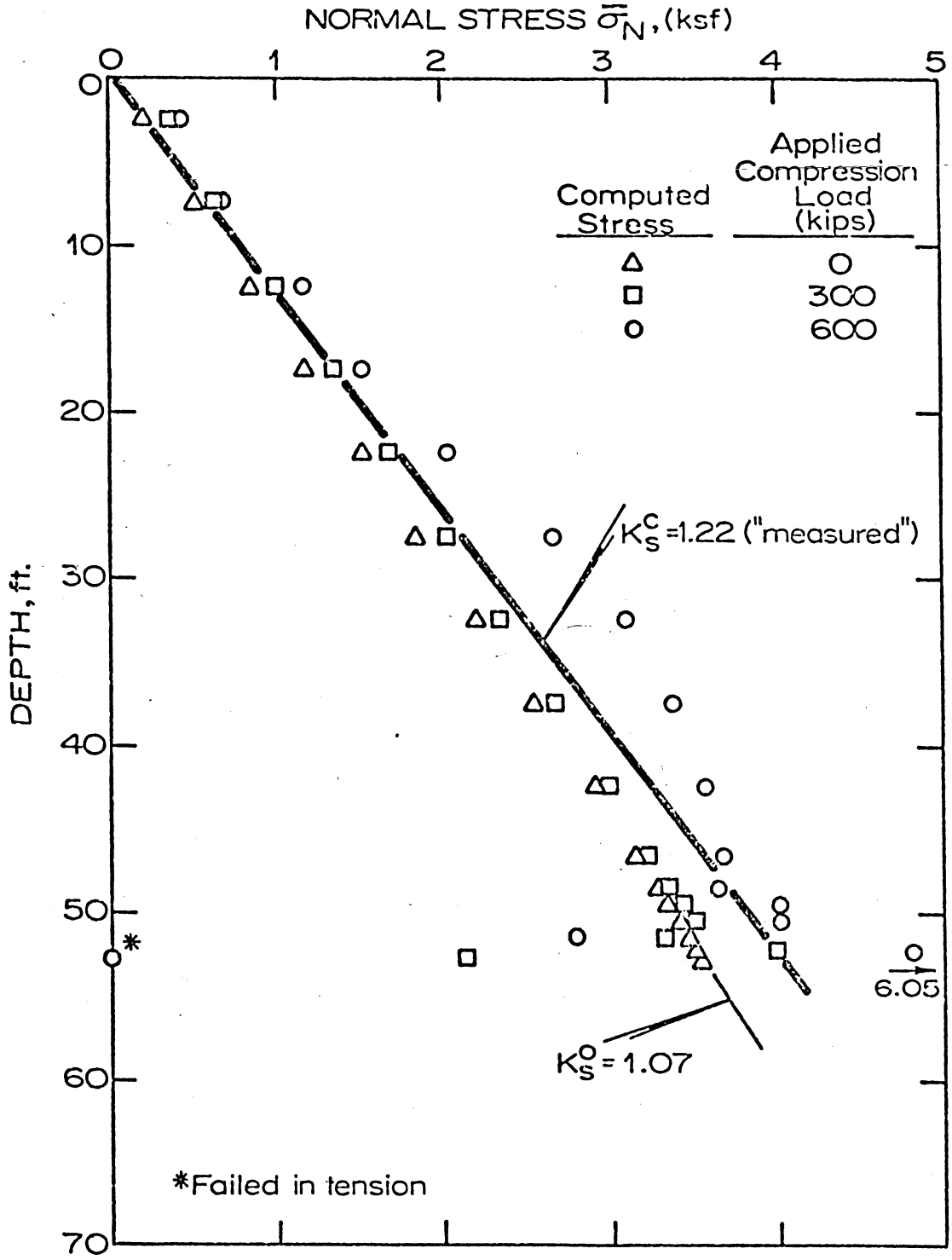

Figure V-8. Cyclic Compression Test Results: AXISYM predictions of Pile-Soil Interface Normal Stress Distribution, LD4TP2.

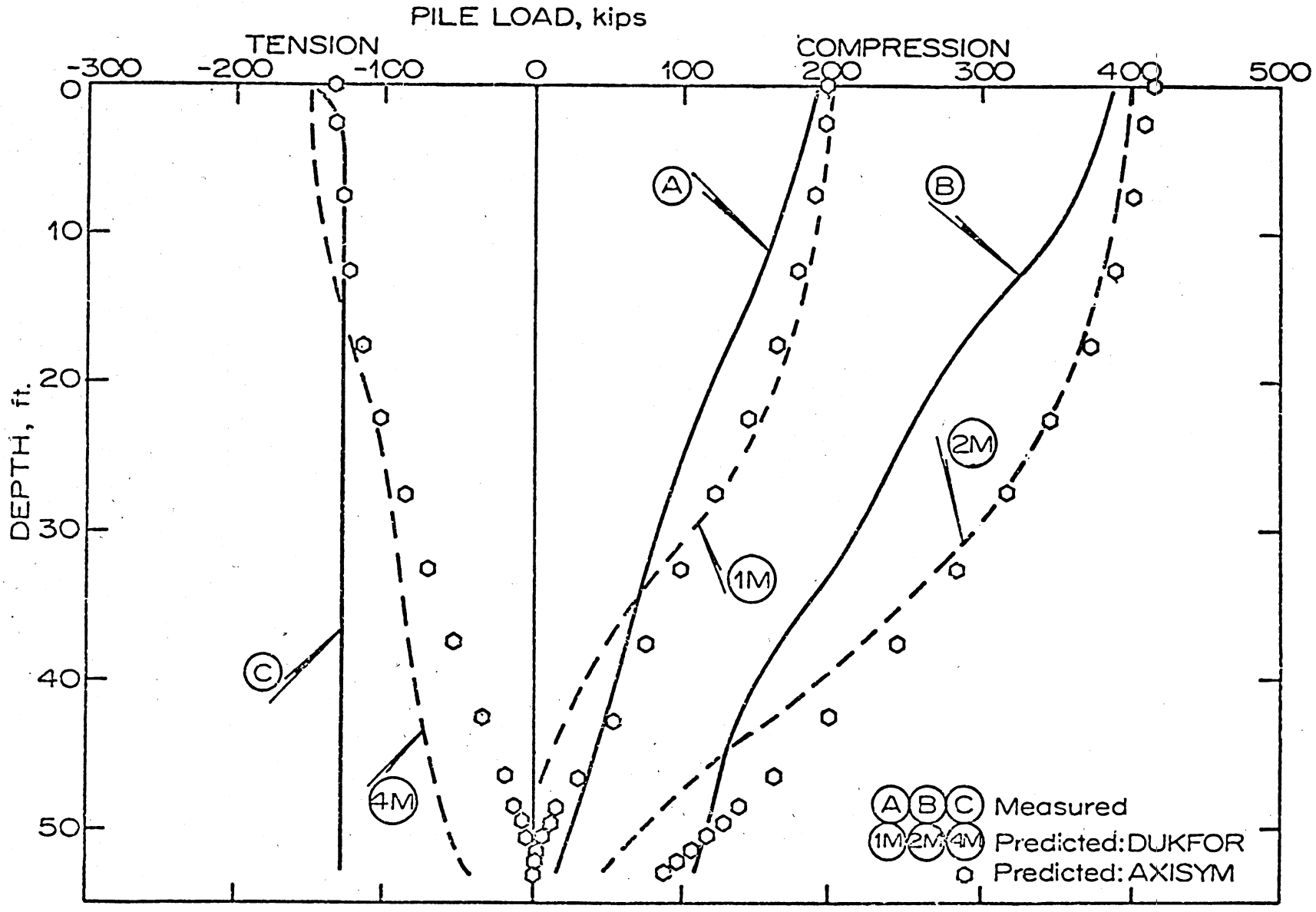

Figure V-9. Pile Test Results: Load Distribution Data; AXISYM Versus DUKFOR, LD4TP2.

increase in $\bar{\sigma}_n$ the AXISYM predictions of load distribution show discrepancies with field measurements similar to the DUKFOR predictions. The curves drawn in figure V-9 are the same as those given in figure V-5. It is extremely interesting to note that the "mobilized" curves from DUKFOR (D/CC-CT) in compression give predictions quite similar to results obtained using AXISYM with mobilized parameters. This apparent strain-hardening behavior is not properly modeled by either analytical method.

With these observations in mind one would expect that AXISYM analysis of tension test behavior will demonstrate a reduction in $\bar{\sigma}_n$ due to vertical stress relief near the pile shaft. Figure V-10 describes AXISYM and DUKFOR results assuming an initially stress-free pile. The predictions should most closely resemble the replotted final reload cycle (which is free of residual compression loads). AXISYM predicts greater displacements closer to the reload cycle data than those predicted by DUKFOR. Figure V-11 demonstrates the tendency of $\bar{\sigma}_n$ to decrease with increasing tension loads, a kind of strain-softening behavior. Note that in figure V-10 the relative effects of residual compression loads on the gross displacement behavior in tension are quite significant. This is due to the manner in which the shaft resistance is mobilized with depth, see figure III-4 and the accompanying discussion. The axisymmetric idealization does not properly account for these residual loads and, therefore, it is limited in this respect.

AXISYM results provide data describing the behavior in the vicinity of the tip during compression loading. Figure V-12 describes the change in normal (vertical) stress in the horizontal plane of soil-soil interface elements at the pile tip elevation. The initial conditions

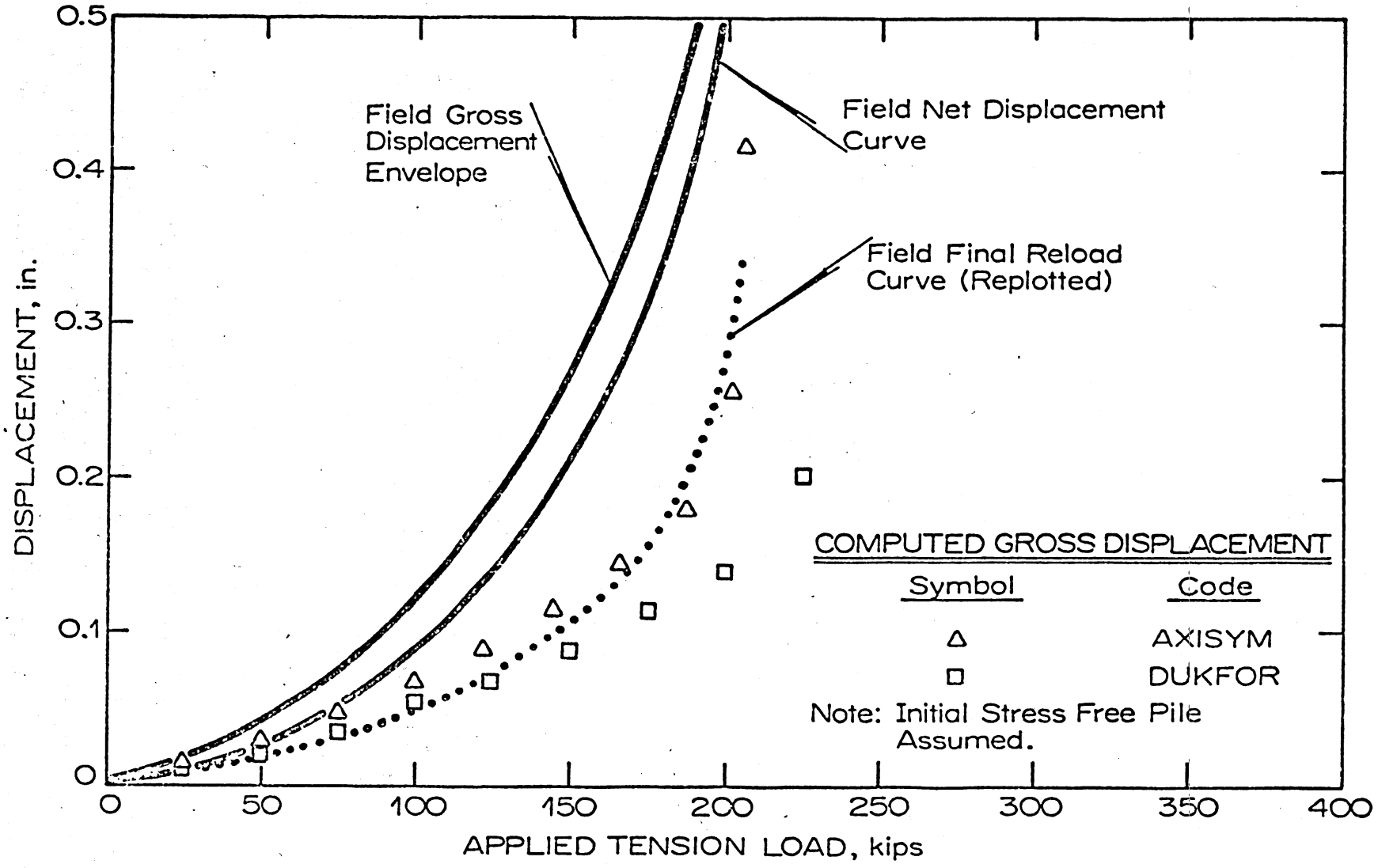

Figure V-10. Cyclic Tension Test Results: Load-Displacement Data; AXISYM Versus DUKFOR, LD4TP2.

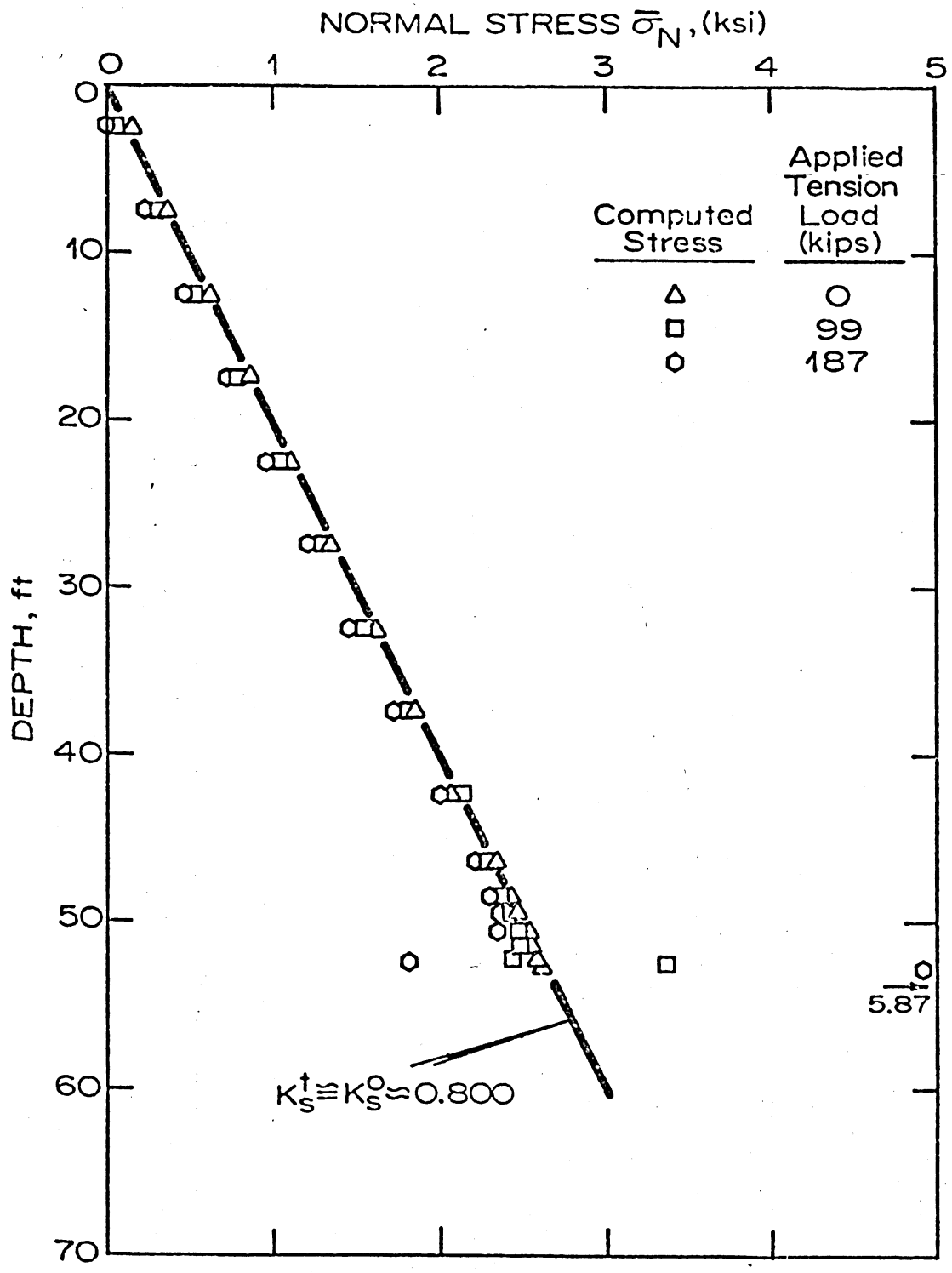

Figure V-11. Cyclic Tension Test Results: AXISYM Predictions of Pile-Soil Interface Normal Stress Distribution, LD4TP2.

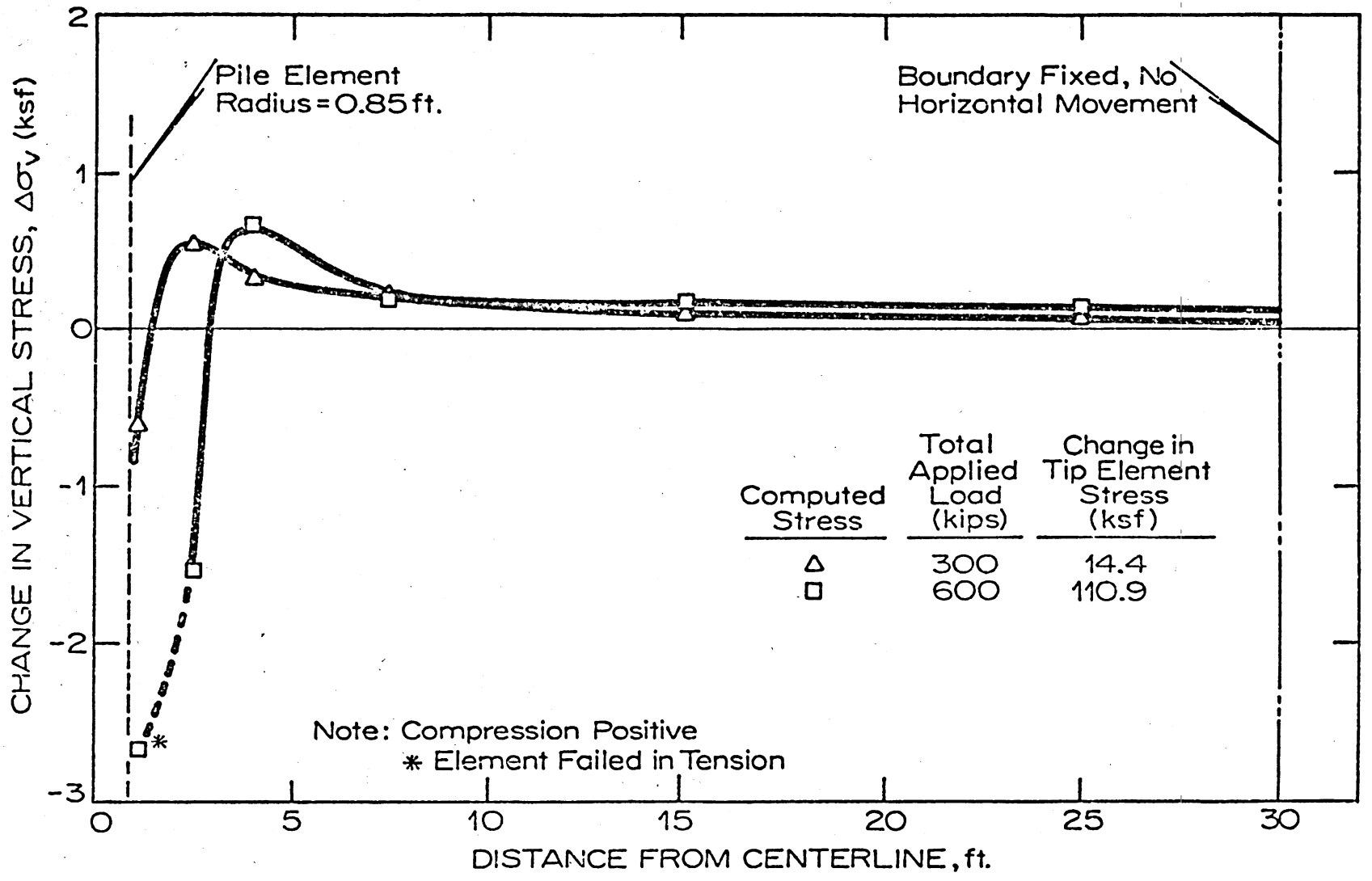

Figure V-12. Cyclic Compression Test Results: AXISYM Predictions of Normal Stress on the Horizontal Plane at the Pile Point, LD4TP2.

(zero change) are approximately the in situ overburden stresses. The extension phenomenon immediately adjacent to the pile tip is clearly demonstrated by the decrease in vertical stress in the first interface element. With increasing radius, however, the transmission of compression stresses due to shaft load transferred above the tip causes an increase in vertical stress. As penetration proceeds AXISYM predicts that the extension zone widens and tensile strains increase.

These data clearly demonstrate the complex nature of the tip bearing capacity problem. The in situ effective overburden stress at this depth is approximately 3.5 ksf. The predicted changes in vertical stress shown in figure V-12 are, therefore, relatively large. In the actual field problem the magnitudes of these stresses are, no doubt, a function of stress/strain history, pile-soil system geometry, shear strength and deformation properties in the vicinity of the point. There is no bearing capacity theory which rationally incorporates all these factors.

A final item of importance concerns the stress distribution beneath the pile point. AXISYM predictions of vertical stress distribution along the soil element centroids beneath the FE pile point are given in figure V-13. Results at two applied load levels are plotted in terms of the change in vertical stress. Boussinesq's solution for the vertical stress distribution in a semi-infinite linear elastic half space is also plotted for the higher tip load (as determined at the same locations.) Note that the AXISYM results exceed Boussinesq's values by as much as a factor of 2 between 2 ft and 10 ft (1 and 6 pile diameters) beneath the tip. The Boussinesq values plotted in the figure neglect the shaft load transferred through the soil and also neglect the response of the soil

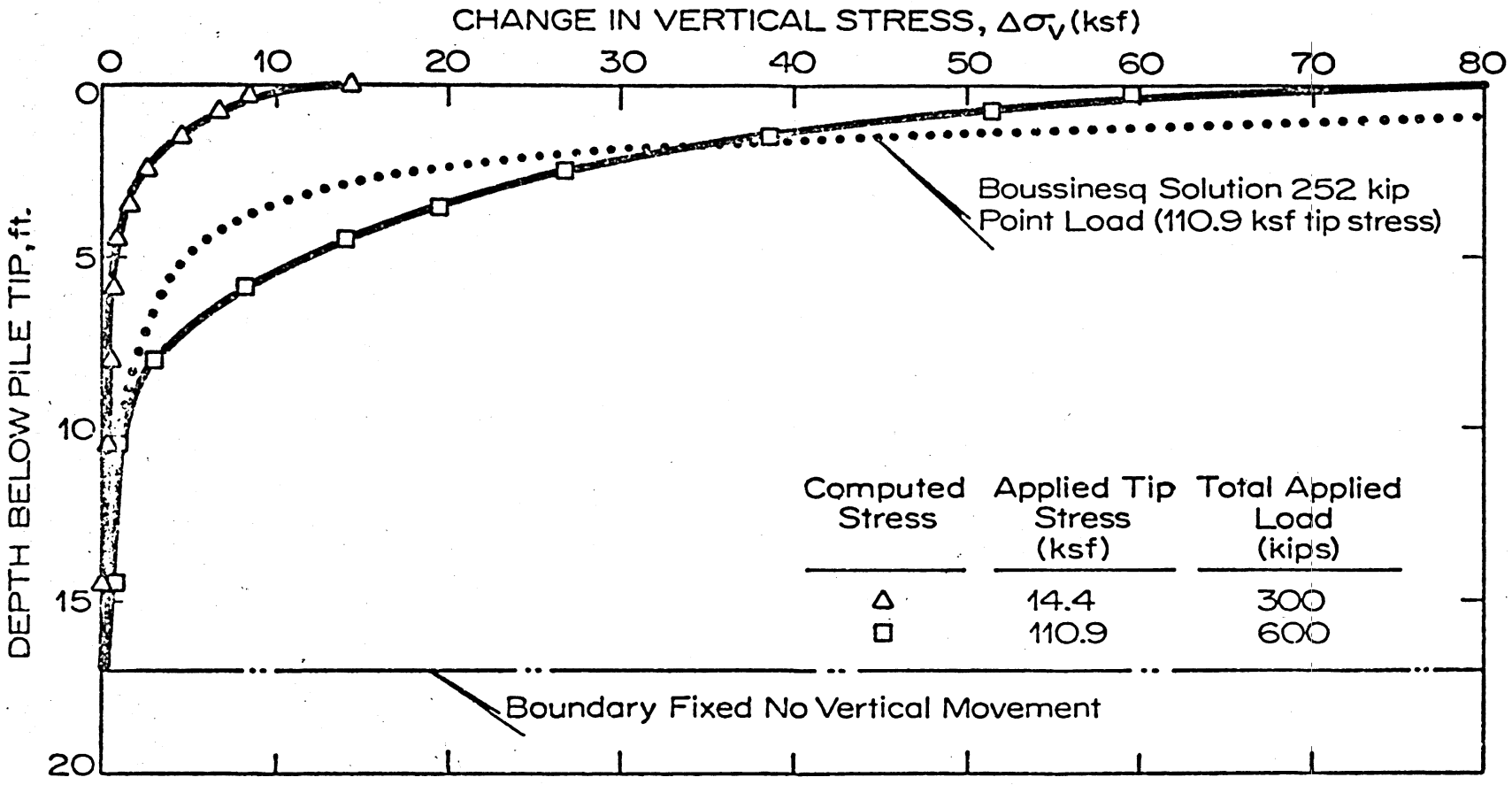

Figure V-13. Cyclic Compression Test Results: AXISYM Predictions of Vertical Stress Distribution Beneath the Pile Point, LD4TP2.

above the pile point. These two effects should neutralize one another to some extent. Boussinesq's solution typically is assumed to be conservative (predicting higher stresses) for this purpose, since it neglects the effects of overburden materials. Mindlin's solution would predict essentially half the Boussinesq results due to point load alone. Neither of these methods appears to predict as high stresses, and therefore, as large displacements as the AXISYM model describes.

It appears that the consideration of nonlinear deformation properties, and more importantly, punching failure conditions beneath the pile point transmit compression stresses deeper than the elastic solution permits. Tip settlement predictions at higher load levels should differ more from the Boussinesq distribution than at lower levels. This observation has its greatest importance with piles designed for end bearing. Piles having appreciable (positive) skin friction resistance will generally not transmit much of the design load to the tip.

Summary

AXISYM predictions of LD4TP2 load test behavior provide some very useful data. In order to predict compression load-displacement behavior well, the effects of residual driving load distribution must be simulated. Since AXISYM analyses assume an initially stress free pile the "mobilized" lateral earth pressure coefficient, K_s^c, must be specified. The tension load displacement predictions resembled the final reload cycle quite closely; the fact that these data poorly estimate the tension load gross displacements is due to the exclusion of residual compression loads in the analysis. Incorporation of residual compression loads in the AXISYM

analysis is not practicable with the present version of AXISYM.

Compression load distribution predictions demonstrate a slight tendency toward the measured field behavior. AXISYM predicts an increase in normal stress, $\bar{\sigma}_n$, on the pile shaft due to compression load transfer through the soil elements. The increase in shaft resistance predicted by AXISYM still appears to be small compared with the field-measured response. This is, no doubt, due to the effects of pile driving on the stress-deformation state in the vicinity of the pile shaft. A more accurate simulation of these effects on the surrounding soil would better approximate the "strain-hardening" phenomenon. The tension test load distribution predictions demonstrate the reverse effects: a reduction in $\bar{\sigma}_n$ due to the decrease in confining stress during tension load transfer to the soil, a "strain-softening" behavior.

Some parametric studies were performed using AXISYM to determine solution convergence criteria. These results are described in Chapter VI. Based upon comparisons between AXISYM and DUKFOR results, DUKFOR is clearly the more rational procedure for analyzing impact-driven pile behavior. Both methods show considerable potential in analyzing pile-soil interaction problems, though the restrictive assumptions required for AXISYM, presently, are better suited for bored or buried pile problems. For these reasons it was decided to concentrate the remaining research effort on applications of DUKFOR. The following pile test analyses were all performed exclusively using DUKFOR.

DUKFOR Analyses: Additional LD4 Piles

Impact-Driven Piles

In addition to LD4TP2, two other fully driven test piles at LD4 (LD4TP1 and LD4TP3) were analyzed using the dynamic/static DUKFOR analysis procedures. As mentioned previously, the shaft load transfer mechanism assigned throughout these analyses employs directly the LD4 sand-on-steel interface shear test data, as reduced to average hyperbolic fit curves. For all the driven cases the K_s^c and Q_p values, adjusted for residual point loads were used, see Table V-3. The assumed initial tangent point quake values, $QUAKE_p$, are listed for all the LD4 test piles in Table V-5.

Pile driving analyses were performed on these test piles to obtain correlated damping parameters in the same manner as presented in figures V-1 and V-2. The respective damping parameters are listed in Table V-5. Both piles were load tested monotonically to failure; first in compression, then in tension. DUKFOR dynamic/static analyses simulated the entire installation and load test sequence. Analyses using the "stress-free" assumptions gave essentially the same compression load-displacement predictions, such that these data are not plotted hereafter.

LD4TP1. Compression load-displacement results for LD4TP1 are described in figure V-14. The DUKFOR predictions are plotted as data points along with the measured load-displacement curve. The DUKFOR predictions show excellent agreement with field measurements.

Tension test predictions for three different assumed loading histories driven (D)/compression (C) - tension (T), stressfree (SF)/C-T and

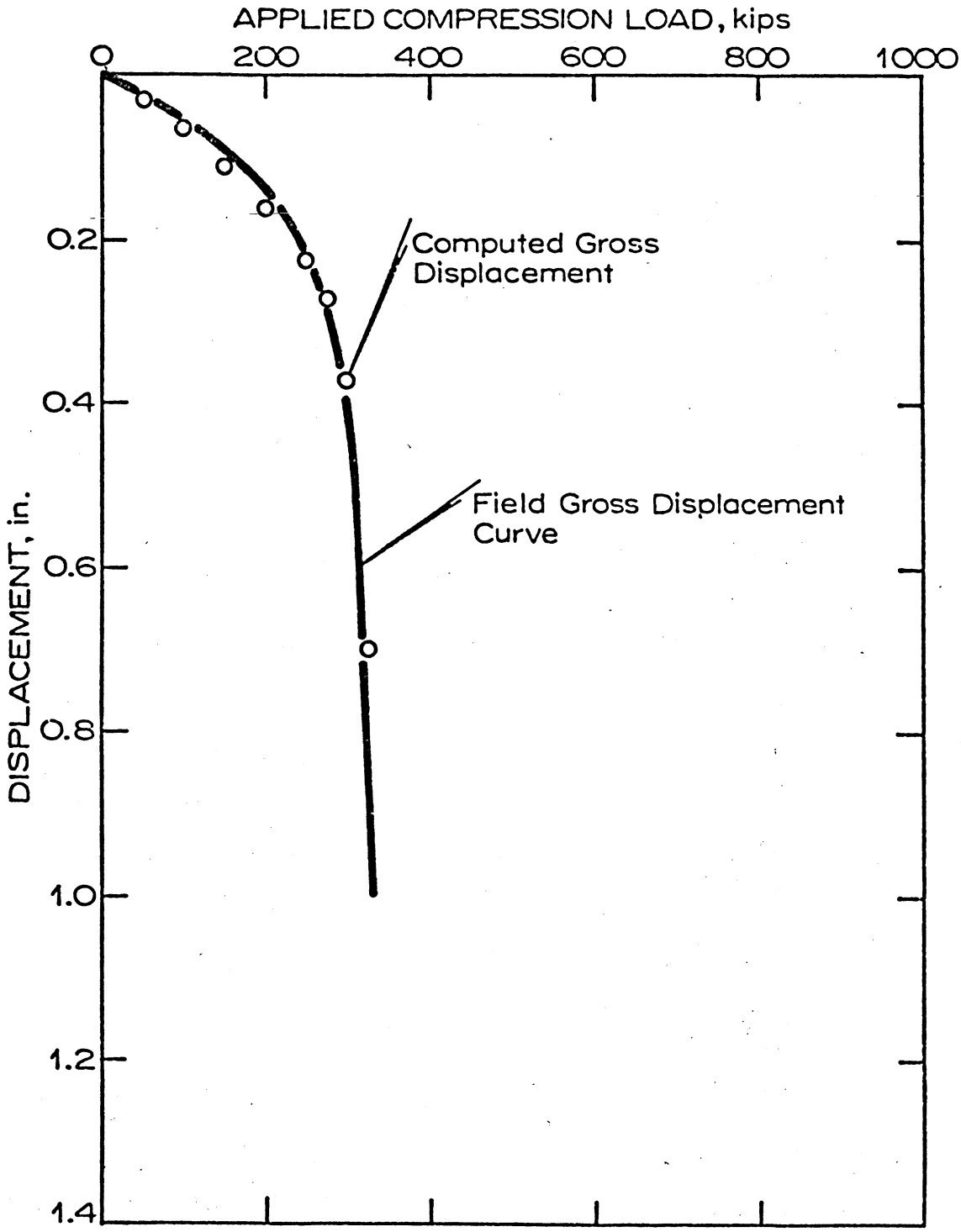

Figure V-14. Compression Test Results: Load-Displacement Data, LD4TP1.

SF/T, are presented in figure V-15. None of the assumed loading histories predicts the measured load-displacement data very well except in the early stages.

The load distribution data for LD4TP1 is presented in figure V-16. The measured residual point load was 74 kips; DUKFOR predicts this value as 110 kips. Two sets of predicted compression and tension load distributions are shown in figure V-16: the first set represents the DUKFOR predictions which incorporate the predicted residual driving load distribution, curves (1), (2), (3), and (4); the second set of predicted curves (1M), (2M) and (4M) represent the "mobilized" load distributions which are "uncorrected" for the residual driving load distribution by subtracting curve (0) (the residual driving load distribution) from curves (1), (2) and (4), respectively. Since LD4 load distribution measurements are uncorrected for residual loads, the measured data (curves (A), (B) and (C)) should be compared with the "mobilized" load distribution predictions.

Agreement between predicted and measured compression load distributions (compare (1M) with (A) and (2M) with (B)) is better at the lower load level. At the higher load level the observed data indicate a more rapid decrease in load in the upper half of the pile, indicating a continuing increase in the corresponding skin friction, which DUKFOR does not include. The skin friction appears to increase to a level above that assumed in the DUKFOR analysis. As this develops at higher load levels, after significant pile-soil relative displacement, this phenomenon is apparently due to an increase in $\bar{\sigma}_n$. For LD4TP2 analyses this behavior was termed strain-hardening response of the system. AXISYM analyses of LD4TP2 demonstrated the tendency toward reduced $\bar{\sigma}_n$ as a result of tension

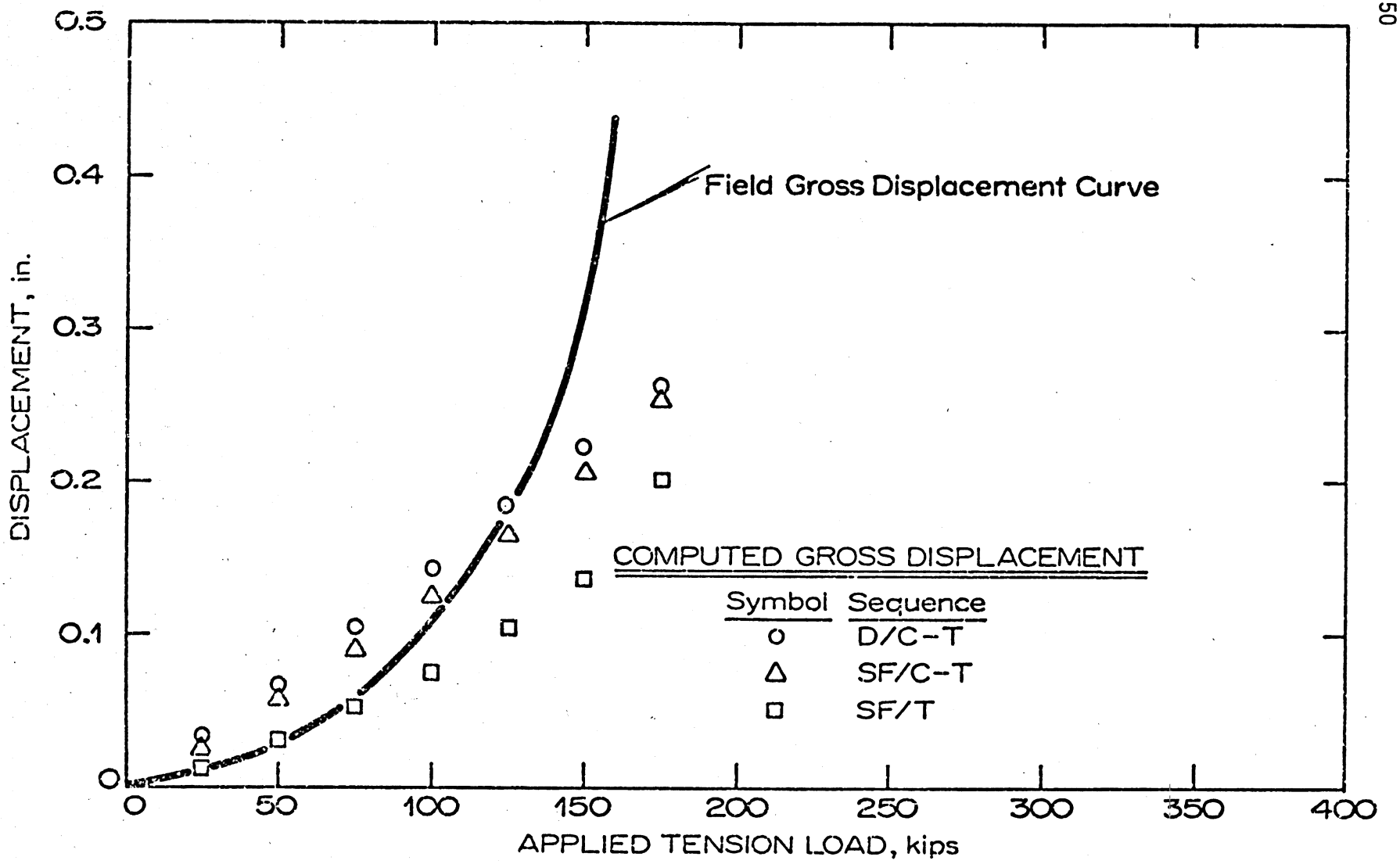

Figure 15. Tension Test Results: Load-Displacement Data, LD4TP1.

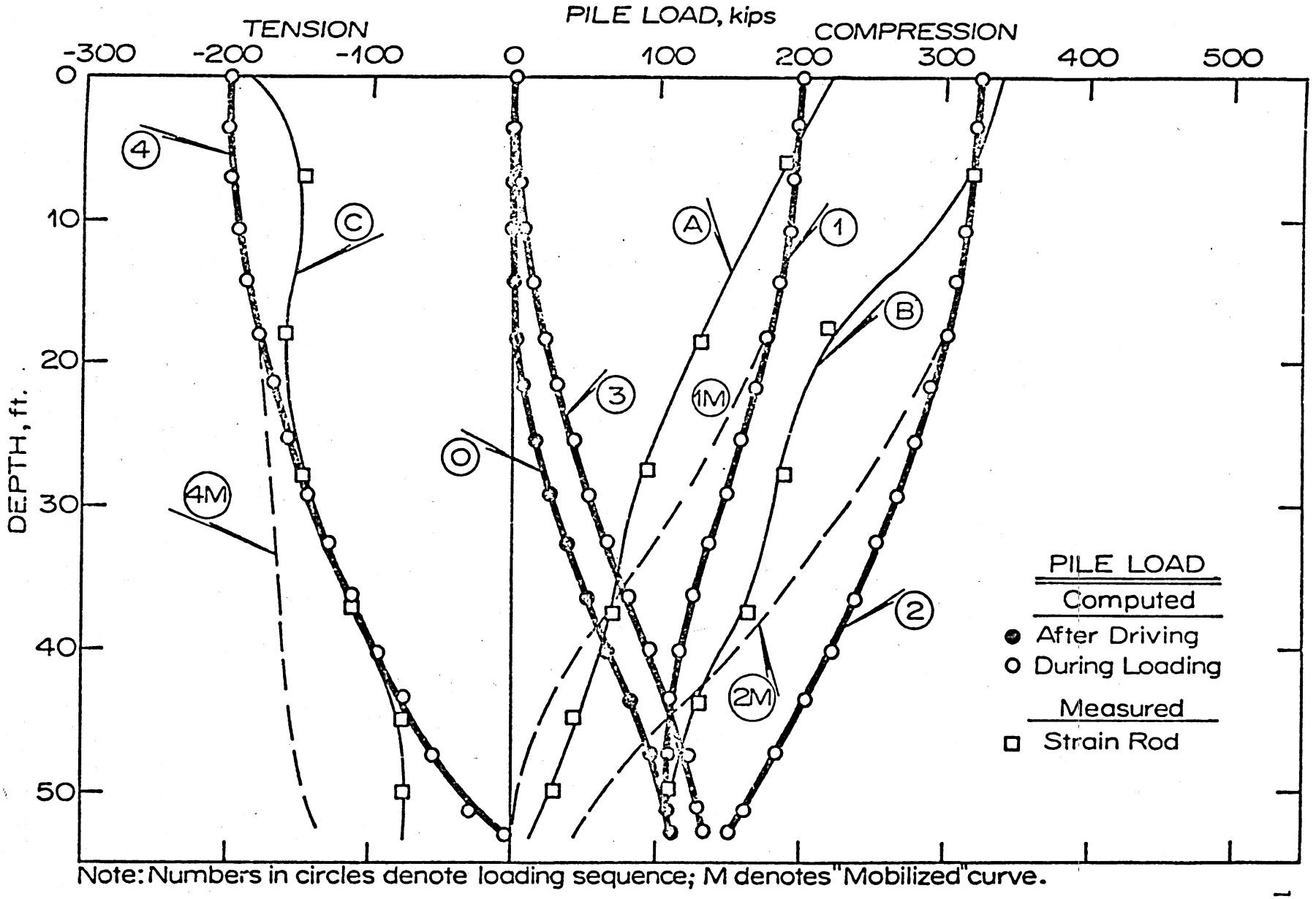

Figure V-16. Load Test Results: Load Distribution Data, LD4TP1.

load transferred to the surrounding soil. The assumptions employed in the DUKFOR analyses do not incorporate these effects directly.

LD4TP3. As with the preceding LD4 test piles, the dynamic analyses of LD4TP3 were performed to determine correlated damping values, see Table V-5. Using the dynamic/static analysis procedure with the correlated damping parameters, the D/C-T loading case was studied. Compression load-displacement predictions are provided in figure V-17. As noted for LD4TP1 and LD4TP2, the computed gross displacements agree closely with the field-measured curve.

Figure V-18 shows the predicted tension load-displacement data for comparison with field data. The computed results which incorporate residual compression loads from the loading history (D/C-T and SF/C-T) give twice the predicted displacement of the SF/T loading case. Moreover, these first two simulated loading cases better approximate the field data, indicating the importance of residual compression loads on tension load-displacement behavior. The lack of a strain-softening simulation in the DUKFOR analyses causes a stiffer response at higher load levels, as noted for the previous pile test predictions.

The load distribution data for LD4TP3 are shown in figure V-19. The predicted residual point load of 103 kips agrees reasonably well with the 96 kips measured (see curve (O).). The load transfer at higher compression loads exhibits increase in skin friction in the upper pile section, resulting in lower measured pile loads in this portion than DUKFOR predicts. This phenomenon was noted for LD4TP1 and LD4TP2 analyses previously. The measured tension load distribution curve (C) shows a break that is probably a measurement error for the 37 ft depth strain rod.

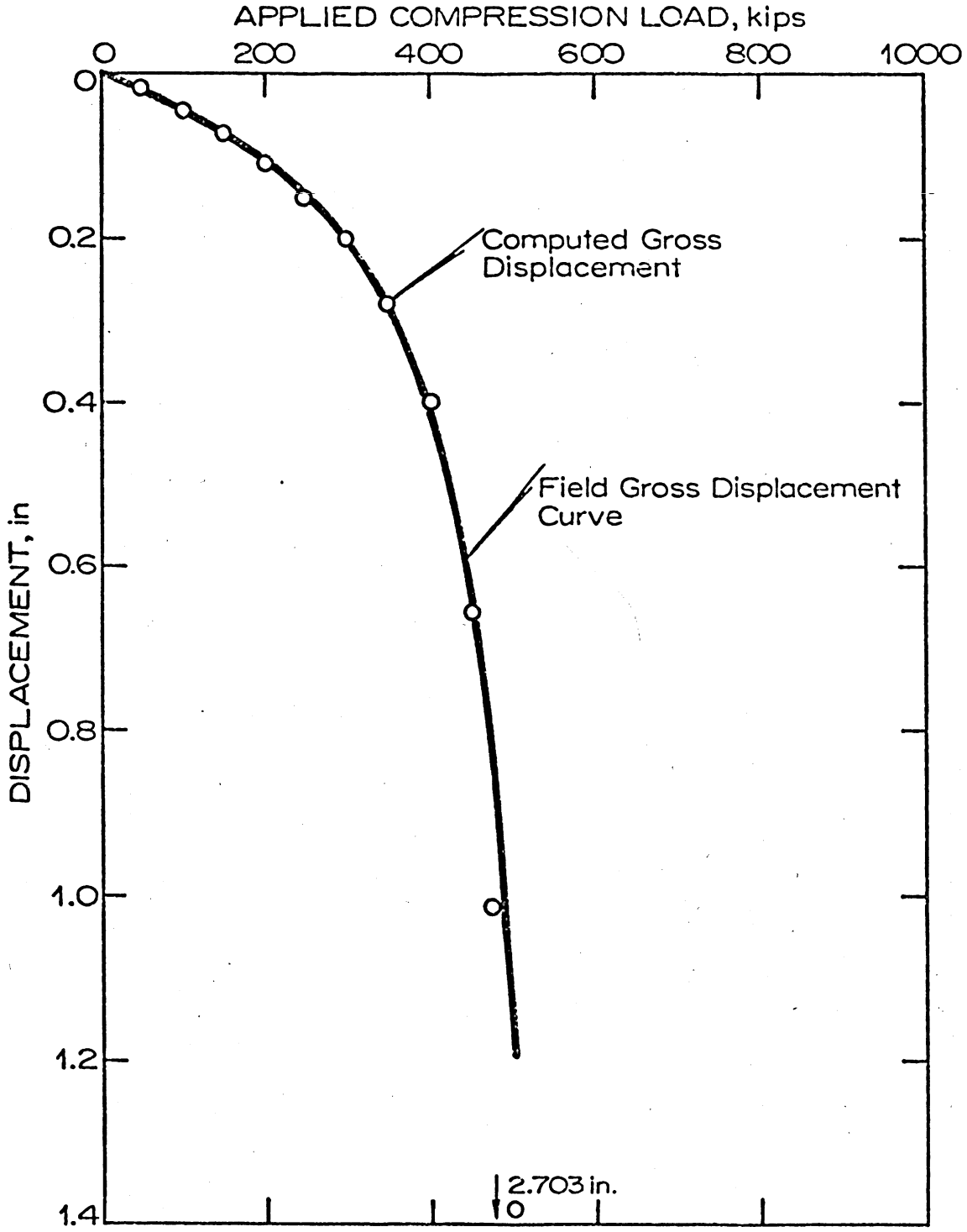

Figure V-17. Compression Test Results: Load-Displacement Data, LD4TP3.

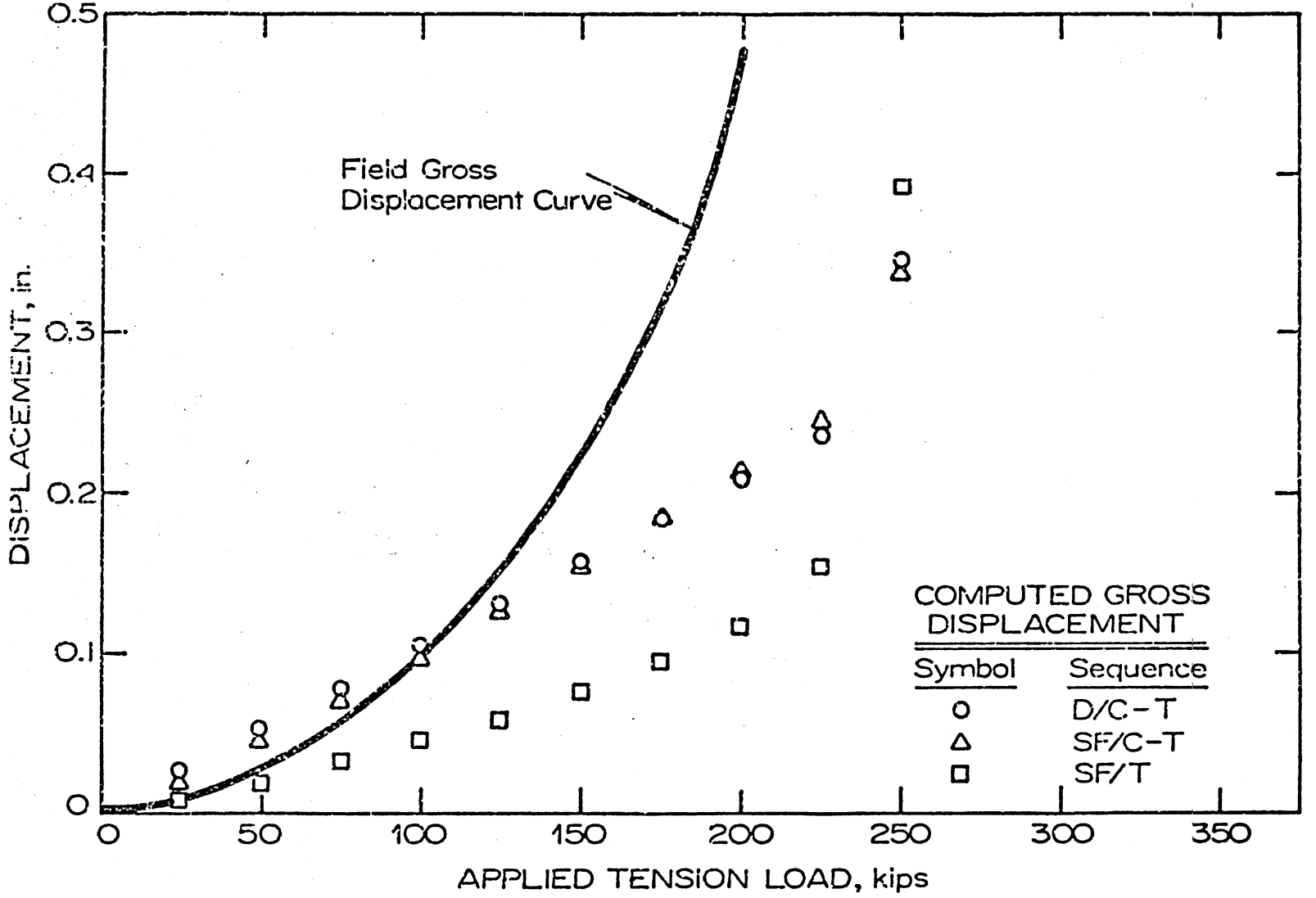

Figure 18. Tension Test Results: Load-Displacement Data, LD4TP3.

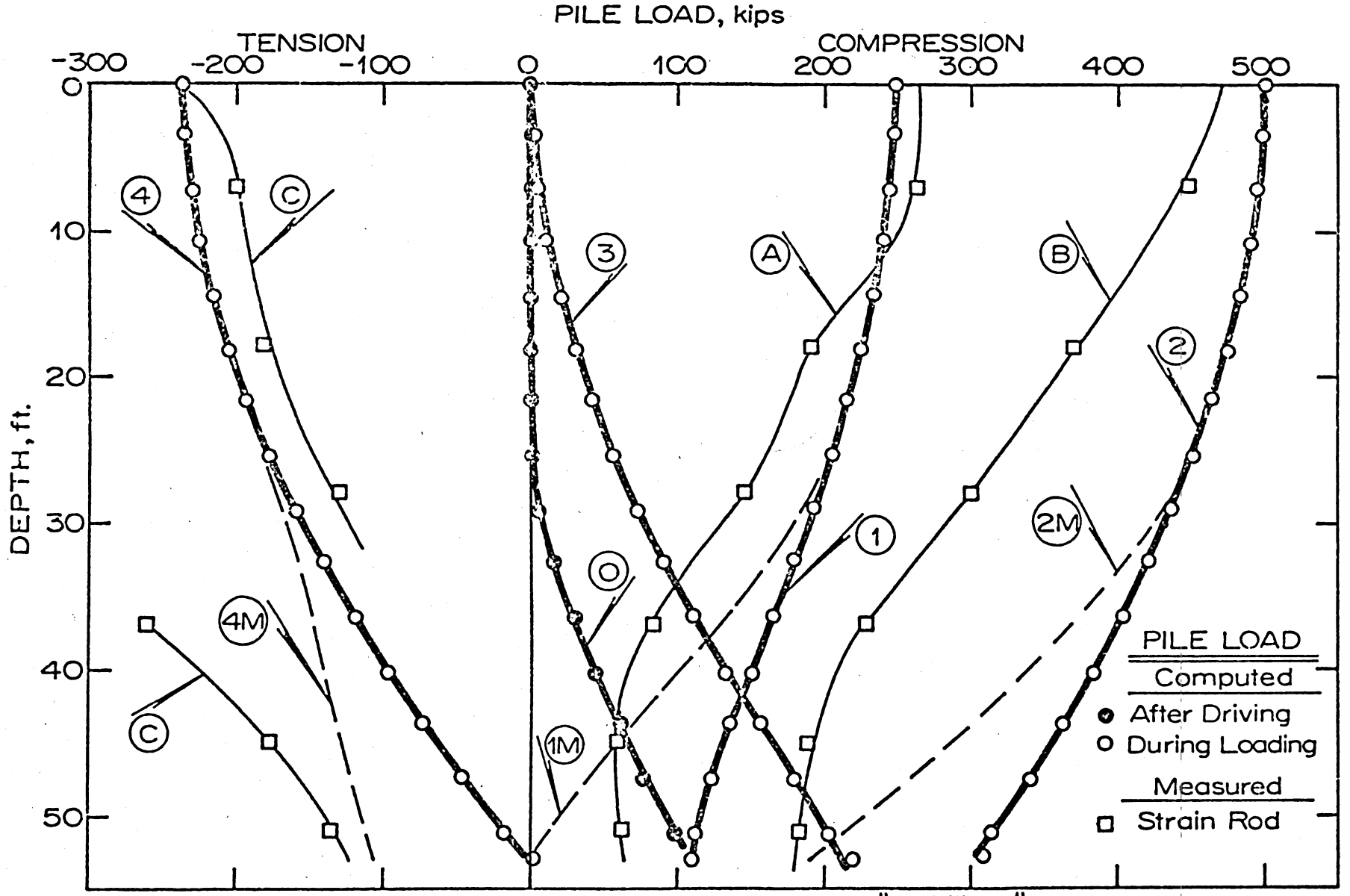

Note: Numbers in circles denote loading sequence; M denotes "Mobilized" curve.

Figure V-19. Load Test Results: Load Distribution Data, LD4TP3.

Bodine-Driven Pile

LD4TP10 was driven to grade using the Bodine vibratory driver. Load test measurements indicated the residual driving loads were negligible.[76] This appears reasonable since the vibratory driver caused penetration by transmission of high frequency, low amplitude longitudinal stress waves in "resonance" with the pile-soil system. In order to analyze the static load test an initially stress free pile is assumed. The compression load-displacement predictions (Figure V-20) give close agreement with the measured behavior.

It should be noted in Table V-5 that an unusually large initial tangent point quake is used in the analysis of LD4TP10. This value was determined from measured tip load-displacement data.[86] It is approximately four times the value assigned for LD4TP2, an identical pile that was impact driven. It is also significant that the low measured point bearing value in Table V-3 corresponds to a one inch point displacement, roughly 6 percent of the point diameter. The point bearing capacity was not fully mobilized in the pile test and the displacement required to fully mobilize point bearing appears to be much greater than that for the impact-driven pile. LD4TP10 behaved much like a bored pile in this respect. The shaft bearing capacity of LD4TP10 slightly exceeds that of LD4TP2, however, suggesting that the lateral soil compression due to installation is about the same in either case.

Tension load-displacement data for LD4TP10 are presented in figure V-21. The predicted data points are reasonably close to the field curve up to 150 kips. Thereafter, the field data suggests a softer response. The computed data are obtained from a SF/C-T analysis. The load distri-

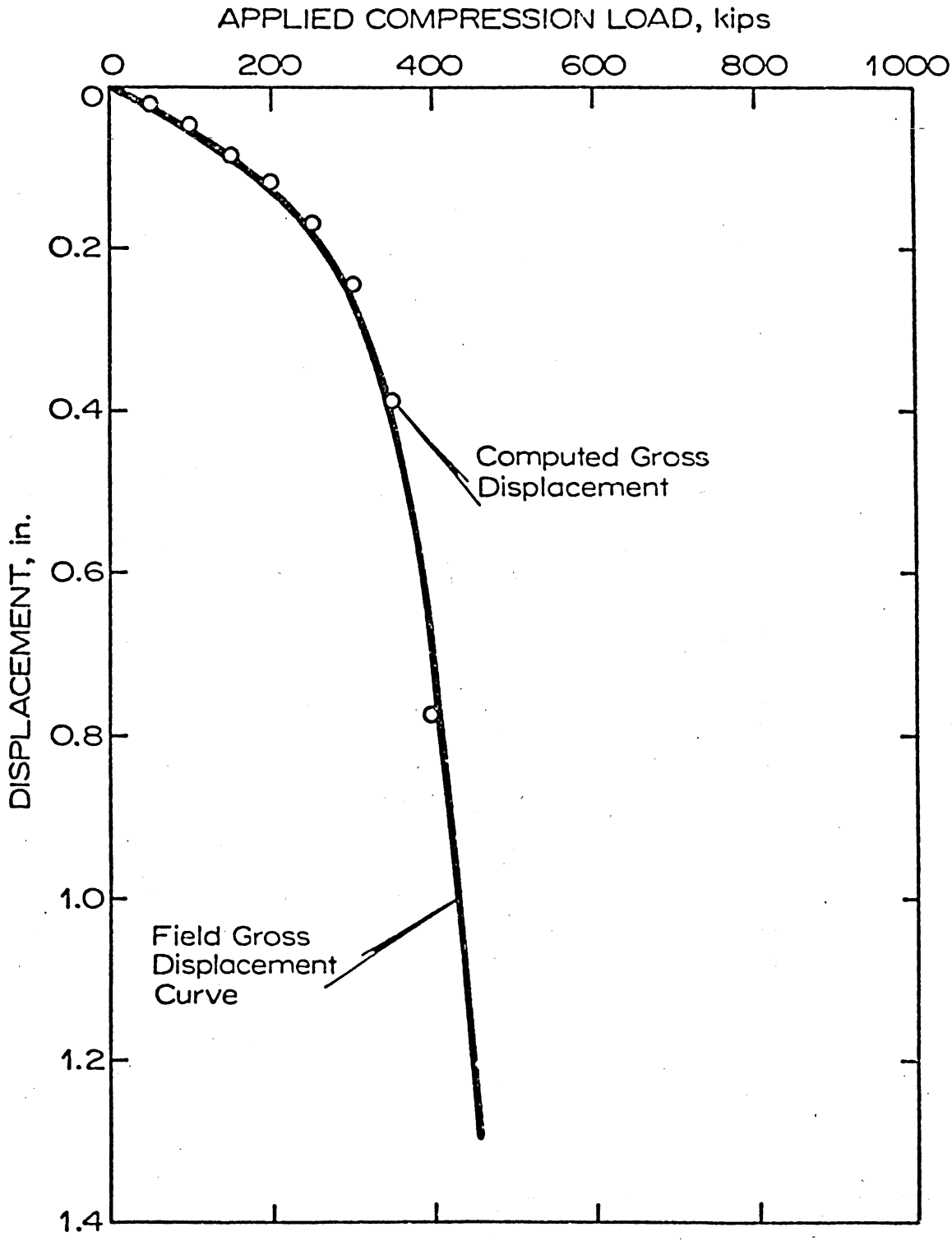

Figure V-20. Compression Test Results: Load-Displacement Data, LD4TP10.

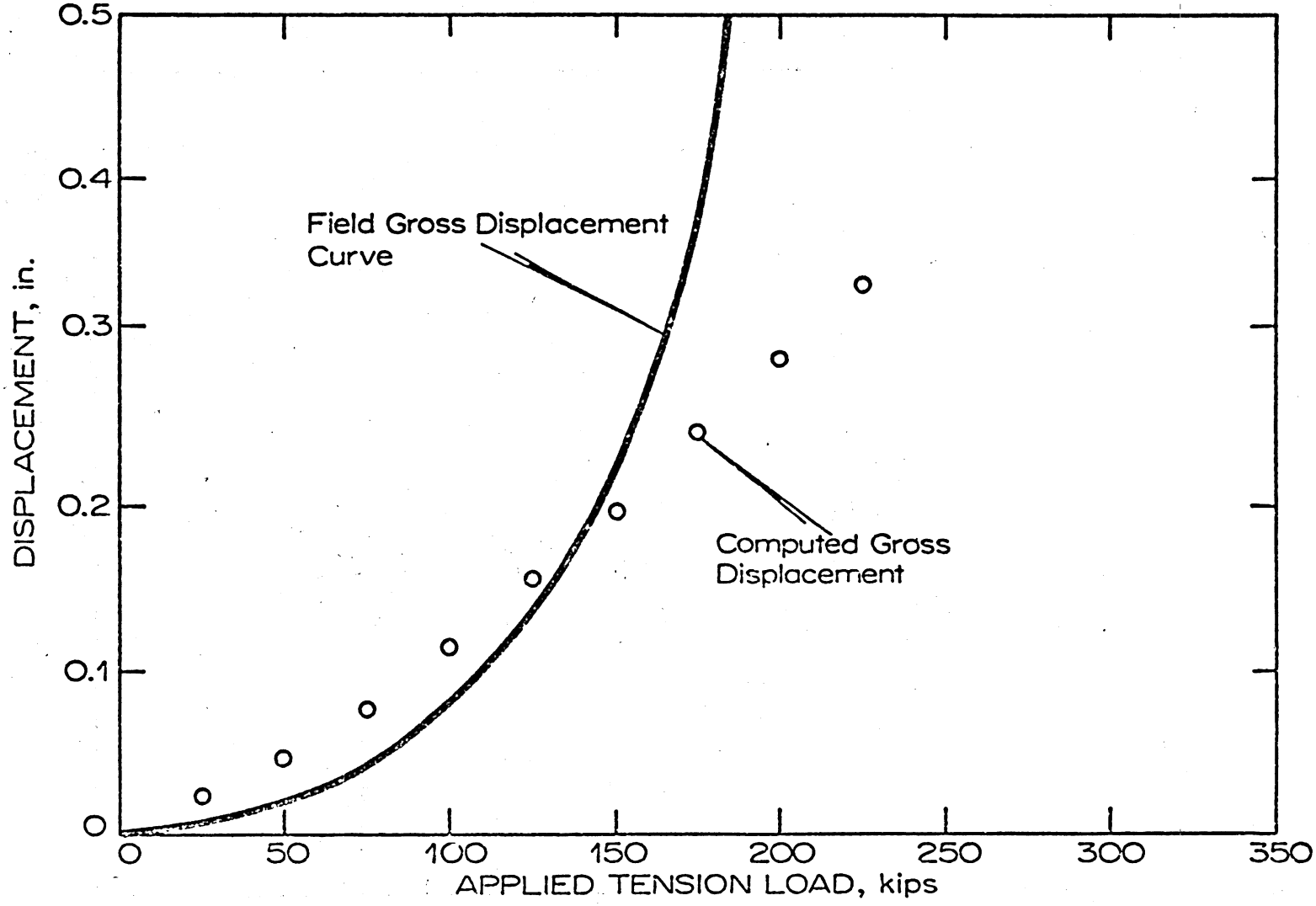

Figure V-21. Tension Test Results: Load-Displacement Data, LD4TP10.

bution data for LD4TP10 are given in figure V-22. The field measurements indicate a much higher shaft resistance in the upper length of the pile than DUKFOR predicts. The increase in skin friction in the upper half of the pile from curve (A) to curve (B) is quite pronounced. The measured tension load distribution curve (C) suggests that the gages were zeroed at the start of the tension test since a tension point load is "mobilized". As no residual compression load was measured for this pile for the start of the compression test, the point tension load measured (curve (C)) should roughly resemble the difference between curves (4) and (3), which it does.

Jetted and Driven Pile

LD4TP16 was jetted to 40 ft embedment and impact driven the remaining 13 ft to grade. For the purposes of these analyses it is assumed that the final driving redensified the soil along the pile shaft, giving a constant K_s^c value along the shaft. No doubt the field conditions are far more complex, but it was found that this simplification gave quite satisfactory predictions. The dynamic/static simulation of driving and load testing was used for this pile. From the blow count correlation study for damping parameters, higher J_s and J_p values were obtained for LD4TP16 than for the preceding fully driven piles, LD4TP1, LD4TP2 and LD4TP3 (see Table V-5). Using the correlated damping values in the dynamic/static procedure DUKFOR predicted a residual point load of 92 kips, as compared with an 80 kip load measured.

Figure V-23 gives the compression load-displacement predicted and field-measured data for LD4TP16. As in all the preceding analyses, the computed displacements provide excellent agreement. The tension load-

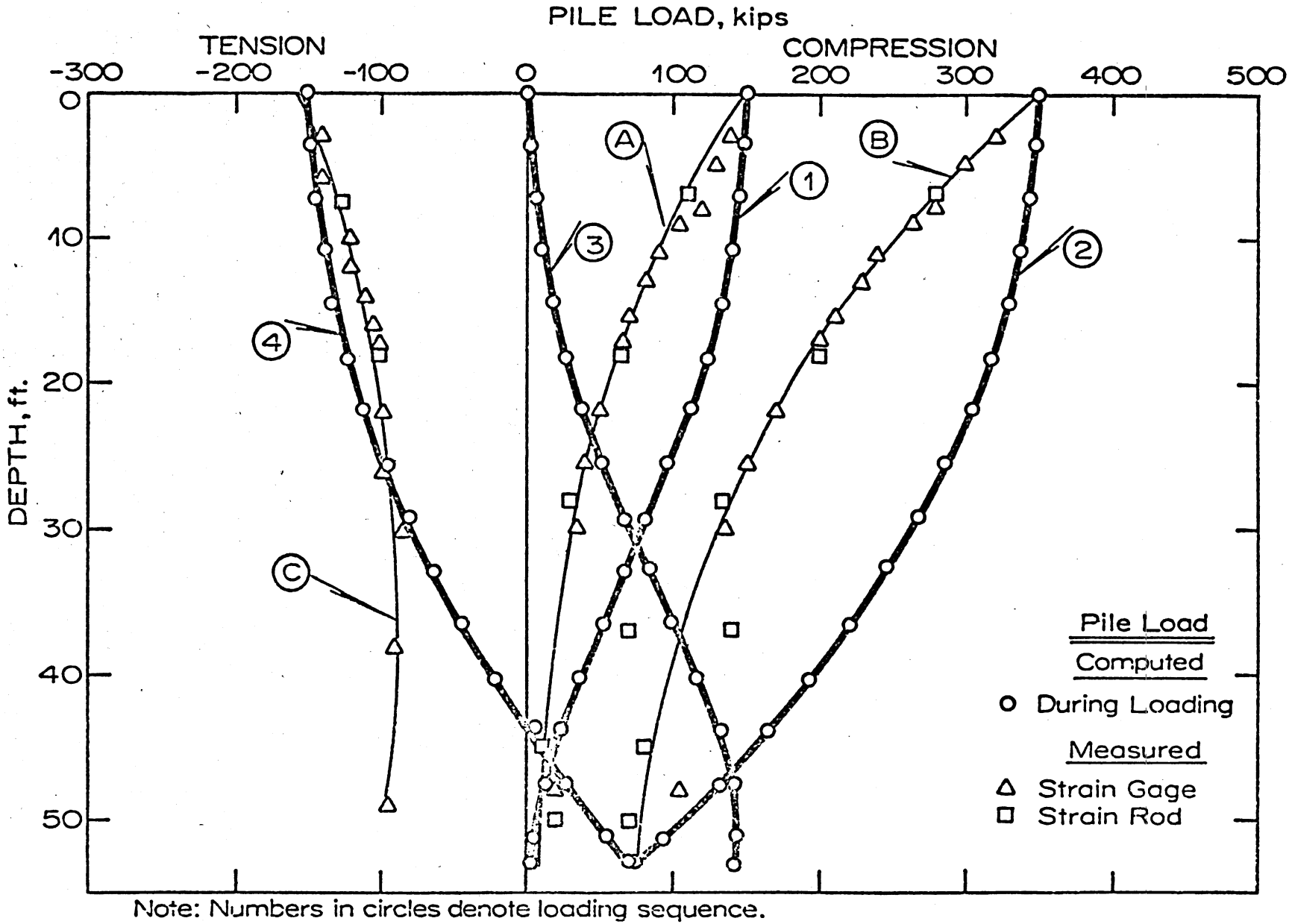

Note: Numbers in circles denote loading sequence.

Figure V-22. Load Test Results: Load Distribution Data, LD4TP10.

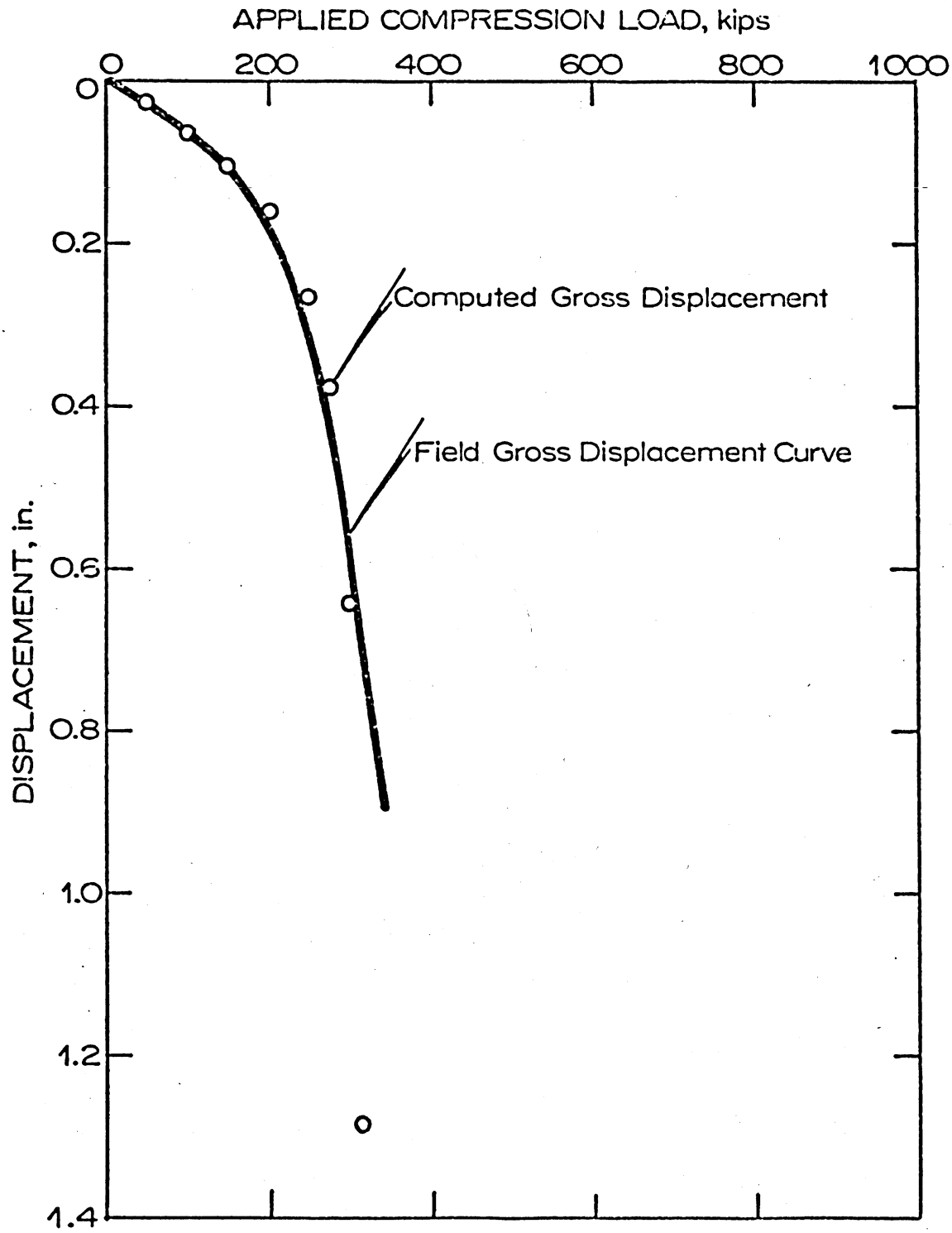

Figure V-23. Compression Test Results: Load-Displacement Data, LD4TP16.

displacement predictions are also reasonably good, see figure V-24. The load distribution data in figure V-25 indicate closer agreement between predicted "mobilized" curves (1M), (2M), and (4M) and measured data curves (A), (B) and (C), respectively, than any of the previous cases. Jetting and subsequent driving caused a lower K_s^c values and apparently reduced the strain hardening effects found in the previous cases. It appears that the tendency toward strain hardening is more pronounced for stiffer pile-soil systems having higher shaft capacities.

Tip penetration during the load test reached only 0.7 inches, about 4 percent of the base diameter. The lower point capacity reported for LD4TP16 (see Table V-3) is most likely caused by insufficient penetration which did not mobilize full bearing capacity. The point load transfer measurements roughly satisfied the point quake criterion applied for impact-driven piles ($QUAKE_p$ = 0.05 in/ft), suggesting that the final 13 ft of driven penetration established impact-driven pile-soil system characteristics near the pile point. The shaft capacity was well below that of LD4TP2, the identical pile fully impact driven, a direct result of jetting.

Comments on Point Bearing Capacity

Measurements of point bearing capacity, q_o, (assuming failure conditions) for the three impact-driven piles, LD4TP1, LD4TP2 and LD4TP3, were q_o = 175, 153 and 141 ksf, respectively. This is somewhat surprising since all the piles were driven to the same embedment (53 ft) such that one would assume that the effective overburden pressure ($\bar{\sigma}_v$ = 3.46 ksf) and the in situ coefficient of lateral earth pressure at rest would be the same for each case. This suggests two possibilities; either the full point

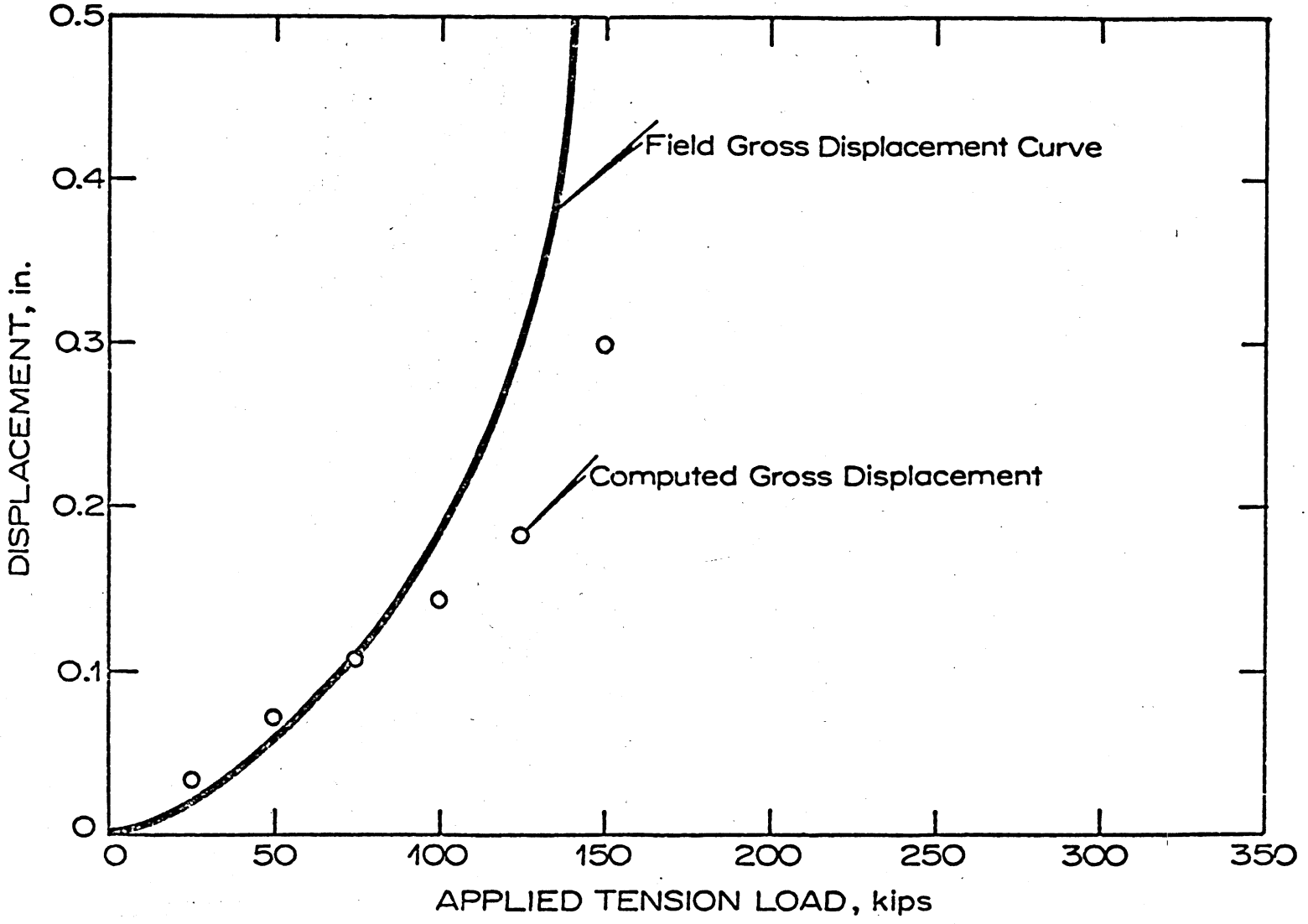

Figure V-24. Tension Test Results: Load-Displacement Data, LD4TP16.

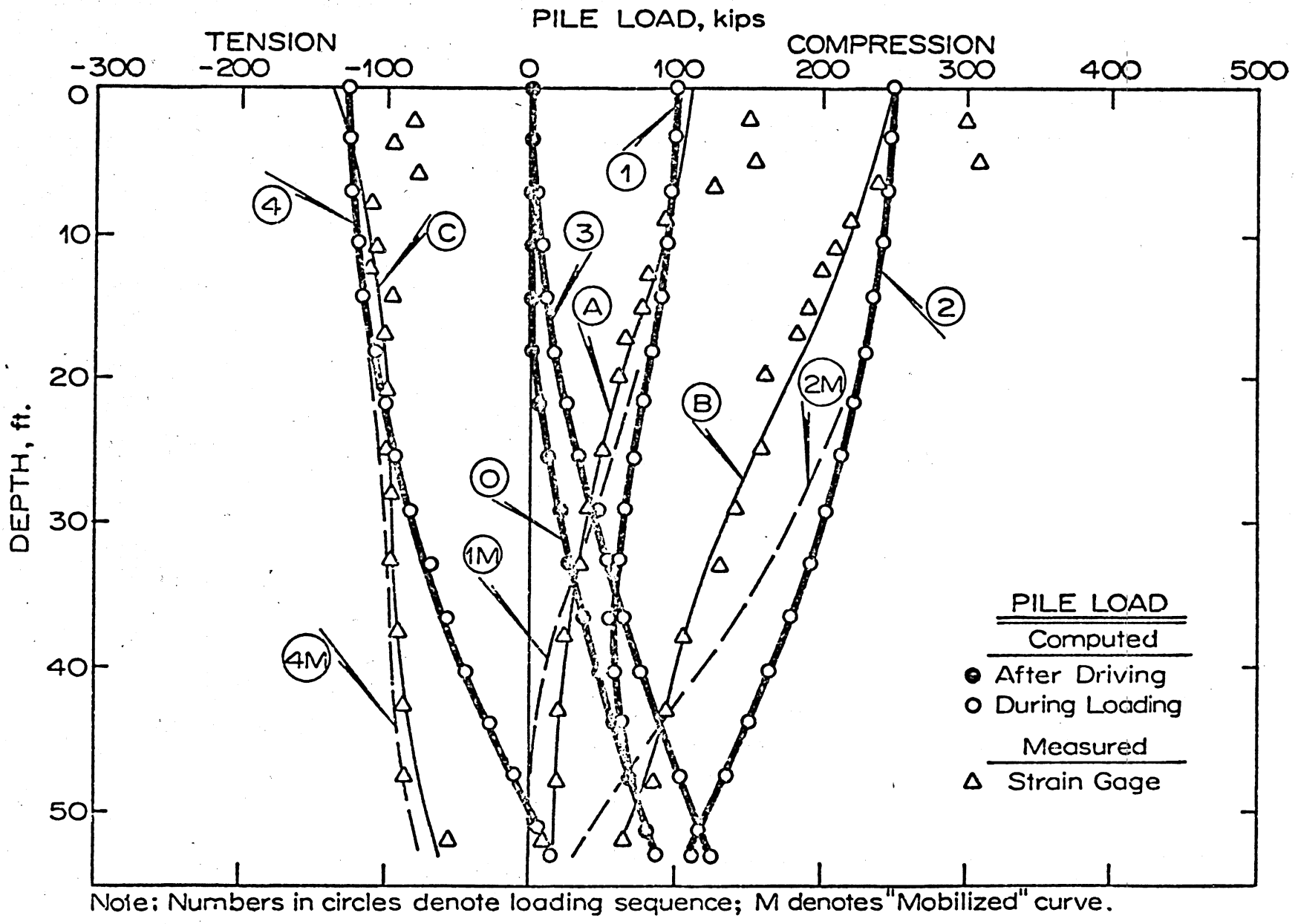

Figure V-25. Load Test Results: Load Distribution Data, LD4TP16.

bearing capacity was not mobilized, or there is a scale-dependent relationship for point bearing. It is conspicuous that q_o seems to decrease with increasing pile diameter.

Careful examination of the measurements reported by Fruco and Associates[86] reveals that the measured tip displacements were greater than 10 percent of the base diameter only for LD4TP1. The measurements indicate that LD4TP2 and LD4TP3 pile tips were displaced only six percent of the base diameter. Point load-displacement data for these piles indicate that the tip bearing force was still increasing in each case. Tip bearing capacity was apparently not fully developed for these two piles. The Bodine driven pile (LD4TP10) and the jetted and driven pile (LD4TP16) showed the same effects; the point displacements were 6 percent and 4 percent of the pile diameters, respectively.

These observations highlight the need to interpret pile load test data carefully. Though the tip bearing values were probably not fully mobilized for any but LD4TP1, they were apparently close enough to permit fairly accurate simulation of the load-displacement behavior. The high damping values for LD4TP16 may be the direct result of underestimating the point bearing value. A higher viscous damping resistance would be required to compensate for a low point bearing value in order to correlate the dynamic resistance to driving with the measured blow count. In order to obtain an accurate estimate of point bearing capacity, the pile point must penetrate a sufficient distance during the load test. For impact-driven piles 10 percent of the point diameter should be enough point displacement. For buried, bored or vibratory driven piles two to four times that amount of displacement is necessary.

Summary

DUKFOR pile driving analyses of all the LD4 impact driven piles gave generally satisfactory predictions. The correlation of damping parameters with measured blow counts was shown to generate interdependent damping values, J_p and J_s, which are not unique soil constants. Attempts to use predicted residual point loads as a second means of determining J_p and J_s values were not successful. The predicted residual point loads exceded the measured values in every case. This discrepancy will be examined parametrically in Chapter VI. It is due to limitations in the problem idealization and necessary assumptions. The shapes of the residual load distribution curves in each case are reasonable approximations within the constraints of the assumptions applied in the mathematical model. Comparisons were not available with the cases analyzed, as residual driving load distributions were not measured.

Compression load test simulation provided excellent load-displacement predictions for all the LD4 piles analyzed. The dynamic/static analysis procedure was used for the three fully driven piles and the jetted and driven pile, while the vibratory driven pile was modeled as an initially stress free pile, consistent with field measurements. The predicted compression load distributions tended to overestimate pile loads with depth, indicating higher load transfer in the upper half of the pile. The measured load transfer increased at higher compression load levels in the upper half of the pile. It was attributed to a strain-hardening phenomenon of the overall pile-soil system. This tendency was predicted to a lesser extent using the axisymmetric FE idealization.

The tension load test predictions of displacements were only fair in most cases. As a general rule the pile-soil system behaved softer at higher tension load levels than DUKFOR predicted. AXISYM results showed that this tendency developed because the tension load transferred to the soil reduced the confining stress level near the pile providing a strain softening effect. The influence of residual compression stresses on tension load-displacement behavior is quite important. A much softer response is predicted when these stresses are included in the analysis. The combination of residual compression stresses and strain softening effect causes measured displacements to be larger than either DUKFOR or AXISYM predicts. DUKFOR does not account for the strain softening effects and AXISYM cannot simulate residual compression stresses correctly.

The DUKFOR dynamic/static solution method predicted overall pile-soil interaction behavior remarkably well for each LD4 test pile. As these analyses employed straight forward simplifying assumptions in the idealization, they demonstrate considerable promise for the method. In the next section pile tests from Jonesville Lock and Dam will be used to further evaluate DUKFOR capabilities.

Pile Test Data: Jonesville Lock and Dam

A series of pile tests were performed at Jonesville Lock and Dam (JLD), near Jonesville, Louisiana, by the U.S. Army Engineering District, Vicksburg, and the U.S. Army Engineer Waterways Experiment Station (WES). Furlow[91] reported the results of the overall pile test program.

The pile test site was excavated from elevation 48 ft to -21 ft, the foundation grade, removing almost 70 ft of abandoned course deposits of silts, clays and silty sands. The subsoils below el.-21 ft consist of abandoned course and reworked deposits of dense to very dense gray silty sands with occasional thin layers of gravel or silt down to -75 ft. The dry unit weights ranged between 100 and 110 pcf (relative densities between 51 and 108 percent). A hard to very hard Tertiary clay (unconfined strengths of 8 to 16 tsf) exists below elevation -76 ft, 55 ft below grade.[91]

Laboratory triaxial and interface shear tests obtained for the load test design were reported by Furlow.[91] In conjunction with a subsequent FE study of one JLD pile (JLDTP2A), Desai and Holloway[56] performed a series of drained triaxial and interface shear tests (sand-on-mortar) using JLD sand. The tests were performed on samples prepared at 60, 80, and 100 percent relative densities for several different confining stresses. Average deformation and failure parameters generated from these tests are given in the Appendix. For all the DUKFOR JLD analyses the interface shear properties of 100 percent relative density sand-on-mortar (see Appendix) were assumed due to densification near the pile shaft from impact driving.

A Vulcan 016 single-acting air hammer was used to drive all the test piles. Information describing the hammer assembly components is pro-

vided in Table V-6. Test piles 1, 2 and 3 were driven to 38 ft, 45 ft and 54 ft embedment, respectively. JLDTP2A was jetted and driven 39 ft, and driven the final 6 ft to 45 ft embedment. Pile data and field measurements are listed in Table V-7. All the Piles yielded a relatively high blow count between 35 and 39 ft embedment; JLDTP1 was embedded 38 ft with a final blow count of 66 B/ft. The boring logs and pile driving behavior suggest a very dense lense of gravelly material exists at that depth.

JLD test piles were not instrumented to measure load distributions such that residual point loads are unknown. In fact, without load transfer measurements along the pile length the magnitudes of point capacity, Q_p, and shaft capacity Q_p^c are indeterminant. As a result it was assumed that the shaft capacity in tension, Q_s^t, is identical to that in compression, Q_s^c ($Q_s^c = Q_s^t$). The LD4 pile tests measurement for the impact-driven piles suggest this is a reasonable approximation, see Tables V-3 and V-4. Using this assumption the point bearing capacity is computed as $Q_p = Q_{max}^c - Q_{max}^t$, where of course, $Q_{max}^t = Q_s^t$. Bearing capacity estimates using this assumption are summarized in Table V-8.

The JLD test piles were loaded to failure in cyclic compression and cyclic tension. The cyclic compression loading was applied in increasing steps spaced at 80-kip intervals until failure occurred, with complete unload after each step. Forty-kip intervals were used in the subsequent cyclic tension tests.

Table V-6

IMPACT HAMMER ASSEMBLY DATA, JLD

Hammer	
Vulcan 016 single-acting air hammer	
Ram Weight, W_1	16,250 lb.
Stroke	3 ft.
Rated Energy	48,750 ft-lb.
Efficiency (assumed)	.85
Cap Block	
Asbestos	
Cross-section (assumed)	255 in.^{2}
Thickness	6 in.
Coefficient of Restitution	0.6
Secant Modulus (stress level dependent)	4.14×10^4 lb/in.^{2}
Helmet	
Weight, W_2	3000 lb.
Cushion Block	
Oak	
Cross-section 18 in. square	324 in.^{2}
Thickness	6 in.
Coefficient of restitution	0.47
Secant Modulus (stress level dependent)	2.94×10^4 lb/in.^{2}

Table V-7

PILE DATA AND FIELD MEASUREMENTS, JLD

Test Pile[2]	Length (FT)	Embedment (FT)	Blow Count Final Foot[2] (Blows/FT)	Maximum Compression Load, Q^c_{max} (KIPS)	Maximum Tension Load, Q^t_{max} (KIPS)
1	39.5	38	66	800	260
2	46.5	45	27	680	280
3	55.5	54	41	765	260
2A[3]	46.5	45	19	485	144

NOTES:

1. All piles prestressed, reinforced concrete, 18-in. square section.
2. Driven using Vulcan 016 hammer, see Table V-6 for driving system data.
3. JLDTP2A jetted and driven 39 ft., driven final 6 ft.

Table V-8

BEARING CAPACITY ESTIMATES, JLD

Test	Q^c_{max} (KIPS)	$Q^t_{max} = Q^t_s$ (KIPS)	$K^t_s = K^{c\,a}_s$	Q_p Estimated[b] (KIPS)
1	800	260	0.981	540
2	680	280	0.772	400
3	765	260	0.509	505
2A	485	144	0.397	341

Notes:

a. In lieu of load transfer measurements it is assumed that $Q^c_s = Q^t_s$. To determine $K^c_s = K^t_s$ the in situ effective overburden pressure is assumed and the interface friction angle $\delta = 37.9^o$ is prescribed, WT at 4 ft. depth.

b. Computed as: $Q_p = Q^c_{max} - Q^t_{max}$

DUKFOR Analyses: JLD Piles

Pile Driving Analyses

A representative pile of the load test series, JLDTP2, was selected for a comprehensive parametric check to validate the various input parameters and analysis procedures. From the investigations it was determined that most of the discretization and integration criteria developed for LD4TP2 were satisfactory; FACTOR = 4, PILSEG = 15, and NBLOWS = 5. The value of NPASS, the number of stress wave front passes through the system, was the only parameter changed; it was increased from 6 to 8. This was done to account for the influence of higher impedance piling of shorter lengths on solution convergence. The value of initial tangent point quake was assumed as 0.075 in., consistent with the 0.05 in. per foot of base width developed for LD4 analyses.

The blow count correlations for damping parameters were performed in the same manner as the previous analyses for all the JLD test piles. A plot of blow count versus shaft damping value for JLDTP2 is shown in Figure V-26. These data indicate that even the assignment of no viscous damping gives predicted blow counts greater than measured. Since "negative damping" is inappropriate within the nonlinear viscous rheologic model (figure II-3), $J_s = J_p = 0$ were assumed. These values along with those determined for the remaining test piles are listed in Table V-9.

The soil damping parameters from the JLD piles are quite low relative to those obtained from LD4 analyses, Table V-5. If damping values from LD4TP2 (J_p = 0.10 sec/ft and J_s = 0.05 sec/ft) are assumed for JLDTP2, the predicted blow count (47 B/ft in Figure V-26) would be much higher

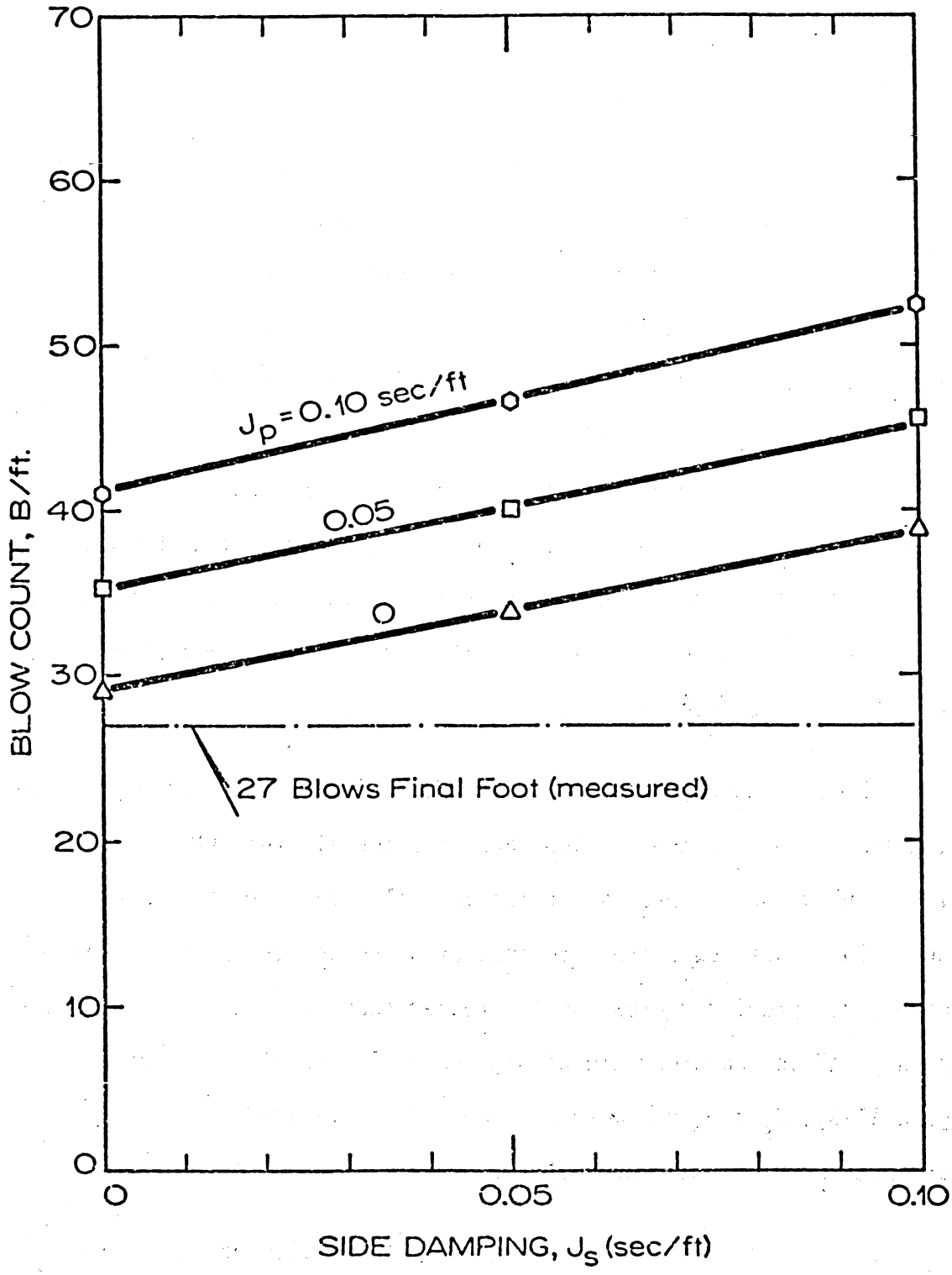

Figure V-26. Pile Driving Results: Evaluation of Damping Affects on Predicted Blow Count, JLDTP2.

Table V-9

SOIL PARAMETERS EMPLOYED IN PILE TEST ANALYSES, JLD

TEST PILE	Correlated* Damping Parameters	
	J_p (sec/ft)	J_s (sec/ft)
1	0.05	0.054
2	0.	0.
3	0.	0.04
2A	0.	0.03

*Correlations made with measured blow counts.

than that measured. These results demonstrate the sensitivity of blow count predictions to assumed damping values. Predicted static resistance based upon the wave equation results and measured blow counts, depends on the damping parameters used. Damping parameters assigned as average or "best" values from one site may be much different from those determined at a different site using exactly the same correlation procedures.

Variations of predicted residual point load with assumed damping values are described in Figure V-27. For JLDTP2 the residual point load predictions are relatively insensitive to damping parameters. As previously mentioned, no measurements were made to determine actual residual loads. The predicted residual driving load distributions for each JLD test pile, using the blow count correlated damping values in Table V-9, are shown in Figure V-28. These data indicate wide variations among the different piles, showing significant differences from those obtained in LD4 analyses. The effects of different hammer-pile-soil system conditions on pile driving behavior and residual load distribution are analyzed in Chapter VI.

Compression Test Analyses

Having obtained correlated damping parameters from pile driving analyses of each test pile, these values were used in dynamic/static DUKFOR analyses. As with the LD4 test piles, the pile driving/load testing behavior was modeled continuously. Driven/cyclic compression-cyclic tension simulations (D/CC-CT) were performed for all the JLD test piles. The results of the cyclic compression test studies are discussed in this section.

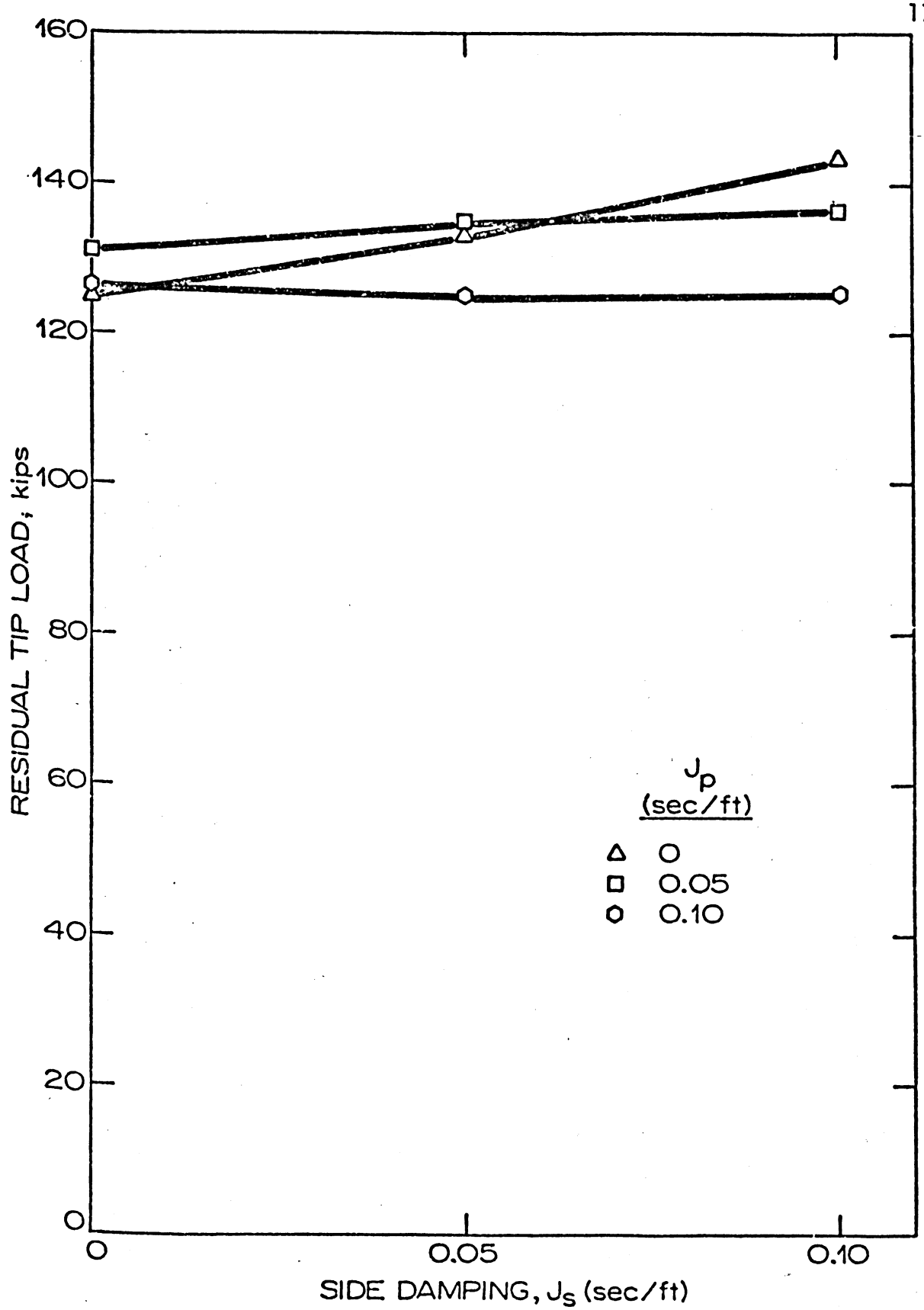

Figure V-27. Pile Driving Results: Evaluation of Damping Effects on Predicted Residual Point Load, JLDTP2.

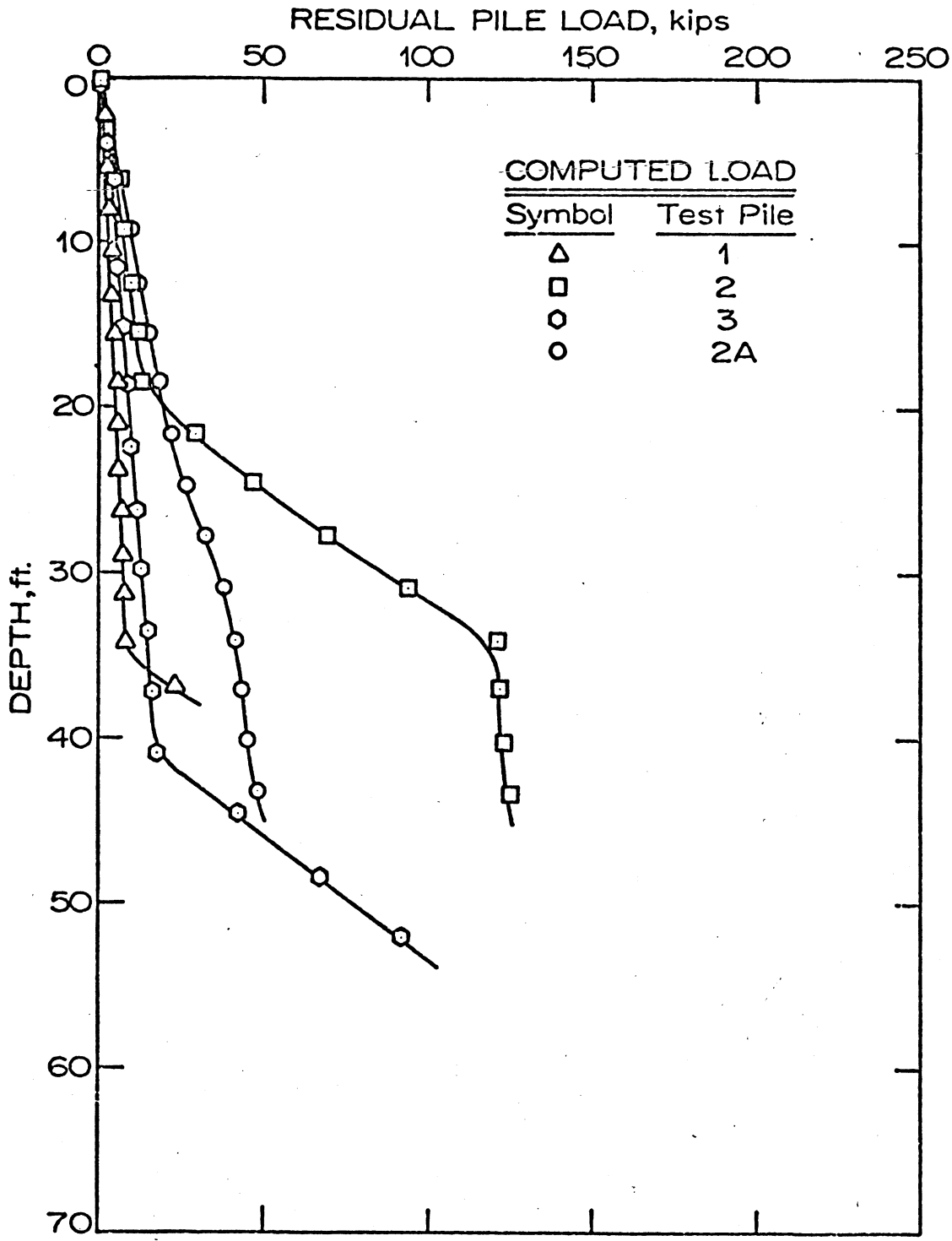

Figure V-28. Pile Driving Results: Residual Load Distributions, JLD Test Piles.

JLDTP1. Predicted cyclic compression load-displacement results for JLDTP1 are shown as data points in Figure V-29. The curves drawn in Figure V-29 represent field measurements of net and gross displacements versus load. Predicted gross displacements agreed quite well with field measurements. Very near plunging failure the predictions exceed the measured gross displacments, indicating that the DUKFOR model was too soft in that range. The net displacement predictions corroborate this observation; DUKFOR predicts greater permanent (net) settlement than described by field data.

JLDTP1 was embedded 38 ft into the dense gravelly stratum between 35 ft and 39 ft depth. The backcalculation of Q_p indicates a very high value (540 kips in Table V-8) at this shallow depth, consistent with the high blow counts obtained penetrating this layer. At applied loads approaching plunging failure it is expected that the shaft bearing capacity has already been mobilized. Larger predicted gross and net settlements at high load levels suggest that the point load transfer model is not stiff enough; i.e. $QUAKE_p$ is too large. The value of $QUAKE_p$ = 0.075 in. was assumed from experience with LD4 test piles embedded in medium dense sands. Results from JLDTP1 analysis in Figure V-29 indicate that the point quake value for points embedded in dense gravelly deposits should be smaller, such that the initial tangent stiffness will be greater.

JLDTP2. Cyclic compression load-displacement predictions for JLDTP2 are described in Figure V-30. Once again, the computed gross displacements are excellent. The predicted net displacements represent the field data reasonably well. DUKFOR predicts that plunging failure develops at a slightly lower applied load than field measurements show.

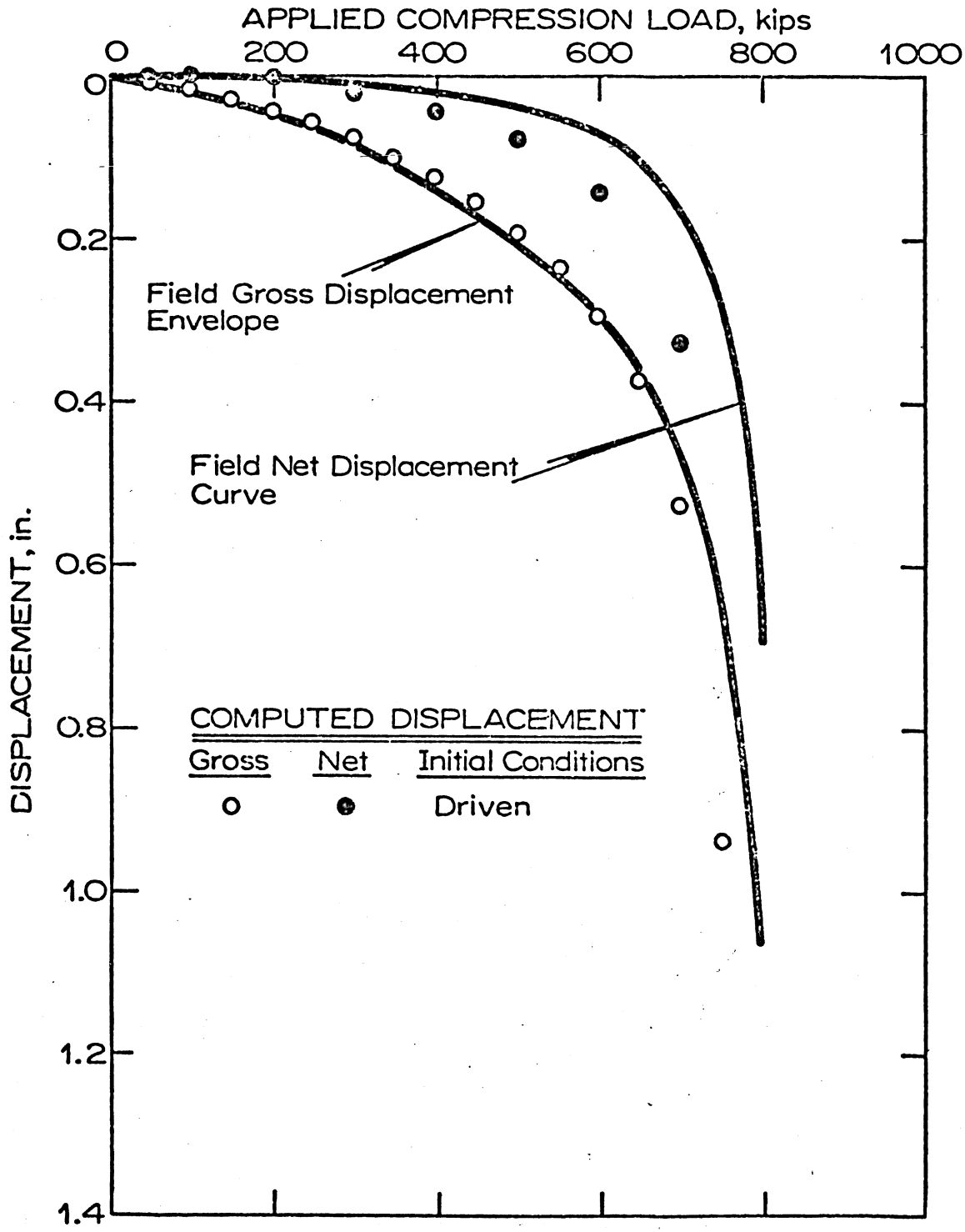

Figure V-29. Cyclic Compression Test Results: Load-Displacement Data, JLDTP1.

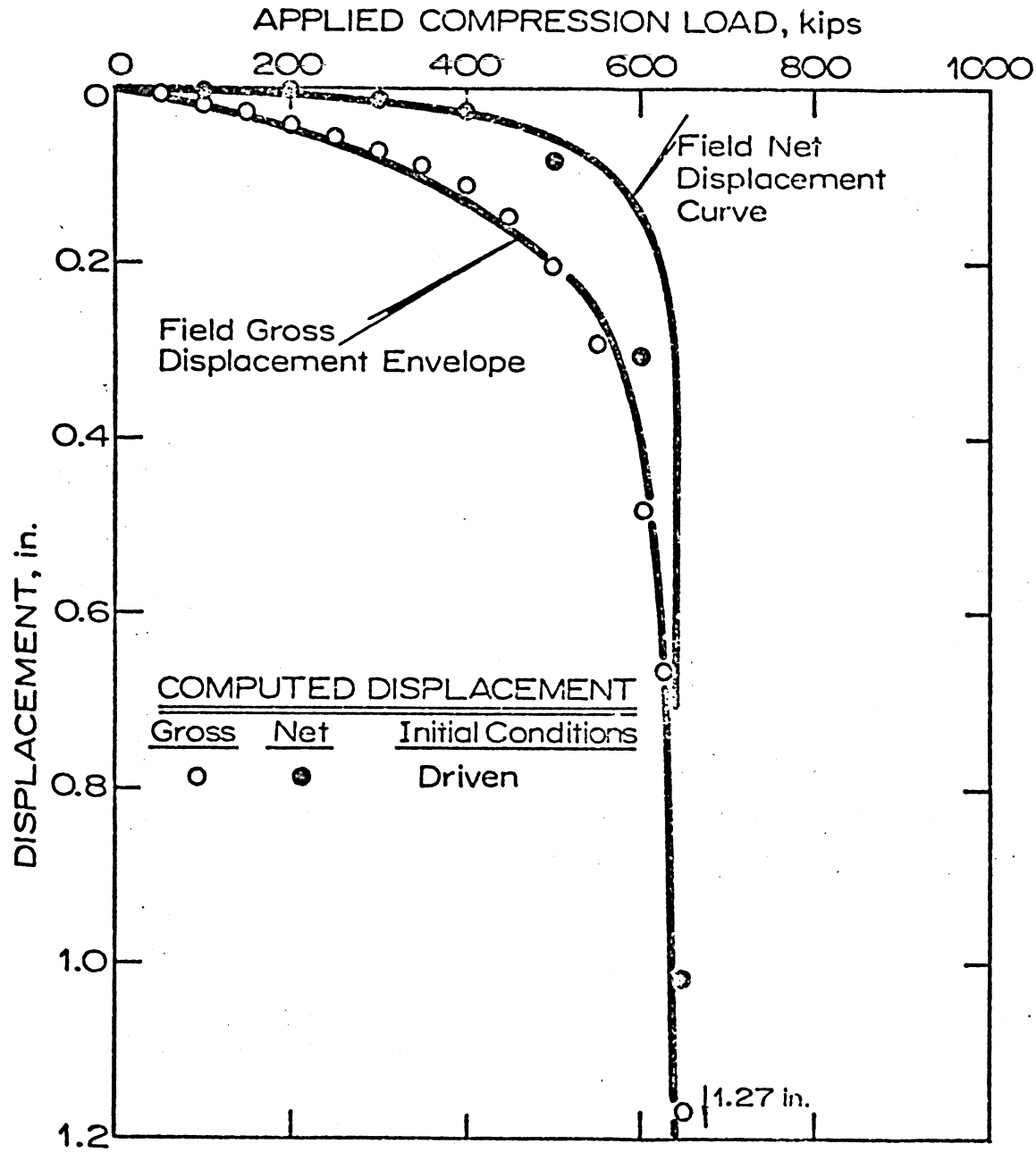

Figure V-30. Cyclic Compression Test Results: Load-Displacement Data, JLDTP2.

JLDTP3. Figure V-31 provides DUKFOR cyclic compression load-displacement predictions of JLDTP3. The computed gross and net displacements follow a trend toward overestimating the filed measured values, especially at thigher load levels. As with JLDTP1 one might suspect that a stiffer point resistance behavior is responsible, since the pile point is embedded one foot above the hard to very hard Tertiary clay stratum. If a stiffer point load transfer model were used (lower $QUAKE_p$) the predictions would be improved.

JLDTP2A. This test pile was jetted and driven to 39 ft embedment and driven (without jetting) the final 6 ft to grade. As with LD4TP16 it is assumed for the analysis that the value of K_s^c is constant with depth. The D/CC-CT simulation predictions of load-displacement behavior show excellent agreement with both gross and net displacement field measurements, see Figure V-32. Note, however, the prediction of less displacement at lower load levels. This suggests that the skin friction resistance is overestimated in the upper portion of the pile, where jetting was used. This is a reasonable expectation.

In order to model the jetted and driven pile-soil system a "two layer" soil profile could be used. For the final 6 ft driven the value of K_s^c could be assumed as that of a driven pile, e.g. $K_s^c = 0.772$ (corresponding to JLDTP2). The magnitude of load transferred in the lower 6 ft of embedment can then be directly computed as 84 kips. Subtracting that from Q_s^t (144 kips) suggests that the upper 39 ft of embedment provides 60 kips resistance. If it is further assumed that K_s^c is constant in the jetted region, the value of K_s^c would compute as 0.168. Such a low value of K_s^c in the upper 39 ft would definitely cause larger predicted displacements, both in compression and tension loading.

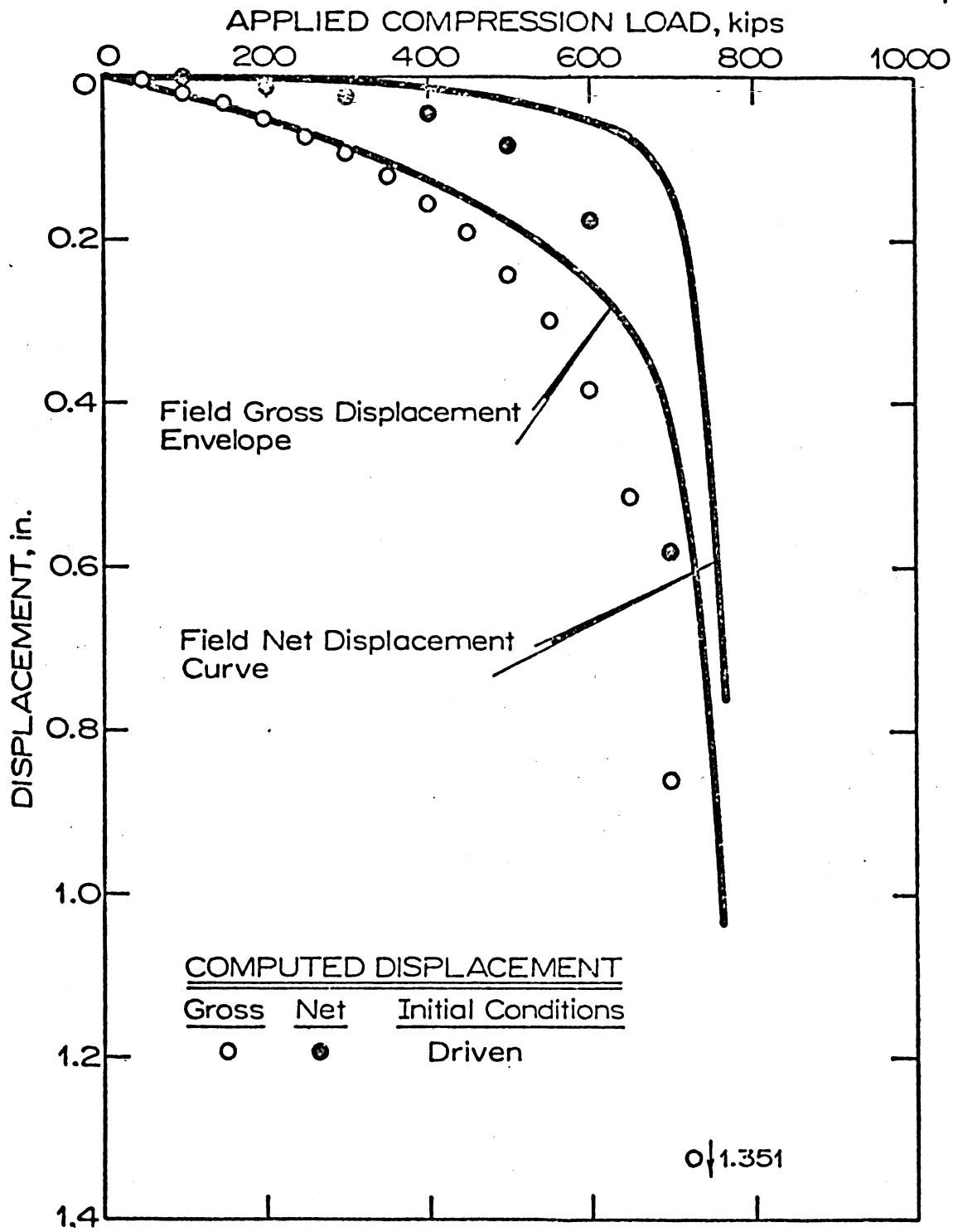

Figure V-31. Cyclic Compression Test Results: Load Displacement Data, JLDTP3.

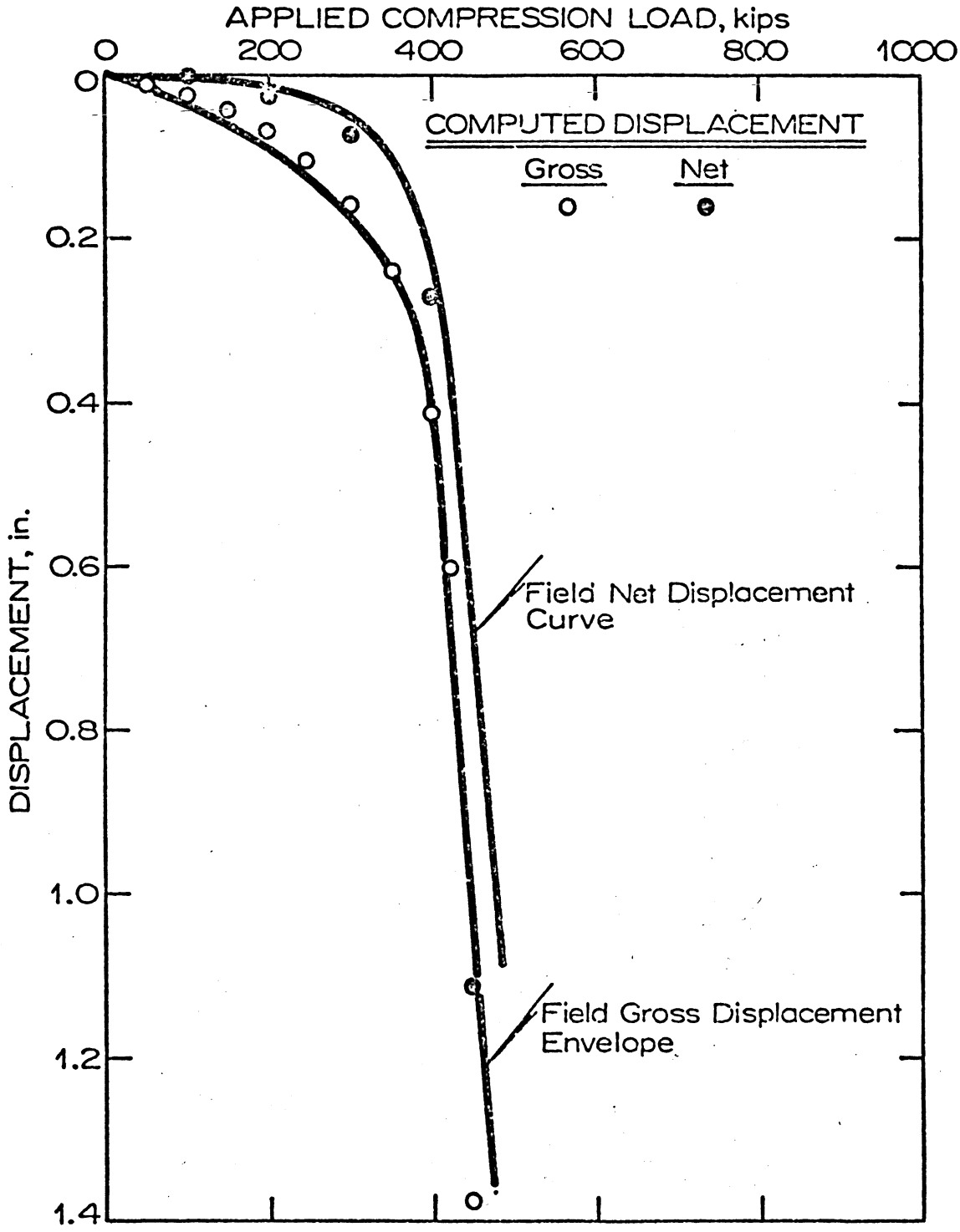

Figure V-3.2. Cyclic Compression Test Results: Load-Displacement Data, JLDTP2A.

JLDTP2A was analyzed in a previous study by Desai and Holloway[56] using an axisymmetric FE idealization. The JLD soil profile was modeled more rigorously as a three layered system, see Figure III-3. The load-displacement predictions of that study are given in Figure V-33 for comparison. Note that three values of lateral earth pressure coefficients were assumed with elasticity compatible Poisson's ratios to compare with the field measured data. Note the larger value of K_s^c (K_o in Figure V-33) required to simulate the JLDTP2A compression load-displacement behavior. The FE analyses assumed an initially stress free pile such that the parameters described in Figure V-33 are mobilized lateral earth pressure coefficients. The DUKFOR D/CC-CT analyses used $K_s^c = 0.4$, see Table V-8, corresponding to a value "corrected" for residual compression load distribution.

Tension Test Analyses

The tension test analyses for JLD test piles were performed in the same fashion as previous LD4 analyses. The direct simulation of the overall loading history was done using the D/CC-CT analysis of each JLD test pile. In addition a SF/T case was used to provide the direct comparison of residual compression load effects on tension test predictions. As all the JLD test piles were loaded in cyclic tension to failure, the comparisons between the SF/T case and the final reload cycle replotted at the origin should give reasonably close agreement. As noted for LD4TP2 analyses, the final reload cycle to failure in tension should most closely approximate a residual compression free pile, such that the stress free pile assumption is nearly correct.

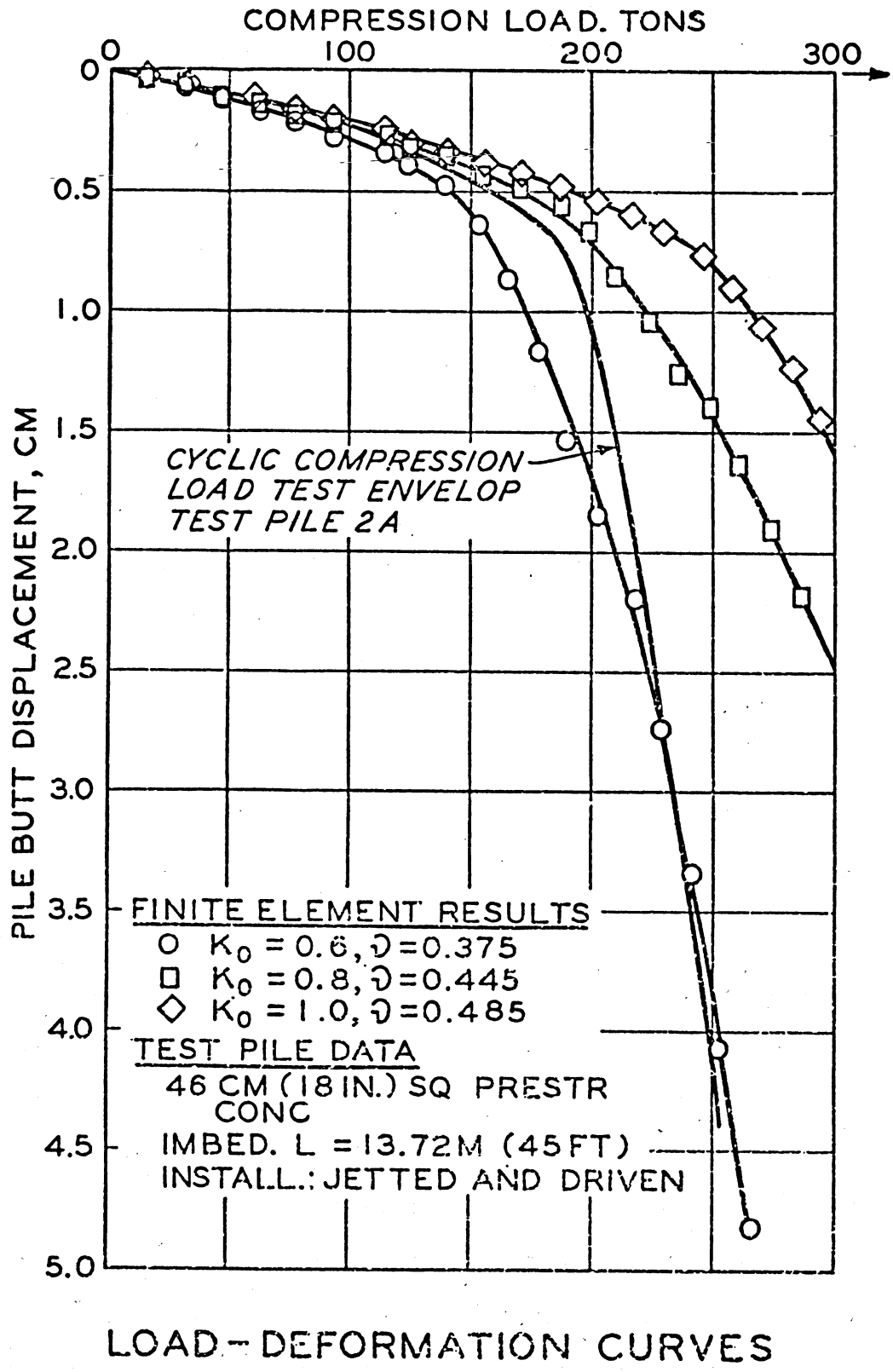

Figure V-33. Cyclic Compression Test Results: Load-Displacement Data; Axisymmetric FE Predictions from Desai and Holloway.[56]

It is interesting to note that the magnitude of backcalculated K_s^t values decreases with increasing pile embedment. The cause of this tendency is not readily apparent. Perhaps K_s decreases along the pile with depth. Without load distribution measurements this cannot be determined.

JLDTP1. Tension load-displacement predictions for JLDTP1 are presented in Figure V-34. The gross and net displacement predictions are reasonable up to -100 kips applied load. Thereafter, the field data indicate a much softer response (much larger displacements) than DUKFOR predicts. The explanation of this discrepancy could be the reduction of $\bar{\sigma}_n$, the normal stress on the pile shaft with increasing tension load transfer to the surrounding soil. This causes a strain-softening effect due to the reduction of confining stress level along the pile shaft. AXISYM results for LD4TP2 demonstrated this tendancy in Figure V-11. DUKFOR does not account for this behavior directly.

The computed displacements for the SF/T case provide good agreement with the replotted final reload cycle, verifying that the stress free pile assumptions approximate this behavior accurately.

JLDTP2. Tension load-displacement predictions for JLDTP2 are shown in Figure V-35. DUKFOR does much better in estimating JLDTP2 gross and net displacements than in the JLDTP1 analysis. It appears that the strain-softening phenomenon is less pronounced for this case. The primary differences are the depth of embedment and the values of K_s^t. It appears that for a lesser value of K_s^t the strain-softening tendency is not as dominant in the behavior. This seems reasonable since the tension load transferred at a given depth is less for the pile having a lower K_s^t value.

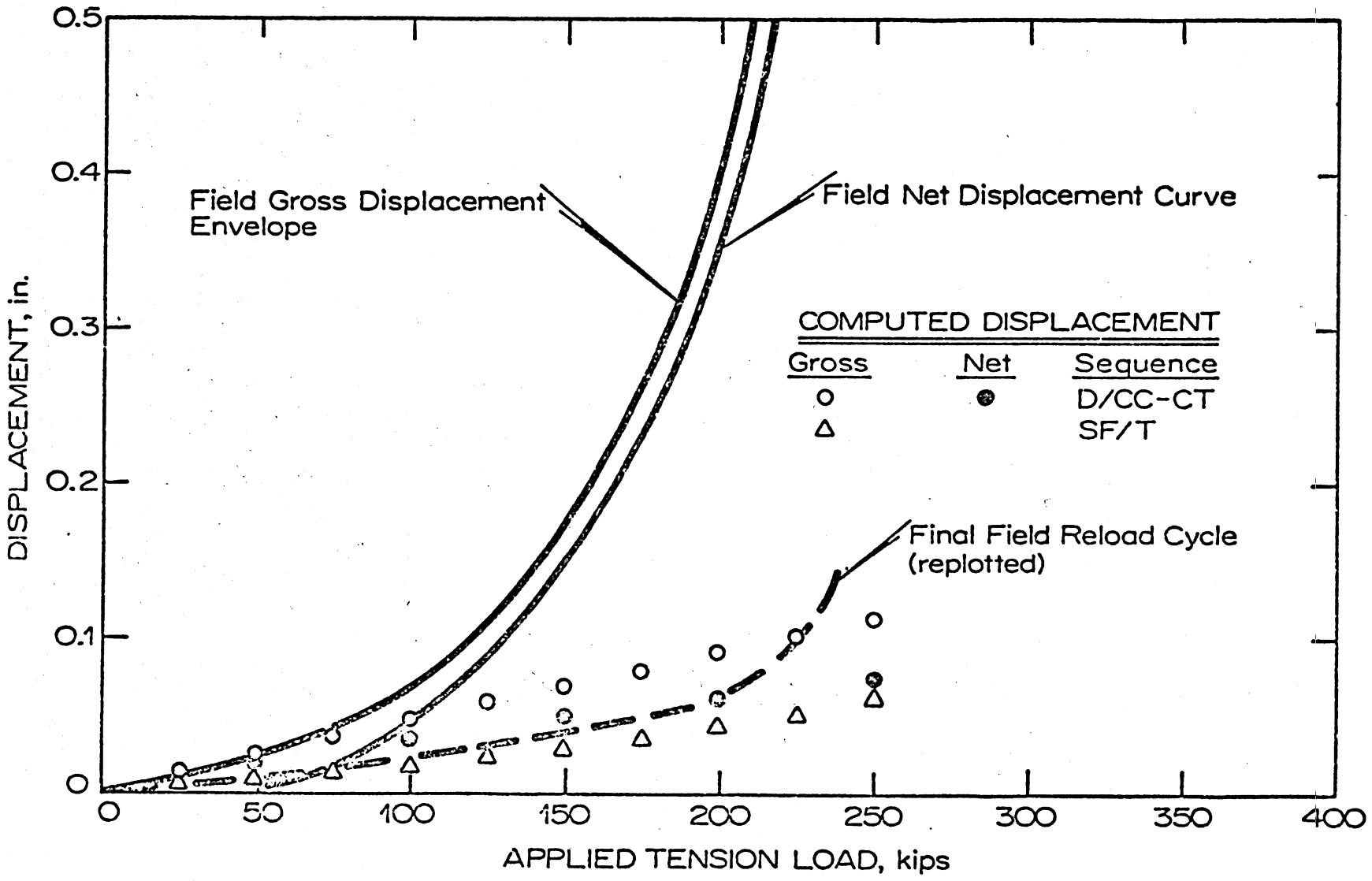

Figure V-34. Cyclic Tension Test Results: Load-Displacement Data, JLDTP1.

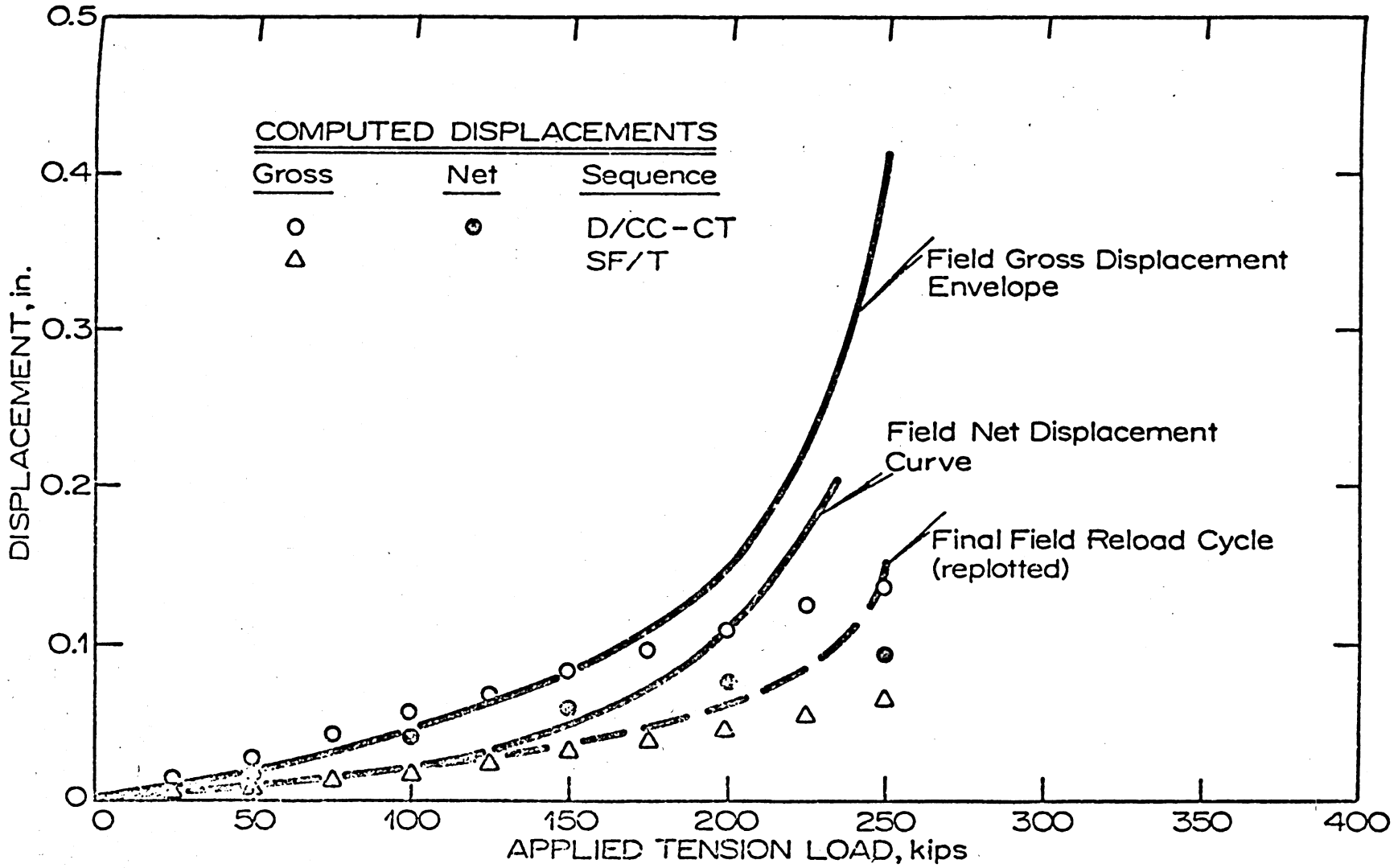

Figure V-35. Cyclic Tension Test Results: Load-Displacement Data, JLDTP2.

The SF/T case provides an excellent approximation of the final reload cycle.

JLDTP3. Figure V-36 describes tension load-displacement data for JLDTP3. The computed gross displacements agree reasonably well with field data up through -150 kips applied load. Thereafter, the softer response of the physical system develops. For this case the net displacement predictions overestimate the measured data. The SF/T simulation estimates the final reload cycle quite well. The only differences develop at the higher loads near failure where the strain softening effects predominate.

JLDTP2A. The data in Figure V-37 suggest that the DUKFOR model of the behavior is too stiff throughout the loading case. Even the SF/T case poorly approximates the final reload cycle. This is not surprising since these analyses assumed a constant K_s^t value along the full length. JLDTP2A was jetted 39 ft and driven the final 6 ft. If adjustment to K_s^t were made in a two layer assumption, the upper 39 ft would be assigned a much reduced K_s^t value. An example was discussed in the compression test analysis of JLDTP2A given previously. Were a lower K_s^t value used for the jetted depth, DUKFOR would predict larger displacements, since the load would be transferred to greater depths causing larger elastic deformations. The two layered model of a jetted and driven pile is more important for analyzing the tension test behavior.

Summary

Analyses of JLD test piles further verified the capabilities and limitations of the DUKFOR methods. Pile driving analyses provided blow count correlated damping values that are significantly lower than the parameters obtained from LD4 analyses. The differences in J_p and J_s

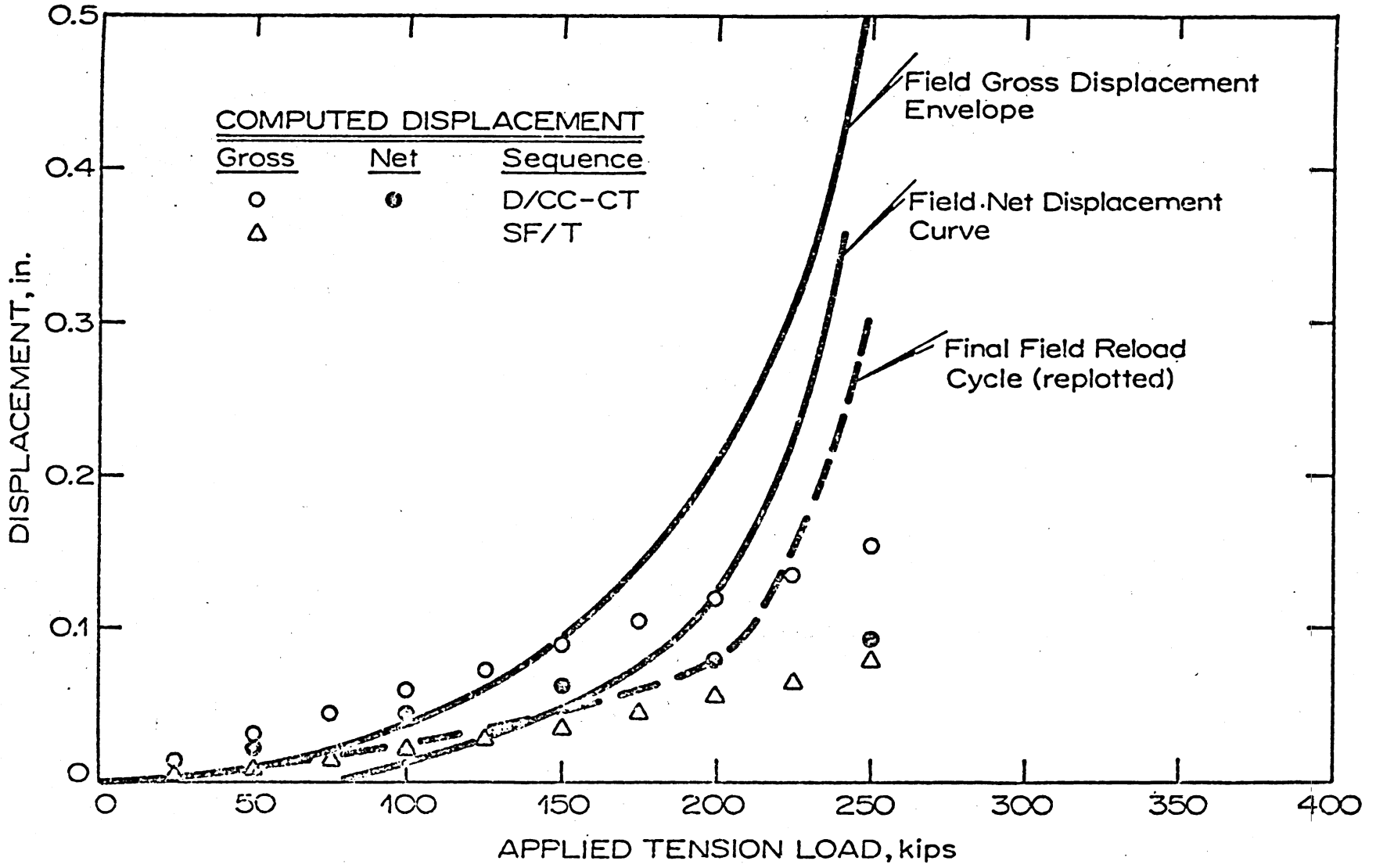

Figure V-36. Cyclic Tension Test Results: Load-Displacement Data, JLDTP3.

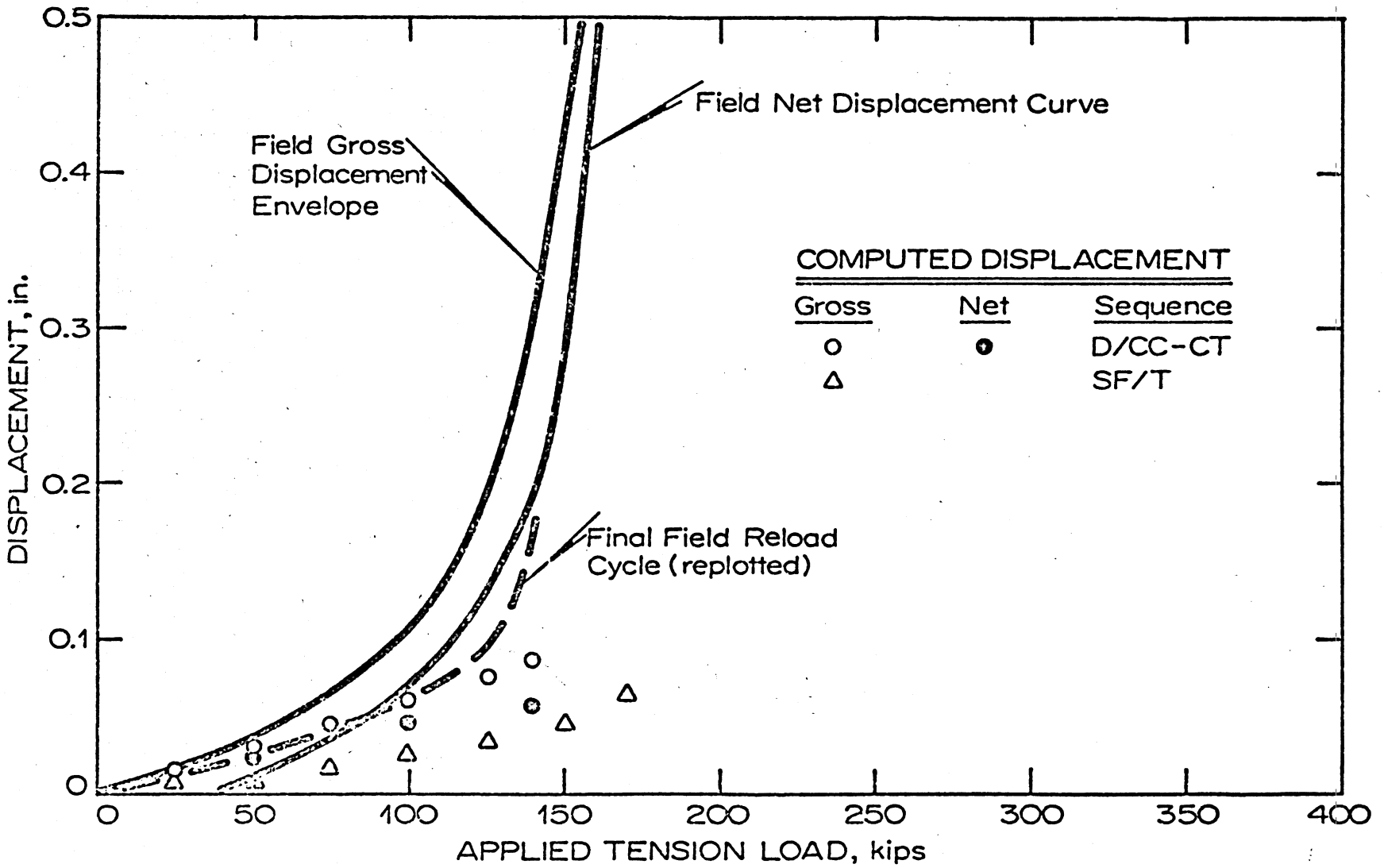

Figure V-37. Cyclic Tension Test Results: Load-Displacement Data, JLDTP2A.

values between JLD and LD4 test piles may be attributed to different dynamic deformation characteristics for the sands at the two sites. The pile driving system and piling used at JLD are significantly different from those at LD4. These may also affect pile driving characteristics, though the differences would be incorporated in the blow count correlations for damping values.

The cyclic compression load-displacement predictions provided some interesting observations. For two test piles, JLDTP1 and JLDTP3, DUKFOR predicted greater displacements than were actually measured. The discrepancies were attributed to the assumption of too soft a point resistance model in the DUKFOR ANALYSES. JLDTP1 was embedded in a dense gravelly layer, while JLDTP3 was driven to within one foot of the very hard Tertiany clay substratum. Both of these conditions would cause a stiffer point bearing response than that assumed. The value of initial tangent point quake was established from point load transfer measurements in medium dense sand at LD4. For JLDTP2 and JLDTP2A the predicted displacements were excellent. Points of these piles were embedded in a medium dense stratum.

DUKFOR predictions of cyclic tension load-displacement behavior demonstrated a stiffer response than field measurements indicate. The softer response of the actual pile-soil system has been explained as a strain-softening phenomenon which DUKFOR does not incorporate directly. The final reload cycles for the three fully driven piles (JLDTP1, 2 and 3) were accurately predicted assuming an initially stress free pile (SF/T case). This is consistent with the expectation that residual compression stresses would be absent in the final tension load cycle to failure.

Analyses of JLDTP2A, a jetted and driven pile, indicate that the reduced skin friction in the jetting zone needs to be accounted for in order to better predict the tension load-displacement behavior.

From tension test analyses it has been noted that two conditions dominate the load-displacement behavior: the residual compression load distribution at the start of the test causes greater displacements than would be expected for an initially stress free pile; and the apparent strain softening of the pile-soil system due to the reduction in effective confining stress by tension load transfer to the surrounding soil, which also increases measured displacements. DUKFOR incorporates residual compression loads in the analysis, but cannot directly simulate the strain softening effects. AXISYM can accommodate the relief of confining stress with tension loading and exhibit the strain softening response; however, the incorporation of residual compression load distributions is not readily available in the present version of AXISYM. As a result both computer codes are limited in their capability to predict tension load-displacement behavior.

Chapter VI

PARAMETRIC ANALYSES

Convergence and Stability

AXISYM

The axisymmetric FE idealization of a pile-soil interaction problem requires that a mathematical model be "designed" which accurately incorporates the significant features of the behavior. The AXISYM analyses of LD4TP2 demonstrate the particular simplifications needed to simulate static load test behavior of an impact-driven pile. Some of the important aspects of the analyses are discussed below.

Residual load effects. Discussion in Chapter III and analyses of LD4 pile tests in Chapter V demonstrated the importance of residual loads on load test interpretation. It was shown that the assumption of an initially stress free pile at the start of a compression load test leads to the measurement of mobilized shaft and point bearing capacities. The existence of significant residual compression loads at the pile point causes the mobilized point bearing capacity to be less than the actual point bearing value. As a result the apparent (mobilized) shaft capacity exceeds the actual shaft capacity by the difference between the actual and mobilized point bearing capacities.

The AXISYM analysis of the compression test on LD4TP2 required the assumption of an initially stress free pile. In order to simulate the compression load-displacement behavior it was necessary to assign the back-calculated mobilized coefficient of lateral earth pressure, K_s^c, in order to "accurately" predict the mobilized shaft capacity and load-displacement behavior. This artificial soil stress state would not be necessary in modeling a pile-soil system for which residual loads were small or absent, such as bored or buried piles. Data for LD4TP10 suggest that vibratory driven piles are relatively free of residual driving loads and could be simulated directly by AXISYM.

Discretization. The effects of discretization on solution convergence can be evaluated by direct analyses. The refined mesh given in Figure IV-3 was designed as the best approximation to the problem. The influence of mesh refinement is generally ignored in geotechnical practice. Two less refined meshes were used to evaluate their effects on the predicted displacements. A coarse mesh was designed using basically 10 ft x 10 ft soil element dimensions and 10 ft pile segment lengths. A 3 ft tip segment and 2 ft butt segment were included in the rectangular element system. A medium mesh was generated by subdividing the 10 ft dimensions to 5 ft x 5 ft maximum dimensions. The refined mesh, of course, uses much more refinement in the vicinity of the tip and in the radial direction near the pile. The lines of interface elements remained the same in each case, though element lengths varied, of course.

Load-displacement predictions using the three FE meshes are presented in Figure VI-1. There is a considerable difference in load-displacement results from one case to the next. The fact that the refined

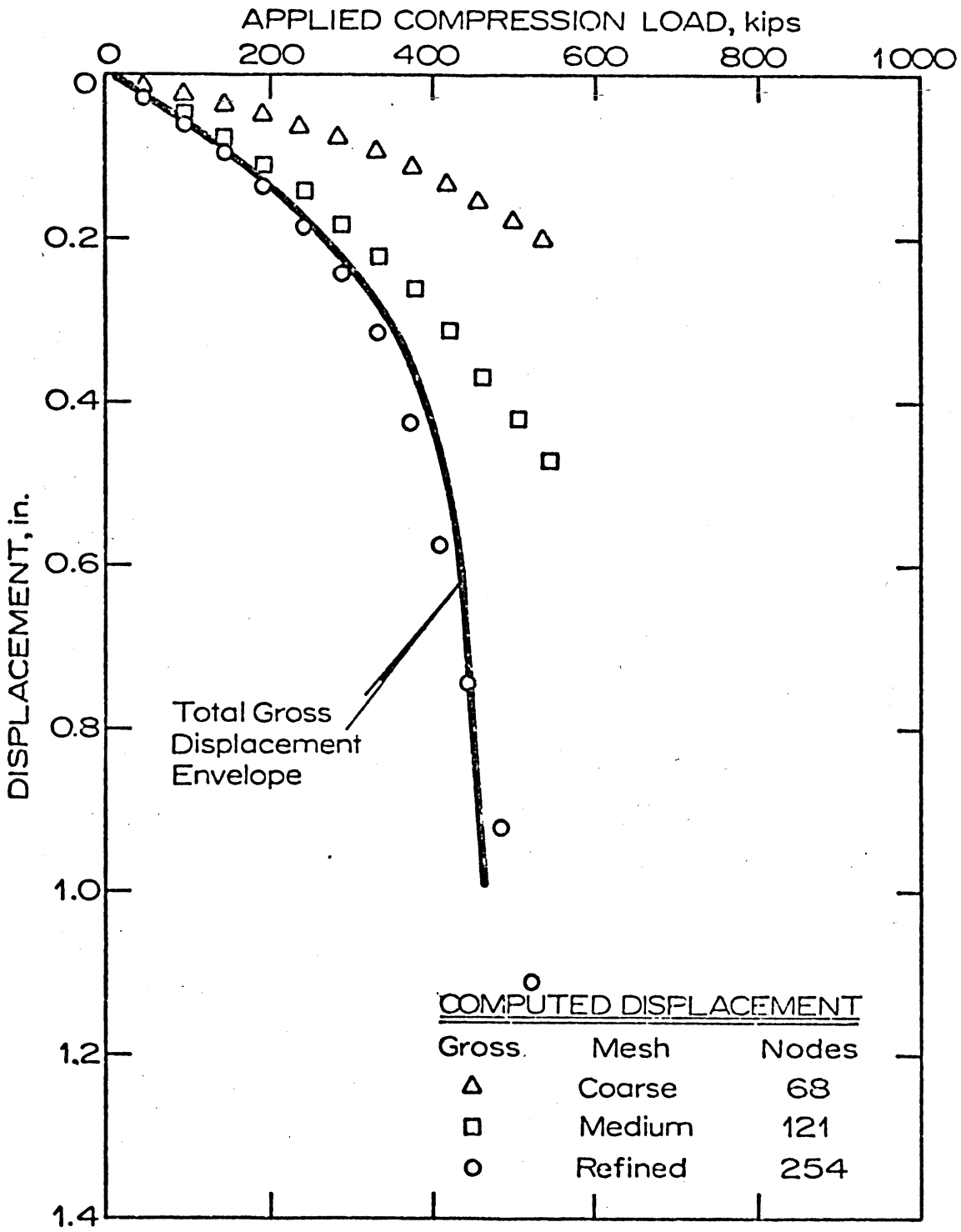

Figure VI-1. Cyclic Compression Test Results: Mesh Refinement Comparison for Load-Displacement Predictions, LD4TP2.

mesh most closely approximates the field measurements does not necessarily mean that the solution to the problem, as formulated, has actually converged. The fact that the results agree well with the field behavior make the comparisons with DUKFOR results more meaningful. Is it possible that a finer mesh might give significantly different results? For applications of FE techniques in practice such a question is rarely resolved. For the purpose of these investigations it is of minor importance. Nevertheless, these data demonstrate the importance of mesh design in applications of the FE method.

A second discretization concern involves selecting the loading increment magnitude. The AXISYM incremental, piecewise-linear displacement formulation uses the elemental tangent moduli based on current element stress level. One would expect that the AXISYM results predict a stiffer response (less displacement) than the convergent solution. The larger the load increment applied, the greater the inaccuracy, especially for highly nonlinear behavior. Iterations on the load step, employing revised estimates of moduli, provide for more rapid convergence for larger load increment magnitudes. There is clearly a trade-off in such an approach. The alternative is to reduce increment size, especially near dominant nonlinear portions of the load path. For pile test analyses load increments applied near plunging failure could be reduced to minimize overshoot problems.

A check was made to determine the influence of load increment magnitude. The refined mesh described in figure IV-3 was used for this purpose. Increment sizes of 25, 50, and 100 kips, respectively, were applied to 600 kips total load in three separate cases. It was found that

computed displacements and stresses were essentially the same for the 25 kips and 50 kip increment cases. The 100 kip increment results gave good agreement with the other two cases up to 400 kips applied load. Thereafter, the predictions underestimated the displacements somewhat. For the analyses described herein a 50 kip compression load increment was used. For the tension test analyses a 25 kip load increment was used.

Constituitive model. The stability of the constitutive model behavior is only a minor problem for monotonic loading conditions. Except in the vicinity of the pile point (which was isolated by the joint element configuration, see Figure IV-3) the elements behaved well. In other words, tensile failure and singularity conditions at the corner of the pile point did not propagate to adjacent soil elements.

Load reversal (e.g. compression unloading) caused erratic soil element behavior in the vicinity of the pile. At the start of the compression unload a number of soil and interface elements were at or near failure. Upon unloading the AXISYM constitutive model provides two choices. If the relatively small loading modulus is assigned in one of these elements a small reduction in shear stress is accompanied by a small reduction in confining stress level such that the element remains failed. On the other hand, if the relatively large unload/reload modulus is assigned the large pile displacement causes an excess reduction in confining stress and often results in failure in the opposite shear sense. One possible solution to the problem is to use very small loading increments and iterate at each loading step. The additional cost is excessive. An alternative would be the modification of the constituitive model in some manner.

Pile-soil interaction problems involve a complex combination of element stress paths in the vicinity of the pile. Due to the stress path-dependent nature of soil deformation behavior a common practice is to perform deformation testing (in situ and/or laboratory testing) using stress path(s) similar to that expected in the physical system. A battery of highly complicated stress path tests would be required to "accurately" model the pile-soil system thoroughly. For the AXISYM analyses of LD4TP2, however, the deformation properties from triaxial tests on JLD sand were used to model the soil behavior. As the load-displacement predictions were reasonably close to the field measurements, it appears that the load-displacement behavior is not very sensitive to the inaccuracies in the constitutive modeling techniques and assumed parameters.

DUKFOR

Pile driving solution stability and convergence criteria for DUKFOR are primary concerns in program usage. The guidelines in the literature for wave equation analyses have proven quite satisfactory, as in Smith's algorithm (e.g. TAMFOR.) Smith recommended that at least ten pile segments, ten ft in length or less, would provide satisfactory results. He also recommended that one-half the critical time increment in the system ($\Delta t = \Delta t_{crit}/2$) would be a satisfactory integration time step. For single blow analyses terminated upon achievement of maximum tip penetration, these guidelines are adequate.

DUKFOR analyzes a series of "complete" hammer blows to better simulate the physical behavior. The algorithm details were described in Chapter IV. LD4TP2 and JLDTP2 were analyzed to evaluate the effects of different parameters on the numerical solutions.

Figure VI-2 demonstrates solution convergence and stability quite effectively. The results using two very different sets of assumptions are plotted as relative peak resultant force on the pile versus time for LD4TP2. For the case PILSEG = 11, $\Delta t = \Delta t_{crit}$ the data clearly describe numerical instability. The resultant force magnitude diverges with time. For a freely suspended rod this assumption should give the exact solution.[8] The pile-soil interaction effects cause drastic instability, as Smith suggested.

For the case of PILSEG = 15, $\Delta t = \Delta t_{crit}/4$ (FACTOR = 4) a highly stable behavior is shown. The envelope of peak resultant forces converges rapidly with time. The envelope of these data remains essentially the same for subsequent hammer blows, providing static equilibration is satisfactorily performed.

Two points in time are labeled in Figure VI-2. Point A represents the instant when maximum penetration has been reached and rebound starts; the moment when TAMFOR would terminate the integration. If one subtracts the initial tangent quake from the maximum tip displacement of the first blow, (assuming full tip rebound) the predicted blow count is 44 B/ft. If the solution is statically equilibrated after point B , the predicted blow count is 38 B/ft. The fact that this value agrees with the measured blow count is no revelation. The damping parameters used for the analysis were correlated with blow count. The fact that it agrees fairly well with the TAMFOR-type assumptions indicates the relative insensitivity to residual loads of blow counts in this range.

Point B in Figure VI-2 signifies a very important integration interval for LD4TP2. The assignment of the minimum integration interval

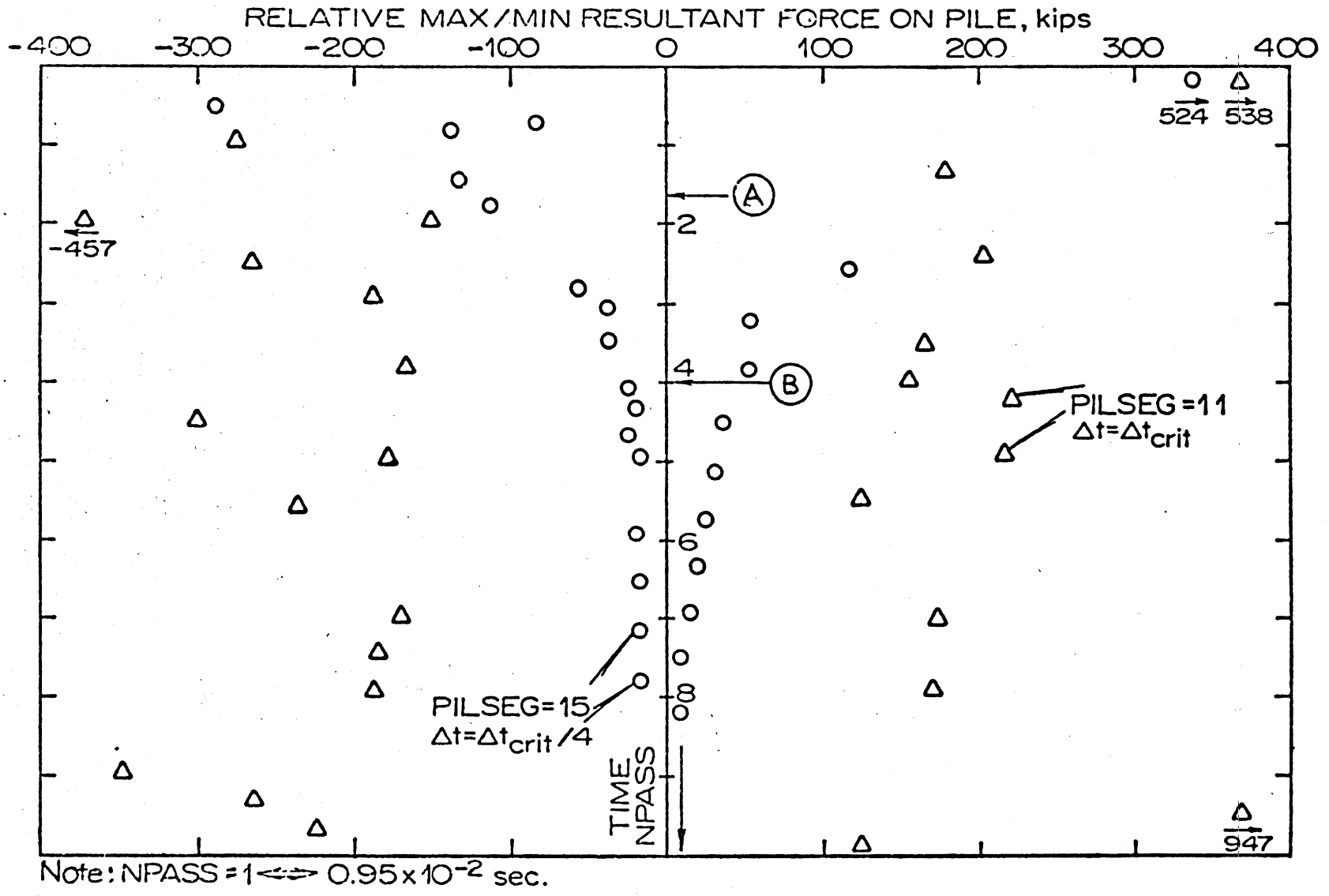

Figure VI-2. Pile Driving Results: Resultant Driving Force versus Time, LD4TP2.

per blow NPASS $\geq$ 4 gave essentially identical results. Five blow analyses using NPASS = 4, 6, 8, and 15 showed the same results for a given blow, regardless of NPASS. This implies that for this case (LD4TP2) the ram impact energy has performed all its useful work within 0.04 seconds. The remaining motion occurring in the system after NPASS = 4 is analogous to the free vibrations of a (not so) simple damped oscillator about the static equilibrium configuration.

For analyses described herein the static equilibration of inertia forces (equation IV-10) is performed after NPASS stress wave front passes, when the amplitude of the total resultant force is less than 1 kip (RESCK = 1). This would correspond to an instant in time when the oscillating resultant force passed across or near to the time axis. It should be noted that the resultant forces on particular pile segments may be appreciably larger than 1 kip. Stress waves "bounce" within the system thereafter, but the pile driving forces have been expended. Since an incremental static solution method is used, it is important to equilibrate the inertia forces at a moment when the magnitude of total force on the pile for any time step is generally nonzero, such that static equilibration is a numerical approximation.

The shape of the envelope of peak resultant forces is affected by a number of input parameters. It was found that, for LD4TP2 at least, convergence was more rapid for larger values of PILSEG and FACTOR (greater refinement in space and time). The amplitudes of forces at a given time interval decreased with greater refinement. Nevertheless, for PILSEG $\geq$ 15 and FACTOR $\geq$ 4, static equilibrium results were the same; Figure VI-3 describes 5th blow predictions of residual tip load and blow count versus

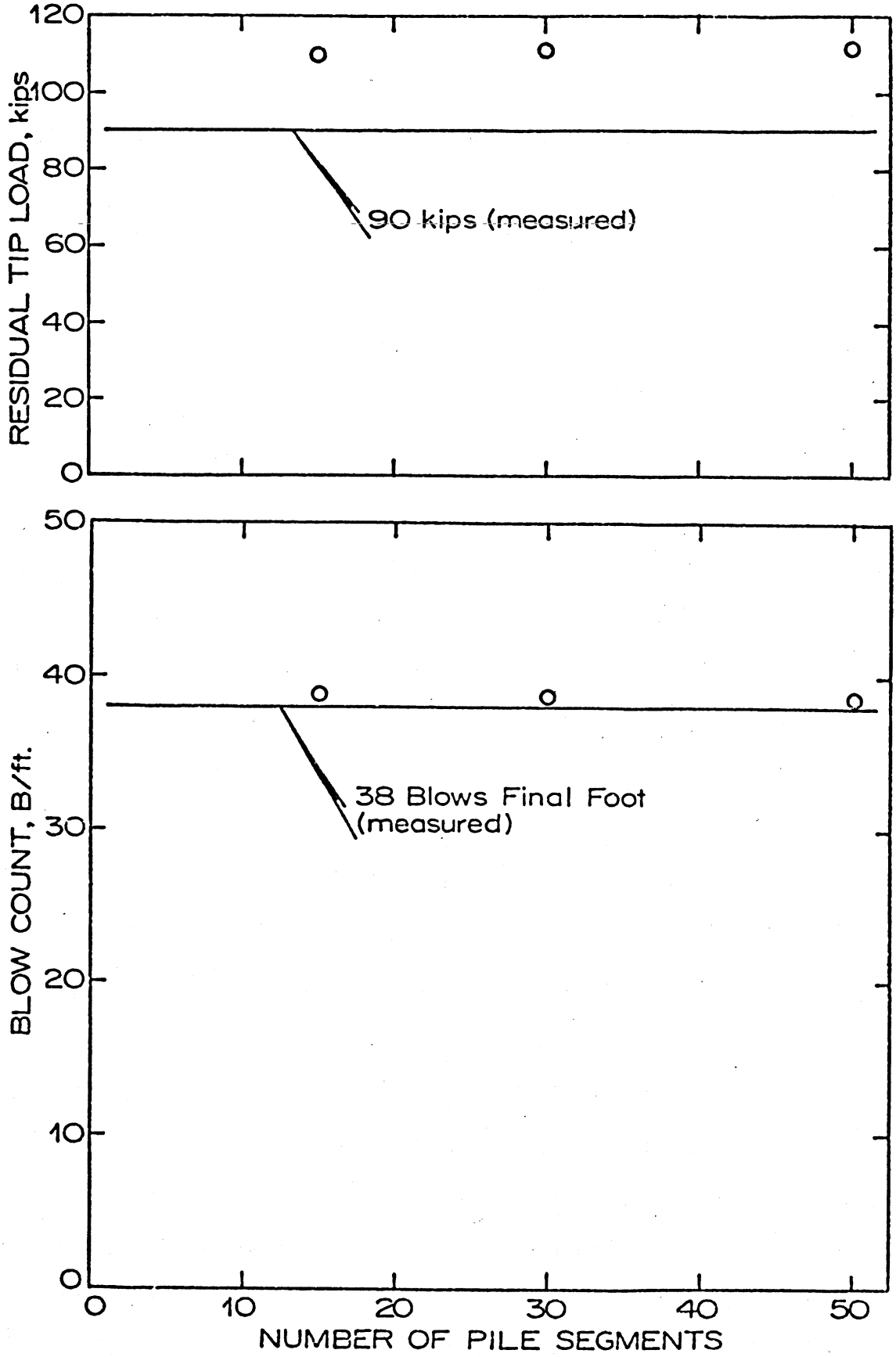

Figure V.I-3. Pile Driving Results: Affects of PILSEG on DUKFOR Predictions, LD4TP2.

PILSEG for LD4TP2. An increase in viscous (resistance) damping for a given system reduced resultant force amplitudes only during the first two wave front passes; thereafter, little difference was noted since the element velocities were relatively low.

One final point noted in the LD4TP2 evaluation is the rapid solution convergence (blow count and residual load distribution) with each blow. It was found that the solution reached a "steady-state" response after the third hammer blow. Residual stresses, blow count, element velocities and peak driving stresses were essentially identical for every blow thereafter using PILSEG = 15 and FACTOR = 4. This "steady-state" behavior was demonstrated for the third through tenth simulated blow, see Figure VI-4. These results describe the remarkable stability and convergence of the wave equation solution of this problem.

For analyses of JLDTP2, a high impedance prestressed concrete pile, it was found that for PILSEG > 20 ($\Delta L < 233$ ft) the multiple blow analyses showed some erratic behavior in blow counts and residual stress distributions. Since JLDTP2 is considerably stiffer than LD4TP2 (equivalent steel cross-section of 70 $in.^2$ versus 24 $in.^2$), and the driving stresses are roughly one-tenth as large, the smaller pile segments caused much smaller relative displacement differences (used to compute spring forces.) This apparently caused errors to propagate in the solution. As a result, for high impedance piling these data indicate that a minimum segment length may be a significant factor.

In terms of pile segment length the data generally suggest that PILSEG $\geq$ 15 and $\Delta L \geq 2.5$ ft are the most reasonable values for use in DUKFOR. It was interesting to note that for both LD4TP2 and JLDTP2 the

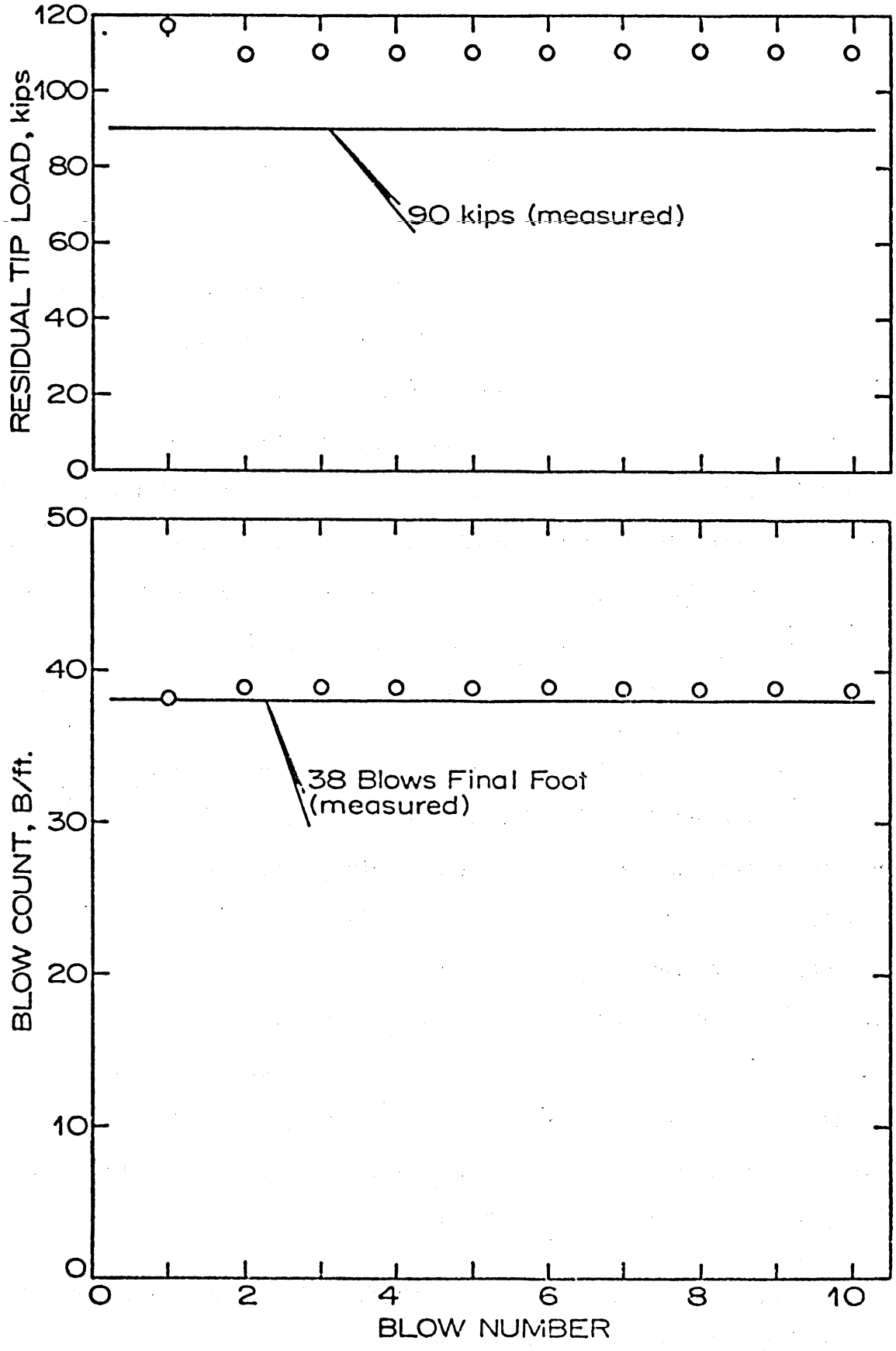

Figure VI-4. Pile Driving Results: Affects of Repeated Blows on DUKFOR Predictions, LD4TP2.

assignment of PILSEG = 5 gave stable steady-state solutions. It was not until PILSEG approached 15, however, that solution convergence was unaffected by PILSEG increase (except as noted above). This is likely due to discretization of the resistance distribution. For PILSEG = 15 and FACTOR = 4 the JLDTP2 behavior for 10 blows was as stable as that described in Figure VI-4 for LD4TP2.

The LD4 analyses were performed assuming NPASS = 6 with no problems whatsoever. The JLD analyses employed NPASS = 8. In general one should increase NPASS for any one of the following: a shorter pile; a higher impedance pile; a lower soil resistance; a greater impact energy; and a greater impact velocity. Any of these factors may increase penetration duration relative to the pile period. For short, high impedance piles there may be an upper limit on NPASS, beyond which numerical errors propagate rapidly. The first indication of potential solution stability problems is manifest in the behavior of element velocities at the end of each blow. If there is no trend toward a steady-state condition from blow to blow, especially if predictions are highly eratic, some revision of the problem description is warranted.

Parametric Analyses: Pile Driving Behavior

The preceding analyses provide assurance that reasonable assignments of hammer assembly-pile-soil system parameters provide acceptable engineering predictions of pile performance. The solutions obtained are remarkably stable and convergent. It was previously mentioned that mathematical models may be only as good as the assumptions and limitations of the technique. It is particularly useful to examine the sensitivity of the

analytical results to differences in resistance behavior models. In addition, other pertinent parametric variations are performed to determine their affects on pile driving performance.

LD4TP2 is used as a "control" case. Throughout this section the parameter variation labelled describes its isolated change relative to LD4TP2 input data. In this manner some general observations are made that provide insights into the pile-soil interaction phenomena. These cases are by no means comprehensive in scope. Experience with TAMFOR and DUKFOR indicates that each field case describes a relatively "unique" problem. The variations of driving system components, pile and soil resistance properties in practice makes the development of comprehensive "design curves" a futile exercise.

One additional fact should be noted. DUKFOR and AXISYM load distribution results only approximately predict the field-measured behavior of the LD4 test piles. The physical load transfer problem is more complex than these idealizations describe. The residual load distributions predicted by DUKFOR are clearly numerical approximations to the real behavior. The detailed shapes of these curves are no doubt inaccurate; however, the overall effects of these inaccuracies are apparently minor. For the purpose of the parametric studies the relative (if not exact) differences observed in the predicted residual driving load distribution curves and blow counts are meaningful.

Interface Shear Stiffness

To determine the effects of the interface shear (IS) deformation model on pile driving performance the hyperbolic stiffness coefficient, k,

was varied. Figure VI-5 compares the LD4TP2 results (corresponding to $\kappa = \bar{\kappa}$, the interface shear test value) with three other cases $\kappa = 2\bar{\kappa}$, $\bar{\kappa}/2$, and $\bar{\kappa}/10$. The pile driving results (after the fifth blow) indicate that a stiffer IS model gives somewhat larger residual loads. This is logical since the stiffer negative skin resistance behavior locks higher stresses in near the tip upon rebound. Reduced stiffness gives a lower level of residual loads. For a much reduced stiffness ($\bar{\kappa}/10$) the would-be residual tip load is greatly dissipated.

The actual value of κ for LD4TP2 may be anywhere in this range. Curves (2), (3) and (4) describe the most probable range of values expected. The residual load distributions and, particularly, blow counts are quite similar. This is quite reassuring since a precise value of κ is unknown. The deformations in the adjacent soil are, no doubt, interrelated with the strain-hardening and strain-softening phenomena noted previously. The influence of compaction and high shear deformations in the soil and at the pile-soil interface make accurate a priori determinations of the load transfer behavior impossible. These data suggest that the analyses are not very sensitive to the interface shear model. In terms of soil profile these results indicate that "soft" deposits should develop lower residual driving loads.

Point Resistance Stiffness

The effects of tip stiffness on LD4TP2 performance are demonstrated in Figure VI-6. The lower value of $QUAKE_p$ denotes a stiffer tip response ($k_{tip} = Q_p/QUAKE_p$). In this case the affects on blow count are minimal once more, but the reverse trend is noted for residual loads; the

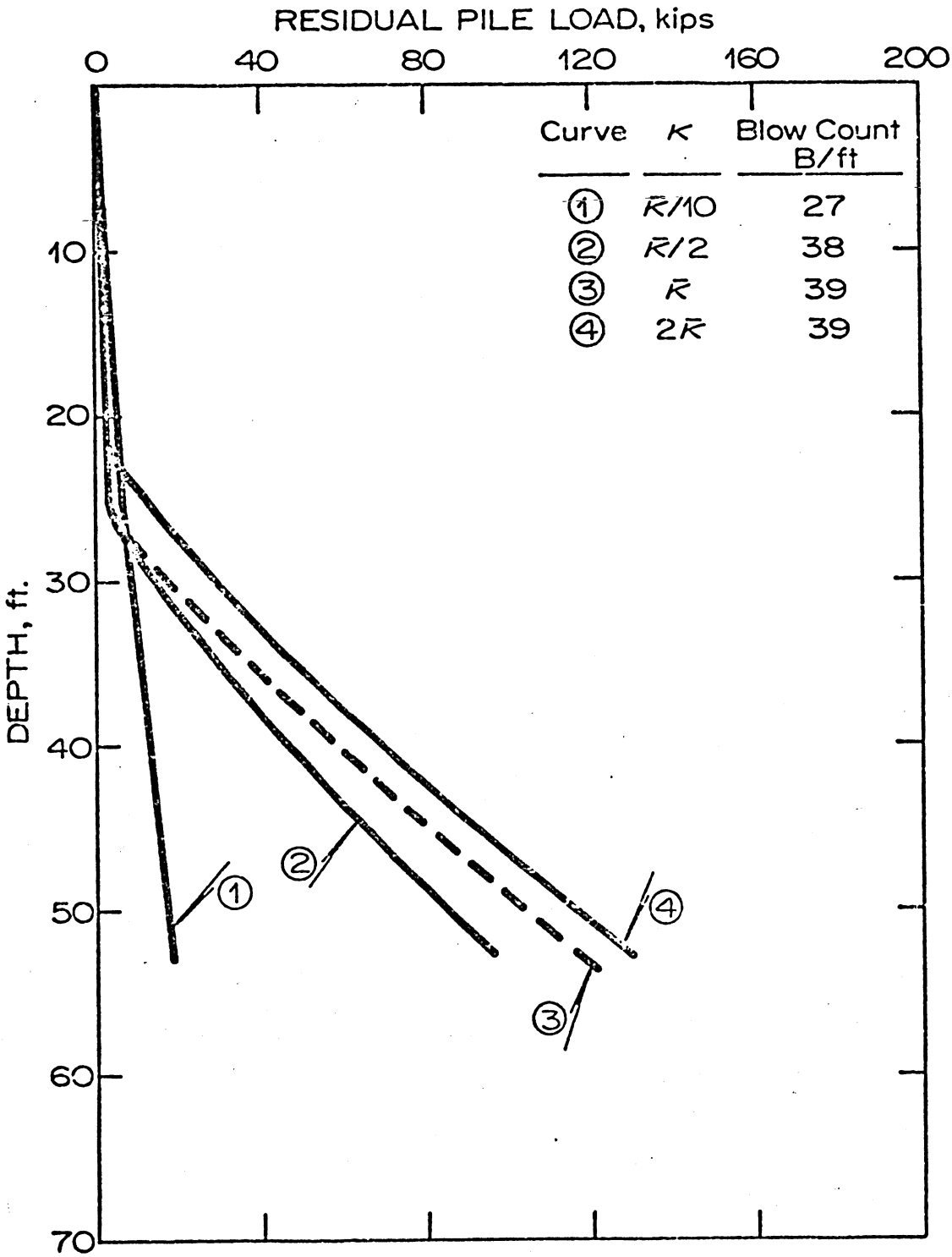

Figure VI-5. Parametric Analyses: Interface Shear Stiffness Affects.

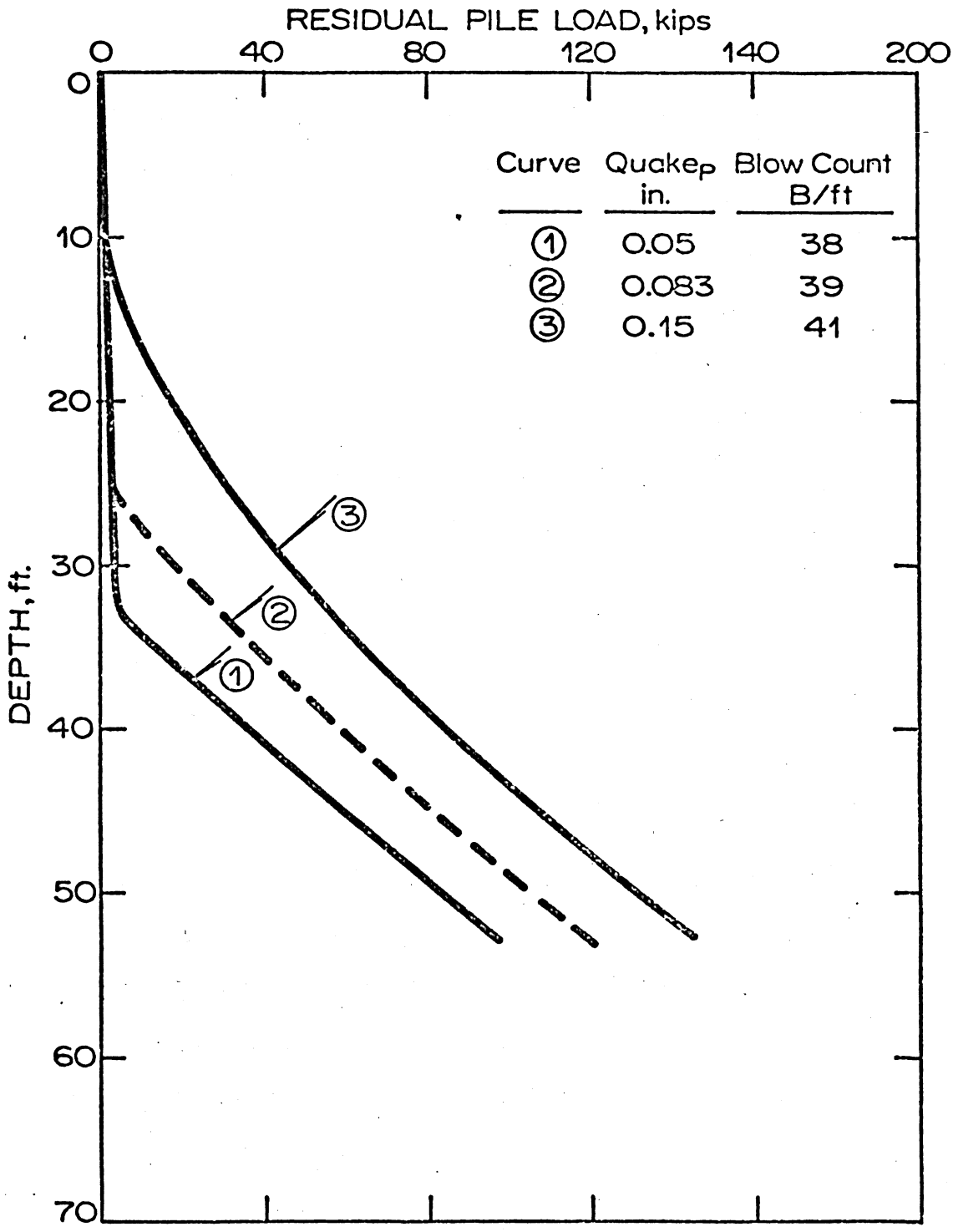

Figure VI-6. Parametric Analyses: Tip Resistance Stiffness Affects.

stiffer tip response gives a lower residual load distribution. In reaching equilibrium after the blow, the tip "spring" is unloading. For the interface behavior this results in (negative) friction loading. The stiffer (unloading) tip spring permits more load to be released from the tip upon rebound, reducing the residual tip load.

Figures VI-5 and VI-6 demonstrate that the measured residual point load for LD4TP2 could be better "predicted" by decreasing $QUAKE_p$ or decreasing κ. With no field measurements from which to develop load transfer relationships (correctly including measured residual load distributions), the actual causes of prediction errors are indeterminant. Nevertheless, the compression load-displacement predictions indicate that such load transfer accuracy is not needed for practical purposes, at least for pile test analyzed herein.

Soil Damping

Blow count increases almost linearly with an increase in J_p or J_s, as shown in Figures V-1 and V-26. The data plotted in Figure VI-7 correspond to results shown in Figure V-1. The affects of damping on predicted residual driving load distributions are rather small. A general trend suggests that greater damping results in somewhat lower residual pile stresses overall, but this is not significant. The minor affects on residual stresses indicate that the predicted load-displacement behavior should be relatively independent of soil damping used in the dynamic analyses. Damping greatly affects the predicted blow count; therefore, bearing capacity predictions from field-measured blow counts are sensitive to damping assumptions.

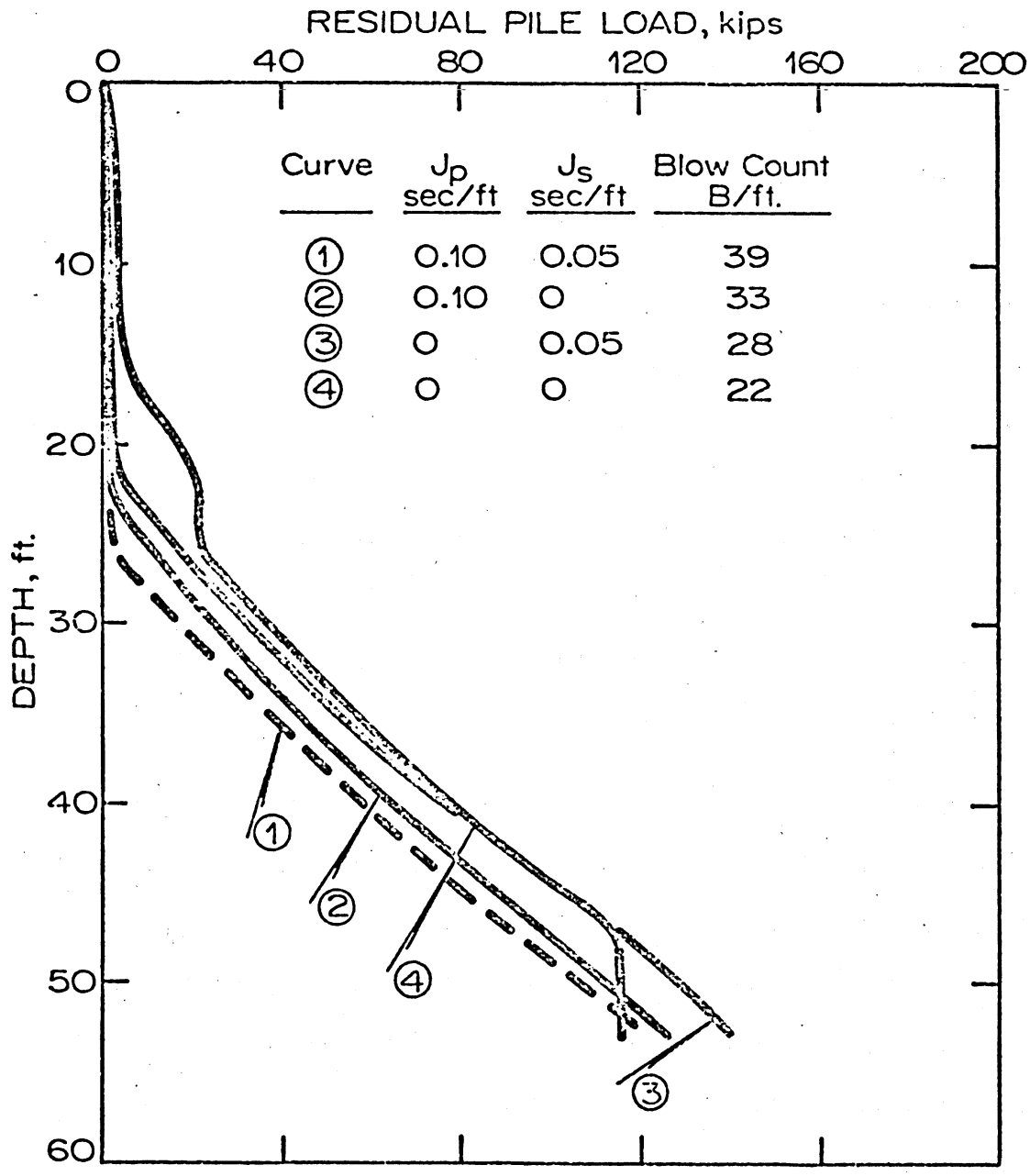

Figure VI-7. Parametric Analyses: Damping Resistance Affects.

Pile Stiffness

According to equation II-9 the ratio of pile impedance, ($\rho c A$), to driving system impedance, $\sqrt{\frac{W_{ram} K_c}{g}}$, should lie between 0.6 and 1.1 to insure efficient energy transmission ($\geq$ 90%). For the Vulcan 140C and micarta capblock, the driving system impedance is approximately 19 kip-sec/in. The range of pile impedances corresponds to an (equivalent) steel cross-section between 79 and 144 sq. in. LD4TP2 (24 sq. in.) provides an inefficient driving combination by these requirements. One would expect that a lighter cross section (e.g. 10 sq.in.) would be less efficient, and a much stiffer cross section (e.g. 70 sq.in.) would vastly improve the driving characteristics. A 70 sq.in. steel section has approximately the same impedance as the 18 in. square prestressed concrete piles at JLD. Pile stiffness affects were analyzed using the LD4 driving system, and the results are presented in Figure VI-8.

Data given in Figure VI-8 provides an interesting comparison of blow counts. For the low impedance pile (curve (1)) the blow count is nearly three times that of LD4TP2. Moreover, the peak driving stress exceeds 51 ksi, such that the ram would probably destroy such a light section. That is not unexpected. LD4TP2 analyses describe peak driving stresses of about 25 ksi. Note that the substantial increase in pile impedance gives only a small increase in penetration per blow over the LD4TP2 section (approximately 15 percent.) Indeed, for these moderate driving conditions the criterion of equation II-9 does not appear to be important.

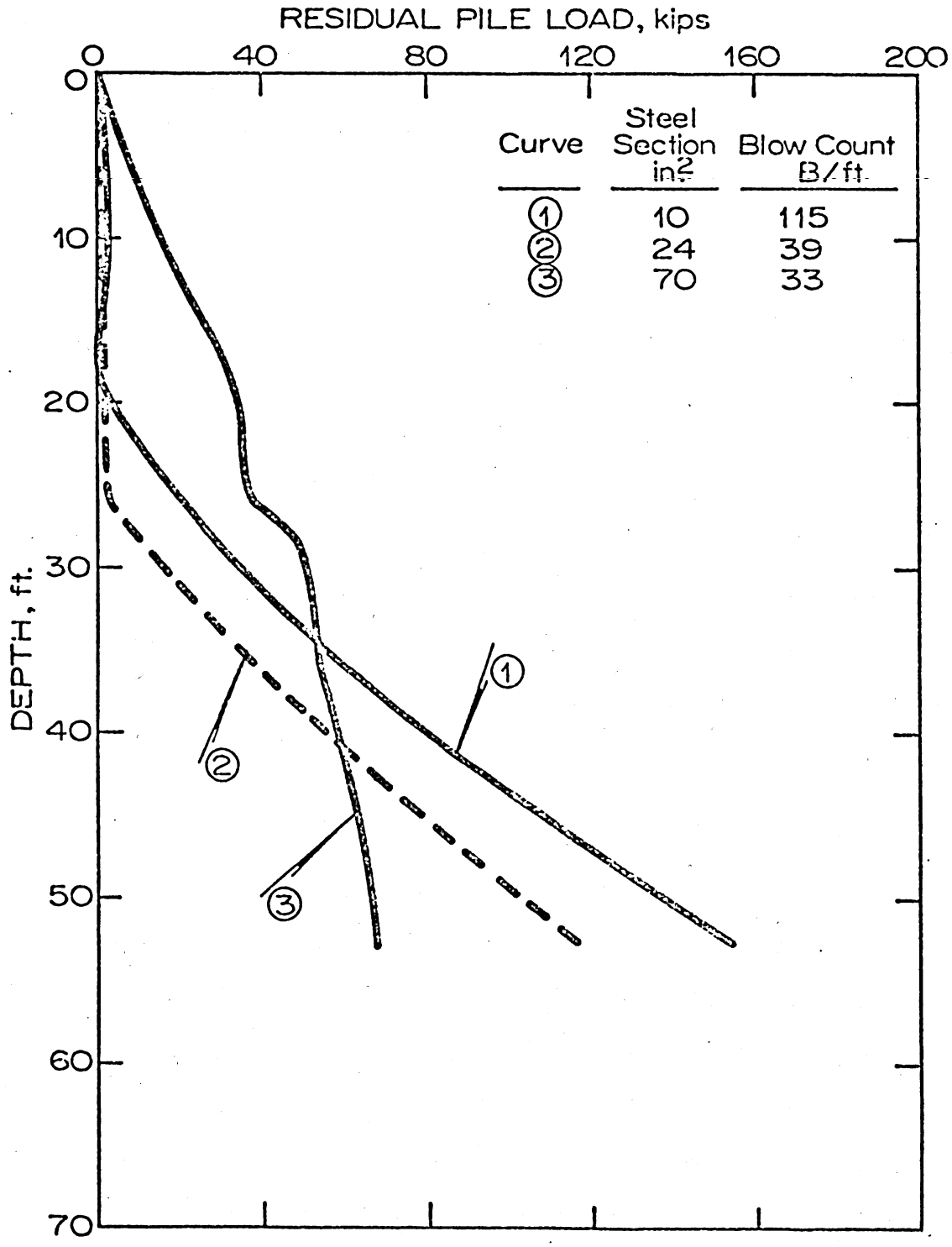

Figure VI-8. Parametric Analyses: Pile Stiffness Affects.

If the criterion were applied to drive the 10 sq.in. - section pile, equation II-9 would recommend an "efficient" 66 lb to 223 lb ram. It is obvious that this range of ram sizes could hardly drive the pile. An "efficient" ram for LD4TP2 would weigh between 383 lb. and 1286 lb. It is also quite likely that such an impedance match would inefficiently drive the pile, though the efficiency of (insufficient) energy transmission would be maximized. The direct application of equation II-9 proves inappropriate for this case.

The residual driving load distributions for the three pile impedance cases are presented in Figure VI-8. The stiffest pile section has the lowest residual point load and the lightest section develops the greatest residual point load. Both blow count and residual load distribution may be significantly affected by changes in pile section stiffness.

Embedment and Penetration Resistance

The influences of penetration resistance and embedment depth on residual load distribution are described in Figure VI-9. As one would suspect, the residual loads and blow counts increase with increasing resistance to penetration. Curves (1), (2), and (3) describe the 55 ft-long steel pipe pile embedded 53 ft (as LD4TP2) having 250, 502, and 750 kip capacities, respectively. Curves (4) and (5) represent 103 ft-long piles embedded 100 ft, with bearing capacities of 245 and 735 kips, respectively. For the 100 ft. embedment piles, (4) and (5), the K_s values were reduced to maintain Q_s and Q_p values the same as those of curves (1) and (3), respectively. These results indicate that curves (4) and (5) closely resemble curves (1) and (3) replotted to the "larger" scale. The magnitude of the

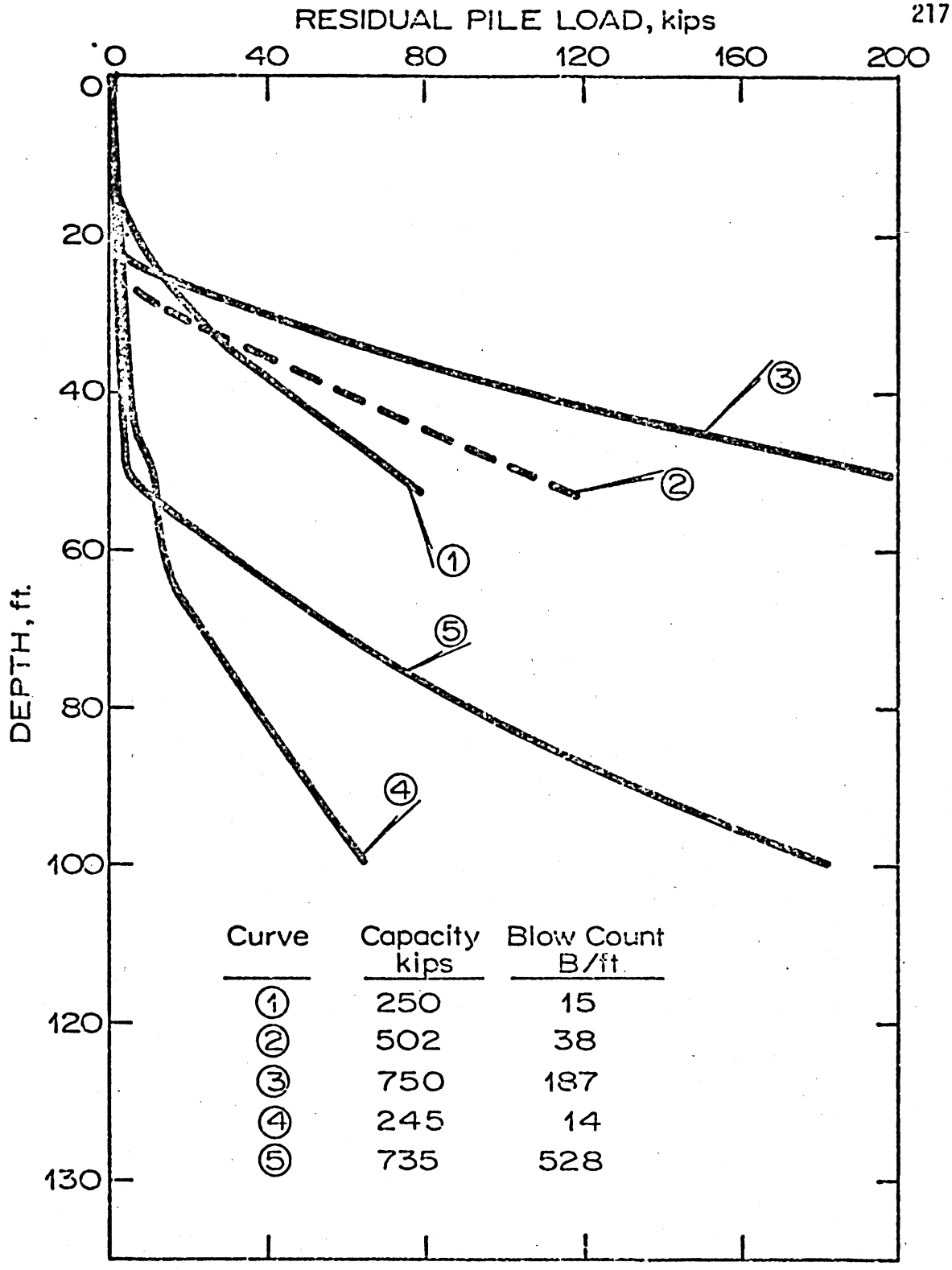

Figure VI-9. Parametric Analyses: Embeddment and Penetration Resistance Affects.

residual point load is dominated by the point capacity, and the slope of the residual load distribution curve is affected by the K_s values, as well.

The depth of embedment for low resistance to penetration has little influence on blow count. For higher capacity piles, however, blow count rises sharply for the same static resistance to penetration. For 490 kip static capacity the blow count increases to 68 B/ft for 100 ft embedment. This could be caused by two possible factors: elastic energy losses (due to a more flexible pile); and greater damping forces (though J_p and J_s were assumed constants from LD4TP2). A comparison was made using $J_p = J_s = 0$ for the 100 ft embedded pile, which predicted 27 B/ft. From Figure V-1 for LD4TP2 the zero damping case predicts 22 B/Ft. Therefore, these elastic losses are only a small part of the increase to 68 B/ft noted above.

The damping parameter J_s in the rheologic model (see equation II-6) is multiplied times the instantaneous elemental velocity and (the absolute value of) the element resistance force to obtain the dynamic resistance component. This suggests that the pile element velocities must be larger in magnitude throughout the 100 ft. embedded length to account for the large blow count increase. If J_p and J_s are constant with depth (a questionable assumption), the dynamic resistance to penetration will increase significantly with increasing penetration, even if Q_s and Q_p were to remain relatively unchanged.

Driving System

Impact energy is a primary concern in equipment selection. Three different cases were simulated to examine the effects of ram energy and

stress wave shape on pile driving performance. The most remarkable fact to be noted is that the impact driving system has no effect on the predicted residual driving load distribution. All of the data plotted almost exactly on the LD4TP2 results. The residual load distribution is a function of pile-soil system properties only, independent of the impact driver.

Table VI-1 presents the results of different driving systems on predicted LD4TP2 performance. Case 2 imparts the same impact energy (36,000 ft-lb) as the Vulcan 140C used at LD4, but with a lighter ram (requiring higher impact velocity). Case 3 uses the same W_{ram} (14,000 lb) as the Vulcan 140C, butt a lower E_{ram} (20,000 ft-lb), and therefore, lower impact velocity. Case 4 describes a "scaled-up" version of the Vulcan 140C with a larger E_{ram} (50,000 ft-lb) larger W_{ram} (19450 lb), having the same impact velocity. The predicted effects of the different systems are quite striking.

For Case 2 the impact velocity and peak stresses in the pile increase by about 50 percent over the control case results. The impact stress wave is increased in magnitude and decreased in duration for the lighter ram, as discussed in Chapter II, see Figure II-6. This case demonstrates a marked increase in driving efficiency which can only be attributed to the peak impact stress. Case 2 results indicate peak impact stresses reach 37 ksi, which could cause pile damage. Recall that one-dimensional analyses assume perfect hammer assembly-pile alignment which is not exactly correct in the physical system. Only a small eccentricity of the driving system or curvature in the upper portion of the pile may cause significant bending stresses in the pile section. These could cause localized pile buckling in case 2 such that a thicker capblock would be advisable. Such a remedy would reduce the impact stresses to a tolerable level and

probably increase the blow count somewhat.

Case 3 of Table VI-1 indicates the increase in blow count with the reduction of E_{ram}, which is as expected. Case 4, however, is particularly surprising since DUKFOR predicts that though E_{ram} and W_{ram} have increased 38 percent over case 1, there is no increase in driving efficiency; i.e. the blow counts are the same. One may only conclude that, for these cases at least, the peak driving stress dominates the pile driving efficiency. The peak driving stresses in case 4 are only slightly larger than those of case 1. These results suggest that an optimum driving system would deliver as large a magnitude impact stress wave as the pile can safely sustain without damage. As an example, for a given hammer the capblock thickness could be determined which will maximize penetration per blow and protect ram and pile from damage. The wave equation analysis offers the only means of properly optimizing the pile driving solution.

Program Capabilities and Limitations: AXISYM

Capabilities

The axisymmetric problem idealization models the single pile load test behavior of the entire pile-soil system. As such the analyses include deformations in the adjacent soil mass. It was found that the observed strain-hardening in compression loading and strain-softening in tension loading for LD4 test piles were predicted to a lesser extent by AXISYM for LD4TP2. No doubt a modification of soil properties (e.g. decreasing compressibility) could improve the predictions. A zone of

Table VI-I

DRIVING SYSTEM AFFECTS ON PILE PENETRATION

Case	E_{ram} (ft-lb)	W_{ram} (lb)	BLOW COUNT (B/ft)
1*	36,000	14,000	39
2	36,000	6,000	15
3	20,000	14,000	121
4	50,000	19,450	39

* Vulcan 140C, used at LD4.

highly compacted and sheared soil surrounds an impact-driven pile. Accurate simulation of the material properties and initial stress state within such a zone is a difficult task. The axisymmetric idealization at the present time is best suited for bored piles and piers, since the necessary initial conditions (stress-free pile) are essentially satisfied for these problems.

Limitations

The primary technical deficiency in AXISYM applications involves the neglect of residual loads. For impact-driven piles the initial conditions for the static formulation (AXISYM) must incorporate "mobilized" K_s^c values to predict effectively the load transfer at the pile shaft. The mobilized K_s^c values for LD4 test piles are listed in Table V-3. For unloading and load reversal conditions the numerical model behaves poorly. As such the AXISYM predictions of tension test behavior must neglect residual load distributions, which have a profound effect on the pile performance. Improvements in the static rheology models may rectify some of these difficulties. Residual driving effects throughout the pile-soil system make AXISYM analyses of impact-driven piles an artificial simulation.

The cost of analyzing a pile test case also may be a major problem. Since the cost vary widely between computer facilities, as well as between different users of the same system, direct comparisons are difficult. Comparative costs of AXISYM and DUKFOR analyses will be discussed in a subsequent section.

Program Capabilities and Limitations: DUKFOR

Capabilities

It has been demonstrated in previous sections that residual pile stresses may influence profoundly both load test performance and the interpretation of field measurements. DUKFOR provides a dynamic/static formulation which simulates pile driving behavior in a thorough, rational procedure. A series of impact hammer blows may be applied to establish a "steady-state" response, which predicts the effects of previous blows on subsequent pile performance. Since the solution approximates static equilibrium at the end of each blow, an arbitrary static load test sequence may be applied to the driven pile. In this manner the effects of residual driving load distributions are incorporated directly.

The DUKFOR one-dimensional idealization greatly simplifies the interface shear and point resistance rheology. This is a particular advantage in simulating pile driving performance and cyclic load test behavior. Moreover, the dynamic and static problem solutions are relatively inexpensive. This allows the engineer to investigate bounds on his design assumptions directly.

A very important <u>design</u> capability generally overlooked in practice is the selection of compatible and efficient hammer assembly-pile-soil "systems". DUKFOR provides an effective means of optimizing the (total) design within the limits of the analytical assumptions. Due to the nature of pile-soil interaction the design assumptions are not always accurate; however, the elimination of unsuitable solutions to the foundation problem and relative comparisons between different proposed solutions

may produce significant savings.

Limitations

The primary limitations in DUKFOR analyses involve the load transfer idealization. As the one-dimensional model lumps the pile-soil slip and adjacent soil deformations at the mathematical "interface", the parameters must be somewhat arbitrary. For LD4 and JLD analyses it was assumed that properties from interface shear test results represented the load transfer behavior. For driven piles the pile-soil interface and soil deformations are the product of soil compaction and high shear and normal stress levels near the pile shaft. Some tendancies toward stiffening of soil resistance in compression loading and softening in tension loading were noted in the measured data. Though load distribution predictions differ somewhat form field measurements, the load-displacement predictions are generally quite good.

The results of LD4 and JLD analyses suggest that the use of interface shear test properties in load transfer models gives quite satisfactory results. A parametric evaluation of interface shear stiffness effects indicates that parameters within +100 percent and -50 percent of the shear test values made little difference in the pile driving performance. For a case in which one-tenth of the laboratory test parameter was used, both blow count and residual loads were appreciably reduced. For a softer or more compressible soil deposit the actual load transfer along the shaft may describe larger deformations than interface shear tests predict. Bored piles or piers may behave in a similar manner, since compaction phenomena due to impact driving are absent in such cases. Future analyses

of pile tests under these conditions should clarify this point. None were studied for the present investigation. Load transfer measurements by Coyle and Reese[63] could be applied for piles in cohesive soils, if transient phenomena can be predicted.

One additional limitation of DUKFOR analyses is the arbitrary assignment of point load-deformation behavior. Since the static pile design involves an estimate of point bearing capacity, the deformation behavior is the "unknown". For piles in medium to dense sands at LD4 and JLD, a hyperbolic load-displacement model has been applied successfully. For impact-driven piles embedded in relatively uniform deposits, a "standard" initial tangent point quake, $QUAKE_p$, (0.05 in. per foot of point diameter) was assigned. This value was generally consistent with LD4 measurements. For a Bodine-driven pile (LD4TP10) larger deformations with load were measured, similar to what one would expect for a bored or buried pile. A larger $QUAKE_p$ was used in the LD4TP10 analyses, see Table V-5. For two piles at JLD (JLDTP1 and JLDTP3) the existence of a stiffer bearing stratum at or near the pile point indicated that smaller $QUAKE_p$ values should be assigned for such conditions.

Comparative Costs: AXISYM and DUKFOR

A direct comparison of computation costs between AXISYM and DUKFOR analyses should be particularly helpful in considering possible applications of these methods. Both computer codes are operational on the Triangle Universities Computation Center (TUCC) IBM 370 Model 165 system with which Duke University is affiliated, and on the GE/Honeywell 635 computer system at WES. The TUCC computer has a machine cycle time of

80 nanoseconds (0.08×10^{-6} seconds/cycle) versus that of the WES computer 1 microsecond ($1. \times 10^{-6}$sec/cycle). Computer costs are based upon formulae that are rarely the same from facility to facility. Very often the CPU time, etc., involve factors rendering the time in "equivalent" system seconds that are not directly comparable. Such is the case for the data described below.

AXISYM

Representative numbers from identical AXISYM analyses of LD4TP2 are presented in Table VI-2. On the WES system the AXISYM requires 80,000 octal words of core memory during execution. The TUCC system requires 300,000 bytes of core memory, approximately 75.000 octal words. Once the program is operational and/or updated, the compile step need not be repeated. Most computer facilities provide the user with a compiled version of the program which may be stored as a physical object deck, on disk and/or on magnetic tape. Therefore, for production runs the object program may be executed, eleminating the compile step.

The dollar amounts presented in Table V-11 represent "prime time" costs, which describe a reasonable range of normal priority costs one might expect. The primary differences between the TUCC and WES costs involve apparent rate differences. Both TUCC and WES systems provide non-prime rates (for overnight or weekend runs) that cut user costs by as much as 50 percent. When possible the nonprime time runs are advisable, of course. These data represent program computations costs, exclusively. The cost of input preparation will greatly depend on the experience of the user.

Table VI-2

Comparative Costs of AXISYM Analyses, LD4TP2*

	WES		TUCC	
	Time** (min:sec)	Cost*** (dollars)	Time** (min:sec)	Cost*** (dollars)
COMPILE	:30	17	:50	10
EXECUTE				
CPU	10:48		1:39	
I/O	3:12	—	1:43	—
Total Execution Costs		$87		$38

NOTES:

* LD4TP2 analysis using refined mesh of Figure IV-3 (254 nodes, 216 element, 12 x 50 kip compression load increments.)

** The time units are system seconds, which may include various multiplication factors for a particular computer system.

*** These costs are computed for "prime user times" (normal priority.)

DUKFOR

Table VI-3 presents comparative program execution costs of DUKFOR analyses of LD4TP2 on WES and TUCC computer systems. As before, the WES costs are roughly 2.3 times the TUCC costs, describing the difference in charge rates between the two. The compile cost of DUKFOR on TUCC was about two thirds that of AXISYM. For production runs a stored, compiled version of DUKFOR should be used. The DUKFOR costs are separated for three different analysis cases: dynamic only; static only; dynamic/static. The sum of charges in the first two cases is not equal to that of the third case because the I/O time does not double. DUKFOR requires 90,000 bytes of core memory (about 23,000 octal words) on the TUCC system during execution.

A comparison between AXISYM and DUKFOR execution costs of analyzing LD4TP2 indicates a large difference, as expected. If the DUKFOR dynamic/static solution is considered, the solution costs one-tenth that of AXISYM. Detailed results of the two LD4TP2 analyses were discussed previously in Chapter V. Actually, a direct comparison of the "static only" DUKFOR costs with AXISYM indicates that essentially identical predictions were obtained for less than 3 percent of the cost of the AXISYM analysis. Indeed, the DUKFOR "static only" costs include both cyclic compression and cyclic tension test behavior, while the AXISYM data involves only the compression test simulation. An increase in load increment size and/or decrease in mesh refinement would reduce the AXISYM analysis costs, but this could possibly change the predicted results.

Table VI-3

COMPARATIVE COSTS OF DUKFOR
Analyses, LD4TP2*

	WES		TUCC	
	Time** (min:sec)	Cost*** (dollars)	Time** (Min:sec)	Cost*** (dollars)
Pile Driving				
Analysis (dynamic only)				
EXECUTE				
CPU			0:15.7	
I/O			0:04.4	
Separate Analysis Cost				$ 3.36
Load Test				
Analysis (static only)				
EXECUTE				
CPU			0:02.3	
I/O			0:03.9	
Separate Analysis Cost				$ 1.01
Complete				
Analysis (dynamic/static)				
EXECUTE				
CPU	1:42.2		0:18.0	
I/O	0:14.4		0:04.9	
Total analysis cost		$ 8.83		$ 3.84

Table VI-3 (con'd)

Notes:

* LD4TP2 analysis using PILSEG = 15, NPASS = 6, FACTOR = 4, IBLOWS = 5; cyclic compression/cyclic tension load test simulated.

** The time units are system seconds, which may include various multiplication factors for a particular computer system.

*** These costs are computed for "prime user times" (normal priority.)

These data describe the relative solution economy of DUKFOR over AXISYM usage in obtaining solutions of comparable accuracy in predicting field measurements. The input requirements to DUKFOR are typical design parameters, alleviating most of the mesh and material property preparation costs involved in using AXISYM. From both technical and practical considerations, DUKFOR better models pile-soil interaction behavior, especially for impact driven piles.

Chapter VII

CONCLUSIONS AND RECOMMENDATIONS

Pile foundation design is as much an art as a science in engineering practice. Solutions frequently rely heavily on engineering judgment due to difficulties in modeling the complex nature of pile-soil interaction behavior. It was the purpose of this study to undertake the analysis of single vertical piles in cohesionless soils, incorporating for the first time the sequential simulation of pile driving and axial load tests. It was determined to keep the analysis as straightforward as possible, relying primarily on basic soil mechanics concepts.

The primary end product of this research project is a combined dynamic/static, one-dimensional discrete element computer code, DUKFOR, which was devised to simulate pile-soil interaction in a reasonable manner. The dynamic wave equation solution method was employed which permits multiple blow analyses of impact driving, modeling the physical process more accurately than previous wave equation computer codes. The static solution algorithm is used to equilibrate the stresses at the end of each simulated hammer blow, thus determining residual pile-soil stresses due to driving. In this manner initial conditions are provided

for the application of a subsequent hammer blow or for the start of static load test simulation. DUKFOR permits the analysis of pile performance due to any arbitrary axial loading sequence.

An additional product of this research effort is an axisymmetric finite element code, AXISYM, which was developed to compare static load test predictions with those from DUKFOR. AXISYM models axisymmetric or plane strain boundary pressure or concentrated load problems using a piecewise linear, incremental/iterative formulation. One-dimensional interface slip elements are provided in the code to describe interelement displacements across selected element boundaries. These slip elements were placed between the pile and the soil to model pile-soil interface behavior. They were used also in the soil immediately beneath the pile point to simulate the relative movements caused by punching of the point into the soil; in this case the interface elements were placed between adjacent soil elements.

Both the AXISYM and DUKFOR codes were used in analyses of instrumented pile tests so that predicted and observed results could be compared. In one case a detailed study was made using both codes; eight other pile load tests were analyzed using DUKFOR alone. In addition, parametric investigations were made to determine stability and convergence criteria for each of the computer codes. Finally, a parameter study was made using DUKFOR to evaluate the effects of various hammer assembly-pile-soil system characteristics on pile driving performance. The results of these studies provide some meaningful insights into the phenomena of pile-soil interaction in cohesionless soils.

Basic Capabilities of DUKFOR

The present version of DUKFOR provides for impact simulation of single- and double-acting pile drivers, exclusively. No attempt was made to simulate diesel hammer behavior nor to apply the impact as a force-time record. Both of these options could be incorporated in future updates of DUKFOR.

Due to its problem formulation DUKFOR offers a number of advantages over other wave equation programs. First, all of the soil parameters except dynamic damping are directly obtained from conventional test programs involving triaxial and interface tests. The straightforward application of data from these tests proved successful in analyzing the instrumented pile load tests. The second and most important difference between DUKFOR and other codes is that it can model the application of a series of individual hammer blows followed by an arbitrary static load sequence. Static equilibrium conditions are established at the end of each simulated blow providing the initial conditions for subsequent behavior simulation. After several hammer blows the method converges to a "steady-state" solution, whereafter predicted blow counts and residual stress distributions are duplicated for each subsequent simulated blow. The solution is stable and convergent, obtaining the steady-state conditions within 3 to 5 simulated blows in every case studied. Having obtained the steady-state pile driving solution, the static equilibrium conditions after the last hammer blow may be applied as initial conditions for load test simulation using the DUKFOR static solution algorithm.

The primary difficulty in applying DUKFOR or other wave equation methods to pile driving analyses lies in defining the soil

resistance rheology or damping. The complex phenomena of pile-soil interaction and the variability of soil deposits in nature make accurate determination of the dynamic load transfer behavior extremely difficult. As such, simplified resistance models are assumed in pile driving analyses.

The magnitudes of predicted blow counts greatly depend on the soil resistance rheology, specifically on the magnitude of the viscous damping forces assumed. It was shown in this work that the nonlinear, viscous damping parameters commonly employed in analyses are not unique soil properties, but rather, interdependent correlation constants. From site to site these damping values may differ significantly, even though the soils are apparently similar. The use of correlated damping parameters from Lock and Dam No. 4, Arkansas River, Arkansas (LD4) analyses to predict Jonesville Lock and Dam, Ouachita and Black Rivers, Arkansas and Louisiana (JLD) pile capacities from blow counts alone gives very poor estimates of the measured pile capacities. The use of wave equation results from any code to predict pile capacities from driving records without pile test verification requires the utmost caution.

Pile Test Analyses

Conventional analytical methods for predicting single pile performance have important limitations. Limit equilibrium methods generally ignore significant factors which directly affect pile performance. Soil compressibility and the complete stress-deformation state in the vicinity of the pile are implicitly ignored by most limit equilibrium models.

Axisymmetric finite element (FE) solutions at present offer the

most rigorous mathematical approximation of static pile-soil interaction. Deformation and failure behavior of the various components of the pile-soil system can be modeled directly. Residual driving load distributions, however, cannot be conveniently incorporated in the formulations presently available. Analyses using the axisymmetric FE code, AXISYM, demonstrate that artificial approximations are required to compensate for the effects of residual driving stresses on load test behavior. For example, to obtain good agreement with observed compression test results a value of k_s of 1.3 was assumed in the FE analyses, a value well above that actually measured (0.9). Axisymmetric FE solutions are best, in fact, suited for modeling the behavior of bored or buried single piles where residual stress effects are minimal.

The one-dimensional DUKFOR representation of the installation and load test behavior generally simulated load test behavior well. Predictions of compression load-displacement behavior were remarkably accurate for all nine test piles studied. Pile load distributions predicted by DUKFOR also compared fairly well with available field measurements. However, at loads approaching compression failure the field measurements suggest an increasing contribution of skin friction in the upper half of the pile. DUKFOR did not predict this behavior directly. The results from the AXISYM code suggest that the phenomenon is due to a strain-hardening effect causing an increase in confining stress level and thus skin friction along the upper pile shaft. Such behavior cannot be readily accommodated by the DUKFOR type of formulation.

Tension load-displacement predictions using DUKFOR are fairly accurate at lower load levels. For loads approaching tension failure DUKFOR underestimated the measured displacements in most cases. This

appears to be caused by a strain-softening tendency, the reverse of that observed in the compression analyses, that is not simulated in DUKFOR. AXISYM analyses show that the strain-softening behavior is related to a decrease in confining stress level due to tension load transfer to the surrounding soil. The DUKFOR and AXISYM analyses indicate that tension test performance is directly affected by the strain-softening phenomena and residual compression load distributions caused by previous driving and/or compression load testing. DUKFOR incorporates residual loads in load test simulation, but the strain-softening effects are not directly included. AXISYM approximates the strain-softening effects, but it is impractical to simulate residual load effects using AXISYM. Both codes are limited in these respects for tension test analyses.

Residual Load Effects

Impact pile driving and/or compression load application generally cause the development of residual compression load distributions at the end of driving or load testing. The existence of these residual load distributions has a direct effect on the subsequent pile performance.

For impact-driven displacement piles a significant residual point load often develops during driving. It appears that the residual load distribution depends directly on the pile-soil system only, independent of the impact pile driver used. When a residual point load remains after driving it is clear that a portion of the point bearing capacity has already been mobilized. Analyses of load distribution measurements (gages zeroed at the start of the load test) commonly ignore these residual load conditions. For compression load testing to failure

the measured point bearing value in such cases is only that mobilized from the start of the load test. The actual point capacity is the mobilized (measured) value plus the residual point load. If residual loads are ignored, the magnitude of tip capacity is underestimated. This mistake could be important in designs which rely on such load test results.

Residual compression loads also directly affect the manner in which shaft resistance is mobilized. For compression load-displacement behavior residual compression loads cause a stiffer response (less displacement) than an initially stress-free pile having the exact same total capacity since there is effectively greater mobilized shaft resistance.

Tension load-displacement behavior is also strongly influenced by residual compression load in the pile. In this case the residual shaft resistance after driving is mobilized along the upper shaft in the negative sense (same as that to be induced by tension loading). The application of tension load requires that the mobilized shaft resistance must develop at greater depth, causing larger butt displacements than would be observed for an initially stress-free pile. DUKFOR provides a reasonable analytical method for incorporating residual loads induced by driving in cohesionless soils.

Driving System Analysis

In addition to the functions previously described, DUKFOR may be used effectively in designing the hammer assembly-pile-soil system. Consideration of installation problems is often overlooked in foundation design. The DUKFOR wave equation solution offers an effective means of comparing different pile driving systems directly. For example, DUKFOR

parametric analyses of LD4 Test Pile 2 (LD4TP2) show that the penetration per blow increases markedly with increasing peak impact stress. The capblock cushion thickness could have been designed to maintain peak stresses below tolerable levels, while maximizing the penetration per blow.

Summation

The methods developed herein are useful engineering tools for evaluating the performance of single piles in sand. DUKFOR offers a practical and economical means of predicting pile driving and load test behavior within the limits of the one-dimensional idealization. However, arching effects within the surrounding soil are not accounted for in the solution. AXISYM, representative of a finite element-type solution, provides a more rigorous mathematical formulation of pile-soil system behavior; however, it requires far greater computational effort and more refined determination of the in-situ conditions than can usually be justified for practical purposes. Further, residual stress effects are not readily accommodated in such codes.

Thus, both of the analytical procedures have advantages and disadvantages. In the final analysis it would appear that the DUKFOR code offers the practical designer the most readily useful tool, because of its advantages of economy and simplicity. Based upon the results of this study, further improvements could yet be made in the DUKFOR formulation to enhance its capabilities. Useful future efforts could be directed towards the representation of soil arching effects and the simulation of other types of force inputs to the top of the pile.

A more complete analytical model of pile-soil interaction can well be developed in future studies. Nevertheless, it is apparent from the results of this study that the true nature of these problems necessitates a full measure of engineering judgment in obtaining a solution. Sound engineering judgment and rational analytical methods represent the best applications in practice, a goal towards which this effort is dedicated.

APPENDIX

Appendix

MATERIAL BEHAVIOR REPRESENTATIONS

A significant amount of engineering research into pile-soil interaction has involved obtaining representative models of the component behaviors. For impact pile driving problems the hammer assembly, pile, pile-soil interface and soil properties all share important roles in measured/predicted behavior. A summary of the available data on the various system components is given below.

Impact Hammers

Impact pile drivers may include a vast assortment of driving accessories needed to adapt the hammer to the pile and to the driving conditions. As DUKFOR does not simulate vibratory hammer behavior, impact pile drivers will be discussed exclusively.

A schematic diagram of three major types of impact pile drivers is given in figure A-1. The simplest hammer in the group is the drop hammer. The ram mass is raised mechanically to a prescribed stroke and released. The free-fall force of gravity imparts kinetic energy to the mass which strikes the pile driving assembly, transmitting driving energy to the pile. The rated hammer energy, E_{ram}, is given as the net potential energy at the moment of release, $W_{ram}h$. To account for energy losses, a mechanical

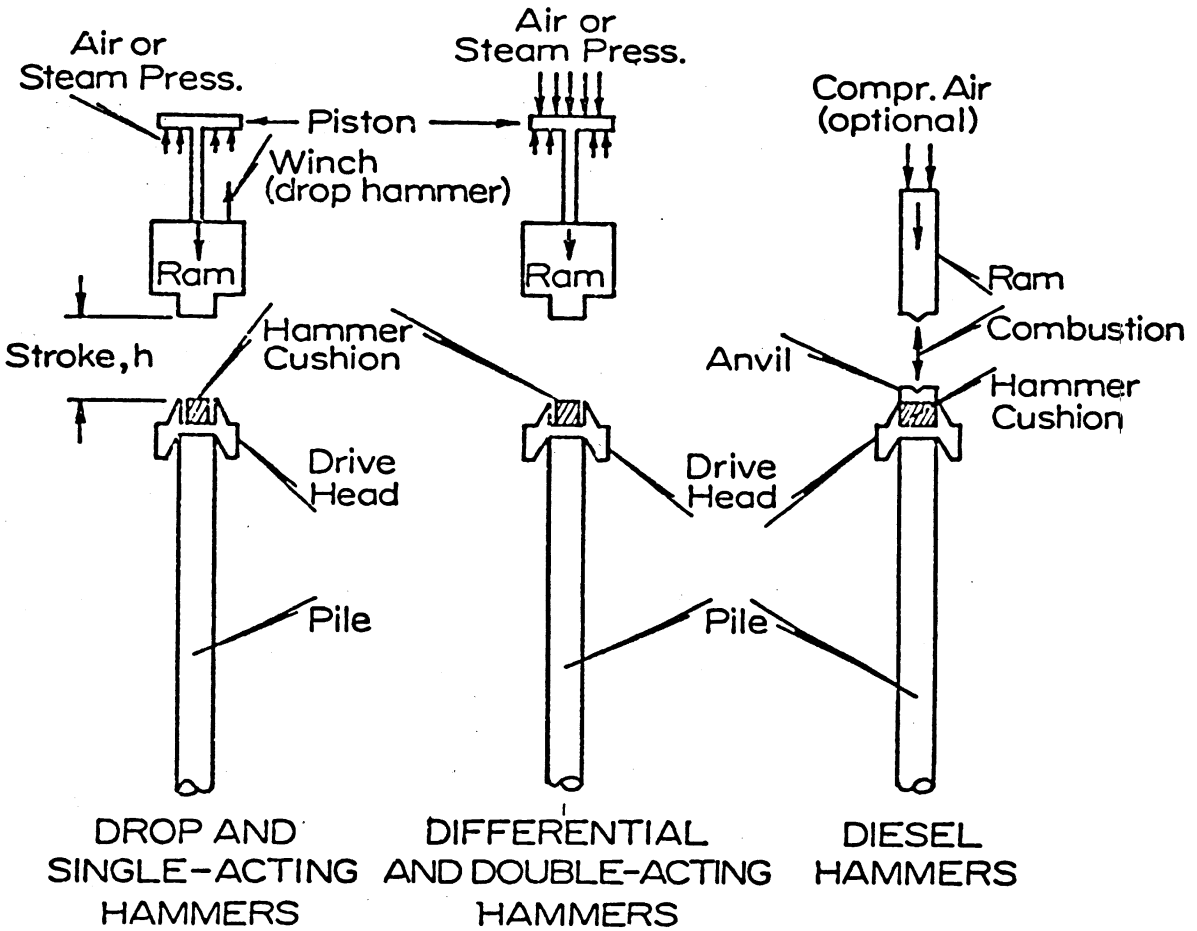

Figure A-1. Schematic Diagram of Impact Pile Drivers.

efficiency factor, η, is applied to compute an "equivalent" free-fall (100% efficient) stroke, h_e, as

$$h_e = E_{ram}\eta / W_{ram} \quad , \text{ ft} \tag{A-1}$$

such that the ram velocity at impact may be written as

$$V_R = \sqrt{2gh_e} \quad , \text{ ft/sec} \tag{A-2}$$

Single-acting hammers increase impact frequency by using steam or air pressure to raise the ram to the required stroke. Single-acting hammers obtain driving rates as high as 60 blows per minute, and a wide range of rated energy values are commercially available. Equivalent stroke and impact velocity are determined using equations A-1 and A-2, respectively. Single-acting and drop hammers generally are assumed to operate in the range of 75 to 85 percent mechanical efficiency.[12] The higher efficiencies would probably correspond to hammers with heavier rams.

Double- and differential-acting hammers increase impact velocity and, therefore, increase the impact energy of the ram by applying the steam or air pressure on the downward stroke as well. In general, these hammers require a shorter stroke for the same ram mass and rated energy, such that the driving rate is approximately doubled to about 120 blows per minute. The mechanical efficiency of these types of hammers is approximately 85 percent,[12] and the equivalent stroke and impact velocity are computed using equations A1 and A2, as before. DUKFOR may be used directly to simulate these types of pile drivers.

Diesel hammers operate using the explosive combustion of a diesel fuel/air mixture during ram-anvil impact. The explosive force returns the ram to its peak stroke and also performs useful work in driving the pile. Thus the shape of the stress wave transmitted to the pile is significantly altered by the explosive force behavior. Closed-ended diesel hammers impart an accelerating force during the downward stroke similar to the effects of the double-acting pile driving system.

The rated kinetic impact energy, E_K, for an open-ended diesel hammer may be written as

$$E_K = W_{ram} (h-d) \qquad \text{(A-3)}$$

where d is the distance from the exhaust ports to the anvil. Equation A-3 assumes that the ram velocity remains constant after passing the exhaust ports. The rated explosive energy performing useful work, E_E, is generally assumed on the same order as the quantity[12]

$$E_E \cong W_{ram}\, d \qquad \text{(A-4)}$$

giving the rated hammer energy equivalent to the free-fall value, $W_{ram}\, h$. Using the above assumptions the mechanical efficiency of open-ended diesel hammers is given as 100 percent. An equivalent stroke for a closed-ended system depends on the measured bounce chamber pressures during driving. Manufacturers' charts may then be used to determine h_e and E_{ram}.[12]

The behavior of diesel pile drivers is a highly complex phenomenon for which no rational model is currently available in practice.[80,92] Pile penetration per blow depends to a large extent on the shape of the transmitted stress wave shape. The Texas A&M University program approximation of diesel hammer behavior (e.g. TAMFOR) has been shown to poorly represent the measured results.[92] Based upon these observations, no attempt was made to simulate diesel hammers in DUKFOR.

One manner by which these difficulties may be overcome is to measure the force pulse transmitted at the pile butt. Such a force-time history could supply the input to the pile-soil system model, eliminating the impact simulation problem. DUKFOR does not presently provide this option. Note that the shape of the transmitted force pulse may depend upon the pile-soil system response as well as the hammer assembly properties, such that no "standard" record would be suitable. Properties of commercially available pile drivers are given in Table A-1.[5]

Cushion Materials

Numerous combinations of accessory elements may be included in the hammer assembly. The fundamental purposes in selecting necessary driving accessories are four fold: to prevent hammer damage during impact; to prevent pile damage during driving; to adapt the connection between the hammer and the pile; and to obtain the most efficient combination of these elements to drive the pile economically. All four of these purposes are usually interdependent for a particular pile driving problem. This section discusses the mechanical properties of cushion materials.

Table A-1

IMPACT PILE-DRIVER DATA (AFTER PAROLA[5])

Rated Energy ft-lb	Make of Hammer	Size	Type	Blows per min	Stroke at Rated Energy in.	Weight Striking Parts, lb	Total Weight lb	Length of Hammer	Air cfm	A.S.M.E. Boiler H.P.	Steam or Air psi	Size of Hose in.	$\sqrt{E_r \times W_1}$ Rating $(ft\text{-}lb^2)^{1/2}$
Energy over 100,000 ft-lb													
180,000	Vulcan	060	Single-act.	62	36	60,000	121,000	18' 6"	4626	740	130	(2)4	103,900
130,000	McKiernan-Terry	S-40	Single-act.	55	39	40,000	96,000	16' 0"	—	375	150	4	72,100
120,000	Vulcan	040	Single-act.	60	36	40,000	87,500	17' 11"	3400	535	120	(2)3	69,300
113,478	Super-Vulcan	400C	Differential	100	16 1/2	40,000	83,000	16' 9"	4659	700	150	5	67,400
Energy 50,000 to 100,000 ft-lb													
97,500	McKiernan-Terry	S-30	Single-act.	60	39	30,000	86,000	16' 0"	—	280	113	4	54,000
79,600	Kobe	K42	Diesel	45-60	98	9,200	22,000	14' 6"	—	—	—	—	27,100
60,000	Vulcan	020	Single-act.	60	36	20,000	39,000	15' 0"	1756	278	120	3	34,600
60,000	McKiernan-Terry	S20	Single-act.	60	36	20,000	38,650	18' 5"	1720	280	150	3	34,600
56,500	Kobe	K32	Diesel	45-60	98	7,060	15,400	13' 7"	—	—	—	—	20,000
50,200	Super-Vulcan	200C	Differential	98	15 1/2	20,000	39,050	13' 2"	1746	260	142	3	31,700
Energy 30,000 to 50,000 ft-lb													
48,750	Vulcan	016	Single-act.	60	36	16,250	30,250	14' 6"	1290	210	110	3	28,100
48,750	Raymond	0000	Single-act.	46	39	15,000	23,000	—	—	85	140	2 1/2	27,000
44,500	Kobe	K22	Diesel	45-60	98	4,850	10,600	13' 4"	—	—	—	—	14,700
42,000	Vulcan	014	Single-act.	60	36	14,000	27,500	14' 6"	1282	200	110	3	24,200
40,600	Raymond	000	Single-act.	50	39	12,500	21,000	15' 7"	—	70	135	2 1/2	22,500
39,800	Delmag	D-22	Diesel	42-60	n/a	4,850	10,054	12' 10 1/2"	—	—	—	—	13,900
37,500	McKiernan-Terry	S14	Single-act.	60	32	14,000	31,600	14' 10"	1260	190	100	3	23,000
36,000	Super-Vulcan	140C	Differential	103	15 1/2	14,000	27,984	12' 3"	1425	211	140	3	22,000
32,500	McKiernan-Terry	S10	Single-act.	55	39	10,000	22,200	14' 1"	1000	140	80	2 1/2	18,000
32,500	Vulcan	010	Single-act.	50	39	10,000	15,750	15' 0"	1002	157	105	2 1/2	18,000
32,500	Raymond	00	Single-act.	50	39	10,000	18,500	15' 0"	—	55	125	2	18,000
32,000	McKiernan-Terry	DE-40	Diesel	48	96	4,000	11.275	15' 0"	—	—	—	—	11,300
30,225	Vulcan	OR	Single-act.	50	39	9,300	16,765	15' 0"	1020	—	100	2 1/2	16,800
Energy 20,000 to 30,000 ft-lb													
26,300	Link-Belt	520	Diesel	80-84	43 1/6	5,070	12,545	18' 6"	—	—	—	—	11,500
26,000	McKiernan-Terry	C-8	Double-act.	77-85	20	8,000	18,750	9' 9"	875	110	100	2 1/2	14,400
26,000	Vulcan	08	Single-act.	50	39	8,000	16,750	15' 0"	880	127	80	2 1/2	14,000
26,000	McKiernan-Terry	S8	Single-act.	55	39	8,000	18,100	14' 4"	850	119	80	2 1/2	14,400
24,450	Super-Vulcan	80C	Differential	111	16 1/2	8,000	17,885	11' 4"	1245	180	120	2 1/2	14,000
24,450	Vulcan	8M	Differential	111	n/a	8,000	18,400	10' 6"	1245	180	120	2 1/2	14,000
24,370	Vulcan	0	Single-act.	50	39	7,500	16,250	15' 0"	841	—	80	2 1/2	13,500
24,000	McKiernan-Terry	C-826	Double-act.	85-95	18	8,000	17,750	12' 2"	875	120	125	2 1/2	13,900
22,600	Delmag	D-12	Diesel	42-60	n/a	2,750	5,440	12' 7 3/4"	—	—	—	—	7,900
22,400	McKiernan-Terry	DE-30	Diesel	48	96	2,800	9,075	15' 0"	—	—	—	—	7,900
24,400	Kobe	K13	Diesel	45-60	98	2,870	6,400	12' 8"	—	—	—	—	8,400
Energy 10,000 to 20,000 ft-lb													
19,875	Union	0	Double-act.	110	24	3,000	14,500	10' 1"	800	—	125	2	6,360
19,850	McKiernan-Terry	11B3	Double-act.	95	19	5,000	14,500	11' 1"	900	126	100	2 1/2	9,780
19,500	Vulcan	06	Single-act.	60	36	6,500	11,200	13' 0"	625	94	100	2	11,200
19,200	Super-Vulcan	65C	Differential	117	15 1/2	6,500	14,886	12' 1"	991	152	150	2	11,200
18,250	Link-Belt	440	Diesel	86-90	36 7/8	4,000	10,300	14' 6 1/4"	—	—	—	—	8,540
16,250	McKiernan-Terry	S5	Single-act.	60	39	5,000	12,375	13' 3"	600	84	80	2	9,000
16,000	McKiernan-Terry	DE-20	Diesel	48	96	2,000	6,325	13' 3"	—	—	—	—	5,660
16,000	McKiernan-Terry	C5	Compound	110	18	5,000	11,880	8' 9"	585	56	100	2 1/2	8,940
15,100	Super-Vulcan	50C	Differential	120	15 1/2	5,000	11,782	10' 2"	880	125	120	2	8,690
15,100	Vulcan	5M	Differential	120	15 1/2	5,000	12,900	9' 4"	880	125	120	2	8,690
15,000	Vulcan	1	Single-act.	60	36	5,000	10,100	13' 0"	565	81	80	2	8,660
15,000	Link-Belt	312	Diesel	100-105	30 7/8	3,857	10,375	10' 0"	—	—	—	—	7,610
13,100	McKiernan-Terry	10B3	Double-act.	105	19	3,000	10,650	9' 4"	750	104	100	2 1/2	6,270
12,725	Union	1	Double-act.	125	21	1,600	10,000	8' 2"	600	—	100	1 1/2	4,530
Energy 5,000 to 10,000 ft-lb													
9,040	Delmag	D5	Diesel	42-60	n/a	1,100	2,401	11' 2 1/2"	—	—	—	—	3,150
9,000	McKiernan-Terry	C-3	Double-act.	130-140	16	3,000	8,500	7' 9 1/2"	450	60	100	2	5,200
9,000	McKiernan-Terry	S3	Single-act.	65	36	3,000	8,800	12' 4"	400	57	80	1 1/2	5,200
8,800	McKiernan-Terry	DE-10	Diesel	48	96	11,000	3,518	12' 2"	—	—	—	—	3,110
8,750	McKiernan-Terry	983	Double-act.	145	17	1,600	7,000	8' 2"	600	85	100	2	3,740
8,280	Union	1 1/2A	Double-act.	135	18	1,500	9,200	8' 4"	450	—	100	1 1/2	3,520
8,100	Link-Belt	180	Diesel	90-95	37 5/8	1,725	4,550	11' 3"	—	—	—	—	3,740
7,260	Vulcan	2	Single-act.	70	29 3/4	3,000	7,100	12' 0"	336	49	80	1 1/2	4,670
7,260	Super-Vulcan	30C	Differential	133	12 1/2	3,000	7,036	8' 11"	488	70	120	1 1/2	4,670
7,260	Vulcan	3M	Differential	133	n/a	3,000	8,490	7' 11"	488	70	120	1 1/2	4,670
6,500	Link-Belt	105	Diesel	90-98	35 1/4	1,445	3,885	10' 3"	—	—	—	—	3,070
Energy Under 5,000 ft-lb													
4,900	Vulcan	DGH900	Differential	238	10	900	5,000	6' 9"	580	75	78	1 1/2	1,900
3,600	Union	3	Double-act.	160	14	700	4,700	6' 4"	300	—	100	1 1/4	1,600
3,600	McKiernan-Terry	7	Double-act.	225	9 1/2	800	5,000	6' 1"	450	63	100	1 1/2	1,700
445	Union	6	Double-act.	340	7	100	910	3' 10"	75	—	100	3/4	210
386	Vulcan	DGH100A	Differential	303	6	100	786	4' 2"	74	8	60	1	200
356	McKiernan-Terry	3	Double-act.	400	5 3/4	63	675	4' 10"	110	—	100	1	150
320	Union	7A	Double-act.	400	6	80	540	3' 7"	70	—	100	3/4	160

E_r = rated striking energy in foot-pounds; W_1 = weight of striking parts in pounds.

Note: Ram weights of drop hammers vary from 500 to 10,000 lb with variable strokes therefore variable energy.

The basic means of reducing hammer and/or pile damage is the use of cushioning material to "soften" the impact. A vast assortment of materials and a multitude of combinations and dimensions have been used for pile driving cushions. Cushions may be used between the hammer striking parts and a drive head, and between the drivehead and the pile. Indeed, either or both cushions and even the drive head may be absent in a contractor's set up.

Two types of cushions may be distinguished in general; a hard (stiff) cushion of micarta, asbestos, aluminum, or hardwood, gives a high modulus of elasticity and a reasonably high coefficient of restitution; and a soft cushion composed of soft woods, which has a low modulus of elasticity and a low coefficient of restitution.

Laboratory tests on cushion blocks performed at Texas A&M University (TAMU) have shown that the dynamic and static stress-strain behavior of most cushion materials are very similar.[20] Analyses using the TAMU wave equation programs have shown that the use of a bilinear cushion representation is a suitable approximation. The non-linear characteristics of the stress-strain data require the selection of an appropriate secant modulus for the linear load modulus. A stress-strain curve for a micarta cushion block is shown in figure A-2.[12] The value selected for secant modulus depends upon the peak driving stress condition in the cushion. Moreover, the secant modulus and coefficient of restitution may vary, depending on the applied load cycle number. It is recommended that for analyses of piles near bearing that "well-consolidated" cushion properties be selected. The only material which did not exhibit appreciable change in stres-strain behavior with repeated load cycles was the micarta plastic.[20]

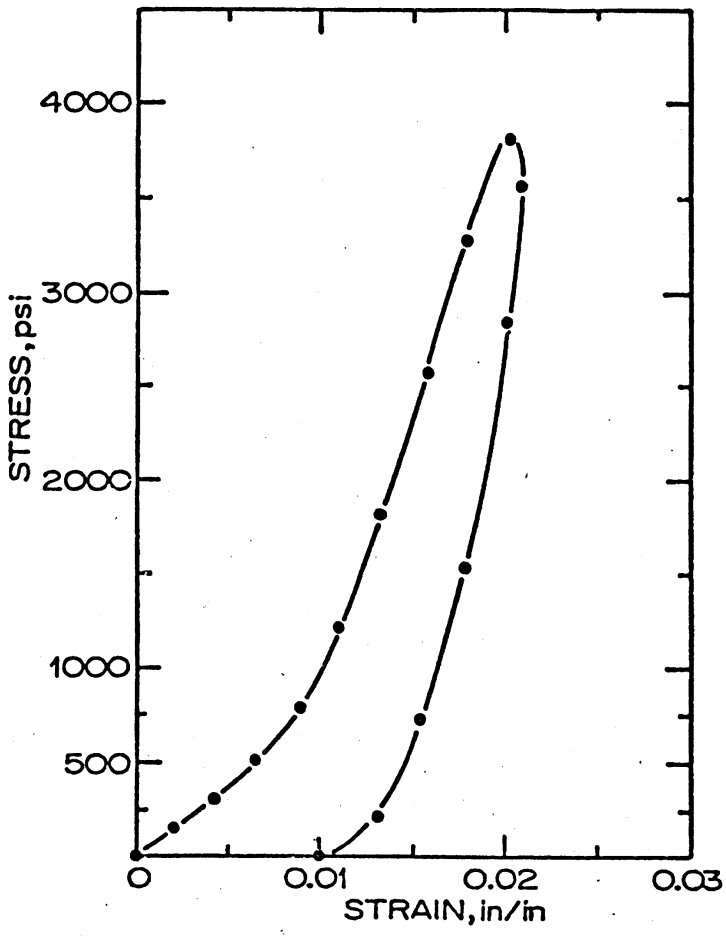

Figure A-2. Micarta Cushion Block Stress-Strain Curve[12]

Table A-2 gives typical secant moduli and coefficients of restitution for various cushion materials based upon TAMU measurements.[12] Should ram stresses or pile stresses become a critical design consideration, these values should be compared with the detailed TAMU laboratory results.[20] A significant difference between the predicted peak cushion stresses and those assumed for secant moduli determination may require re-analysis with a corrected secant modulus. These moduli may affect the impact stress wave transmitted to the pile, which directly affects the pile penetration per blow.

Piling

Pile impedance, moduli and mass densities for steel, concrete and timber piling are listed in Table A3. As discussed in Chapter II, piles having the same impedance and similar resistance distributions would exhibit very similar pile driving behavior. As a general rule the high impedance piling is best used to overcome hard driving resistance. Under easy driving conditions lower impedance piling may drive more efficiently.[5] There is an economic trade-off between installation costs and piling material costs on a typical project. Wave equation methods may be used to evaluate the possible alternatives.

In applications of DUKFOR discussed herein it was found that the criterion given by Smith[7] for pile segment lengths was generally acceptable for low to medium impedance piling ($\rho cA' < 3600$ lb-sec/in. $\approx$ 25 sq.in. steel cross section.) For the nonlinear resistance models and multiple blow analyses performed using DUKFOR it is probably better to employ at least 15 or more (instead of 10 or more[7]) pile segments, none longer than 10 ft.

Table A2

TYPICAL PILE CUSHION MATERIAL PROPERTIES[12]

	E psi	e
Micarta Plastic	450,000	0.80
Oak (Green)	45,000*	0.50
Asbestos Discs	45,000	0.50
Fir Plywood	35,000*	0.40
Pine Plywood	25,000*	0.30
Gum	30,000*	0.25

* Properties of wood with load applied perpendicular to wood grain.

Note: E is a secant modulus value.

Table A3

PILE IMPEDANCES AND PILE TYPES[5]

Pile Impedance ρcA lbs-sec/in.	Steel* Area in.^{2}	Pile Material Concrete* Area in.^{2}	Concrete* Diameter in.	Concrete* Width in.	Wood* Area in.^{2}	Wood* Diameter in.
725	5(Thin Wall pipe)	23.5	5.5	4.8	82	10.2
1450	10	47	7.8	6.9	164	14.5
2900	20	94	11.0	9.7	328	20.4
5800	40(Mandrel)	188	15.5	13.7	656	29.0
8700	60	282	18.0	16.8	984	—

*The following material properties were used to determine pile dimensions from impedances. Subscripts (s = steel, c = concrete, w = wood) are used.

Steel $E_s = 29 \times 10^6$ psi $\quad \rho_s = 15.2 \frac{\text{lbs-sec}^2}{\text{ft}^4}$

$$c_s = \sqrt{E_s/\rho_s} = 16{,}600 \text{ ft/sec} \quad (\rho c)_s = 145 \frac{\text{lbs-sec}}{\text{in.}^3}$$

Concrete $E_c = 4.25 \times 10^6$ psi $\quad \rho_c = 4.65 \frac{\text{lbs-sec}^2}{\text{ft}^4}$

$$c_c = \sqrt{E_c/\rho_c} = 11{,}500 \text{ ft/sec} \quad (\rho c)_c = 30.9 \frac{\text{lbs-sec}}{\text{in.}^3}$$

Wood $E_w = 1.3 \times 10^6$ psi $\quad \rho_w = 1.24 \frac{\text{lbs-sec}^2}{\text{ft}^4}$

$$c_w = \sqrt{E_w/\rho_w} = 12{,}300 \text{ ft.sec} \quad (\rho c)_w = 8.84 \frac{\text{lbs-sec}}{\text{in.}^3}$$

Segment lengths as small as 1 ft were used herein without difficulty; but, of course, such refinement is needless and too expensive in most applications.

For higher impedance piling the 15 or more pile segments guideline is still reasonable. It was found that for high impedance piles ($\rho cA \approx 10{,}000$ lb-sec/in.) the 10 ft maximum segment length was suitable, but segment lengths less than 2 ft caused noticeable solution instability due to apparent round-off errors. For high impedance piling a minimum pile segment length of about 3 ft would be appropriate (i.e. 3 ft $\leq \Delta L \leq$ 10 ft.) The length of the impact stress wave transmitted to the pile governs the maximum segment length which can accurately approximate the stress wave shape. For extremely large pile drivers and very long piling such as used in offshore construction the pile segment length may be larger than 10 ft.

Regardless of pile driving idealizations, DUKFOR analyses should be examined to carefully monitor element velocities at the end of each blow to ensure solution convergence and stability. It should be noted that for single blow calculations after Smith[7] the criteria he recommends provide satisfactory results. In using DUKFOR with repeated blow calculations of longer (time) integration duration the stricter guidelines are needed. The time interval needed for the DUKFOR analyses is one-fourth the critical time interval in the system as discussed in Chapter II.

Piles are generally assumed to behave as linear elastic materials such that for pile driving analyses a Young's Modulus and material density are needed. For most problems this is a reasonable assumption since driving stresses are maintained below the material yield point. Pile material

damping (hysteresis) has been found to have a negligible effect on driving performance.[12] DUKFOR models the pile as a linear elastic material, though a bilinear approximation of a "cushion-like" material could be used, see figure II-4. A damaged pile section may be represented as a different linear or bilinear material if necessary.

Material properties listed in Table A3 should be sufficiently accurate for most practical purposes. It may be worthwhile to measure these properties in the laboratory should there be any doubt. For cast-in-place piles the geometric configuration and pile material properties may require particular attention during installation to insure design performance of the pile itself.

Pile-Soil Interface Properties

Static Behavior

In analyzing pile-soil interaction behavior the load-deformation characteristics at the pile-soil interface must be assigned for the mathematical model. A direct shear testing device may be modified using a block of pile material in place of one half of the "sample." Figure A3 describes such a testing apparatus as used to test sand-on-mortar samples from Jonesville, Louisiana.[56] Interface shear tests may be performed routinely to determine deformation and failure parameters.

Interface shear results from Jonesville sand-on-mortar tests are plotted in figure A-4a.[56] Note the nonlinear, normal stress-dependent behavior of the 80 percent relative density sand-on-mortar. The development of peak and residual strength values indicates a dependency of

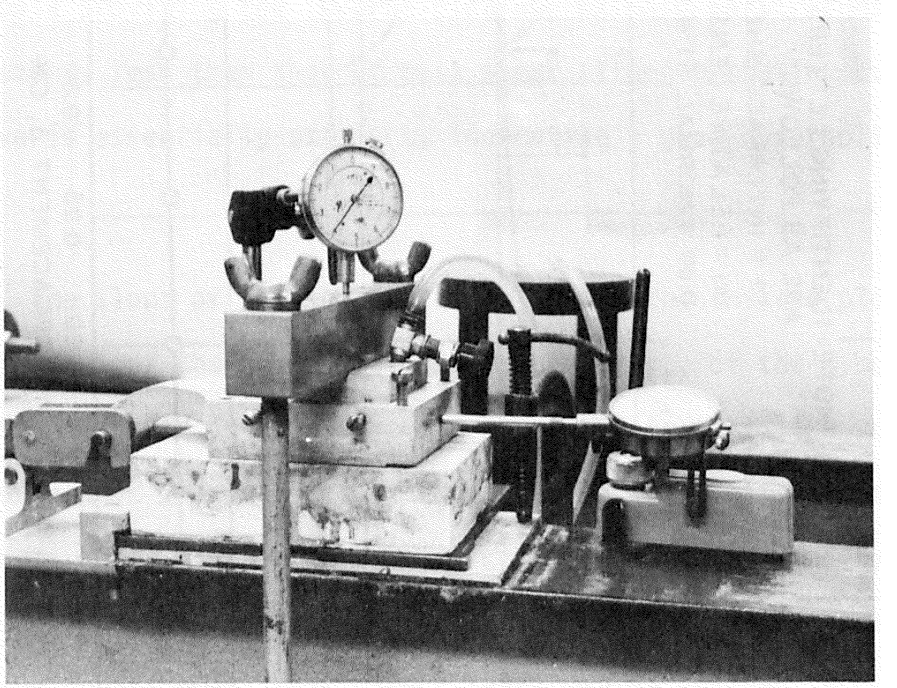

Figure A-3. Interface Shear Testing Device.

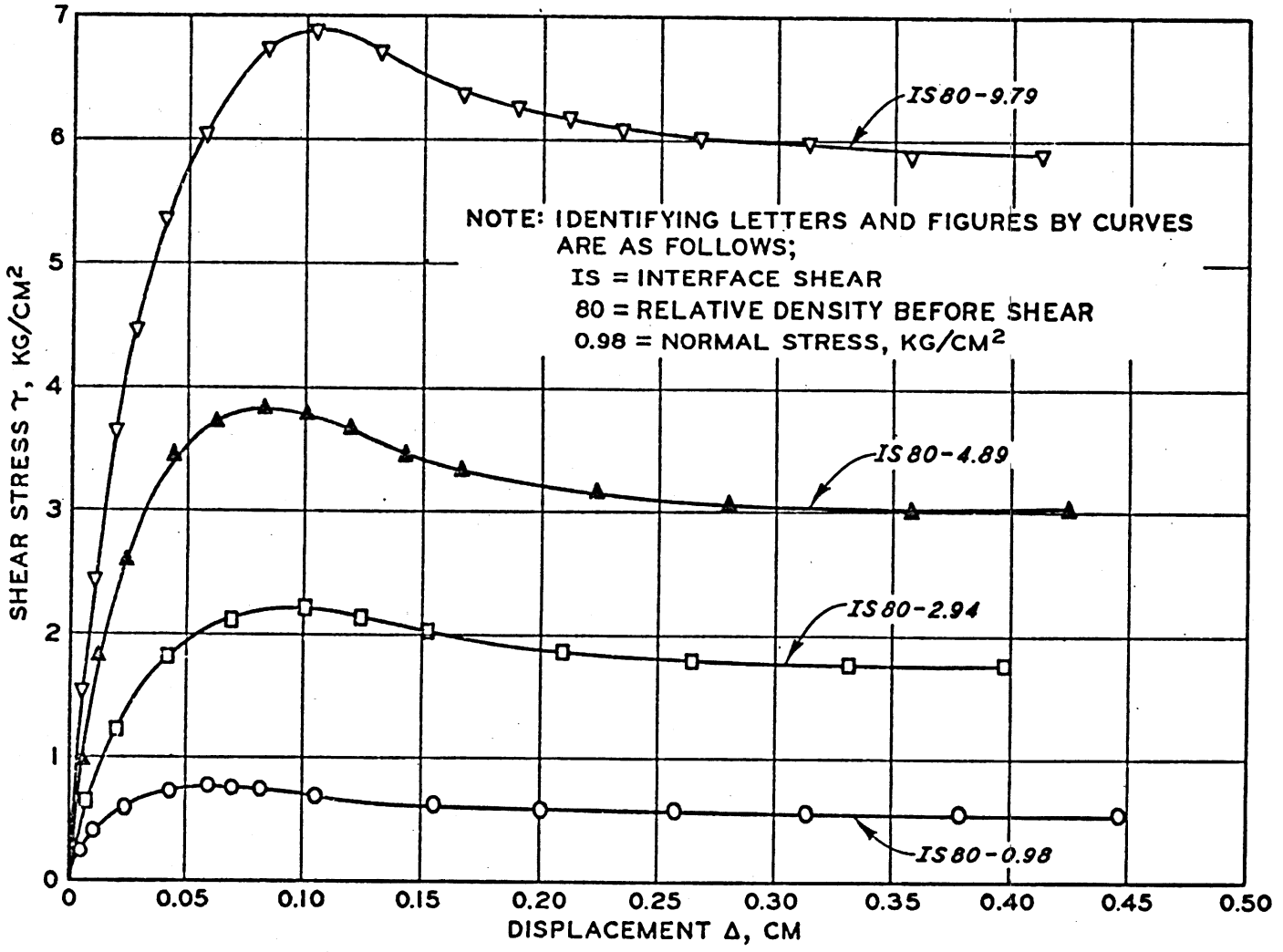

a. SHEAR STRESS VS DISPLACEMENT

Figure A-4. Interface Shear Test Results, JLD Sand-on-Mortar[56].

strength on relative density and shear deformation.

A common method of representing nonlinear behavior has been the use of hyperbolic fits to the laboratory data. Clough and Duncan[81,82] developed the equations to describe interface shear using an inverse plot; relative displacement divided by shear stress (Δ/τ), versus relative displacement (Δ). The data of figure A-4a is presented in this manner in figure A-4b. The shear stress-displacement curve (figure A-4a) resembles a hyperbola providing the inverse plot approximates a straight line. For displacements less than that at peak shear strength the inverse plot of the curve is essentially straight, indicating a good hyperbolic fit in this range.

The slope of the straight line fit on the inverse plot is equal to the reciprocal of the horizontal assymptote, τ_{ult}, of the hyperbola approximating the measured data in figure A-4a. The straight line intercept of the inverse plot is equal to the reciprocal of the initial tangent slope of the hyperbola. These two quantities uniquely define the hyperbola resembling the test results. The equation for the tangent shear stiffness value as a function of shear stress level may be written as

$$\bar{k}_{st} = \bar{k}_{si}\left(1 - \frac{\tau}{\tau_{ult}}\right)^2 \qquad \text{(A-5)}$$

where

$\bar{k}_{st}$ = tangent interface shear stiffness , F/L^3

$\bar{k}_{si}$ = initial tangent shear stiffness , F/L^3

τ = current shear stress , F/L^3

τ_{ult} = shear stress assymptote , F/L^3

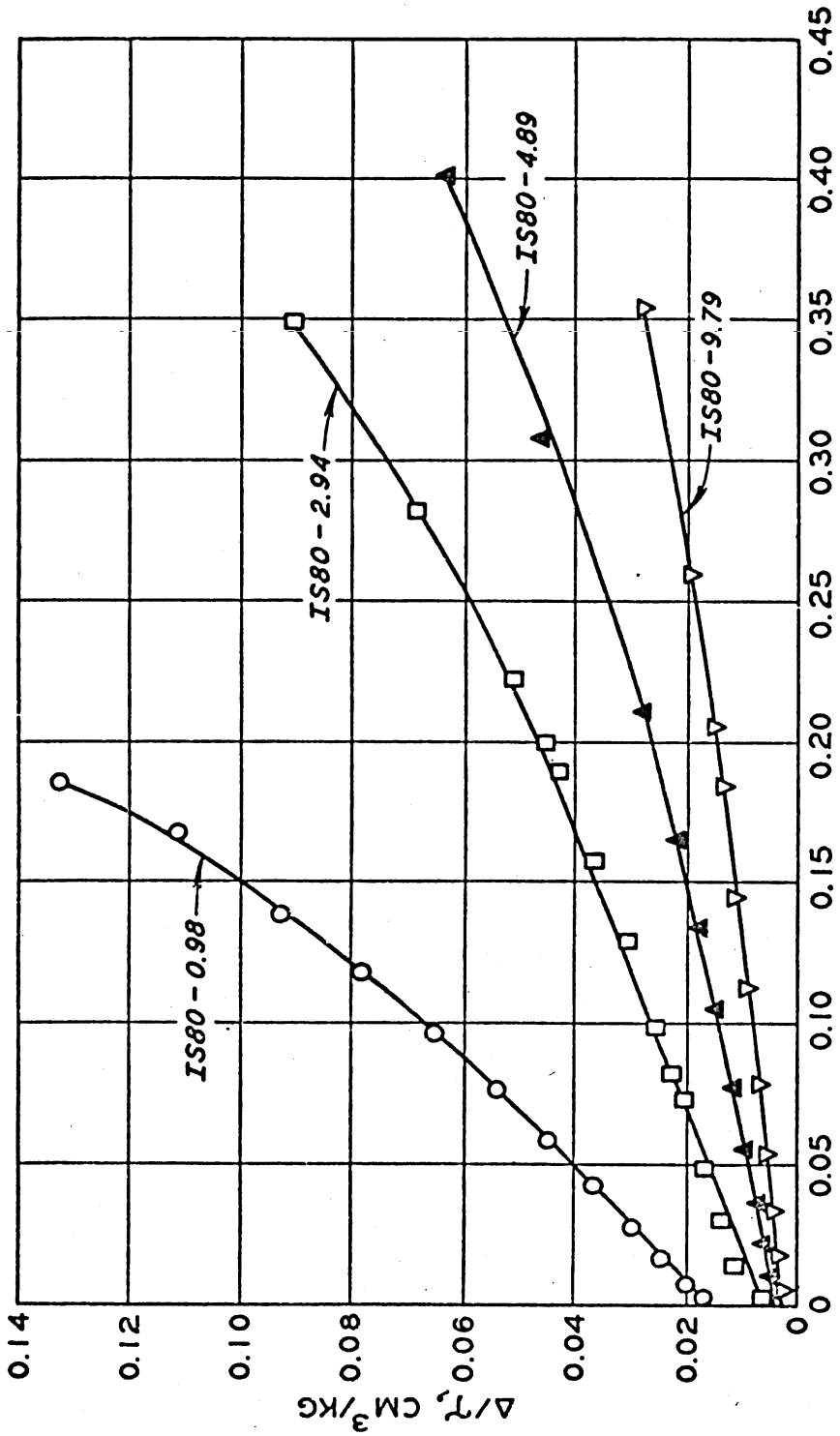

b. TRANSFORMED CURVES-INTERFACE SHEAR TEST RESULTS

Figure 4-A. Interface Shear Test Results, JLD Sand-on-Mortar[56].

The initial tangent shear stiffness, $\bar{k}_{si}$, may be written as a function of effective normal stress,

$$\bar{k}_{si} = \kappa_{IS} \gamma_w \left(\frac{\bar{\sigma}_n}{p_a}\right)^n \qquad \text{(A-6)}$$

where

κ_{IS} = dimensionless interface shear stiffness coefficient

γ_w = unit weight of water , F/L^3

$\bar{\sigma}_n$ = effective normal stress , F/L^2

p_a = atmospheric pressure , F/L^2

n = correlated constant exponent

Equation A-6 represents a straight line approximation to the plot of log $\bar{k}_{si}$ versus log $\bar{\sigma}_n$.

For each test a value of τ_{max} is obtained which may not equal τ_{ult}. A correlation coefficient, R_f, may be used to determine $\tau_{ult} = \tau_{max} / R_f$. The use of all these parameters, recognizing $\tau_{max} = c_a + \bar{\sigma}_n \tan\delta$ (equation IV-3) provides the relationship for $\bar{k}_{st}$ in the form

$$\bar{k}_{st} = \kappa_{IS} \gamma_w \left(\frac{\bar{\sigma}_n}{p_a}\right)^n \left(1 - \frac{\tau R_f}{c_a + \bar{\sigma}_n \tan\delta}\right)^2 \qquad \text{(A-7)}$$

Upon reaching τ_{max} the value of $\bar{k}_{st}$ is set to a small number, simulating failure. All of the parameters in equation A-7 are readily derived from interface shear test results. Parameters obtained from several laboratory test series are listed in Table A-4.

Table A4
INTERFACE SHEAR PROPERTIES

Soil (Classification)	Interface Materials* Dry Density γ_d pcf	Relative Density D_r percent	Modulus Coefficient K_{IS} (Dimensionless)	Exponent n (Dimensionless)	Failure Ratio R_f	Interface Friction Angle δ_{max} deg	δ_{res} deg
Chattahoochee River	Sand/Mortar						
Sand	89	50	2.94×10^4	0.773	0.815	32.3	31.3
(SW)	95	75	3.62×10^4	0.773	0.758	33.6	31.2
	103	100	4.62×10^4	0.773	0.780	33.3	31.3
	Sand/Steel						
	89	50	4.48×10^4	0.602	0.798	22.6	20.6
	95	75	6.92×10^4	0.532	0.777	24.5	21.9
	103	100	9.02×10^4	0.662	0.872	24.8	—
LD4	Sand/Mortar						
Sand	90	0	2.16×10^4	1.15	0.866	29.9	—
(SP-SM)	100	57	2.77×10^4	1.15	0.938	31.3	—
	110	100	5.57×10^4	1.15	0.953	34.6	—
	Sand/Steel						
	90	0	3.51×10^4	1.28	0.949	26.1	—
	100	57	3.51×10^4	1.28	0.989	26.3	—
	110	100	3.51×10^4	1.28	0.985	29.8	—
JLD	Sand/Mortar						
Sand	100	60	5.10×10^4	0.808	0.825	34.5	—
(SP)	103.5	80	6.24×10^4	0.831	0.800	36.9	—
	107	100	7.69×10^4	0.841	0.722	37.9	—

* Values of γ_d and D_r are for the sand specimen tested.

The nonlinear representation of shear stress-displacement behavior discussed above approximates the monotonic loading case. In order to simulate unload/reload behavior, both AXISYM and DUKFOR employ stress level-dependent linear elastic models. In AXISYM the unload/reload stiffness is computed using equation A-6 with an input unload/reload stiffness coefficient replacing κ_{IS}. DUKFOR provides a similar approximation. The initial tangent stiffness is modified by a proportionality constant, RULRL; the ratio of the unload/reload stiffness to the initial tangent stiffness, (RULRL) ($\overline{k}_{si}$). As little laboratory data is available for these loading conditions it was assumed throughout this study that RULRL = 1.

In AXISYM analyses the value of $\overline{\sigma}_n$ is permitted to vary during the load test simulation as a function of the pile-soil system response. As such the variation of $\overline{\sigma}_n$ described a "strain-hardening" shear stress-displacement response during compression loading (increasing $\overline{\sigma}_n$) and a "strain-softening" tendency (decreasing $\overline{\sigma}_n$) during tension loading. DUKFOR approximates this behavior by providing an option assigning $\overline{\sigma}_n$ at failure in compression ($K_s^c \overline{\sigma}_v$) different from that in tension ($K_s^t \overline{\sigma}$).

For all the pile tests analyzed herein using DUKFOR, the interface shear test hyperbolic representation was applied directly as the load transfer function. This assumption modeled the compression test load-displacement behavior quite well in each case. The simulation of tension test behavior was less accurate for most of the cases studied. Though DUKFOR incorporated the effects of residual compression loads on tension test behavior, the load-displacement predictions indicated a stiffer response than that measured. AXISYM results described the strain-softening tendency

in the decrease of $\bar{\sigma}_n$ along the pile shaft at greater tension load levels. Unfortunately, AXISYM cannot correctly incorporate residual compression loads, such that neither AXISYM nor DUKFOR effectively simulates tension test behavior.

DUKFOR compression test load distribution predictions did not accurately estimate the LD4 field measurements. The field data describe an increasing load distribution slope (increasing skin friction) in the upper half of the embedded pile length, giving greater skin friction values than that assumed in DUKFOR analyses. These observations indicate that the assumed triangular skin friction distribution is not an accurate approximation for the LD4 test piles. AXISYM predictions showed a tendency for $\bar{\sigma}_n$ to increase along the pile shaft, showing a strain-hardening effect that the one-dimensional DUKFOR model does not include. Comparison of AXISYM predictions showed that the field behavior was more affected by this phenomenon (larger increases in load distribution slopes) than the axisymmetric model used. This discrepancy is due to the inaccuracy of the rheologic models employed.

Dynamic Behavior

The dynamic behavior models available in DUKFOR include two generalized Kelvin elements: one (after Smith[8]) includes a nonlinear viscous element, given in equation II-6; the other permits a linear viscous damping force, equation IV-3. Discussions of these two formulations are given in Chapters II and IV.

Nonlinear viscous damping parameters for LD4 and JLD test piles obtained using DUKFOR multiple blow analyses are given in Tables V-5 and

V-9, respectively. The description of the correlation procedures used to determine these constants is given in Chapter V. The most recent data published by TAMU researchers is shown in Table II-2. The TAMU values were obtained from single blow analyses correlated with measured blow counts. The TAMU results were generated using estimates of pile capacities during driving as corrected for relaxation or set up effects.

It was shown in Chapter V that correlated damping values are not unique soil properties; rather, they are interdependent correlation coefficients. A change in any of the hammer assembly-pile-soil system properties may alter the correlated value. Extreme caution is advised in using "average" values of damping parameters to verify pile capacities from blow count data alone. Furthermore, the resistance overcome by driving forces to obtain penetration may vary significantly from static load test measurements. Transient phenomena of relaxation or set up may make the "static resistance during driving" a difficult quantity to define.

Point Resistance Behavior

DUKFOR requires point bearing capacity and deformation properties as input to the analyses. As mentioned in Chapter IV either a bilinear or hyperbolic rheologic model of static behavior may be assumed. The dynamic resistance to point penetration is defined using either Smith's nonlinear viscous model (equation II-6) or a linear viscous model (equation IV-3). Since the point resistance force cannot be tensile, it is modeled as a "no tension" element.

In either the bilinear or hyperbolic static models the point resistance is defined uniquely by two parameters: the point bearing capacity, Q_p; and the initial tangent elastic quake, $QUAKE_p$. The initial tangent stiffness is defined as $Q_p/QUAKE_p$. This slope remains constant for the bilinear model until the applied static load exceeds Q_p, whereupon it is set to a very small value. For the hyperbolic model the tangent stiffness is defined in terms of the current point load, Q, as

$$\bar{k}_{tip} = (Q_p/QUAKE_p)(1 - Q/Q_p)^2 \qquad (A\text{-}8)$$

For both the hyperbolic and bilinear models $\bar{k}_{tip}$ is assigned a small value at failure ($Q \geq Q_p$).

The hyperbolic point load transfer model was used throughout this study. From LD4 pile test measurements an approximate criterion was developed for defining $QUAKE_p$. For impact-driven piles in the medium dense sand at LD4 a value of $QUAKE_p$ equal to 0.05 in. per foot of point diameter provided reasonably good hyperbolic fits of the field data. The vibratory-driven pile (LD4TP10) required a much larger value of $QUAKE_p$ (0.325 in. $\cong$ 0.23 in. per foot of pile diameter). Apparently, the vertical compression beneath the point of a vibratory-driven pile is much less than that for an impact-driven pile, more closely resembling the point load transfer response of a bored pile. Denser bearing strata in the vicinity of the pile point would require a stiffer response, and therefore, $QUAKE_p$ would be assigned a smaller value.

The accurate prediction of point bearing capacity is beyond the state of the art. The analytical methods available all have important

limitations. The magnitude of point bearing capacity depends directly upon strength and deformation characteristics of the soil(s) in the vicinity of the point and upon the prevailing effective stress state in that zone. Limit equilibrium methods and elasti-plastic solutions require simplifying assumptions that do not properly model the behavior. Finite element techniques presently require similar assumptions to solve the problem. The FE method offers the greatest potential in this regard; however, convergence and stability of the numerical solution near failure, and the accurate idealization of the initial conditions remain to be solved.

Even without predicting point capacities, pile load tests are often misinterpreted. Often times the load test has not achieved sufficient point penetration to fully mobilize point bearing. For impact-driven piles the residual point loads are usually ignored. The assignment of Q_p in DUKFOR for predicting pile performance requires careful engineering judgement.

Soil Behavior

Cohesionless soils exhibit extremely complex deformation characteristics for which an accurate, all-purpose constitutive model has yet to be found. Figure A-5a shows stress ratio and volume change versus strain data from consolidated-drained triaxial tests on medium dense JLD sand.[56] Note the nonlinear, stress level-dependent stress-strain characteristics which are typical of cohesionless materials. Note the tendency for volume increase in shear (dilatancy) which is quite pronounced for this material.

As a general rule for performing laboratory or in situ tests it is important to approximate the loading conditions of the specific problem. In this manner the stress path-dependency of the material behavior is incorporated in the parameters obtained for the constitutive model. For example, in order to model the transverse cross section of an earth dam, plane strain test results should be used to develop constitutive model parameters. The loading (stress) path simulated in the test should approximate the predominant field behavior whenever possible.

For pile-soil interaction problems the soil element stress path in a FE mesh depends on its location in the pile-soil system and on the manner in which the load is applied to the pile. A series of laboratory tests that would represent all the stress paths satisfactorily is obviously not feasible. Moreover, soil deposits are rarely homogeneous and isotropic in situ, much less after pile installation, such that the detailed refinement of the soil constitutive model is only a small part of the idealization problem.

AXISYM uses a pseudoelastic, piecewise-linear (hyperbolic), stress level-dependent constitutive model for soil behavior based on the standard procedures presented by Duncan and Chang.[93] An inverse plot of the triaxial test data shown in Figure A-5a is given in Figure A-5b. As with the hyperbolic fit of the interface shear results, a family of hyperbolas provides a good stress-strain approximation when the inverse plot resembles a family of straight lines.

As a guide to determining a "best fit" Duncan and Chang suggest the use of a straight line which passes through points in figure A-5b

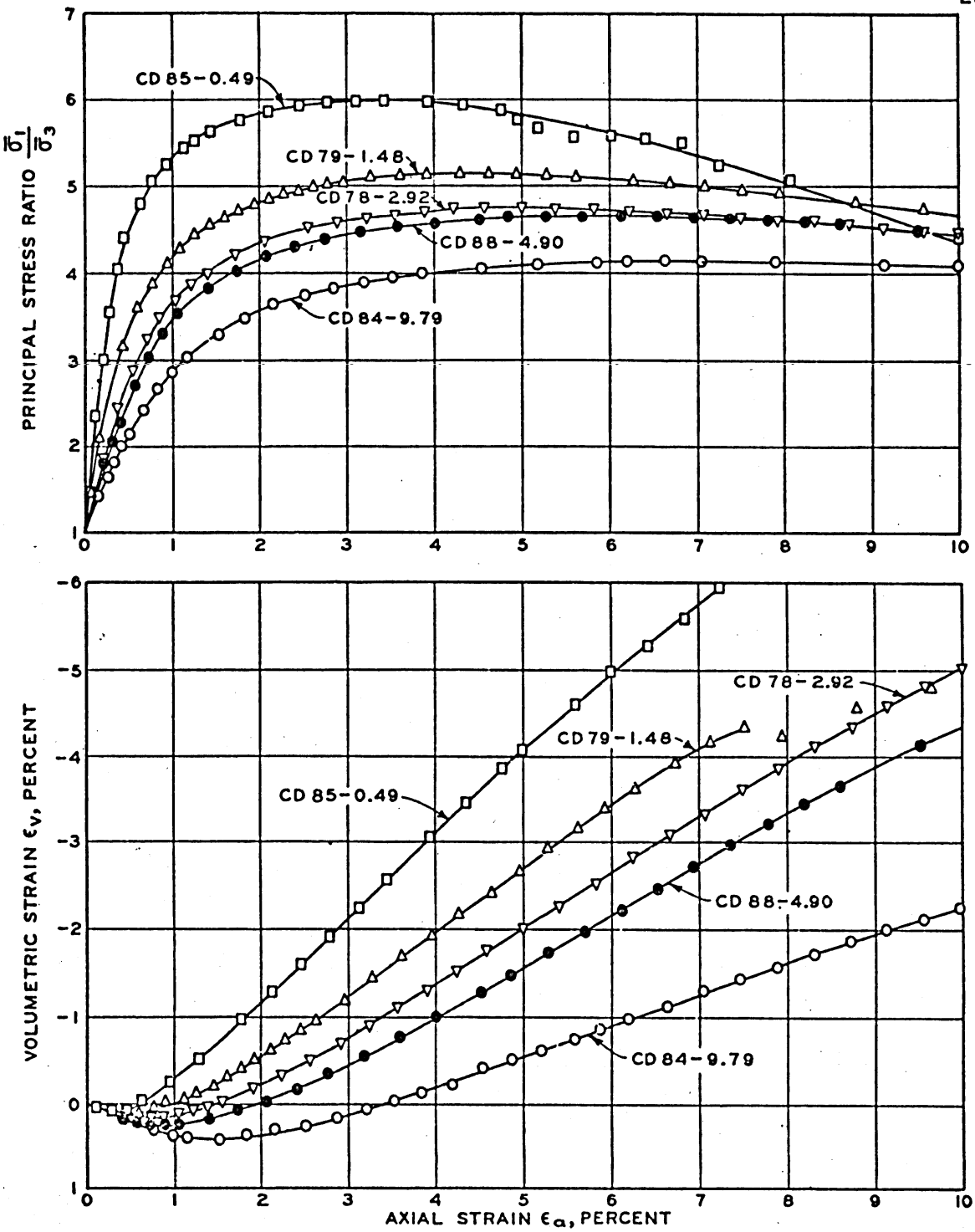

NOTE: IDENTIFYING LETTERS AND FIGURES BY CURVES ARE AS FOLLOWS:
CD = CONSOLIDATED DRAINED TRIAXIAL TEST
85 = RELATIVE DENSITY BEFORE SHEAR, PERCENT
0.49 = EFFECTIVE CONFINING PRESSURE $\bar{\sigma}_3$, KG/CM^2

a. STRESS RATIO AND VOLUMETRIC STRAIN VS AXIAL STRAIN

Figure A-5. Consolidated-Drained Triaxial Test Results, JLD Sand[56].

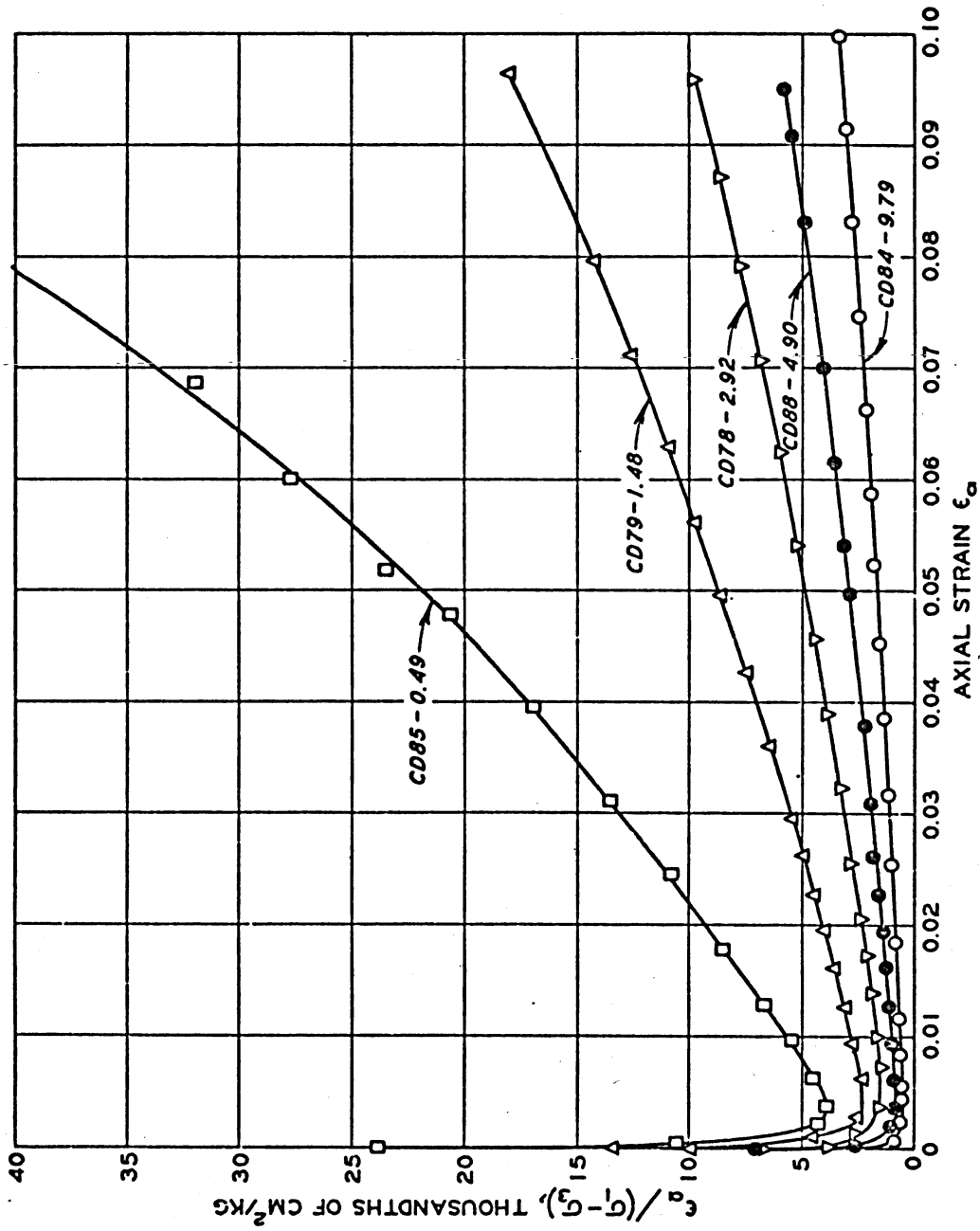

b. TRANSFORMED CURVES-TRIAXIAL TEST RESULTS

Figure A-5. Consolidated-Drained Triaxial Test Results, JLD Sand[56].

corresponding to shear stress levels of 70 and 95 percent of the peak shear stress. That straight line has a slope equal to the reciprocal of the deviator stress (horizontal) assymptote, $(\sigma_1 - \sigma_3)_{ult}$. Its intercept is the reciprocal of the initial tangent modulus, E_i. The failure ratio R_f is defined as

$$R_f = \frac{(\sigma_1 - \sigma_3)_f}{(\sigma_1 - \sigma_3)_{ult}} \tag{A-9}$$

such that the tangent modulus E_t may be defined analogous to that in equation A-5 in the form

$$E_t = E_i\left(1 - \frac{R_f(\sigma_1 - \sigma_3)}{(\sigma_1 - \sigma_3)_f}\right)^2 \tag{A-10}$$

The value of the initial tangent modulus is typically a function of confining stress level. If a plot of log E_i versus log σ_3 (from a series of tests at different σ_3 levels) is approximated by a straight line, its equation provides E_i as

$$E_i = \kappa_S p_a\left(\frac{\bar{\sigma}_3}{p_a}\right)^n \tag{A-11}$$

where κ_S = dimensionless soil modulus coefficient

$\bar{\sigma}_3$ = effective confining stress, F/L^2

n = dimensionless exponent

Thus, the tangent modulus may be written as

$$E_t = \kappa_S p_a\left(\frac{\bar{\sigma}_3}{p_a}\right)^n \left[1 - \frac{R_f(\sigma_1 - \sigma_3)}{(\sigma_1 - \sigma_3)_f}\right]^2 \tag{A-12}$$

and assuming the Mohr-Coulomb failure criterion the deviator stress at failure is given as

$$(\sigma_1 - \sigma_3)_f = \bar{\sigma}_3\left[\tan^2(45 + \phi/2)\right] + 2c \tan(45 + \phi/2) \qquad \text{(A-13)}$$

Thus, the tangent modulus is uniquely defined by the hyperbolic fit parameters κ_S, R_f and n, the Mohr-Coulomb strength parameters c and ϕ, and the stress conditions, $\bar{\sigma}_3$ and $(\sigma_1 - \sigma_3)$. Note that the derivation of E_t assumes that $\bar{\sigma}_3$ is a constant value. It may be necessary to apply small enough loading increments to maintain relatively small changes in $\bar{\sigma}_3$ for each load step. Values of the parameters used for JLD sand (relative density of 80 percent)used in AXISYM analyses of LD4TP2 were:[56]

$$c = 0$$
$$\phi = 32^0$$
$$\kappa_S = 1530.$$
$$n = 0.60$$
$$R_f = 0.89$$

Kulhawy, Duncan and Seed[94] provide hyperbolic fit parameters for a wide variety of soils.

One further item to note is the value assigned for Poisson's ratio. AXISYM provides for two constant values of Poisson's ratio: an initial value to be used in loading and unload/reload of the element; and a failure value which is assigned whenever the Mohr-Coulomb strength (equation A-13) is exceeded in the element. The initial value was assigned as 0.45, and the failure value was assumed as 0.49. These values represent a nearly

incompressible elastic material. The dilatancy behavior cannot be simulated using the pseudoelastic constitutive model in AXISYM. Soil compressibility is a significant factor in pile-soil interaction problems such that the value for Poisson's ratio should be carefully selected.

REFERENCES

1. Sherman, W.C., Holloway, D.M., and Trahan, C.C., "Analysis of Pile Tests," Technical Report S-74-3, U.S. Army Engineer Waterways Experiment Station, Vicksburg, Ms., April, 1974.

2. Holloway, D.M., "Pile-Soil Interaction in Cohesionless Soils," Draft submitted for review, U.S. Army Engineer Waterways Experiment Station, Vicksburg, Ms., April, 1974.

3. Holloway, D.M. "Wave Equation Analyses of Pile Driving," Technical Report, U.S. Army Engineer Waterways Experiment Station, Vicksburg, Ms., 1975.

4. Gendron, G.J., "Pile Driving: Hammers and Driving Methods," Highway Research Record No. 333, Pile Foundations, Highway Research Board, Washington, D.C., 1970.

5. Parola, J.F., 1970. "Mechanics of Impact Pile Driving," Ph.D. Dissertation, University of Illinois at Urbana, Ill.

6. Glanville, W.H., Grime, G., Fox, E.N., and Davies, W.W., 1938. "An Investigation of the Stresses in Reinforced Concrete Piles During Driving," Technical Paper 20, British Building Research Board, Dept. Sci. Ind. Res., 1938.

7. Smith, E.A.L., 1955. "Impact and Longitudinal Wave Transmission," Transactions, American Society of Mechanical Engineers, August 1960.

8. Smith, E.A.L., 1960. "Pile Driving Analysis by the Wave Equation," Journal of Soil Mechanics and Foundations Division, ASCE, Vol.86, SM4, August 1960.

9. Timoshenko, S., and Goodier, J.N., 1951. Theory of Elasticity, McGraw-Hill, New York, 1951.

10. Kolsky, H., 1963. Stress Waves in Solids, Dover, New York, 1963.

11. Crandall, S.H., 1956. Engineering Analysis, McGraw-Hill, New York.

12. Lowery, L.L., Jr., et al., "Pile Driving Analysis-State of the Art," Research Report No. 33-13 (FINAL), Texas Transportation Institute, 1969, Texas A&M University.

List of References (con'd)

13. Goble, G.G., Rausche F., and Moses, F., 1970. "Dynamic Studies on the Bearing Capacity of Piles, Phase III," Final Report to the Ohio Department of Highways, Case Western Reserve University, Cleveland, Ohio, August 1970.

14. Goble, G.G., Moses, F., and Rausche, F., 1970. "Prediction of Pile Behavior from Dynamic Measurements," Proceedings, Conference on Design and Installation of Pile Foundations and Cellular Structures, April, 1970, Lehigh University, Bethlehem, Pa.

15. Goble, G.G., and Rausche, F., 1970. "Pile Load Test by Impact Driving," Highway Research Record No. 333, Pile Foundations, Highway Research Board, Washington, D.C., 1970.

16. Rausche, F., Goble, G.G., Moses, F., 1971. "A New Testing Procedure for Axial Pile Strength," Offshore Technology Conference, 1971 Paper Number OTC 1481.

17. Rausche, F., Moses, F., and Goble, G.G., "Soil Resistance Predictions from Pile Dynamics," Journal of the Soil Mechanics and Foundations Division, ASCE, Vol. 98, No. SM9, Proc. Paper 9220, September, 1972, pp. 917-937.

18. Rausche, F., 1970. "Soil Response from Dynamic Analysis and Measurement on Piles," Ph.D. Dissertation, Case Western Reserve University, 1970.

19. Goble, G.G., Walker, F.K., Rausche, F., "Pile Bearing Capacity-Prediction vs. Performance," Proceedings of the Specialty Conference on Performance of Earth and Earth-Supported Structures, Purdue University, Lafayette, Indiana, June 11-14, 1972.

20. Lowery, L.L., Jr., Hirsch, T.J., Samson, C.H., Jr., "Pile Driving Analysis - Simulation of Hammers, Cushions, Piles, and Soil," Research Report No. 33-9, Piling Behavior Research Study No. 2-5-62-33, Texas Transportation Institute, Texas A&M University, College Station, Texas, August, 1967.

21. _____, 1968. "Piling Analysis Wave Equation Computer Program Utilization Manual," Research Report 33-11, Texas Transportation Institute, Texas A&M University, 1968.

22. Bender, C.H., Jr., Lyons, C.G., and Lowery, L.L., Jr., 1969. "Applications of Wave-Equation Analysis to Offshore Pile Foundations," Proceedings, First Annual Offshore Technology Conference, May 18-21, 1969, Houston, Texas.

23. Hirsch, T.J., and Samson, C.H., Jr., "Driving Practices for Prestressed Concrete Piles," Research Report No. 33-3, Texas Transportation Institute, Texas A&M University, 1967.

List of References (con'd)

24. Reeves, G.N., Coyle, H.M. and Hirsch, T.J., "Investigation of Sands Subjected to Dynamic Loadings," Research Report No. 33-7a, Texas Transportation Institute, Texas A&M University, 1976.

25. Gibson, G.C., and Coyle, H.M., "Soil Damping Constants Related to Common Soil Properties in Sands and Clays," Research Report No. 125-1, Texas Transportation Institute, Texas A&M University, 1968.

26. Raba, C.F., and Coyle, H.M. 1968. "The Static and Dynamic Response of a Miniature Friction Pile in Remolded Clay," Paper presented at the Texas Section Meeting, ASCE, San Antonio, Texas, October, 1968.

27. Korb, K.W., and Coyle, H.M. "Dynamic and Static Field Tests on a Small Instrumented Pile," Research Report No. 125-2, Texas Transportation Institute, Texas A&M University, 1969.

28. Bartoskewitz, R.E., and Coyle, H.M. "Wave Equation Prediction of Pile Bearing Capacity Compared with Field Test Results," Research Report No. 125-5, December, 1970.

29. van Reenen, D.A., Coyle, H.M., and Bartoskewitz, R.E., "Investigation of Soil Damping on Full-Scale Test Piles," Research Report No. 125-6, Texas Transportation Institute, Texas A&M University, 1971.

30. Foye, R., Jr., Coyle, H.M., Hirsch, T.J., Bartoskewitz, R.E., and Milberger, L.J., 1972. "Wave Equation Analyses of Full-Scale Test Piles Using Measured Field Data," Research Report No. 125-7, Texas Transportation Institute, Texas A&M Unviersity, 1972.

31. Vesić, A.S., "Ultimate Loads and Settlements of Deep Foundations in Sand," Bearing Capacity and Settlement of Foundations, Proceedings of a Symposium at Duke University, Durham, N.C., April 5/6, 1965, pp. 53-68.

32. Prandtl, L., "Uber die Härte plastischer Körper," Nacher. Kgl. Ges. Wiss. Göttingen, Math.-phys. Klass, 1920, pp. 74-85.

33. Prandtl, L., "Uber die Eindringungsfestigkeit plastischer Baustoffe und die Festigkeit von Schneiden," Zeitschrift fur Angewandte Mathematik und Mechanik 1, No. 1, 1921, pp. 15-20.

34. Reissner, H., Zum Erddruckproblem, Proceedings, First International Conference of Applied Mechanics, Delft, 1924, pp. 295-311.

35. Caquot, A., Equilibre des Massifs à Frottement Interne, Gauthier-Villars, Paris, 1934.

36. Buisman, A.S.K., "De Weerstand van Paalpunten in Zand," De Ingenieur 50, 1935, pp. Bt. 25-28, 31-35.

List of References (con'd)

37. Terzaghi, K., Theorical Soil Mechanics, J. Wiley Sons, New York, 1943.

38. Brinch Hansen, J., "A General Formula for Bearing Capacity," Bulletin No. 11, 1961, The Danish Geotechnical Institute, Copenhagen, Denmark.

39. DeBeer, E.E., "Etude des Fondations sur Pilotis et des Fondations Directes," Annales des Travaux Publics de Belgique 46, 1945, pp. 1-78.

40. Jáky, J., "On the Bearing Capacity of Piles, "Proceedings, Second International Conference on Soil Mechanics and Foundation Engineering, Rotterdam, 1948, Vol. I, pp. 100-103.

41. Meyerhof, G.G., "The Ultimate Bearing Capacity of Foundations," Geotechnique 2, 1951, pp. 301-332.

42. Scott, R.F., Principles of Soil Mechanics, Addison-Wesley, 1963.

43. Meyerhof, G.G., "Recherches sur la Force Portante des Pieux," Supplement, Annales de l'Institut Technique du Bâtiment et des Travaux Publics 6, 1953, No. 63-64 pp. 371-374.

44. Meyerhof, G.G., "Compaction of Sands and Bearing Capacity of Piles," Journal of Soil Mechancis and Foundations Division, ASCE, Vol. 85, No. SM6, Dec. 1959, pp. 1-30.

45. Meyerhof, G.G., "Influence of Roughness of Base and Ground-Water Conditions on the Ultimate Bearing Capacity of Foundations," Geotechnique, 5, Sept. 1955, pp. 227-242.

46. Meyerhof, G.G., "Penetration Tests and Bearing Capacity of Cohesionless Soils," Journal of Soil Mechancis and Foundations Division, ASCE, Vol. 82, No. SM1, Jan. 1956, pp. 1-17.

47. Meyerhof, G.G., "The Ultimate Bearing Capacity of Wedge-Shaped Foundations," Proceedings, Fifth International Converence on Soil Mechanics and Foundation Engineering, Paris, 1961, Vol. II, pp. 105-110.

48. Meyerhof, G.G., "Some Recent Research on the Bearing Capacity of Foundations," Canadian Geotechnical Journal, Vol. I, No. 1, Sept. 1963, pp. 16-26.

49. Berezantzev, V.G., and Yaroshenko, V.A., "Osobennosti Deformirovania Peschanych Osnovanii Pod Fundamentami Glubokogo Zalozhenia," Osnovania I Fundamenty, Vol. 4, No. 1, pp. 3-7.

List of References (con'd)

50. Vesić, A.S., "A Study of Bearing Capacity of Deep Foundations Final Report," Project B-189, Georgia Institute of Technology, Atlanta, Ga., 1967, pp. xvi + 264.

51. Vesić, A.S., "Bearing Capacity of Deep Foundations in Sand," Stresses in Soils and Layered Systems, Highway Research Record No. 39, 1963, pp. 112-153.

52. Kérisel, J., "Fondations Profondes en Milieux Sableux: Variation de la Force Portante Limite en Fonction de la Densite, de la Profondeur, du Diamètre, et de la Vitesse d'Enfoncement," Proceedings, Fifth International Conference on Soil Mechanics and Foundation Engineering, Paris, Vol. II, pp. 78-83.

53. Kerisel, J., "Deep Foundations-Basic Experimental Facts," Proceedings, North American Conference on Deep Foundations, Mexico City, 1964, pp. 5-44.

54. Robinsky, E.I., and Morrison, C.F., "Sand Displacement and Compaction Around Model Friction Piles," Canadian Geotechnical Journal, Vol. I, No. 2, pp. 81-93.

55. Ellison, R.D., "An Analytical Study of the Mechanics of Single Pile Foundations," Ph.D. Dissertation, Carnegie-Mellon University, Pittsburg, Pa., 1969.

56. Desai, C.S., and Holloway, D.M., "Load-Deformation Analysis of Deep Pile Foundations," Proceedings, Symposium on Applications of the Finite Element Method to Problems in Geotechnical Engineering, U.S. Army Engineer Waterways Experiment Station, 1-4 May, 1972, Vicksburg, Miss.

57. Al-Awkati, Z., "On Problems of Soil Bearing Capacity at Depth," Ph.D. Dissertation, Duke University, Durham, N.C. 1975.

58. Vesić, A.S., "Foundation Engineering," Lecture notes, Fall 1974, Duke University, Durham, N.C.

59. Vesić, A.S., "Load Transfer in Pile-Soil Systems," Proceedings, Conference on Design and Installation of Pile Foundations and Cellular Structures, Lehigh University, Bethlehem, PA., April, 1970, pp. 47-73.

60. Leonards, G.A., "Summary and Review of Part II," Pile Foundations, Highway Research Record No. 333, 1970, pp. 55-59.

61. Seed, H.B., and Reese, L.C. (1957), "The Action of Soft Clay Along Friction Piles," Proceedings, ASCE, Vol. 81, Paper No. 842, pp. 1-28.

List of References (con'd)

62. Reese, L.C., "Load versus Settlement for an Axially Loaded Pile," Proceedings, Symposium on Bearing Capacity of Piles, Part 2, Central Building Research Institute, Rookee, India, February, 1964, Cement and Concrete, New Delhi, India, pp. 18-38.

63. Coyle, H.M., and Reese, L.C., "Load Transfer for Axially Loaded Piles in Clay" Journal of the Soil Mechanics and Foundations Division, ASCE, Vol. 92, No. SM2, March, 1966.

64. Reese, L.C., Hudson, W.R., and Vijayvergiya, V.N., "An Investigation of the Interaction between Bored Piles and Soil; Proceedings, Seventh International Conference on Soil Mechanics and Foundation Engineering, Mexico City, 1969, Vol. 2, pp. 211-215.

65. Coyle, H.M., and Sulaiman, I.H., "Skin Friction for Steel Piles in Sand," Journal of the Soil Mechanics and Foundations Division, ASCE, Vol. 93, SM6, Nov. 1967.

66. D'Appolonia, E., and Romualdi, J.P., "Load Transfer in End-Bearing Steel Hl-Piles," Journal of the Soil Mechanics and Foundations Division, ASCE, Vol. 89, SM2, pp. 1-25.

67. Mindlin, R.D., "Force at a Point in the Interior of a Semi-Infinite Solid," Physics, Vol. 7, No. 5, 1936.

68. Thurman, A.G., and D'Appolonia, E., "Computed Movement of Friction and End-Bearing Piles Embedded in Uniform and Stratified Soils," Proceedings, The Sixth International Conference on Soil Mechanics and Foundation Engineering, 1965, pp. 323-327.

69. Poulos, H.G., and Davis, E.H., "The Settlement Behavior of Single Axially-Loaded Incompressible Piles and Piers," Geotechnique, Vol. 18, 1968, pp. 351-371.

70. Poulos, H.G., and Mattes, N.S., "The Behaviro of Axially-Loaded End-Bearing Piles," Geotechnique, Vol. 19, 1969, pp. 285-300.

71. Poulos, H.G., "Load-Settlement Prediction for Piles and Piers," Journal of the Soil Mechanics and Foundations Division, ASCE, Vol. 98, SM9, Sept. 1972, pp. 879-897.

72. Zienkiewicz, O.C., The Finite Element Method in Engineering Science, McGraw-Hill, London, 1971.

73. Desai, C.S., and Abel, J.F., Introduction to the Finite Element Method, Van Nostrand Reinhold, New York, 1972.

74. Ellison, R.D., D'Appolonia, E., and Thiers, G.R., "Load-Deformation Mechansim for Bored Piles," Journal of the Soil Mechanics and Foundations Division, ASCE, Vol. 97, SM4, April 1971, pp. 661-678.

List of References (con'd)

75. Desai, C.S., "Numerical Design-Analysis for Piles in Sands," Journal of the Geotechnical Engineering Division, ASCE, Vol. 100, GT6, June, 1974, pp. 613-635.

76. Hunter, A.H. and Davison, M.T. (1969), "Measurements of Pile Load Transfer," Performance of Deep Foundations, ASTM STP 444, American Society for Testing and Materials, 1969, pp. 106-117.

77. Hanna, T.H., and Tan, R.H.S. (1973), "The Behavior of Long Piles Under Compressive Loads in Sand," Canadian Geotechnical Journal, Vol. 10, No. 3, August, 1973.

78. Holloway, D.M., "DUKFOR: Utilization Guidelines," Draft Report submitted for review, U.S. Army Engineer Waterways Experiment Station, Vicksburg, Ms., Nov. 1974.

79. Holloway, D.M., "Users' Guide, Program AXISYM," Draft Report submitted for review, U.S. Army Engineer Waterways Experiment Station, Vicksburg, Ms., Nov. 1974.

80. Davisson, M.T., "Pile Driving Analyses by the One-Dimensional Wave Equation," Paper Presented to the Metropolitan Section (NYC) Continuing Education Seminar, 1974.

81. Clough, G.W., and Duncan, J.M., "Finite Element Analyses of Port Allen and Old River Locks," Contract Report S-69-6, U.S. Army Engineer Waterways Experiment Station, Vicksburg, Ms., Sept., 1969.

82. Duncan, J.M., and Clough, G.W., "Finite Element Analysis of Port Allen Lock," Journal of the Soil Mechanics and Foundations Division, ASCE Vol. 97, No. SM8, August, 1971.

83. Conte, S.D., Elementary Numerical Analysis, McGraw-Hill, New York, 1965.

84. Clough, G.W., and Tsui, Y., "Performance of Tied-Back Walls in Clay," Journal of the Geotechnical Engineering Division, ASCE, Vol. 100, No. GT12, December, 1974.

85. Doherty, W.P., Wilson, E.L., Taylor, R.L., "Stress Analysis of Axisymmetric Solids Utilizing Higher-Order Quadrilateral Finite Elements" Report No. S.E.S.M. 69-3, Structural Engineering Laboratory, University of California, Berkeley, California, January, 1969.

86. Fruco and Associates, "Pile Driving and Loading Tests: Lock and Dam No. 4, Arkansas River and Tributaries, Arkansas and Oklahoma," Report for the U.S. Army Engineer District, Little Rock, CE, September, 1964.

List of References (con'd)

87. "Results of Tests in Foundation Materials, Lock and Dam No. 4, Arkansas River Navigation Project, Little Rock District," U.S. Army Engineer Division Laboratory, Southwestern, CE, SWDGL Reports No. 7920 and 7932, Dallas, Texas, 1962.

88. Desai, C.S., Jeng, Y.S., and Johnson, L.D., unpublished research in the Soil Mechanics Division, Soils and Pavements Laboratory, U.S. Army Engineer Waterways Experiment Station, Vicksburg, Ms., 1973.

89. Desai, C.S., unpublished research in the Soils Mechanics Division, Soils and Pavements Laboratory, U.S. Army Engineer Waterways Experiment Station, Vicksburg, Ms., 1973.

90. Vesić, A.S., "Tests On Instrumented Piles, Ogeechee River Site," Journal of the Soil Mechanics and Foundations Division, American Society of Civil Engineers, Vol. 96, No. SM2, Proceedings Paper 7170, March 1970, pp. 561-584.

91. Furlow, C.R., "Pile Tests, Jonesville Lock and Dam, Ouachita and Black Rivers, Arkansas and Louisiana," Technical Report S-68-10, U.S. Army Engineer Waterways Experiment Station, Vicksburg, Ms., 1968.

92. Davisson, M.T., "Pile Load Capacity," Proceedings, Design, Construction, and Performance of Deep Foundations, Continuing Education Seminar, San Franscisco Section, ASCE, given at the University of California, Berkely, February-March, 1975.

93. Duncan, J.M., and Chang, C.-Y., "Nonlinear Analysis of Stress and Strain in Soils," Journal of Soil Mechanics and Foundation Engineering Division, ASCE, Vol. 97, No. SM10, Oct. 1971.

94. Kulhawy, F.H., Duncan, J.M., and Seed, H.B., "Finite Element Analyses of Stresses and Movements in Embankments during Construction," Contract Report S-69-8, for the U.S. Army Engineer Waterwyas Experiment Station, Vicksburg, Ms., Nov. 1969.